Combining Capillary Electrochromatography with Ion Trap Accumulation and Time-of-Flight Mass Spectrometry

A Thesis Submitted for the

Degree of Doctor of Philosophy by

David Charles Simpson

School of Chemistry

College of Science and Engineering

University of Edinburgh

Final Copy

December 2002

Declaration

This thesis was composed by myself and is based on work that I carried out at the University of Edinburgh since registration for the PhD degree in October 1998. Collaborations have been indicated clearly.

David Charles Simpson

December 2002

Abstract

Capillary electrochromatography (CEC) is a rapidly developing liquid chromatographic technique in which electroosmotic flow (EOF) is used to propel mobile phase through the chromatographic column. The use of EOF results in reduced band dispersion when compared with pressurised flow, but narrow capillaries are required to avoid dispersion due to heating that arises from the required application of high electrical potentials. Measurement of UV absorbance in these narrow capillaries is therefore relatively insensitive, demanding improved detection methods. This work presents an alternative strategy that is based on the combination of ion trap accumulation with time-of-flight mass spectrometry.

Electrospray is most often used to transfer analytes from solution to the gas phase, concomitant with ionisation, when interfacing CEC to mass spectrometry. The small volumetric flow rates encountered in CEC, however, raise the possibility of other types of interface being effective. The work presented here describes the development of a novel interface in which a pulsed IR laser is used to vaporise chromatographic eluent, followed by ionisation using a pulsed UV laser. Vaporisation and ionisation both occur within the ion trap to remove the possibility of transmission losses. Ionisation laser wavelength is varied to impart a degree of selectivity. The presence of vaporised solvent and analyte ions inside the trap offers the possibility of performing ion-molecule chemistry.

In developing this instrument, the electrochromatographic column was separated from the interface by an electrically grounded junction and a transfer capillary. To preserve chromatographic efficiency, the fluid dynamics of this junction between the column and the transfer capillary were investigated both computationally and experimentally. Simulations of the fluid dynamics of the junction are presented. In order to test the interface without the intermittent, chromatographic, delivery of analyte, a continuous leak inlet was employed. The performance of the instrument was evaluated with polycyclic aromatic hydrocarbons because they are important environmental pollutants and because they are amenable to laser ionisation at 266 nm. Expressed as a number of theoretical plates per metre, an average chromatographic efficiency of 95,000 was obtained with a test mixture that consisted of acenaphthene, biphenyl, fluorene, naphthalene and phenanthrene. Furthermore, using the leak inlet, naphthalene was detected as a 100 nM solution in acetonitrile.

Acknowledgements

I would like to acknowledge the help and support that I have received from various sources during the course of my PhD. First and foremost, I would like to thank my supervisor, Pat Langridge-Smith. I would also like to give particular thanks to Sandy Yates, with whom I shared the project during my first year in Edinburgh. On the computational side, I would like to acknowledge the contributions of George Alder to the fluid flow simulations, and David Kilgour to the data acquisition software. Financial assistance was provided primarily by the EPSRC, but also by ICI in the form of a CASE studentship.

In writing this thesis, help has come from a number of additional sources. Thanks should go to Perdita Barran, John Knox, Gordon McDougall and George Alder. John Knox deserves special thanks for his extensive knowledge of chromatographic theory, which he was always willing to share, providing help and ideas throughout the course of the project. Assistance of a more practical kind came from Bob Boughtflower and Clare Paterson at Glaxo in Stevenage. Without their donations of instrumentation and expertise this project would not have been possible. Mention should also be made of Beth Watchman who popped in with an interesting CE problem that provided me with something to do in the dark days of leaking column-packing chambers. The guys at ICI who've at some point been involved in my project are Tony Jackson, Steve Rumbelow, Bill Dollard and Mike Taylor. Thanks especially go to Bill for spending so long trying to fix the LCT.

Finally, looking back to early days in the lab, I must thank Alison, Angela and Michel for introducing me to the union and compulsory morning and afternoon tea breaks. Those early days were followed by the opening of Room 4, which Logan, DPAK and Chris turned into their own special little den. More recently, Nick, Jennifer, Richard, Adriana and Perdita have changed the character of the group once again, Thanks to all of them for making Lab 73 into a fun place to work for the past four years.

Examination by Gwyn Lord and John Monaghan, Tuesday 19th November 2002.

Contents

Abbreviations and Symbols

a	Used to denote flatness of surface, which in a capillary is equal to r_i AND forward peak width at 10% height used to quantify peak asymmetry
A	van Deemter term relating to dispersion due to differing migration path length and speed
ADC	Analogue to Digital Converter
AMP	Adenosine 5'-monophosphate
APCI	Atmospheric Pressure Chemical Ionisation
API	Atmospheric Pressure Ionisation
APPI	Atmospheric Pressure Photoionisation
b	Rearward peak width at 10% height used to quantify peak asymmetry
B	van Deemter term relating to dispersion due to diffusion
C	van Deemter term relating to dispersion due to slow mass transfer
CCBC	Capillary Column Butt Connector (chromatographic union)
CE	Capillary Electrophoresis
CEC	Capillary Electrochromatography
CFD	Computational Fluid Dynamics
CFFAB	Continuous Flow Fast Atom Bombardment
CI	Chemical Ionisation
CIA	Capillary Ion Analyser (instrument for CE and CEC)
C_m	Concentration of solute in mobile phase AND van Deemter term relating to dispersion due to slow mass transfer in the mobile phase
CMP	Cytidine 5'-monophosphate
C_P	Peak capacity
C_s	Concentration of solute in stationary phase AND van Deemter term relating to dispersion due to slow mass transfer in the stationary phase
δ	Electrical double layer thickness
D	van Deemter term, which replaced C_m term and which in conjunction with the A term is used to describe mobile phase process contributing to dispersion AND length of TOF/MS drift region
d_c	Inner diameter of column (CFD calculations)
ΔEPE	Electrical Potential Energy difference
d_f	GLC film thickness
d_i	Inner diameter (of a circular cylindrical tube)
D_m	Diffusion constant of solute in the mobile phase
d_p	Diameter of chromatographic packing particle
ΔP	Pressure difference
D_s	Diffusion constant of solute in the stationary phase
d_t	Inner diameter of transfer capillary (CFD calculations)
EI	Electron Impact
EOF	Electroosmotic Flow

ESI	Electrospray Ionisation
FAB	Fast Atom Bombardment
F_V	Volumetric flow rate
γ	Geometrical factor that represents the retarding effect of chromatographic packing materials on diffusion
GC	Gas Chromatography
GLC	Gas Liquid Chromatography
GMP	Guanosine 5'-monophosphate
h	Reduced plate height, which is equal to H/d_p
H	Plate height or height equivalent to a theoretical plate
HPLC	High Performance Liquid Chromatography
HPMC	Hydroxypropylmethyl cellulose
ID	Inner Diameter (of a circular cylindrical tube)
IEEE	Institute of Electrical and Electronics Engineers
IP	Ionisation Potential
ITS	Ion Trap Storage
κ	Inverse of electrical double layer thickness, δ
k'	Phase capacity ratio
λ	Geometrical factor that represents the regularity of column packing AND wavelength
L	Column length or distance migrated by centre of analyte band
L_1	Distance between simulation start point and junction (CFD calculations)
L_2	Distance from junction to end of conical inlet (CFD calculations)
L_3	Distance from end of conical inlet to detection point (CFD calculations)
LC	Liquid Chromatography
LIF	Laser Induced Fluorescence
μ	Mean of a Gaussian curve
MALDI	Matrix Assisted Laser Desorption Ionisation
MCP	Microchannel Plate
μ_E	Electrophoretic steady state velocity
μ_{EO}	Electroosmotic flow steady state velocity at infinite distance from a surface
MS	Mass Spectrometry
m/z	Mass to charge ratio of an ion
N	Plate number
N_R	Reynolds number
OD	Outer Diameter (of a circular cylindrical tube)
ODS	Octadecylsilyl (type of stationary phase for LC)
PAH	Polycyclic Aromatic Hydrocarbon
PEC	Pressurised Electrochromatography
PEEK	Polyetheretherketone
R	Chromatographic resolution
REMPI	Resonantly Enhanced Multiphoton Ionisation
rf	Radio Frequency

r_h	Hydrodynamic radius
r_i	Inner radius (of a circular cylindrical tube)
σ	Standard deviation of a Gaussian curve
S	Distance between the source and liner electrodes in a single-field ion extraction TOF/MS
σ_0	Charge density at a surface
σ^2	Variance of a Gaussian curve
S_a	Distance through which an ion is accelerated in a single-field ion extraction TOF/MS
SCX	Strong Cation Exchange (type of stationary phase for LC)
SIMS	Secondary Ion Mass Spectrometry
t_D	Time spent by an ion in the drift region of a TOF/MS
TLC	Thin Layer Chromatography
t_m	Average time for mobile phase to pass through column
TMP	Thymidine 5'-monophosphate
TOF	Time-of-Flight
t_r	Average time spent by a solute on column, which is equal to $t_m + t_s$, and which is also known as the retention time
TRIS	Tris(hydroxymethyl)aminomethane
t_s	Average time spent by a solute in the stationary phase
t_S	Time spent by an ion in the source region of a TOF/MS
u	Average fluid velocity in axial direction, which is equal to L/t_m
u_D	Drift velocity in TOF/MS
u_r	Axial fluid velocity at radial position, r
v	Reduced velocity, which is equal to ud_p/D_m
V_D	Electrical potential applied to the electrode used in two-field ion extraction TOF/MS to draw ions out of the source region
V_{DEF}	Electrical potential applied to deflector plates in TOF/MS
V_F	Electrical potential applied to central electrode of an Einzel lens
V_L	Electrical potential applied to TOF/MS drift region liner
V_m	Volume of mobile phase
V_R	Electrical potential applied to the reflectron
V_s	Volume of stationary phase
V_S	Electrical potential applied to source electrode in TOF/MS
$w_{10\%}$	10% height width of a Gaussian curve
$w_{1/2}$	Half height width of a Gaussian curve
w_b	Base width of Gaussian curve, equal to exactly $4 \times \sigma$
ψ	Electrical potential
ψ_0	Electrical potential at surface
YAG	Yttrium Aluminium Garnet
ψ_d	Electrical potential at Stern plane
ζ	Electrical potential at shear plane: the *zeta* potential
ZDV	Zero Dead Volume (chromatographic union)

1. Introduction

The work described in this thesis has focused on the development of an instrument for performing on-line capillary electrochromatography mass spectrometry (CEC/MS), based on a hybrid ion trap time-of-flight (TOF) mass spectrometer. The ion trap provides decoupling of the different timescales required for CEC separation and TOF mass spectrometry. The instrument incorporates a novel laser vaporisation laser ionisation interface, in which analytes are vaporised directly from the end of a capillary coupling the working CEC column to the mass spectrometer. Detection is accomplished using UV photoionisation of the vaporised neutrals.

CEC is a rapidly developing separation technique in which electroosmotic flow (EOF) is used to propel mobile phase through the chromatographic column. EOF arises from the application of a gradient in electrical potential across the column, with CEC often being regarded as a replacement for high-performance liquid chromatography (HPLC). In contrast to CEC, mobile phase is propelled through the column in HPLC by the application of a pressure gradient across the column. The term 'column' in both cases refers to the tube that is used to encapsulate the stationary phase along with the stationary phase itself, which typically consists of a thin layer of material bonded to an inert support. The inert support is most commonly composed of porous silica particles, but porous polymeric monoliths can also be encountered. Solutes partition between the phases, with those that have a high affinity for the stationary phase taking longer to pass through the column than those that do not. Mobile phase flow through the column can be considered as an array of streams between which solutes can diffuse.

Stream homogeneity, in both flow rate and path length, is critical to maximising separation efficiency. Flow rate homogeneity is improved when EOF is used because flow originates from the surfaces, making stream flow rate largely independent of proximity to a surface. In the case of pressurised flow, due to frictional drag, stream velocity is zero at the surface and increases with increasing distance from the surface. Identical solute molecules will pass through the column at more varied rates when vastly differing stream flow rates exist, causing narrow injected bands to

spread. Path length homogeneity can also be improved by EOF, but in this case, not directly. Moving to smaller particles will reduce path length variation but will increase the pressure necessary to force mobile phase through the column at an acceptable flow rate. Commercial instrumentation is usually limited to 6000 psi, meaning that it is impossible to use the smallest particles in HPLC. No such limitation exists with EOF, allowing much smaller particles to be used in CEC.

EOF does, however, introduce some limitations. The mobile phase must be an electrolyte, and the surface must be charged when in contact with the mobile phase. The application of high electrical potentials across electrolyte filled columns results in resistive heating, which limits column size due to the requirement for effective radiation of generated heat to the environment. As column temperature rises, chromatographic efficiency is reduced [1]. Narrow columns and hence low volumetric flow rates introduce detection sensitivity problems. Measurements of UV absorbance in columns that have an inner diameter (ID) in the region of 100 μm are relatively insensitive, while connecting large volume detection cells reduces separation efficiency. The logical detection strategy is therefore to utilise mass spectrometry. As well as providing enhanced sensitivity, the mass spectrometer would be expected to supply a considerable amount of additional information that could lead to the identification of a solute. To a certain degree, the mass spectrometer also allows overlapping solute bands to be resolved.

Electrospray ionisation (ESI) has become the technique of choice for converting ions and molecules in solution to gas phase ions for the purpose of mass spectrometric analysis, and would be expected to be the most obvious route for the interfacing of CEC to mass spectrometry. The best results, however, are obtained for compounds that pre-exist as ions in solution. This preference for ions is very similar to that shown by the particle bombardment techniques, fast atom bombardment (FAB) and secondary ion mass spectrometry (SIMS). ESI, although most effective for compounds that pre-exist as ions in solution, is also effective with compounds that can be ionised in solution by acid/base chemistry or by adduct formation. For this reason, volatile organic acids such as formic acid are commonly employed additives. ESI is therefore very effective for compounds such as proteins and peptides, which

contain basic amino acid residues, but several important classes of compounds are not well analysed by the technique. For example, the polycyclic aromatic hydrocarbons (PAHs) studied in this work give much improved ESI signals only when ions are preformed in solution using charge-transfer complexation [2]. The low volumetric flow rates encountered in CEC offer the possibility of other interfacing strategies being effective.

The need for new mass spectrometric techniques that are applicable to compounds unsuitable for ESI is evidenced by the recent development of atmospheric pressure photoionisation (APPI) [3]. APPI has been designed for non-polar analytes, and relies on the fact that most organic molecules have ionisation potentials (IPs) in the range 7 – 10 eV, while most common solvents have relatively high IPs (water, IP = 12.6 eV; methanol, IP = 10.8 eV; acetonitrile, IP = 12.2 eV). The use of a krypton discharge lamp to provide 10.0 eV and 10.6 eV photons provides the possibility of being able to produce analyte ions without ionising the solvent, therefore reducing background. Dopants, however, such as toluene (IP = 8.83 eV) and acetone (IP = 9.70 eV), were necessary in the reported work to improve ionisation efficiency.

The approach adopted in the work described in this thesis is also based on photoionisation. As with APPI, it was hoped that only analytes would be ionised, allowing neutrals to be pumped away. However, rather than using high-energy photons from a discharge lamp, lower energy photons from a laser were used. For ionisation, a quadrupled Nd^{3+}:YAG laser was used to provide 4.66 eV photons (266 nm). Using photons of this energy naturally requires more than one photon to be absorbed for ionisation. Such multiphoton ionisation is enhanced by choosing a laser wavelength that corresponds to excitation of the molecule into an intermediate electronic state, which must then be followed by a further photon for ionisation. The presence of a real intermediate state improves the efficiency of the process, adding a degree of selectivity. A certain class of compounds can therefore largely be analysed without interference from other compounds present. The use of a laser also means that ionisation can be limited to a small volume, with the use of a pulsed laser allowing ionisation to be limited in duration also.

Laser ionisation requires that analyte molecules be transferred from the solution phase to the gas phase. In this work the technique by which this was accomplished was laser vaporisation, using an IR laser to effect fast heating of chromatographic eluate. Laser vaporisation relies on fast heating to break bonds between analyte and solvent before enough time has elapsed for bonds inside the analyte to break. Ideally the CEC column outlet would be subjected to irradiation for the purpose of analyte vaporisation, but it was decided that a significant operational simplification would be achieved by terminating the column in a union, using a short length of unpacked capillary to transfer eluate to the vaporisation point.

The mass spectrometer chosen for this work consisted of an ion trap that could only be used for ion storage and a TOF mass analyser. The purpose of the ion trap was to accumulate ions from a number of laser ionisation events, before ejection into the TOF mass analyser. The ion trap ring electrode contained four drilled holes, with the capillary carrying the eluate being mounted in one, using a ceramic sleeve for insulation. The capillary terminus and the ceramic sleeve were mounted so that they were flush with the inner surface of the ring electrode, with the vaporisation laser entering the trap through an opposite drilled hole. The ionisation laser entered the trap through a third drilled hole, leaving the trap through the fourth and final drilled hole. The paths of the two lasers intersected in the centre of the trap, with the beams being at right angles to each other. Both vaporisation and ionisation were performed inside the trap to remove the possibility of transmission losses.

TOF spectra were collected using an oscilloscope, but were transferred to a computer for storage and analysis. The connection between the oscilloscope and the computer was by IEEE-488 cable, with National Instruments' (Austin, TX, USA) [4] LabVIEW software being used to write programs both for data acquisition and processing. The most significant problem with this approach was that a little over one second was required for the transfer of a single TOF spectrum from the oscilloscope to the computer. For this reason the oscilloscope was instructed to sum ten TOF spectra, which were then transferred to the computer. Only after data transfer was complete could the oscilloscope begin collecting data again. This was a major shortcoming of the entire instrumental system.

One further aim of the project was the implementation of gradient elution. Being able to vary the relative proportions of mobile phase constituents during a chromatographic run has been shown to significantly improve the effectiveness of the technique. A method where two inlet buffer vials are used and the potentials applied to these vials are varied to produce the gradient has been demonstrated [5]. Most investigators, however, have reported the use of gradient pumps designed for HPLC being used to provide what could be regarded as a continually renewed inlet reservoir [6,7]. In such systems, the solvent mixture from the HPLC system is passed by the column inlet, with running potential being applied at the junction with the CEC column. The column therefore draws in whatever mobile phase, or analyte from the injection valve, that is passing at any particular time. Such a configuration is illustrated in Figure 1.1.

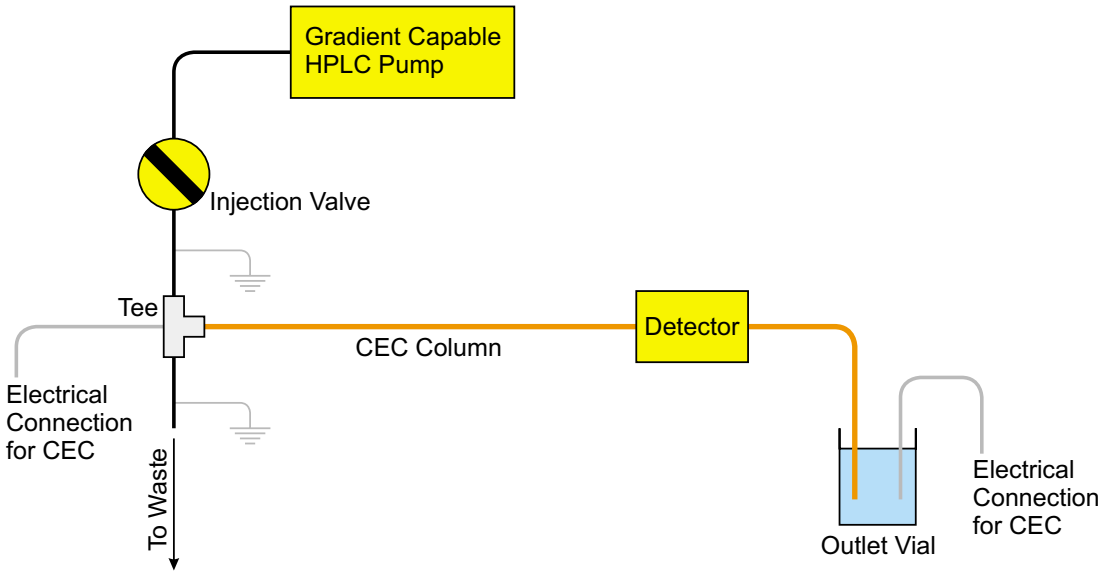

Figure 1.1. Instrumental system for performing gradient CEC.

Some form of restriction is often used on the waste line to raise system pressure and obtain a hybrid pressurised and EOF system. The use of part pressurised flow will naturally reduce chromatographic efficiency somewhat, but a more reliable instrumental analytical technique is obtained. Another aim was to investigate the performance of novel stationary phases as the stationary phases most often used in CEC were designed for HPLC, suggesting that differing strategies more suited to the new technique might yield improved results.

In Chapter 2 of this thesis, an introduction to both chromatography and electrophoresis is provided, together with an explanation of how these techniques are combined in CEC. Emphasis is then placed on explaining the methods used to quantify chromatographic performance. Some issues relating to the practice of CEC are also discussed. In Chapter 3, a review of the development of interfaces between liquid chromatography (LC) and mass spectrometry is given, followed by an examination of those techniques that have been applied to CEC. This is then followed by brief descriptions of TOF mass spectrometry, ion trap storage, laser desorption, laser ionisation, and finally, ion trap storage time-of-flight (ITS/TOF) mass spectrometry. A detailed description of the various items of instrumentation used in this work is given in Chapter 4, including tests that were carried out to evaluate the performance of some of these items of equipment.

The development of, and experiments performed to demonstrate the effectiveness of, the capillary junctions required in this work are described in Chapter 5. Termination of the CEC column in the ion trap ring electrode would have been ideal, but the use of a transfer capillary between the column and the vaporisation point was chosen both as a simplification and to allow separate optimisation of the chromatographic and the mass spectrometric systems. Work directed towards producing the best possible junction is fully described, focusing on simulations, imaging, and the building of test systems. Reproducibility in CEC is also investigated. Extensive characterisation of the mass spectrometric system is presented in Chapter 6, along with imaging of the effects of laser irradiation on liquids entering a vacuum chamber. The CEC/MS data obtained for test mixtures of PAHs is then displayed, followed by a description of unsuccessful attempts to implement continuous flow matrix assisted laser desorption ionisation (MALDI) using an IR laser. Chapter 7 provides an overall conclusion, while associated work on CE systems is presented in Appendix A.

---

[1] J. H. Knox, *Chromatographia*, **1988**, *26*, 329-337.

[2] G. J. Van Berkel, S. A. McLuckey and G. L. Glish, *Anal. Chem.*, **1991**, *63*, 2064-2068.

[3] D. B. Robb, T. R. Covey and A. P. Bruins, *Anal. Chem.*, **2000**, *72*, 3653-3659.

[4] Further information available from http://www.ni.com

[5] C. Yan, R. Dadoo, R. N. Zare, D. J. Rakestraw and D. S. Anex, *Anal. Chem.*, **1996**, *68*, 2726-2730.

[6] B. Behnke and E. Bayer, *J. Chromatogr.*, **1994**, *680*, 93-98.

[7] C. G. Huber, G. Choudhary and C. Horváth, *Anal. Chem.*, **1997**, *69*, 4429-4436.

2. Capillary Electrochromatography

When performing a chromatographic separation, an analyte mixture is in some way added as a discrete band to a mobile phase stream that is then passed through a stationary phase. As analyte molecules are washed through the stationary phase by the mobile phase, they regularly move from one phase to the other. The residence time in the stationary phase causes molecules to fall behind the mobile phase. Identical molecules should migrate at approximately the same rate, while conditions must be chosen so that differing molecules migrate at different rates. If differing molecules pass through the system at sufficiently different rates, a separation is achieved. An electrophoretic separation on the other hand is based upon differing ions having different migration rates in an electrical field. Cations are attracted to the cathode, while anions are attracted to the anode, with migration rate being proportional to ionic charge and inversely proportional to the drag experienced while moving. Chromatography can provide separation of both charged and uncharged analytes, while electrophoresis can only separate charged analytes. With the modes of operation of the two techniques being quite different, the combination of the two can greatly increase separation power.

The separation of five overlapping analyte bands is illustrated in Figure 2.1. The separation could be either chromatographic or, provided that all five analytes migrate in the same direction, electrophoretic. The chromatograms on the left-hand side of the figure are coloured to distinguish each analyte band while those on the right-hand side of the figure show the bands added together. The five pairs of chromatograms shown are consecutive in time and are separated by the same time interval. The representation of the separation process shown on the right-hand side of the figure can be likened to watching the migration of five analytes that have the same colour in a transparent tube filled with a transparent mobile phase or electrophoretic medium. Individual analyte bands are represented by Gaussian curves since bands achieve this concentration profile rapidly as they pass through a column. The illustration shown here, however, is idealised because the initial band profile would be expected to differ significantly from Gaussian, becoming Gaussian only after migrating a short distance. The analyte bands would also be expected to widen as they passed through the column.

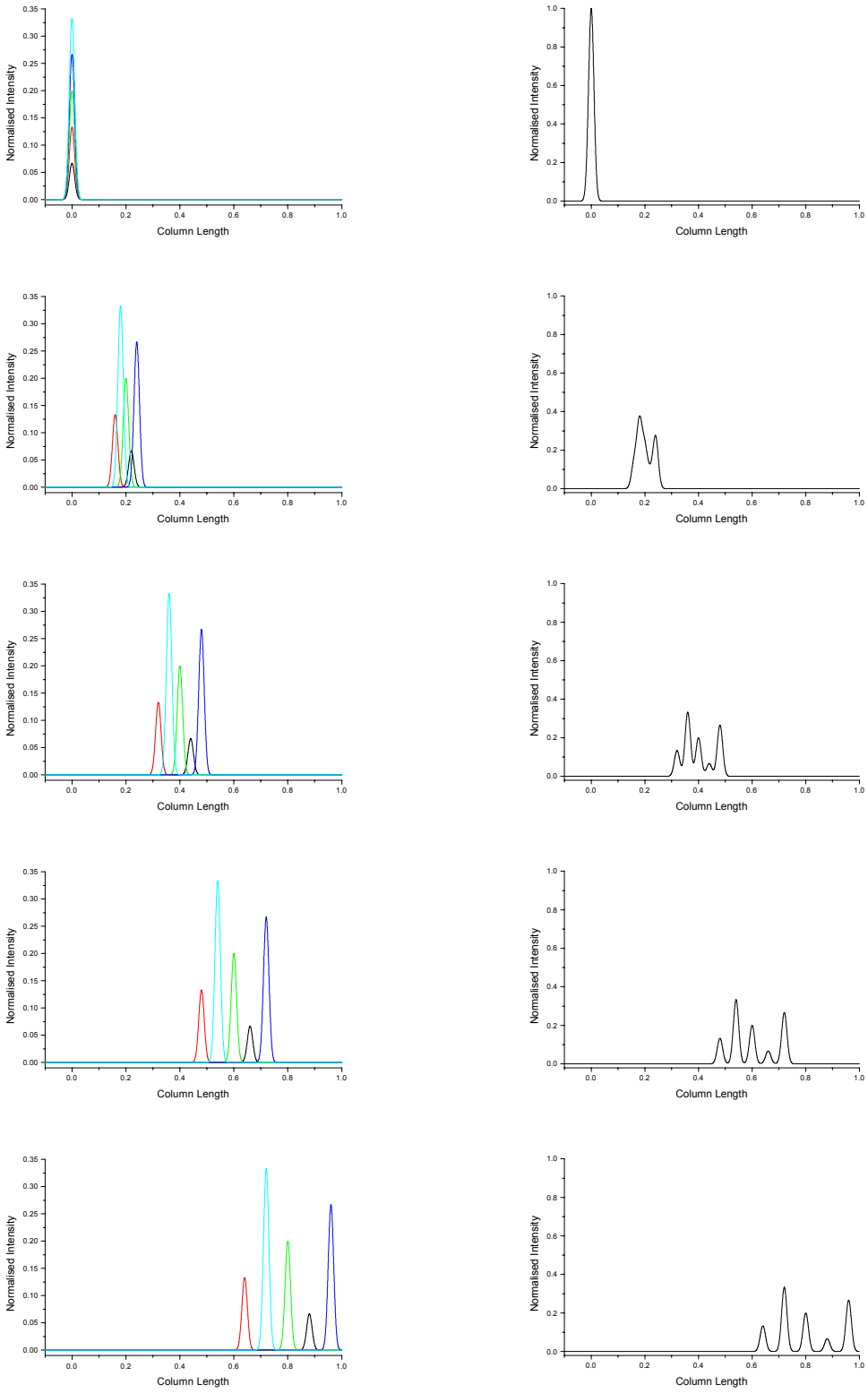

Figure 2.1. Representation of the separation process. The chromatograms on the left are coloured to distinguish individual analytes while those on the right are the result of adding the individual analyte bands together.

In each chromatogram in Figure 2.1, the horizontal axis refers to column length, with the word column simply referring to the tube in which the separation is performed. It must be noted, however, that both techniques are not exclusively performed in columns. In chromatography, the column is filled with stationary phase through which the mobile phase flows, whilst in electrophoresis, the column is filled with a medium that provides the drag required for separation, but which does not have to move itself. If the electrophoretic medium does move, however, it becomes possible to elute ions that migrate in both directions past a fixed position detector.

Chromatography can be subdivided into gas chromatography (GC) and LC, dependent upon whether the mobile phase employed is a liquid or a gas. It would be expected that a GC technique would be chosen for the separation of compounds that are both volatile and thermally stable, while LC techniques can be applied to a much wider range of compounds. The most widely used LC technique today is HPLC, which is characterised by the use of columns that are packed with solid support particles that are coated with chromatographic material. These coatings are chemically bonded to the support particles and are most commonly based on long chain hydrocarbons. As mobile phase passes around and over these coatings, there is partitioning between the phases and chromatographic action is obtained. This method of providing a stationary phase has the advantage that many different groups can be bound to the support particles to obtain the correct selectivity, while the coatings are long-lasting and reliable. HPLC is particularly suitable for compounds with characteristics such as high polarity, high molecular weight, thermal instability, and a tendency to ionise in solution [1].

Mobile phase is forced though HPLC columns by application of relatively high pressures. In common separation methods, applied pressures of between 400 and 4000 psi are regularly used. As mobile phase moves through the column, friction from support particle surfaces causes mobile phase velocity to vary significantly. Close to surfaces, the magnitude of mobile phase velocity is small, while towards the centre of pores between particles it is comparatively large. The particles are also not in a perfectly regular arrangement, so routes of both varying length and varying flow rate exist, which are followed by solutes through the packed bed. Diffusion allows switching between these routes, but does not nullify their effect. Variations in migration rate for identical molecules contribute to the band dispersion.

A solution to this problem, and hence an improvement in performance, is offered by the use of EOF to drive mobile phase through the chromatographic column. EOF requires the application of an electrical potential gradient across the column, but reduces dispersion by delivering close to constant mobile phase velocity across each pore. A further advantage of EOF is that smaller solid support particles can be used to reduce variation in migration path length, further reducing dispersion. Reduction of support particle size is restricted with pressurised flow because the applied pressure required to maintain the same flow rate increases rapidly as particle size and hence channel diameter falls. Flow rate must be maintained to avoid excessive dispersion arising from diffusion. Most commercial HPLC systems are limited to an maximum operating pressure of 6000 psi, fixing the minimum particle size at around 3 μm. Much higher pressures have been employed in HPLC to allow the utilisation of smaller particles [2], but technical difficulties have so far prevented widespread use. This limit does not apply when EOF is utilised to drive mobile phase through the column. Use of EOF, however, results in a technique that differs significantly from HPLC, which is known as electrochromatography.

The combination of electrophoresis with chromatography was first reported by Strain in 1939 [3]. In this work an improvement in chromatographic resolution was obtained by the application of an electrical potential gradient, although application of a small pressure gradient was used to suppress EOF. The adoption at around that time of solid stabilising media in electrophoresis to suppress convection no doubt also led to many nominally electrophoretic separations having some chromatographic character. In 1950, Synge reported the separation of electrically neutral carbohydrates in an agar gel [4], leading to the development of thin-layer chromatography (TLC) systems that utilised EOF to drive mobile phase flow [5,6]. There was then a long gap until 1974 when Pretorius *et al.* reported the next significant event in the development of electrochromatography [7]. In this work, the improvement in chromatographic performance gained by replacing pressurised flow with EOF was demonstrated. The columns used by Pretorius *et al.* were constructed of quartz, had an ID equal to 1 mm, and were packed with bare silica particles (for some analytes a bare silica surface can act as a stationary phase). The next instance of electrochromatography was reported by Jorgenson and Lukacs in 1981 [8], with the technique now being better referred to as CEC, due to the use of narrower (170 μm ID) pulled glass capillaries. These authors,

however, considered pressurised flow chromatography to be superior due to greater control over the mobile phase flow characteristics. This work was augmented by Tsuda *et al.* in 1982 who reported the use of narrow capillaries (30 μm ID), internally coated with a stationary phase, for what has become known as open tubular CEC [9]. Stevens and Cortez followed this by an investigation into EOF in very short packed columns, noting the effect of different stationary and mobile phases [10]. Popularisation of the technique had to wait, however, until the publication of papers by Knox and Grant in 1987 and 1991 [11,12], and Knox alone in 1988 [13], in which the performance improvement available from utilisation of EOF was described. Since 1991, a large body of literature has become available, culminating in the recent publication of two books on this subject [14,15]. All that remains for the use of CEC to become widespread is the development of good commercial instrumentation, which in turn will drive the development of appropriate stationary phases to add selectivity to the enhanced separation power.

2.1. Pressurised Solvent Flow in a Chromatographic Context

In a cylindrical tube through which a fluid is flowing, due to the application of a pressure gradient, if all fluid flowing through a small part of the cross-sectional area at one particular point is in some way labelled, two distinct types of flow can be observed. At low flow rates, a stream is observed that remains largely intact over long distances, spreading slightly due to the action of molecular diffusion. This case is referred to as laminar flow. At high flow rates, however, the labelled stream shows a chaotic, fluctuating type of motion. Rapid mixing is observed, occurring over a length scale comparable with the internal diameter of the tube. This type of flow is known as turbulent flow. The difference between the two types of flow is illustrated in Figure 2.2, representing the introduction of a stream of labelled fluid moving at the same linear velocity as that found in the larger tube.

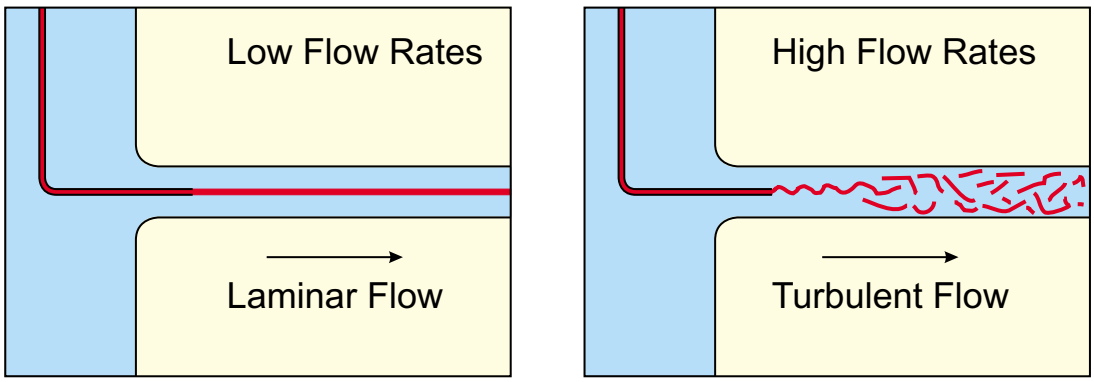

Figure 2.2. Comparison of the effect of introducing a stream of labelled fluid into a tube where laminar flow conditions are found versus one where turbulent flow conditions are found.

In a laminar flow system, fluid velocity is related to distance from the inner wall of the tube, since it is governed by friction from the tube walls. In a cylindrical tube, laminar sheets of fluid have the same velocity, hence giving rise to the name. In a circular cylindrical tube these sheets will be annular. The transition from laminar to turbulent flow, with increasing flow rate, occurs at a Reynolds number, $N_R > 2100$ in an open tube [16]. N_R can be calculated using Equation 2.1 for Newtonian liquids (constant viscosity).

$$N_R = \frac{\rho u d_i}{\eta} \qquad \text{Equation 2.1}$$

In the above expression, ρ is the density of the fluid, u is the average flow velocity, d_i is the ID of the tube, and η is the viscosity of the fluid. For acetonitrile ($\rho = 779.3$ kg m^{-3} (298 K) [17] and $\eta = 0.369 \times 10^{-3}$ N m^{-2} s (298 K) [17]) flowing through a tube of $d_i = 100$ µm at a typical chromatographic flow rate of 1 mm s^{-1}, $N_R = 0.21$. Although it would appear difficult to reach turbulent flow conditions for liquids in open tubes, such conditions have been investigated in open tubular GC [18]. In a packed column, however, the array of support particles will produce a very complex system that is expected to be laminar in character. Flow streams converging from different directions in particular arrangements of support particles, however, are likely to result in some localised turbulent character. In a recent paper Knox stated that turbulent flow will occur in GC at typical operating velocities but will only occur at very high linear flow velocities in LC systems [19]. Under laminar flow conditions in a circular cylindrical

tube, the magnitude of the fluid velocity in the direction of flow at any radial point r, u_r, is given by Equation 2.2.

$$u_r = \frac{1}{4\eta}\frac{\Delta P}{L}\left(r_i^2 - r^2\right) \qquad \text{Equation 2.2}$$

In this expression, ΔP is the pressure drop across the tube, L is the length of the tube and r_i is the internal radius of the tube. This relationship has been plotted in Figure 2.3, illustrating the parabolic velocity profile found. This velocity profile gives the magnitude of the velocity at radial positions as a proportion of that found at the centre of the tube, where the magnitude of the velocity is greatest. This is the variation that will be found in channels between stationary phase support particles that will lead to dispersion. Turbulence, however, will act to flatten out this profile, but it must be remembered that the high flow rates that will lead to turbulence will lead to dispersion arising from molecules in the stationary phase being left behind. The importance of this cause of dispersion rises with increasing flow rate, meaning that turbulent flow is unlikely to be the answer to reducing dispersion.

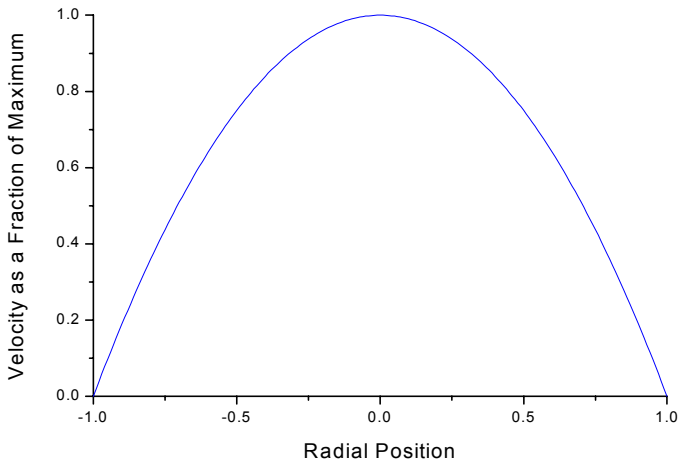

Figure 2.3. Parabolic variation in fluid flow velocity across the diameter of a cylindrical capillary as a fraction of the maximum velocity.

Integration of Equation 2.2 across the internal cross-sectional area of the circular symmetrical tube can then be used to give the volumetric flow rate, F_V, as shown in Equation 2.3. This relationship has been used during this work to estimate F_V for liquids

flowing through capillaries under applied pressure gradient and laminar flow conditions. A more careful consideration of the flow rate must also take account of the density and the surface tension of the liquid [20].

$$F_V = \frac{\pi r_i^4}{8\eta}\frac{\Delta P}{L} \qquad \text{Equation 2.3}$$

2.2. The Origin of Electroosmotic Flow

As outlined above, laminar flow resulting from the application of a pressure gradient will contribute to band dispersion. EOF offers superior flow characteristics that reduce band dispersion. A good theoretical description of the phenomenon is found in Grant's PhD thesis [21], with a more general description of the properties of charged liquid-solid interfaces being found in Shaw's textbook [22]. Silica surfaces become charged when placed in contact with aqueous solutions, with the magnitude of this charge being pH dependent. The isoelectric point of silica remains a matter of dispute, with values between 1 and 4 having been reported [23]. At typical chromatographic pH a silica surface acquires a significant net negative charge due to dissociation of acidic surface silanol (SiOH) groups. Electrostatic forces result in the attraction of a balancing layer of excess cations to this anionic surface, with random thermal motion acting against this tendency. A simple model proposed by both Gouy and Chapman assumes that ions can be regarded as point charges and that they are distributed in solution close to the surface according to a Boltzmann distribution. Their model of the diffuse electrical double layer is illustrated in Figure 2.4.

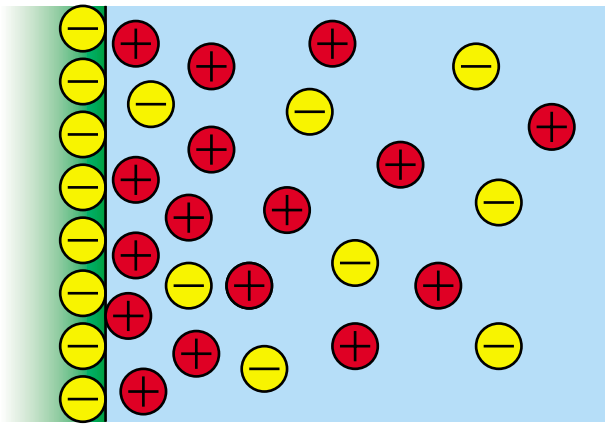

Figure 2.4. Schematic representation of the Gouy-Chapman model of the diffuse electrical double layer for an anionic (e.g. silica) surface. Note that overall electroneutrality must be maintained.

The variation in potential, ψ, with distance from the surface can be derived from the Poisson-Boltzmann distribution, with application of the Debye-Hückel approximation (small potentials), resulting in Equation 2.4.

$$\psi = \psi_0 \exp(-\kappa x) \qquad \text{Equation 2.4}$$

The potential, which at the surface is denoted ψ_0, falls in a roughly exponential manner with increasing distance from the surface, x. κ is a constant as defined in Equation 2.5

$$\kappa = \left(\frac{2F^2 I}{\varepsilon_0 \varepsilon_r RT} \right)^{1/2} \qquad \text{Equation 2.5}$$

where F is the Faraday constant, I is the ionic strength of the solution (expressed in mol m^{-3}), ε_0 is the permittivity of a vacuum, ε_r is the relative dielectric constant of the solution, R is the gas constant and T is the temperature. The inverse of κ is referred to as the double layer thickness, δ, which is defined as the distance over which ψ_0 decays by a factor of e. For an A^+B^- electrolyte (e.g. ammonium acetate) at a concentration in water of 50 mM (50 mol m^{-3}), the double layer thickness is approximately 1.4 nm (using a value of 80 for the relative dielectric constant of water at room temperature). The same calculation for a 5 mM solution gives a value of approximately 4.3 nm.

The requirement for overall electrical neutrality allows the potential at the surface, ψ_0, to be related to the charge density at the surface, σ_0, via Equation 2.6 (provided that ψ_0 is small).

$$\sigma_0 = \varepsilon_0 \varepsilon_r \kappa \psi_0 \qquad \text{Equation 2.6}$$

The Gouy-Chapman model, however, does not consider ions held firmly to the surface by adsorption. Such ions must be treated in a different manner to those that are not adsorbed and hence are free to move. Essentially, instead of utilising ψ_0 as the surface potential, the potential at the shear plane between immobile and mobile ions must be considered. This potential is termed the ζ potential. Stern's model, which divides the electrical double layer into two parts separated by a plane located at roughly a hydrated ion radius from the surface, is illustrated in Figure 2.5. Potential falls linearly between the surface and the Stern plane and then exponentially beyond the Stern plane. The potential at the Stern plane is denoted ψ_d, and is very similar to ζ. It is possible to determine ζ experimentally, but not ψ_d. A typical value for the ζ potential of a silica surface in contact with an aqueous electrolyte solution with an ionic strength of 0.01 mol dm^{-3} at pH 8 is 40 mV [23].

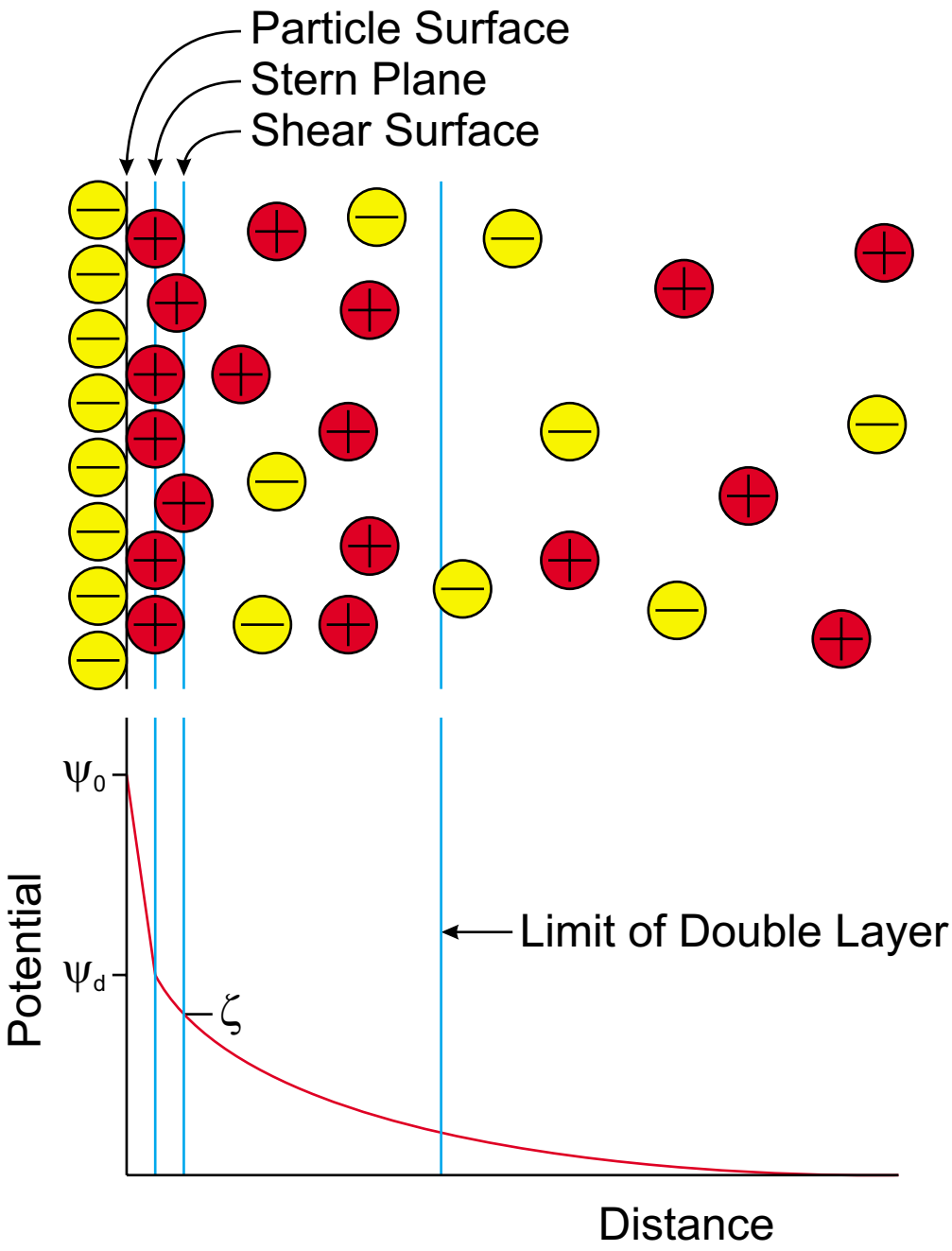

Figure 2.5. Schematic representation of the structure of the electrical double layer according to Stern's theory.

When an electrical field is applied parallel to the surface the non-adsorbed excess ions will move towards the oppositely charged electrode, dragging the bulk solution along with them due to appreciable frictional forces, giving rise to EOF. The Smoluchowski equation describes the EOF velocity at an infinite distance from a surface,

$$\mu_{EO} = \frac{\varepsilon_0 \varepsilon_r \zeta E}{\eta}$$ Equation 2.7

where μ_{EO} is the EOF velocity. The above expression, however, is valid only when the product κa is large, where a in the case of a cylindrical capillary refers to the internal radius of a capillary. The channels through a column packed with small particles are often regarded as bundled interconnecting cylindrical capillaries. Rice and Whitehead [24] made a detailed study of the effect of varying κa on the EOF velocity profile for cylindrical capillaries. At low values of κa, where there is significant electrical double layer overlap, there is significant deviation from plug flow, while at high values of κa the flow profile is flat except right at the surface, with the Smoluchowski velocity being achieved over the majority of the capillary diameter. The variation in velocity profile across a capillary diameter for various values of κa is illustrated in Figure 2.6 (for comparison Figure 2.3 shows the velocity profile found with laminar flow).

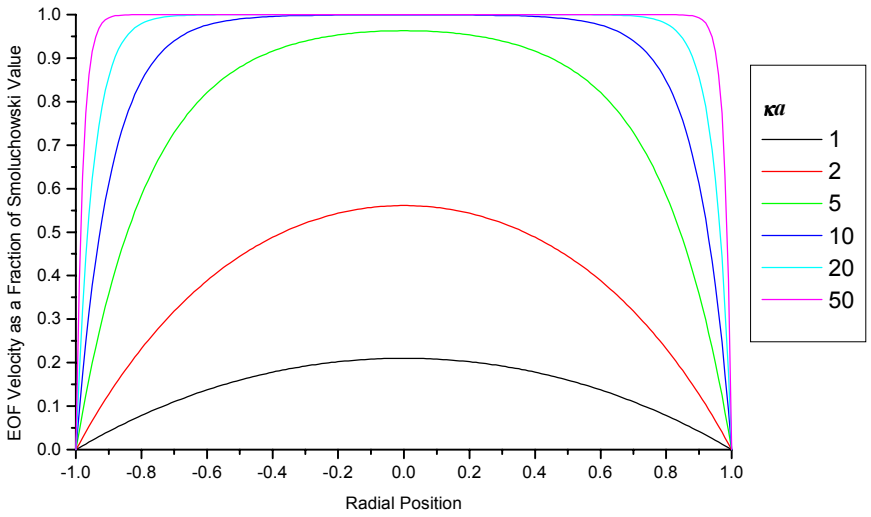

Figure 2.6. Variation in fluid flow velocity across the diameter of a cylindrical capillary as a fraction of the maximum velocity under EOF conditions.

Knox and Grant suggested that EOF velocity is acceptable when $\kappa a > 5$. In the case of columns packed with small particles this means that a significant loss in EOF rate will be found only when the particle diameter is less than forty times the double layer

thickness, δ [11]. For 50 mM and 5 mM aqueous electrolyte solutions this fixes the minimum particle size at 55 nm and 170 nm, respectively, much smaller than the particles currently used in HPLC.

2.3. Effects Arising from the Use of Electroosmotic Flow

When an electrical potential gradient is applied across a chromatographic column to produce EOF, charged molecules, as well as being swept through the column by EOF, will be attracted to the oppositely charged electrode. This attractive force will result in a velocity towards the appropriate electrode that is superimposed onto the EOF velocity. This superimposed velocity is given by Equation 2.8,

$$\mu_E = \frac{qE}{6\pi\eta r_h} \qquad \text{Equation 2.8}$$

where μ_E is the steady state velocity, q is the charge on the molecule, E is the field gradient, and r_h is the hydrodynamic radius of the molecule. The superimposed velocity is proportional to charge and inversely proportional to size, and is illustrated diagrammatically in Figure 2.7. Essentially, larger ions will experience more drag and hence will move more slowly than smaller ions.

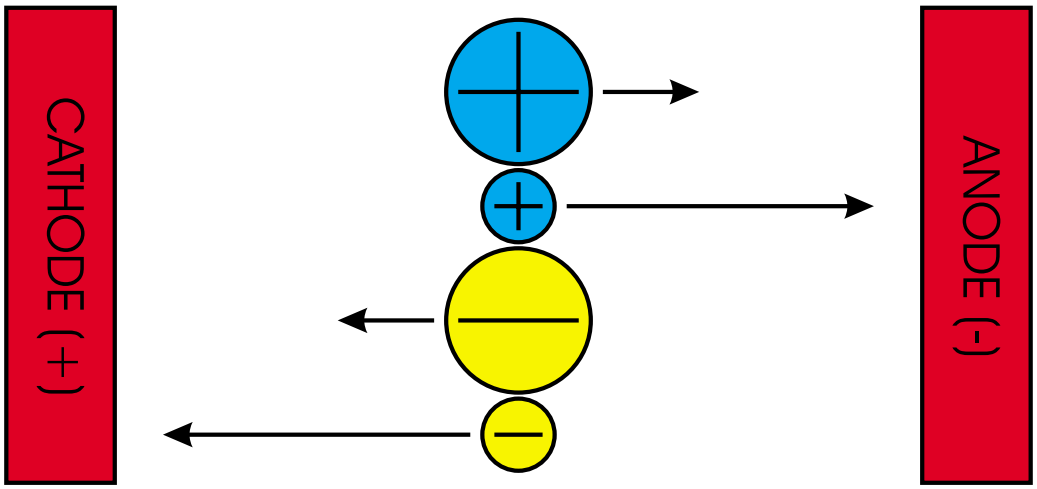

Figure 2.7. Simple representation of electrophoresis for molecules differing in size and charge. The arrow size indicates the steady state velocity obtained.

This form of separation is known as electrophoresis and is superimposed onto EOF, as is represented in Figure 2.8. This figure shows the relative position of a group of

cations, anions and neutrals after a short time under the influence of both electrophoresis and EOF. Initially all molecules were at the green line. Figure 2.8 shows the situation after EOF has caused labelled mobile phase to reach the blue line. Flow is from the cathode to the anode because the surface is negatively charged. Molecules of varying sizes are carried forward by the bulk flow, while ions either outpace or fall behind the bulk flow. Electrophoresis, for the negatively charged surface case, will give small anions a larger velocity towards the cathode than large anions of like charge, meaning that small anions will fall further behind the bulk flow than large anions. Similarly, small cations will outpace larger cations of like charge, all outpacing the bulk flow. The combination of electrophoresis and EOF results in CE. The addition of a chromatographic stationary phase results in CEC.

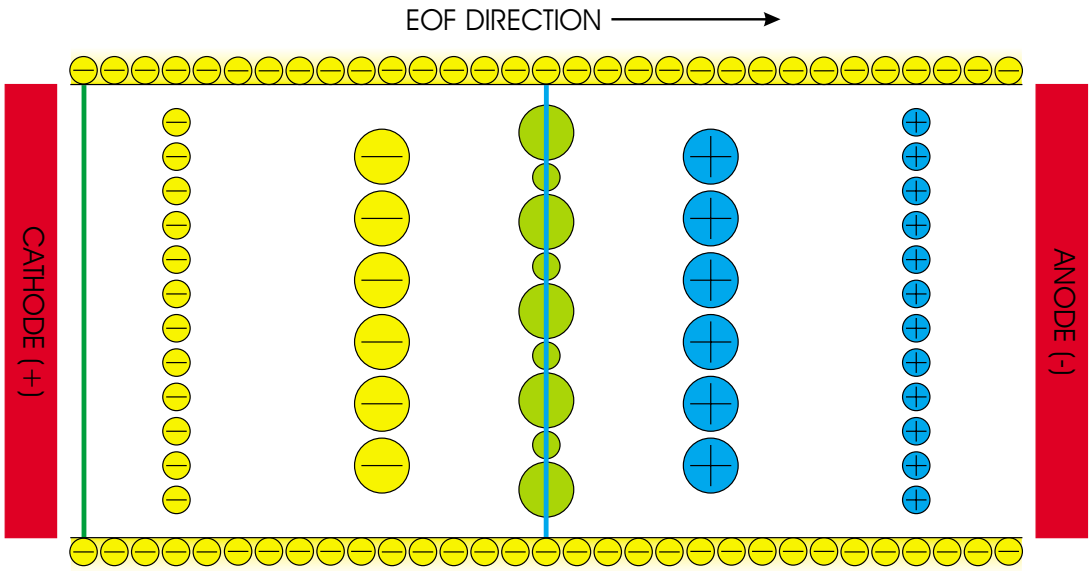

Figure 2.8. Diagrammatic representation of an electrophoretic separation superimposed onto an electroosmotic system.

The combination of electrophoresis and EOF utilised in CE has the advantage over electrophoresis alone in that cations and anions can both be analysed in the same run, although neutrals are not separated. The addition of a chromatographic stationary phase also allows neutrals to be separated. In both CE and CEC, analytes start at one end of the column and all but the most highly charged small anions (negatively charged surface case) will eventually reach the other end, allowing detection simply by monitoring species passing a particular point. This makes automation much simpler than in techniques such as gel electrophoresis (a type of electrophoresis carried out in porous

gels that do not support EOF), where the whole separation medium must be investigated for analyte bands.

Whereas electrophoresis is usually regarded as a beneficial side effect of EOF, resistive heating is an important problem. When EOF is used to drive mobile phase through a chromatographic column, current flows and heat are generated. EOF is directly responsible for very little of this current, the majority being due to the conductivity of the column. The centre of the column will become hotter than areas closer to the wall resulting in temperature gradients that in CE result in convection currents, which will degrade the separation. In CEC the presence of stationary phase support particles will suppress convection to a degree, but will still result in some degradation of separation efficiency. Parabolic temperature variation across the column will result in a parabolic velocity profile superimposed on the flat EOF velocity profile due to changes in viscosity with temperature [13]. Heating can also result in the formation of gas bubbles that can block the column, destroying the separation and necessitating the refilling of the column with fresh mobile phase. To avoid difficulties caused by heating, dilute or poorly conductive electrolytes and narrow capillaries (to allow heat to dissipate into the environment) must be used.

A further effect arising from the use of EOF originates from the necessary presence of a charged surface. This surface is prone to strong interactions with certain analytes, forcing manufacturers of HPLC stationary phases to attempt to cap charged surface groups. These attempts, while unable to remove all charges, are sufficient to significantly reduce EOF, making some modern HPLC stationary phases unsuitable for CEC. This has resulted in the development of stationary phases that contain charged groups for the purpose of supporting EOF.

2.4. Optimisation of Chromatographic Performance

Most chromatographic separations start with a number of solutes being present in the same localised area, whether this is a spot on a TLC plate or an injected band in HPLC. To achieve an effective separation, these solutes must migrate through the chromatographic medium at sufficiently differing rates so that they no longer overlap. The phase capacity ratio, k', is a measure of the degree of retention of a solute in a particular system, and can be defined as the ratio of the amount of solute in the

stationary phase to the amount in the mobile phase. Naturally, therefore, k' also equals the ratio of the time spent by a solute in the stationary phase to the time spent in the mobile phase, which is especially useful in systems where the time taken for solutes to pass through the chromatographic medium is measured. These relationships are expressed mathematically in Equation 2.9,

$$k' = \frac{C_s V_s}{C_m V_m} = \frac{t_s}{t_m} = \frac{t_r - t_m}{t_m} \qquad \text{Equation 2.9}$$

where C_s is the concentration of the solute in the stationary phase and V_s is the volume of the stationary phase. Likewise, C_m is the concentration of the solute in the mobile phase and V_m is the volume of the mobile phase. In the next part of the expression, t_s represents the time spent by a solute in the stationary phase, while t_m represents the time spent in the mobile phase. The sum of t_s and t_m is the total time spent in the system, better known in column chromatography as the retention time, t_r. This is the elapsed time between injection and the peak maximum of the chromatographic band of interest passing the detector. Values of between 1 and 10 for k' are usually deemed to be acceptable [25], with lower values indicating a reduced likelihood of achieving a separation and higher values indicating excessively long analysis times.

While differences in migration rate are naturally essential if the detection method cannot distinguish between different solutes, control of band spreading is also important. Analyte bands start with a certain width and then spread as they pass through a system, resulting in bands that cannot be resolved if their migration rates are not sufficiently different. Successful chromatography is therefore a balance between migration rate differences and control of band spreading. The latter tends to be most important in circumstances where separation of a large number of analytes is required. In a chromatogram that contains a large number of peaks, obtaining narrow peaks is essential. Altering relative migration rates in this case will simply rearrange the peaks.

2.4.1. The Role of the Plate Model in Quantification of Band Spreading

Band spreading is quantified by comparing peak width with retention time. By far the most successful of the early attempts to explain the processes leading to band dispersion

was reported by Martin and Synge in 1941 [26]. Their plate model assumes that a chromatographic column can be represented by a series of mixing cells, the plates. The term 'plates' is used because this theoretical description of the chromatographic process originates from concepts developed for distillation. Aliquots of mobile phase can be added to and removed from the cells, while stationary phase does not leave the cells. Equilibrium of solutes between the phases in the cell is achieved within a small, but finite, period of time. Partition of solutes between the phases is assumed to be concentration independent. Flow of mobile phase through the column is represented by all mobile phase being removed from the final cell and replaced with the mobile phase from the penultimate cell. Simultaneously, mobile phase from the cell previous to the penultimate cell is moved to the penultimate cell, and so on, simultaneously, right back to the first cell being filled with fresh mobile phase. This movement of mobile phase along the series of mixing cells is instantaneous, with rounds of movement being separated by the equilibration time. A greater number of mixing cells will result in a greater probability of the desired separation being achieved, but will require more time. A single step in the process is illustrated in Figure 2.9.

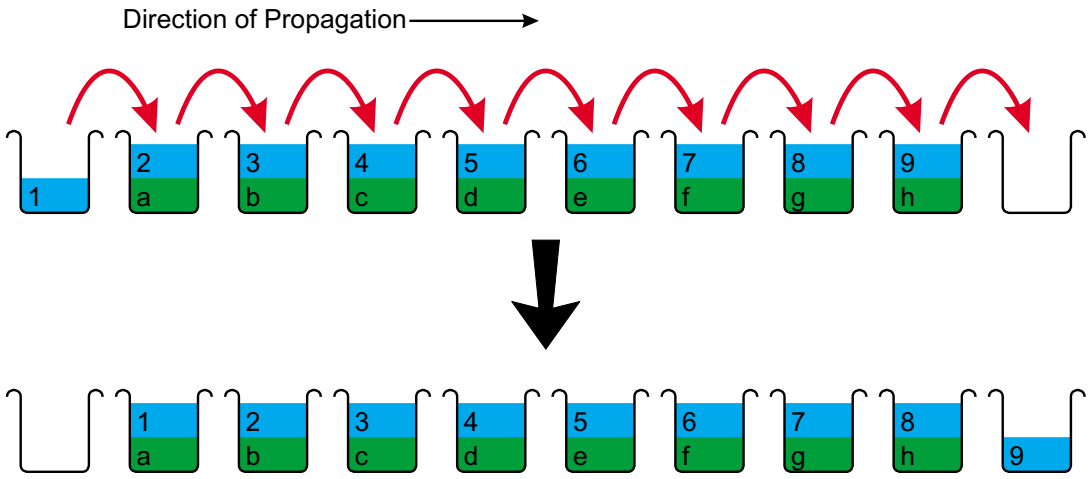

Figure 2.9. Representation of the plate model. Beakers containing stationary phase (coloured green and labelled a to h) represent the mixing cells (plates). Aliquots of mobile phase (coloured blue and labelled 1 to 9) move along the series as indicated, while stationary phase does not leave the cells.

Injection of a sample onto the column is represented by adding a mixture of analytes dissolved in mobile phase to the first cell, instead of fresh mobile phase. Over a number of rounds of movement, as mobile phase advances though the series of cells, separation

may be achieved by means of different analytes moving through the series of mixing cells at differing rates. The important characteristics of the system are therefore the size and number of mixing cells along with the time required for achieving equilibrium. In this model, equilibration time is assumed to be constant regardless of cell size. When considering chromatographic columns, cell size and the number of cells must naturally be linked to the size of the column. Under certain conditions there will be more cells than under other conditions. For example, raising flow rate, with equilibration time fixed, will demand larger cells. This will lower the total number of cells and hence the effectiveness of the separation, but the amount of time required for separation will be reduced. It must be remembered that performance indicators are related to a particular column, mobile phase, flow rate, analyte, etc. Results for one set of conditions may of course, however, be used as a guide to what might be expected under different but related conditions.

Since most chromatographic columns have constant cross-sectional area along their length, cell size is replaced by cell length. Since this theory was developed at a time when columns were typically mounted vertically, using gravity to drive mobile phase through the column, cell length is replaced with *H*, the plate height (or alternatively the height equivalent to a theoretical plate). The number of plates, *N*, is now naturally related to the plate height by the distance migrated by the centre of the band, *L*. This is equivalent to the distance migrated by a spot in TLC, but in elution chromatography, it is the length of the column. Since in early chromatographic systems detection was performed simply by viewing the progress of coloured bands, migration distance could easily be related to band width in length units. With elution chromatography it is equivalent to compare retention time to peak width in time units.

2.4.2. Obtaining Plate Model Characteristics from Experimental Data

As mentioned above, in plate theory, an analyte band starts entirely within the first plate. On being washed through a small number of plates, a highly discontinuous concentration profile is obtained, with solute being distributed between plates according to the Poisson distribution. After fifty plates much of the abrupt discontinuity is gone, with neighbouring plates having fairy similar concentrations. However, concentration profile is still governed by the Poisson distribution. At a later stage, usually when the

band centre has migrated through around a hundred plates, the concentration profile is reasonably smooth and continuous. Although still Poisson, the concentration profile can now be approximated by a Gaussian curve (sometimes termed a normal distribution curve). Plate theory states that the standard deviation of the Gaussian curve, σ, is equal to the square root of the product of the plate height, H, and the distance migrated by the centre of the band, L, as defined in Equation 2.10. Although the discontinuous nature of the early part of the separation is clearly a failure of the plate model, other theories of band spreading also predict that the eventual concentration profile will be approximately Gaussian, making this a useful prediction of the plate model.

$$\sigma = \sqrt{HL} \qquad \text{Equation 2.10}$$

The shape of a Gaussian curve, shown as a black line, is illustrated in Figure 2.10. The mathematical form is defined by the expression in Equation 2.11. In this expression the constant, μ, refers to the mean of the curve, with the curve being symmetrical about μ. Viewing the curve as a chromatographic peak, peak widths at various proportions of peak height can easily be calculated as multiples of σ, allowing measurements taken from experimental data to be used to determine plate model characteristics. Perhaps the two most important peak widths are the half height width, $w_{1/2}$, equal to $2\sigma\sqrt{2\ln 2}$ (2.35σ), and the 10% height width, $w_{10\%}$, equal to $2\sigma\sqrt{2\ln 10}$ (4.29σ).

$$y = \left(\frac{1}{\sigma\sqrt{2\pi}}\right)\exp\left(-\left(\frac{(x-\mu)^2}{2\sigma^2}\right)\right) \qquad \text{Equation 2.11}$$

With columns of fixed length, rather than use Equation 2.10, it is more common to produce an expression in terms of plate number, N, as shown in Equation 2.12. This expression is then easily modified from length to time units, allowing t_r to replace L, as shown in Equation 2.13. Naturally, σ must be expressed in the appropriate units.

$$N = \left(\frac{L}{H}\right) = \left(\frac{L}{\sigma}\right)^2 \qquad \text{Equation 2.12}$$

$$N = \left(\frac{t_r}{\sigma} \right)$$ Equation 2.13

When dealing with chromatographic peaks that approximate Gaussian curves it is normally better to measure the base width of the peak, w_b, in order to obtain the standard deviation of the peak. Base width is obtained by drawing tangents to the curve though the inflection points to either side of the apex of the curve, and is defined as the distance between the points at which these tangents intersect the horizontal axis. This is illustrated graphically in Figure 2.10. From Equation 2.11 it can be shown that $w_b = 4\sigma$.

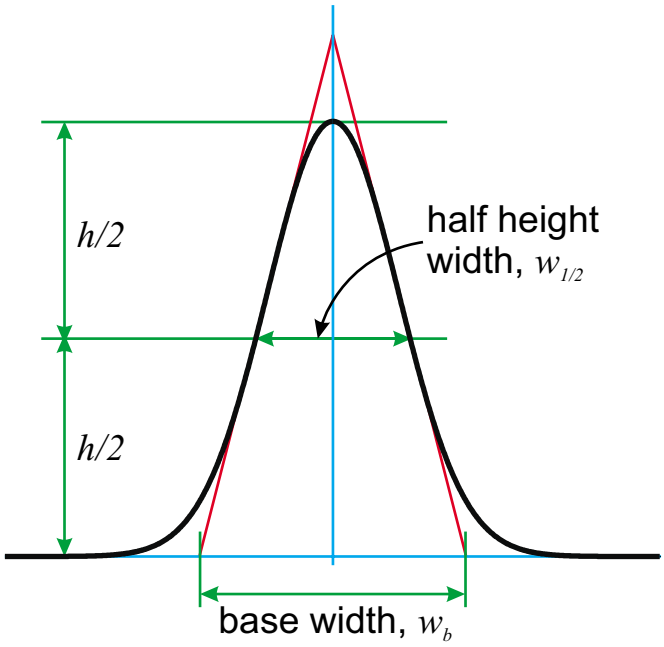

Figure 2.10. Graphical description of the definition of base width for a Gaussian shaped peak. Tangents to the curve (red lines) are drawn through the inflection points to either side of the apex. The distance between the points at which these tangents intersect the horizontal axis is the base width of the peak, which is equal to four times the standard deviation of the Gaussian curve.

Base width is easy to measure provided that the peak is symmetrical and the baseline is level, with a noisy baseline merely reducing the accuracy of a measurement. An expression for the efficiency of the separation in terms of plate number and base width is readily obtained from Equation 2.13 and is given below.

$$N = 16\left(\frac{t_r}{w_b}\right)^2 \qquad \text{Equation 2.14}$$

Asymmetrical peaks, however, will make accurate measurement of w_b difficult. The half height width, $w_{1/2}$, also defined in Figure 2.10, provides an alternative measurement that can also be related to σ, as mentioned above. The half height width is commonly used because asymmetry has a much less pronounced effect towards the apex of the peak, and has been used extensively in this work to calculate efficiencies as plate numbers. The expression for calculating the plate number using $w_{1/2}$ is given in Equation 2.15.

$$N = 8\ln 2\left(\frac{t_r}{w_{1/2}}\right)^2 = 5.545\left(\frac{t_r}{w_{1/2}}\right)^2 \qquad \text{Equation 2.15}$$

Although plate numbers are widely quoted, an advantage of plate height is that it is independent of the column length, making comparisons between columns of differing lengths easier. An alternative way to aid comparison is to give the number of plates per metre of column. Hence a separation performed on a column of length 0.5 m with an efficiency of 100,000 plates could be described either as having an efficiency of 200,000 plates per metre or as having a plate height of 5 μm.

2.4.3. The Identification of the Processes Leading to Band Spreading

The theoretical plate model, introduced into chromatography because of its effectiveness in describing distillation procedures, suffers from a near total failure to describe the physical and molecular events occurring in chromatography. For example, consecutive, but isolated, mixing cells clearly cannot describe the effect of molecular diffusion on chromatographic efficiency. The theory would seem to state that slowing down the separation would increase N, while in reality diffusion at very low flow rates would reduce the effectiveness of the separation. The description of chromatographic peaks in terms of Gaussian curves, and hence H as defined in Equation 2.10, means that plate theory terminology is in widespread use. This is probably due to their ease of extraction from experimental data.

Since the plate model is only loosely related to the real physical processes that occur in the column, it is of little use as a basis for work focused on improving performance. The contribution of van Deemter *et al.* was to produce an equation, which indicated that the processes leading to band broadening could be considered to be both independent and random, and hence could be added together. Their original work was published in 1956 [27], while the final version was presented at an informal symposium of the Gas Chromatography Discussion Group in 1957 [28]. This final version is reproduced elsewhere [29]. Their approach was designed for the then new technique of gas liquid chromatography (GLC), which is GC where an inert support medium is coated with a liquid that acts as the stationary phase. The equation they produced is now found in many textbooks [25,30,31], and is given in Equation 2.16.

$$H = A + \left(\frac{B}{u}\right) + C_m u + C_s u \qquad \text{Equation 2.16}$$

where

$$A = 2\lambda d_p$$

$$B = 2\gamma D_m$$

$$C_m = \left(\frac{1}{100}\right)\left(\frac{k'}{1+k'}\right)^2\left(\frac{d_p^2}{D_m}\right)$$

$$C_s = \left(\frac{2}{3}\right)\left(\frac{k'}{(1+k')^2}\right)\left(\frac{d_f^2}{D_s}\right)$$

This expression is given in terms of H and the mobile phase liner velocity, $u = (L/t_r)$. A, B, C_m and C_s are constants each made up of a number of other constants as defined above and explained in more detail below. The general form of Equation 2.16, the underlying physical processes, and the identity of the constants have been the subject of considerable debate. In the following sections, the identities of these terms will be explained, but a full mathematical treatment will be avoided. By fitting experimental data to their expression, van Deemter *et al.* attempted to identify which processes were most significant for the purpose of determining where development work could most profitably be focused. Their expression and the reasoning behind it have been improved on many occasions, but the general concept has survived. A careful mathematical treatment of the origin of this expression and numerous improvements are given in

Giddings' book [32]. Supplementary to this are a number of review papers, with the explanation offered by Grushka *et al.* being particularly straightforward [33].

(1) The van Deemter *A* Term

Flow through a packed bed, under laminar flow conditions, can be regarded as being divided into streams that follow different paths through the bed. These streamlines can be envisaged as having to follow tortuous paths around particles or, in contrast, flowing directly between particles for some distance. Solutes caught up in one stream will move through the packed bed at different rates to solutes in other streams, naturally leading to band broadening. The complex array of streams, following different routes and moving at different speeds, would be very difficult to model even today, but it is clear that a more uniform packed bed will reduce variation. The A term contribution to H will be reduced by packing columns with smaller particles, with d_p in Equation 2.16 referring to packing particle diameter, and λ being a geometrical factor that represents the quality of packing. As this contribution to H was assumed to only be dependent on packing geometry, it was deemed to have no dependence on u.

The advantages of using EOF to drive mobile phase through the column are clearly demonstrated by this term. EOF allows the use of much smaller particles since there is no maximum pressure limit, and the flat flow profile generated reduces the variation between streams. In a pressure drive system, streams that follow paths in spaces between particles will suffer little friction and hence will progress rapidly, whereas streams close to particles will endure greater frictional drag and hence will progress more slowly. Using EOF, flow rate will be close to constant across a gap between particles, although this will of course break down in narrow pores as explained above. It is clear that utilisation of EOF will significantly diminish A term dispersion.

(2) The van Deemter *B* Term

The B term is concerned with the effect of molecular diffusion. Since the sample is introduced to the column as a narrow plug, concentration gradients are set up that result in axial spreading of the band. The degree of spreading is proportional to the diffusion coefficient of the solute in the mobile phase, D_m, and also to the time spent in the column. Dependence on time spent in the column is represented by an inverse proportionality to u, while a geometrical factor, γ, is introduced to represent the

retarding effect on diffusion of the presence of the support particles. Although D_m is smaller for a liquid mobile phase than for a gaseous mobile phase, *B* term dispersion is still important in LC. Utilisation of EOF will confer no advantage over pressurised flow in limiting such dispersion, but may prove to be a disadvantage if the use of a highly conductive buffer forces low potentials to be applied, and hence low flow rates to be obtained.

(3) The van Deemter *C* Terms, C_m and C_s

C term dispersion is attributed to slow mass transfer, with C_m referring to slow mass transfer in the mobile phase and C_s referring to slow mass transfer in the stationary phase and between the phases. These terms are sometimes bundled together as they are both proportional to *u*, but are better treated separately. The C_m term is proportional to the square of the fractional time spent by the solute in the stationary phase $((k'/(1 + k'))^2)$, d_p^2, and *u*, while being inversely proportional to D_m. This term represents resistance to solute movement between the streams that are described above with relation to the *A* term. If solutes always remained in the same stream, bands would become very wide, with some solute molecules barely moving at all. Rapid diffusion between streams helps to reduce the variance in time taken for solutes to pass through the column.

In contrast, the C_s term describes the contribution of slow mass transfer between the mobile and stationary phases and within the stationary phase. It is proportional to the product of the fractional time spent by a solute in the mobile phase with that spent in the stationary phase $((k'/(1 + k')^2))$, along with *u* and d_f, the GLC film thickness, while being inversely proportional to the diffusion constant of the solute in the stationary phase, D_s. The effect of the C_s term can be thought of by considering solutes making their way through a column. If one solute enters the stationary phase, another solute that remains in the mobile phase will move ahead on the now stationary solute. This naturally leads to broadening that is proportional to *u*. Control of such processes is often regarded as the region of chromatographic performance where there is least room for improvement. Other expressions have been added under the umbrella of the C term, for example a term covering mass transfer into and out of pockets of stagnant mobile phase, such as those that would be found in pores in the silica support particles. The traditionally

assumed relative importance of these terms is illustrated in Figure 2.11 [25]. It can be clearly seen that there is an optimum value of u where H is minimised.

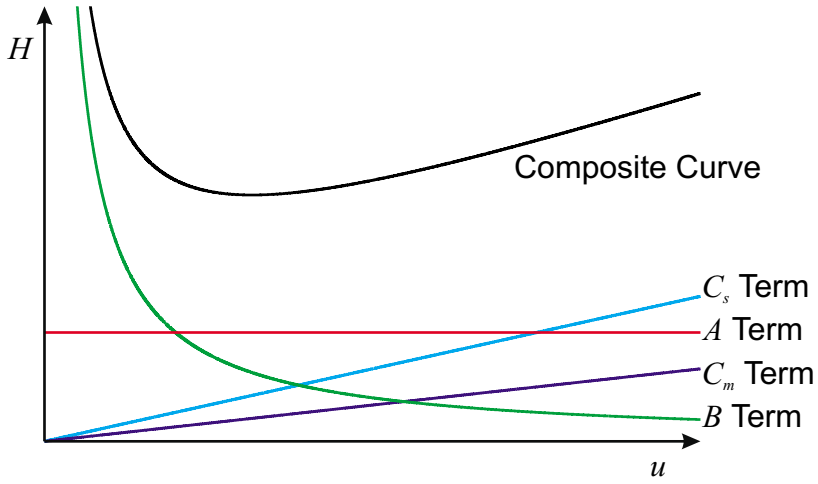

Figure 2.11. Relative importance of the components of the van Deemter equation.

(4) Improvements to the van Deemter Equation

Once the van Deemter equation was widely known, investigators began to try to fit it to their data with the aim of determining where best to focus their attentions to improve their data. Giddings proposed that the A and C_m terms were not independent, and that coupling these terms resulted in a better fit to the experimental data [32], leading to the modified expression that is given as Equation 2.17. It seems reasonable to assume that diffusion between streamlines and the geometrical pattern of these streamlines should be linked.

$$H = (B/u) + C_s u + \frac{1}{(1/A) + (1/C_m u)} \qquad \text{Equation 2.17}$$

Many corrections and improvements have been made to this treatment of the processes leading to band dispersion. Knox, in a recent paper [34], showed that the best fit of the experimental data is now regarded to be given by an expression of the form given in Equation 2.18.

$$h = \left(\frac{B}{v}\right) + \left[\left(\frac{1}{A}\right) + \left(\frac{1}{Dv^n}\right)\right]^{-1} + Cv \qquad \text{Equation 2.18}$$

In this expression, n is typically in the region of 0.5, H has been replaced with $h = H/d_p$, and u has been replaced by $v = ud_p/D_m$. The parameter h is referred to as the reduced plate height and v is referred to as the reduced velocity. These substitutions are made to allow easier comparison of differing chromatographic systems, with Knox and Saleem having shown that when differing diffusion constants are taken into account, the treatment of van Deemter *et al.* can be applied to most chromatographic techniques [35]. The new D term in Equation 2.18 is similar to the previously introduced C_m term. The relative importance of the terms as accepted today is shown in Figure 2.12, with the D term and the A term plotted together. This new treatment has shown that nearly all dispersion previously assigned to processes in the static zone actually occurs in the mobile zone. Substantial improvements in chromatographic performance would therefore seem to be available through being better able to pack columns, by being able to use smaller particles and by using EOF to provide a constant flow velocity across a channel diameter. There seems ample scope for CEC to deliver chromatographic efficiencies not available with any other chromatographic technique. The greatest advances in reducing A term dispersion would be likely to come from using perfectly regular packed beds such as those that could be produced by photolithography.

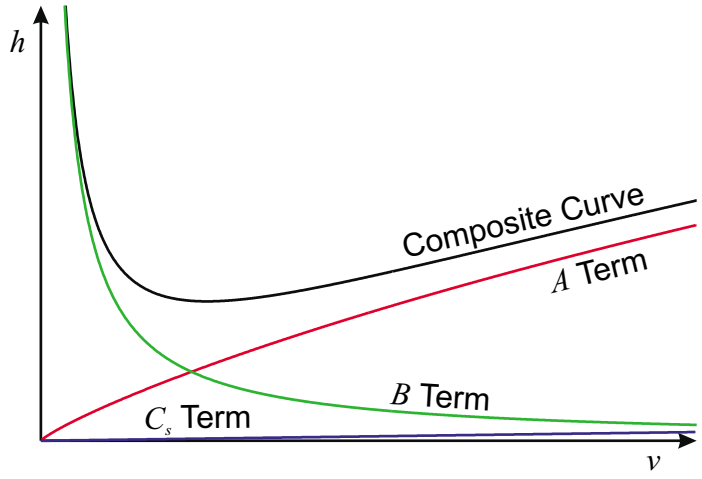

Figure 2.12. Terms contributing to band dispersion as set out in Equation 2.18.

2.4.4. Other Performance Indicators

(1) Resolution

A measure of chromatographic performance that is not linked to plate theory is resolution. This can be calculated by dividing the difference between the retention times

of two peaks by their average base width, as shown in Equation 2.19. Obtaining a resolution of unity is usually defined as an acceptable standard, with resolutions greater than one being wasteful and resolutions less than one being inefficient. It must be remembered of course that a resolution of unity does not mean baseline resolution.

$$R = \frac{t_{r,2} - t_{r,1}}{0.5\left(w_{b,1} + w_{b,2}\right)} \qquad \text{Equation 2.19}$$

(2) Peak Asymmetry Factor

Peak asymmetry is often a valuable indicator of chromatographic problems, and is usually measured by comparing the forward half width of the peak with the rearward half width of the peak at 10% of peak height. These quantities, *a* and *b* respectively, are illustrated in Figure 2.13. By convention the rearward width is divided by the forward width, with asymmetry factors greater than one indicating tailing and those less than one indicating fronting. Tailing tends to be caused by adsorption of analytes to the stationary phase, while fronting usually results from overloading the column. Asymmetry makes parameters such as plate numbers meaningless, as plate theory assumes Gaussian peaks, but plate numbers are often calculated for moderately tailing peaks.

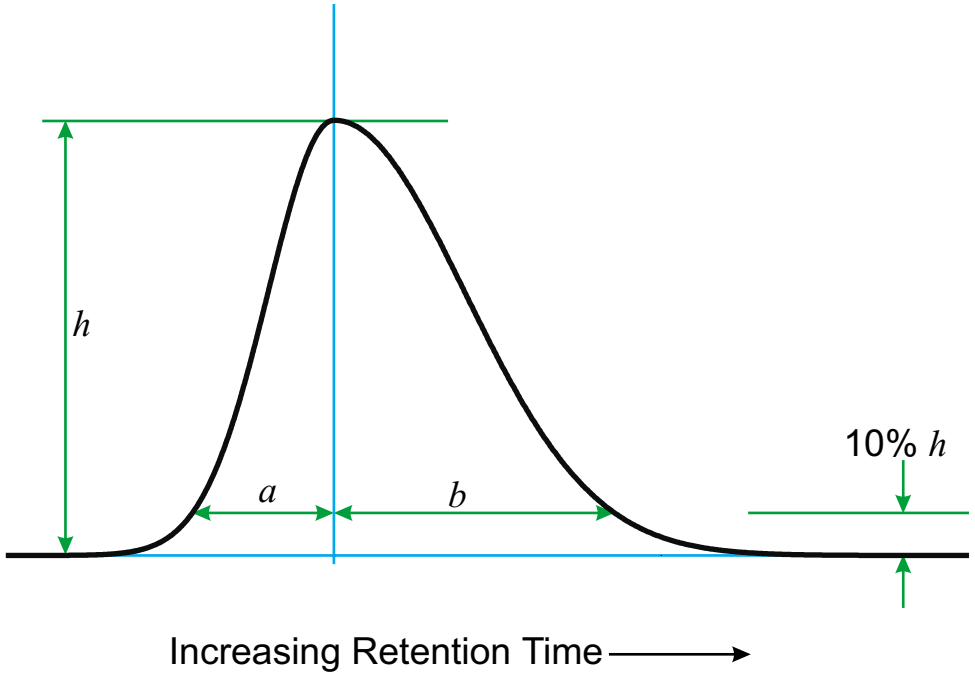

Figure 2.13. Illustration of the measurements necessary for the calculation of the peak asymmetry factor.

(3) Peak Capacity

A further way of describing chromatographic efficiency is via peak capacity, which is designed to give an improved idea of the ability of a chromatographic system to provide the answer to an analytical problem. Peak capacity, a term first described by Giddings [36], has been related to conventional chromatographic parameters by Grushka [37], and is simply the maximum number of peaks that will fit into a chromatogram with a resolution of unity between consecutive peaks. Peak capacity, C_P, is defined in terms of plate number, N, retention time, t_r, and the retention time of an unretained component, t_m, as shown in Equation 2.20. The retention time of an unretained component needs to be included because it is not possible for peaks to be found before mobile phase has made its way through the column. Further to this, Davis and Giddings calculated that to adequately resolve 90% of the components of a mixture, the peak capacity of the separation must be 19.0 times larger than the number of components [38]. Therefore, a chromatogram must be approximately 95% vacant to provide a 90% probability that a given compound of interest will appear as an isolated peak.

$$C_P = 1 + \frac{\sqrt{N}}{4} \ln \frac{t_r}{t_m} \qquad \text{Equation 2.20}$$

Horváth *et al.* demonstrated that it was possible to approximately double peak capacity by narrowing peaks using gradient elution in LC or by using temperature programming in GC [39]. Temperature programmed open tubular GC is capable of providing peak capacities in the region of 1,000, while utilisation of gradient elution in HPLC is capable of providing peak capacities in the region of 200 [40]. This allows the GC method to resolve approximately 50 components, still retaining a 90% chance of the compound of interest appearing, while the equivalent number for gradient elution in HPLC is in the region of 10. CEC offers the promise of approaching the high peak capacities available with temperature programmed open tubular GC for a LC separation.

2.5. Practical Aspects of Performing CEC

The minimal instrumentation required to perform CEC is illustrated in Figure 2.14. The inlet of the column is dipped in the inlet reservoir, while the outlet is dipped in the outlet reservoir. The inlet reservoir is replaced with the sample reservoir when performing an injection. In more complicated systems, these reservoirs may be constructed so as to allow the system to be pressurised for the purpose of reducing the probability of bubble formation (see below). Another common upgrade is the automation of the injection process, and the supply of a sample carousel rather than a single sample reservoir. Automation would be expected to improve reproducibility.

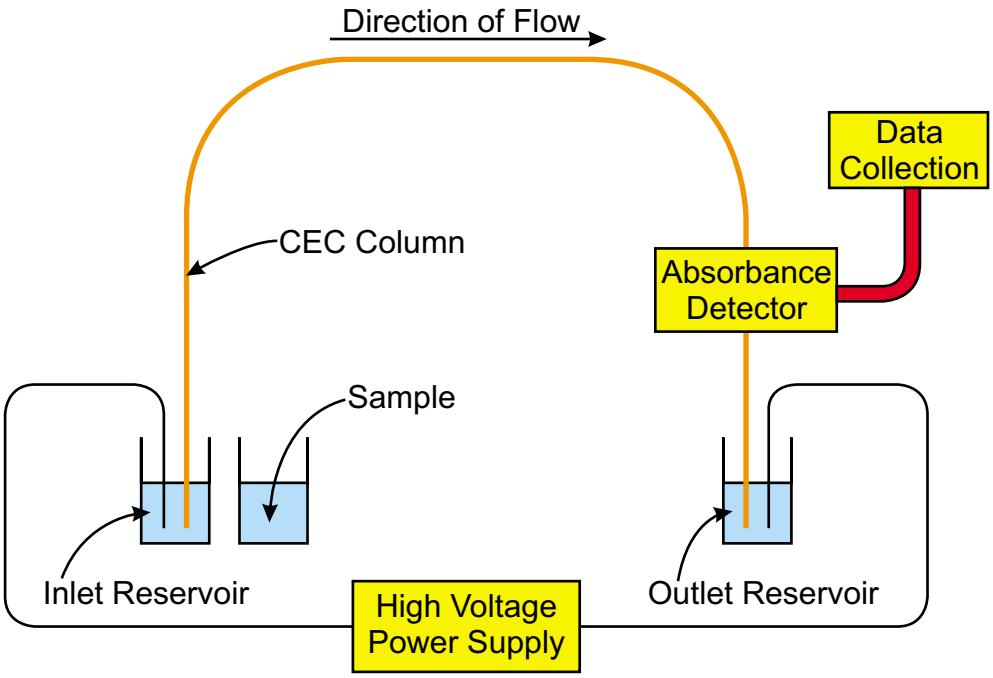

Figure 2.14. Schematic representation of the essential components of an instrument designed for performing CEC.

The high voltage power supply is used to apply an electrical potential between the inlet and outlet reservoirs. For normal operation, with anionic surfaces used to provide the EOF, a potential in the region of +30 kV will be applied to the inlet reservoir while the outlet reservoir will be held at electrical ground. Other configurations are possible, but rarely implemented. Injection is usually achieved by applying a potential of ~ +5 kV to the sample reservoir when it has been substituted for the inlet reservoir. The absorbance detector is placed close to the outlet and is connected to some form of data collection device. Additional to this, and not shown in Figure 2.14, is a high-pressure pump for initial filling of the column with degassed mobile phase. The essential components of an instrument designed for performing CE are identical to those for an instrument designed for performing CEC, with the only difference being that a syringe is sufficient for initial filling of the column. Additional injection strategies are available in CE, however, with more advanced instrumentation allowing injection by siphoning or by application of a vacuum to the outlet vial.

The production of the CEC columns used in this work is described in greater detail at the beginning of Chapter 4, but is summarised briefly here in order to describe the structure of the column. Good descriptions of column packing procedures, similar to

those used in this work, have been provided by Smith and Evans [41], by Boughtflower *et al.* [42,43], and by van den Bosch *et al.* [44]. To produce CEC columns, fused silica capillaries are packed with approximately spherical porous silica particles that are coated with the chromatographic stationary phase. The particles that were used in this work typically had diameters in the region of 3 μm. In order to maintain the integrity of the column, the particles must be retained in some manner, in this work through the production of sintered frits.

One method of producing such frits is to tap a small volume of porous silica particles, which have been moistened with sodium silicate solution, into the end of the capillary. This material is then sintered using a small flame or heating coil to manufacture retaining frits. Heating porous silica particles under pressure, with the pressure being produced by simultaneously flushing the column with water, can also be used for the production of frits [41]. Fused silica is used as tubing both because it can withstand the heating required for the production of frits, but also because it is transparent to UV light, allowing on-column detection. Fused silica capillaries are coated with polymeric materials for protection, which must be removed in order to produce a window for absorbance detection.

A typical CEC column is shown schematically in Figure 2.15, with the configuration being a packed section of capillary, where the separation occurs, followed by an open section of capillary beginning at the absorbance detection window. The packed section of capillary is bounded by retaining frits, and since it is not transparent, forces detection to be performed after the separation medium. Such a column can be mounted in the apparatus illustrated in Figure 2.14.

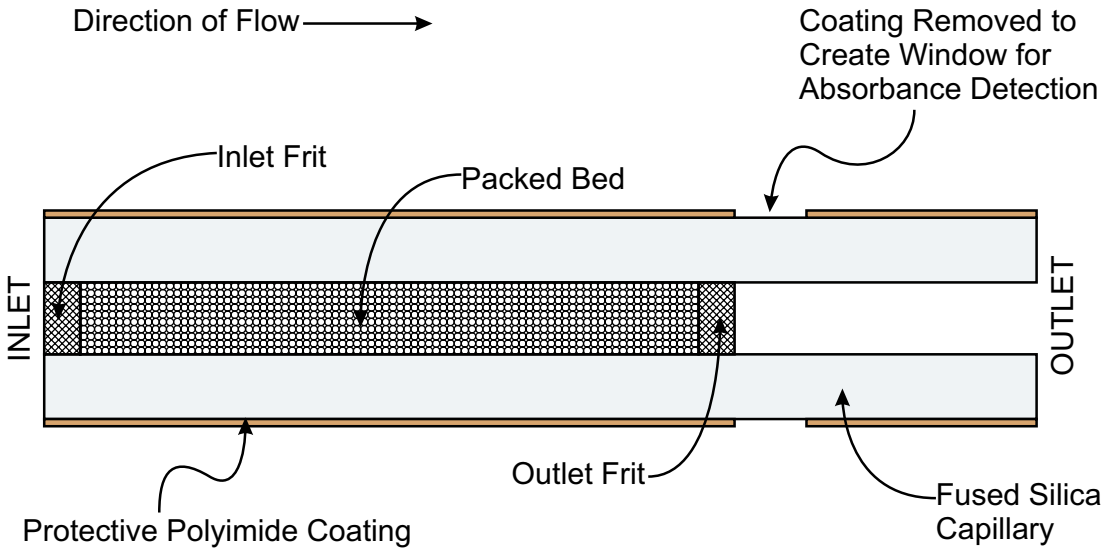

Figure 2.15. Schematic representation of a packed capillary prepared for use as a CEC column.

The most important practical problem in performing CEC is bubble formation, which has recently been the subject of a paper by Carney *et al.* [45]. This problem is regarded as so serious that pressurisation of entire systems has been implemented, increasing instrumental complexity [41,46,47]. When a bubble forms in CE, data is lost, but the column can quickly be flushed and returned to analytical use. Many CE instruments also have the option of programming periodic column flushes to improve reliability, the flushing process being fully automated. In CEC, however, column flushing requires a high-pressure pump to be attached to the column for relatively long periods of time. This process involves a significant risk of damaging the column, with automation being difficult but desirable. Bubble formation can be due purely to heating as detailed by Knox [13], but is more likely to be due to column structures such as retaining frits. Tsuda was first to report bubble formation in electrochromatography, but the relatively large columns utilised meant that this was probably due mostly to heating [48]. Rebscher and Pyell performed experiments, which precluded heating effects, showing that retaining frits were a major cause of bubble formation [49]. Furthermore, van den Bosch *et al.* concluded that bubble formation was most significant when frits were used that differed in their composition from the rest of the packing material, also suggesting that stringent degassing of mobile phases was essential for reliable operation [44]. More recently, the effect of frits on the separation process has been imaged

[50,51]. In this work, permanent frits were constructed out of the packing material, as described by Smith and Evans [41].

2.6. Alternatives to Sintered Frits

As mentioned in the previous section, retaining frits are blamed for many of the problems associated with CEC. A number of alternative stationary phase retention methods have therefore been suggested, with the simplest method of reducing frit effects having been suggested first by Knox and Grant [12]. Briefly, since the stationary phase support particles are negatively charged they will be attracted to the anode. Since the anode is typically the inlet end of the column, there is no need to incorporate an outlet frit into the column, which would be expected to halve the incidence of frit effects, such as bubble formation. The absence of an exit frit, however, would be expected to reduce column stability, and would naturally require mobile phase to be pumped in from the outlet when flushing the column, a drawback when interfacing CEC to other techniques. Another method to reduce frit effects without dispensing with frits entirely is to recoat frits with stationary phase. The sintering process causes the stationary phase to be lost, and this is sometimes blamed for bubble formation. Improved performance with recoated frits has been reported by Carney *et al.* [45]. Some alternative retention strategies are detailed below.

2.6.1. Using Tapers for Retention of Stationary Phase

The concept of forming constrictions in fused silica capillaries for the purpose of retaining stationary phase was introduced to CEC by Lord *et al.* [52]. Capillaries can be pulled to produce doubly tapered constrictions such as that illustrated in Figure 2.16. Such structures can be broken to produce needles or can be strengthened with coaxial tubing and used as illustrated. A further type of constriction can be constructed by heating the capillary without pulling, resulting in what could be described as a double internal taper. This structure must then be split, with the new capillary termini ground to give internal tapers, which can be used as illustrated in Figure 2.17. Stationary phase particles are retained at the constriction by a keystone effect, with liquid flow through such structures having been shown to be adequate. Similar systems have been compared with conventional CEC columns, and found to be superior, by Mayer *et al.* [53]. In one system they tested, a conventional sintered frit was used at the inlet while a constriction,

similar to that illustrated in Figure 2.16, was used prior to the absorbance detection window. They also tested a system where the inlet was produced from a constriction that had been broken to produce a needle, while no outlet retaining structure was present, with the attraction of stationary phase particles to the anode relied upon to maintain the integrity of the column.

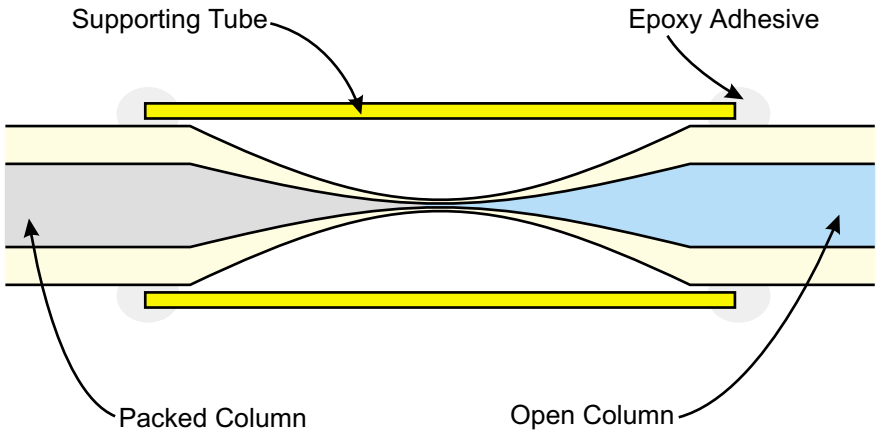

Figure 2.16. Capillary pulled to a double taper for the purpose of retaining stationary phase.

This work has been continued recently, with attention focused on internal taper capillaries [54]. Using heat-shrink tubing to produce capillary joints, structures such as that illustrated in Figure 2.17 have been constructed. The configuration shown would require an inlet frit, but by adding a constriction at the inlet to the unpacked capillary, and reversing the packed capillary, a reliable frit-free CEC system can be produced. Such systems, however, rely very heavily on the quality of the capillary joint, and the heat-shrink tubing forces the detection point away from the end of the packed bed, which is the ideal location.

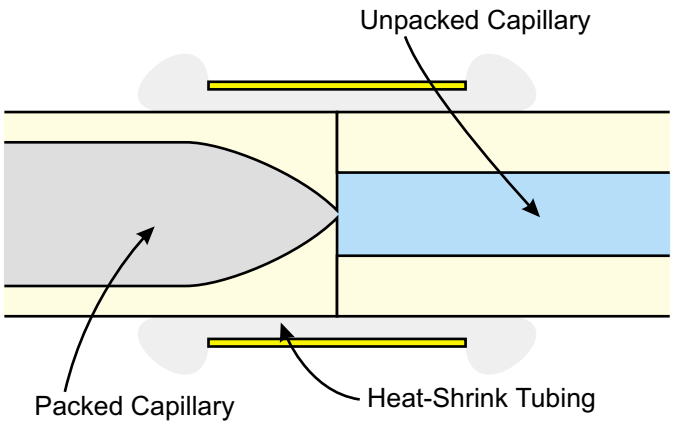

Figure 2.17. Capillary junction between a packed column terminated in an internal taper and an open capillary where absorbance detection is performed.

2.6.2. Polymeric Materials as Stationary Phase Supports

Instead of packing columns with silica particles that have been coated with the desired stationary phase, and hence necessitating the production of retaining structures, columns can be produced by filling capillaries with polymeric materials. One strategy is to fill the capillary with polyacrylamide gels, in which charged additives have been incorporated for the purpose of supporting EOF. Variation in polymerisation mixture has been shown to affect both pore size and analyte migration time, with separation of uncharged low molecular weight compounds having been demonstrated [55,56]. With these initial systems, however, a molecular sieving action was suspected to be the dominant separation mechanism. The same group then added additional components to their polymerisation mixture to achieve a separation more chromatographic in character [57]. This work also included imaging of mobile phase flow through the gel.

Peters *et al.* augmented this work with their report on the production of rigid polymeric monoliths for CEC [58]. Moving from gels to rigid structures allows pressure to be applied for the purpose of column flushing and the suppression of bubble formation. Their system also has a further significant advantage in that fabrication is a one step process. The relative proportions of the ingredients of the polymerisation mixture were again varied to obtain differing retention characteristics, pore sizes and EOF rates. This work was later extended by the same group, with the polymerisation mixtures having been improved [59,60]. Experience gained in polymeric stationary phases for HPLC, however, is not directly transferable to CEC due to the necessary addition of charged

groups required for EOF. Polymeric systems, however, are likely to provide the best chance for the use of CEC to be become widespread, as they offer the promise of columns that are genuinely robust since they do not contain fragile sintered frits. A final technique that has recently been reported involves the entrapment of conventional silica particles in a silicate matrix [61,62]. Columns are packed with normal frits, but following the entrapment process, these frits are removed. The resulting columns were shown to function well, although the stationary phase was damaged to some degree in the entrapment process.

2.6.3. Open Tubular CEC

In open tubular CEC, the stationary phase is simply bonded to the inner surface of the capillary to produce a column. One of the earliest reports of CEC was in fact of open tubular CEC [9], with the possibilities and challenges of the technique having been detailed by Bruin *et al.* [63]. Briefly, for optimum performance, column ID must be less than 10 μm. Such small dimensions are necessitated by the limited rates of mass transfer in LC. Small columns mean that detection cell volumes will be in the region of 100 pL, offering considerable challenges in detection sensitivity. Furthermore, sample capacity is small and the columns can easily become plugged. However, since most chromatographic efficiency is lost due to variation in the routes that a solute may take through the packed bed (see Figure 2.12), a column with only a single available route could offer very high separation efficiencies. For further information, open tubular CEC has recently been reviewed by Dittmann and Rozing [64].

A solution may be offered by using photolithography to produce very regular arrays of channels in silicon chips as reported by He *et al.* [65]. Very regular arrays of narrow interconnecting channels can be produced to offer an idealised chromatographic system. The use of silicon, however, requires that the surface be modified to support EOF in the usual manner. A multi-step process was used to provide the silanol groups necessary for EOF and to provide the stationary phase required for chromatography, while numerous channel configurations were investigated. Although production of single devices is obviously very expensive, mass production could make such instrumentation disposable.

2.7. Detection Strategies

Detection for CEC is, to a significant degree, similar to that in CE. Numerous detection strategies have been investigated, including optical [66] and electrochemical techniques [67]. UV absorbance is by far the most commonly used technique, with other optical and electrochemical techniques tending to be focused on specific problems. Absorbance detection works well due to its simplicity and close to universal response. On-column detection in CEC, however, suffers from a lack of sensitivity, although this is not as severe as that found in open tubular CEC since larger columns are typically used. The use of enlarged detection cells for CEC has been investigated by Paterson [68], but the increased complexity and the loss of chromatographic efficiency, due to poor junctions between column and cell, did not justify the slightly improved sensitivity reported.

An ideal detector for CEC would be universal, quantitative, reliable and sensitive. Mass spectrometry is a technique that is intrinsically close to universal, although the interfaces used to produce ions are often highly selective. It is also a technique that is quantitative, though the selectivity of the interfaces requires calibrations to be performed. The true strength of mass spectrometric detection, however, lies in it being essentially an orthogonal separation technique, which is also sensitive and which can also provide structural information. Of course, it is also possible to perform both mass spectrometric and absorbance detection, maximising the available data. Mass spectrometry can often provide enough information to identify an unknown, especially when tandem techniques are employed. In the following chapter the development of interfaces between chromatography and mass spectrometry is described in some detail, with special attention paid to those employed for CE/MS and CEC/MS.

---

[1] J. H. Knox (Editor), *High-Performance Liquid Chromatography*, Edinburgh University Press, Edinburgh, **1978**.

[2] J. E. MacNair, K. D. Patel and J. W. Jorgenson, *Anal. Chem.*, **1999**, *71*, 700-708.

[3] H. H. Strain, *J. Am. Chem. Soc.*, **1939**, *61*, 1292-1293.

[4] R. L. M. Synge, *Biochem. J.*, **1950**, *46*, xli-xlii.

[5] D. L. Mould and R. L. M. Synge, *Analyst*, **1952**, *77*, 964-969.

[6] D. L. Mould and R. L. M. Synge, *Biochem. J.*, **1954**, *58*, 571-585.

[7] V. Pretorius, B. J. Hopkins and J. D. Schieke, *J. Chromatogr.*, **1974**, *99*, 22-30.

[8] J. W. Jorgenson and K. D. Lukacs, *J. Chromatogr.*, **1981**, *218*, 209-216.

[9] T. Tsuda, K. Nomura and G. Nakagawa, *J. Chromatogr.*, **1982**, *248*, 241-247.

[10] T. S. Stevens and H. J. Cortez, *Anal. Chem.*, **1983**, *55*, 1365-1370.

[11] J. H. Knox and I. H. Grant, *Chromatographia*, **1987**, *24*, 135-143.

[12] J. H. Knox and I. H. Grant, *Chromatographia*, **1991**, *32*, 317-328.

[13] J. H. Knox, *Chromatographia*, **1988**, *26*, 329-337.

[14] I. S. Krull, R. L. Stevenson, K. Mistry and M. E. Swartz, *Capillary Electrochromatography and Pressurized Flow Capillary Electrochromatography, An Introduction*, HNB Publishing, New York, **2000**.

[15] K. D. Bartle and P. Myers (Editors), *Capillary Electrochromatography*, The Royal Society of Chemistry, Cambridge, UK, **2001**.

[16] F. A. Holland and R. Bragg, *Fluid Flow for Chemical Engineers*, Edward Arnold, London, **1995**.

[17] D. R. Lide (Editor), *CRC Handbook of Chemistry and Physics (Seventy Fourth Edition)*, CRC Press, Boca Raton, FL, **1993**.

[18] V. Pretorius and T. W. Smuts, *Anal. Chem.*, **1966**, *38*, 274-281.

[19] J. H. Knox, *J. Chromatogr. A*, **1999**, *831*, 3-15.

[20] V. L. Tal'roze, G. V. Karpov, I. G. Gorodetskii and V. E. Skurat, *Russ. J. Phys. Chem.*, **1968**, *42*, 1658-1664.

[21] I. H. Grant, *Electroosmosis and Electrochromatography in Narrow Bore Packed Capillaries*, PhD Thesis, University of Edinburgh, **1990**. Currently (December 2002) available from http://webex.lib.ed.ac.uk/homes/grant90.html

[22] D. J. Shaw, *Colloid & Surface Chemistry (Fourth Edition)*, Butterworth-Heinemann, Oxford, **1992**.

[23] M. Kosmulski, J. Hartikainen, E. Maczka, W. Janusz and J. B. Rosenholm, *Anal. Chem.*, **2002**, *74*, 253-256.

[24] C. L. Rice and R. Whitehead, *J. Phys. Chem.*, **1965**, *69*, 4017-4024.

[25] H. H. Willard, L. L. Merritt, Jr., J. A. Dean and F. A. Settle, Jr., *Instrumental Methods of Analysis (Seventh Edition)*, Wadsworth, Belmont, CA, **1988**.

[26] A. J. P. Martin and R. L. M. Synge, *Biochem. J.*, **1941**, *35*, 1358-1368.

[27] J. J. van Deemter, F. J. Zuiderweg and A. Klinkenberg, *Chem. Eng. Sci.*, **1956**, *5*, 271-289.

[28] J. J. van Deemter, paper presented at an informal symposium of the Gas Chromatography Discussion Group in Cambridge, UK, 4th October 1957 (see D. H. Desty, *Nature*, **1958**, *181*, 604).

[29] D. H. Desty, A. Goldup and B. H. F. Whyman, *J. Inst. Petrol.*, **1959**, *45*, 287-298.

[30] G. D. Christian, *Analytical Chemistry (Fifth Edition)*, John Wiley & Sons, New York, **1994**.

[31] R. Kellner, J. –M. Mermet, M. Otto and H. M. Widmer (Editors), *Analytical Chemistry*, Wiley-VCH, Weinheim, Germany, **1998**.

[32] J. C. Giddings, *Dynamics of Chromatography, Part I, Principles and Theory*, Marcel Dekker, New York, **1965**.

[33] E. Grushka, L. R. Snyder and J. H. Knox, *J. Chromatogr. Sci.*, **1975**, *13*, 25-37.

[34] J. H. Knox, *J. Chromatogr. A*, **2002**, *960*, 7-18.

[35] J. H. Knox and M. Saleem, *J. Chromatogr. Sci.*, **1969**, *7*, 745-751.

[36] J. C. Giddings, *Anal. Chem.*, **1967**, *39*, 1027-1028.

[37] E. Grushka, *Anal. Chem.*, **1970**, *42*, 1142-1147.

[38] J. M. Davis and J. C. Giddings, *Anal. Chem.*, **1983**, *55*, 418-424.

[39] C. G. Horváth, B. R. Preiss and S. R. Lipsky, *Anal Chem.*, **1967**, *39*, 1422-1428.

[40] J. G. Dorsey, *Microchem. J.*, **1999**, *61*, 6-11.

[41] N. W. Smith and M. B. Evans, *Chromatographia*, **1994**, *38*, 649-657.

[42] R. J. Boughtflower, T. Underwood and C. J. Paterson, *Chromatographia*, **1995**, *40*, 329-335.

[43] R. J. Boughtflower, T. Underwood and J. Maddin, *Chromatographia*, **1995**, *41*, 398-402.

[44] S. E. van den Bosch, S. Heemstra, J. C. Kraak and H. Poppe, *J. Chromatogr. A*, **1996**, *755*, 165-177.

[45] R. A. Carney, M. M. Robson, K. D. Bartle and P. Myers, *J. High Res. Chromatogr.*, **1999**, *22*, 29-32.

[46] N. W. Smith and M. B. Evans, *Chromatographia*, **1995**, *41*, 197-203.

[47] B. Behnke, E. Grom and E. Bayer, *J. Chromatogr. A*, **1995**, *716*, 207-213.

[48] T. Tsuda, *Anal. Chem.*, **1987**, *59*, 521-523.

[49] H. Rebscher and U. Pyell, *Chromatographia*, **1994**, *38*, 737-743.

[50] B. Behnke, J. Johansson, S. Zhang, E. Bayer and S. Nilsson, *J. Chromatogr. A*, **1998**, *818*, 257-259.

[51] B. Behnke, J. Johansson, E. Bayer and S. Nilsson, *Electrophoresis*, **2000**, *21*, 3102-3108.

[52] G. A. Lord, D. B. Gordon, P. Myers and B. W. King, *J. Chromatogr. A*, **1997**, *768*, 9-16.

[53] M. Mayer, E. Rapp, C. Marck and G. J. M. Bruin, *Electrophoresis*, **1999**, *20*, 43-49.

[54] E. Rapp and E. Bayer, *J. Chromatogr. A*, **2000**, *887*, 367-378.

[55] C. Fujimoto, *Anal. Chem.*, **1995**, *67*, 2050-2053.

[56] C. Fujimoto, J. Kino and H. Sawada, *J. Chromatogr. A*, **1995**, *716*, 107-113.

[57] C. Fujimoto, Y. Fujise and E. Matsuzawa, *Anal. Chem.*, **1996**, *68*, 2753-2757.

[58] E. C. Peters, M. Petro, F. Svec and J. M. J. Fréchet, *Anal. Chem.*, **1997**, *69*, 3646-3649.

[59] E. C. Peters, M. Petro, F. Svec and J. M. J. Fréchet, *Anal. Chem.*, **1998**, *70*, 2288-2295.

[60] E. C. Peters, M. Petro, F. Svec and J. M. J. Fréchet, *Anal. Chem.*, **1998**, *70*, 2296-2302.

[61] G. Chirica and V. T. Remcho, *Electrophoresis*, **1999**, *20*, 50-56.

[62] G. S. Chirica and V. T. Remcho, *Electrophoresis*, **2000**, *21*, 3093-3101.

[63] G. J. M. Bruin, P. P. H. Tock, J. C. Kraak and H. Poppe, *J. Chromatogr.*, **1990**, *517*, 557-572.

[64] M. M. Dittman and G. P. Rozing in K. D. Bartle and P. Myers (Editors), *Capillary Electrochromatography*, The Royal Society of Chemistry, Cambridge, UK, **2001**.

[65] B. He, N. Tait and F. Regnier, *Anal. Chem.*, **1998**, *70*, 3790-3797.

[66] S. L. Pentoney, Jr., J. V. Sweedler in J. P. Landers (Editor), *Handbook of Capillary Electrophoresis (Second Edition)*, CRC Press, Boca Raton, FL, **1997**.

[67] C. Haber in J. P. Landers (Editor), *Handbook of Capillary Electrophoresis (Second Edition)*, CRC Press, Boca Raton, FL, **1997**.

[68] C. J. Paterson, *The Development of Capillary Electrochromatography (CEC) and its Coupling with Electrospray Mass Spectrometry*, PhD Thesis, Manchester Metropolitan University, **1998**.

3. Mass Spectrometric Detection for Capillary Electrochromatography

In this chapter, the development of LC/MS interfaces is reviewed, with particular attention being paid to those applied to CE and CEC. The central theme of this thesis is the interfacing of CEC to ITS/TOF mass spectrometry, using laser vaporisation and laser ionisation, so a description of these techniques and the rationale behind the use of them is also given.

3.1. The Development of Interfaces for Coupling Liquid Chromatography to Mass Spectrometry

GC offers higher separation efficiencies than LC [1], so when analytes are both volatile and thermally stable, it is the technique of choice. Most analytes, however, are both involatile and thermally instable, requiring the use of LC techniques. Mass spectrometry is used for detection in chromatography because of the extra information available than with techniques such as UV light absorbance. So much information is available, in fact, that it is often possible to distinguish a small number of analytes that have the same chromatographic retention time. Historically, GC/MS interfaces were developed earlier, first due to their requirement for sample ionisation only (LC/MS interfaces also require sample vaporisation), and second due to the lower pumping speeds required [2,3].

The pumping speed problem can easily be explained. Most mass spectrometers require pressures in the mass analyser in the region of ~ 10^{-5} mbar (~ 10^{-8} atm) to provide an adequate mean free path. Gas entering at 1 cm^3 min^{-1} and 1 atm pressure would therefore require a pumping speed of ~ 1700 L s^{-1} to maintain the required vacuum. However, if liquid acetonitrile (a common mobile phase constituent) is introduced into the source region of the mass spectrometer at a much lower flow rate of 100 µL min^{-1} and 1 atm pressure, a little over 45 cm^3 of vapour would be produced every minute, requiring a pumping speed of ~ 75,000 L s^{-1}. Because of this, GC systems can be directly connected to mass analysers while LC systems must be connected via differentially pumped chambers, increasing instrumental complexity.

This introduces a key advantage of CEC, in that with flow rates of the order of 200 nL min^{-1} (again basing the calculation on acetonitrile) the pumping speed requirement is only 150 L s^{-1}. For CEC/MS, direct connection without differential pumping is achievable.

The sample vaporisation problem, however, has been much harder to solve. The story of LC/MS development is essentially a description of the development of vaporisation strategies. An important point to make is that in GC, analytes, once vaporised, must survive without decomposition for long periods of time. In LC/MS on the other hand, this required survival time can be less than 100 μs. Most early LC/MS interfaces were demonstrated with volatile analytes that could better be analysed by GC/MS, but for the technique to become really useful, universal interfaces were essential. No current interface is universal, but a lab equipped with the most common modern interfaces would be able to study virtually all analytes. The key requirements for an LC/MS instrument are summarised below.

- Retention of chromatographic resolution
- Universal analyte detection
- High sensitivity
- Quantitative response

Over the last 30 years, a great deal of attention has naturally been paid to the on-line interfacing of chromatographic techniques to mass spectrometry. A wide and varied body of literature is available, with early development having been well reviewed by McFadden [2]. A more recent review and a good starting point for reading has been provided by Abian [3], while Gelpí has updated this work, with attention paid to LC techniques only [4]. Development of liquid interfaces for mass spectrometry has largely been accomplished with the use of pressurised flow systems only, due to their reliability and ease of use. Generally first steps were taken using a constant flow of analyte solution, but chromatographic systems were soon substituted. Only later have these systems been modified for techniques such as CE and CEC. In this Section the major types of LC/MS interfaces are reviewed. Interfaces developed for CE/MS and CEC/MS are dealt with in Section 3.2.

3.1.1. Automated Off-line Interfaces

The simplest way to obtain mass spectrometric data from chromatographic eluate is to collect fractions, which may then be subjected to some form of sample preparation, followed by mass spectrometric analysis. Attempts have been made to automate this process, with a good example being the work of Lovins *et al.* [5]. In this work, an interface is described that is based on chromatographic eluate being collected on gold gauze [6]. The gauze is moderately heated to evaporate the mobile phase, while less volatile analytes are retained. Analyte is collected for a defined period of time before the gauze is moved through a high-vacuum valve into the source region of the mass spectrometer. More intense heating is then used to vaporise analytes into a source region where they are subjected to electron impact (EI) ionisation. The cycle time of the interface was given as 3 - 5 minutes, demanding that chromatographic flow be stopped to avoid an unacceptable loss of information. Although modern systems could no doubt better this performance, the ideal of being able to record more than one mass spectrum per second, to retain chromatographic resolution, is clearly unattainable using such a technique. True on-line systems are unlikely to be mechanical devices. This system also suffers from the requirement that analytes be involatile enough to be retained under the first moderate heating event, but volatile and thermally stable enough to be vaporised in the second heating event.

3.1.2. Electron Impact Ionisation of Vaporised Chromatographic Eluate

The simplest way to circumvent the pumping speed and differential pumping problem is to allow only a small fraction of the chromatographic eluate to enter the mass spectrometer. The pumping speed and maximum operating pressure of the system, therefore, determine the maximum allowable flow rate. The first reported LC/MS system arose from work by Tal'roze *et al.*, published in 1968, in which liquids were allowed to enter the source region of a mass spectrometer through a leak inlet at flow rates of less than 1 $\mu L\ min^{-1}$ [7,8]. This leak inlet consisted of a narrow heated capillary, the inlet being placed in a vial containing the analyte solution and the outlet being inside the mass spectrometer. Heating is required to avoid freezing of the solvent and hence blocking of the capillary. As solution flows into the mass

spectrometer it evaporates, with conditions being chosen to ensure that the evaporation boundary is close to the mass spectrometer end of the capillary. The stream of vaporised solvent and analyte was then subjected to EI ionisation. This interface is illustrated in Figure 3.1. In following work, published in 1969, they made a more systematic study of the inlet [9]. They then connected a chromatographic system, detecting the separation of benzene, biphenyl and naphthalene [10]. Although successful, this interface suffered from poor sensitivity due to the low fraction of eluate that could be permitted to enter the mass spectrometer. Moreover, since this system relies on evaporation alone, only volatile analytes could be investigated. Such analytes would have been better analysed by GC/MS.

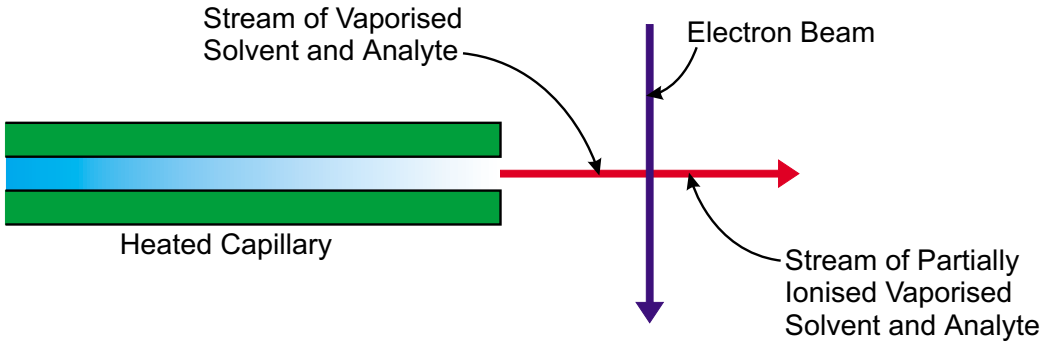

Figure 3.1. Early LC/MS interface based on vaporisation of a small proportion of the chromatographic eluate followed by EI ionisation.

3.1.3. Improving Performance by using a Chemical Ionisation Source

The early interface developed by Tal'roze *et al.* was significantly improved on by Baldwin and McLafferty, who realised that higher flow rates could be accommodated by using evaporated chromatographic solvent as reagent gas in a chemical ionisation (CI) source [11]. In their initial system, analyte solution was placed in a glass capillary that was sealed at one end and drawn out to a narrow needle at the other, as illustrated in Figure 3.2. When placed in a vacuum chamber, air caught in the capillary pushed the analyte solution out through the needle and into the high-vacuum chamber. A spray was formed, which was bombarded with electrons to initiate the CI process. It was possible to allow flow rates of up to 10 μL min^{-1} to enter the system.

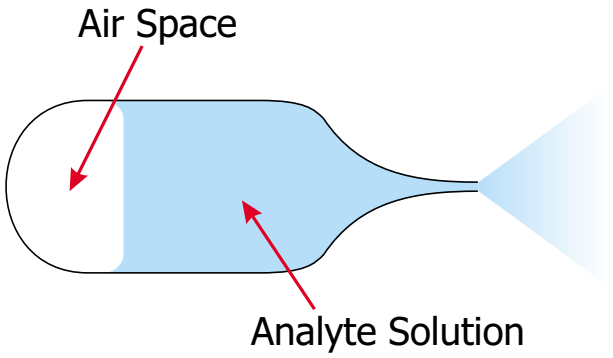

Figure 3.2. Higher flow rates were accommodated by using solvent as CI reagent gas. Initial experiments made use of ampoules such as that shown above.

The following year, using the same principle, a source that was connected to a chromatographic system was reported [12]. Sensitivity was much improved over the EI system because it was possible for a greater proportion of eluate to enter the system. The majority, however, was still sent to waste. The system was claimed to work with all but the most involatile analytes [13]. Hewlett-Packard used this approach to produce a commercial instrument, although a differentially pumped chamber was added to increase the proportion of eluate that could be fed into the ion source region of the mass spectrometer [14]. This family of interfaces, however, although being more widely applicable than the EI interfaces described in Section 3.1.2, are limited to only a small proportion of possible analytes. Mobile phase choice is also restricted due to the requirement for it to act as an effective CI reagent gas.

3.1.4. Atmospheric Pressure Ionisation Mass Spectrometry

In atmospheric pressure ionisation (API) mass spectrometry, analytes in solution are converted to gas-phase ions in a chamber held at approximately atmospheric pressure. In early work, a stream of liquid was sprayed into a heated chamber, supported by a heated carrier gas, with the aim of producing a mixture of solvent vapour and analyte vapour. Ions, produced in some manner, then enter the mass spectrometer through a small aperture. The small size of this aperture allows an adequate vacuum to be maintained in the mass analyser region of the mass spectrometer. Initial studies by Horning *et al.* used a ^{63}Ni source for ionisation

[15,16], while in later studies this was replaced with a corona discharge [17,18]. A comparison of these two techniques was later published, which judged the corona discharge method to be superior [19]. This final design of interface is illustrated in Figure 3.3. The glass wool is presumably present to prevent any large liquid droplets from reaching and passing through the aperture and hence influencing mass analyser vacuum.

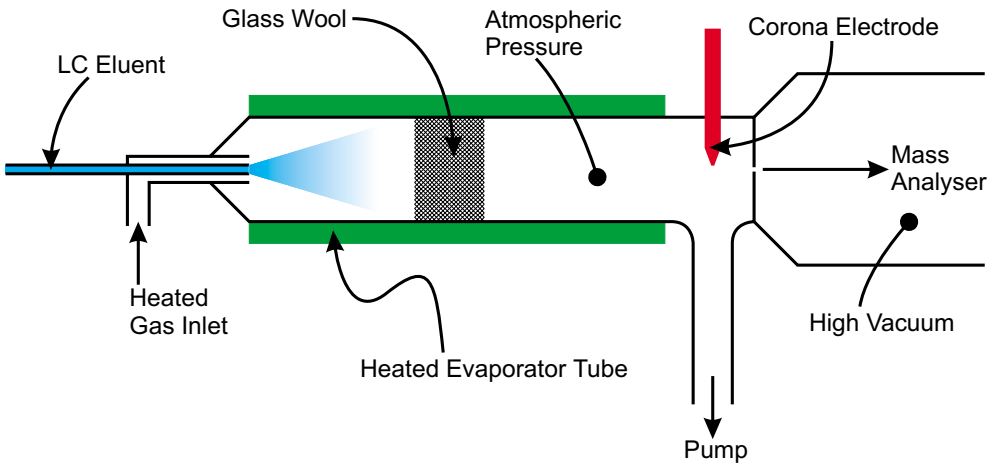

Figure 3.3. Early atmospheric pressure ionisation chamber interface.

This work eventually led to the atmospheric pressure chemical ionisation (APCI) interface that is today commonplace on commercial mass spectrometers. The key advantage of API systems is that all chromatographic eluate can be vaporised, potentially offering much greater sensitivity. Because of the energy required for evaporation of solvent at flow rates in the region of 1 mL min^{-1}, desolvation must be performed at atmospheric pressure and elevated temperatures. An advantage that arises from the differential pumping required in API systems is that solvent molecules are more easily pumped away, due to their lower momentum, enriching the molecular beam in analyte. Early API systems, however, required non-polar solvents and did not respond well with particularly involatile analytes.

3.1.5. Mechanical Transfer

In mechanical transfer interfaces, chromatographic eluate is deposited on a moving wire or belt, which then travels past a low-temperature heater to vaporise the mobile phase, followed by a high-temperature heater to vaporise the analyte for EI

ionisation. The rationale is similar to that used by Lovins *et al.* [5,6] and described earlier. Addition of eluate to the wire or belt and removal of chromatographic mobile phase both occur at atmospheric pressure, with the wire or belt passing through narrow slits into a high-vacuum region where vaporisation of analyte is performed. Scott *et al.* reported the first example of such an interface in 1974 [20], but their choice of a wire to transfer analytes into the mass spectrometer limited sensitivity as the sample capacity of the wire was small. This was improved by McFadden *et al.* [21], who replaced the wire with a stainless steel ribbon, allowing a greater proportion of the eluate to be accepted and hence transported into the mass spectrometer. Early interfaces simply allow eluate to drop onto the wire or belt, but a significant improvement in chromatographic resolution was obtained by employing a gas-assisted nebuliser to evenly coat the belt [22]. Hayes *et al.* demonstrated the performance improvement available from such nebulisation [23].

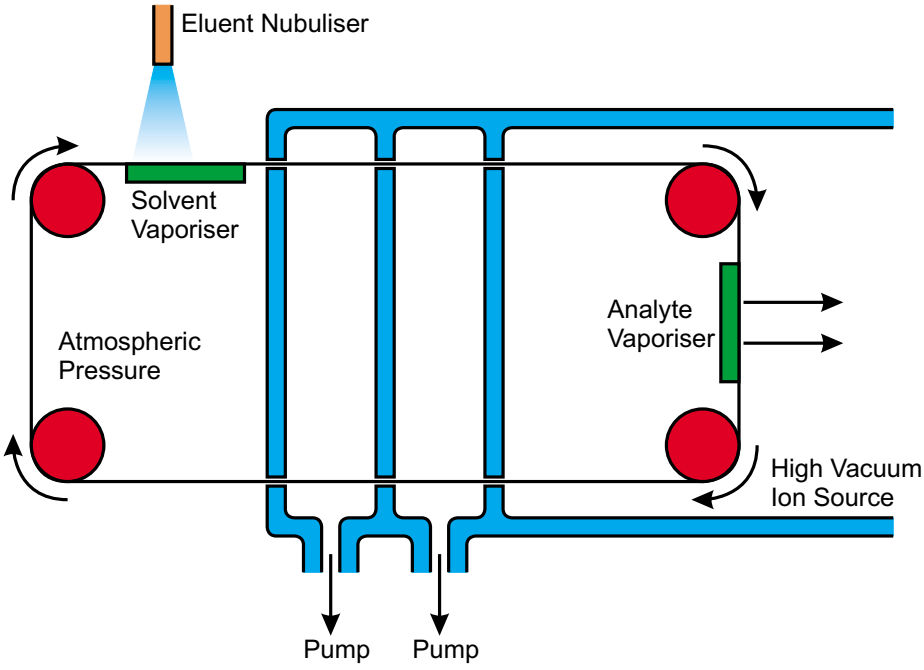

Figure 3.4. Mechanical transfer interface.

An interesting advantage of this interface is that involatile buffers can be used because they will simply not be vaporised off the belt and will exit the vacuum chamber. At this point an extra stage can be added to clean the belt before it returns to the sample source. Chromatographic resolution is typically well preserved in such

systems, especially when a jet is used to deposit eluate on the belt. The major drawback, however, is similar to that for the earlier mentioned work of Lovins *et al.* [5,6], in that the first heater must be hot enough to vaporise all solvent, while retaining analyte for vaporisation by the second heater. Solvent volatility governs the maximum flow rate that can be sprayed onto the belt. With solvents such as water this can be quite limiting.

3.1.6. Enrichment of Analytes over Mobile Phase

In 1975, Jones and Yang reported an interface in which chromatographic eluate was first rapidly vaporised and then passed through a series of selective membranes to provide an enriched stream of analyte vapour to the mass spectrometer [24]. These membranes were chosen because of their ability to reject polar molecules while allowing non-polar molecules to pass. With careful choice of mobile phase and analyte this allows relatively high flow rates to be accepted without endangering mass analyser vacuum. For systems where an appropriate membrane is available, such an approach might prove to be worthwhile, but in general the requirement for thermally stable and volatile molecules makes this technique uncompetitive when compared with GC/MS. However, their general desire to analyte enrich chromatographic eluate is common to many interfaces.

Another enrichment system is the jet separator that is commonly employed in GC/MS. For LC/MS, eluate is first vaporised by passing through a heated steel tube and is then passed through a fine aperture as illustrated in Figure 3.5. All molecules pass through this aperture with approximately the same velocity, but heavier analyte molecules have more momentum and hence are more likely to reach the facing aperture that permits entry to the mass analyser. Such an interface was first reported by Takeuchi *et al.* in 1978 [25]. Although this type of interface does work, flow rates are limited to $< 10\ \mu L\ min^{-1}$, with the requirement for vaporisation meaning that analysis of involatile analytes will be difficult.

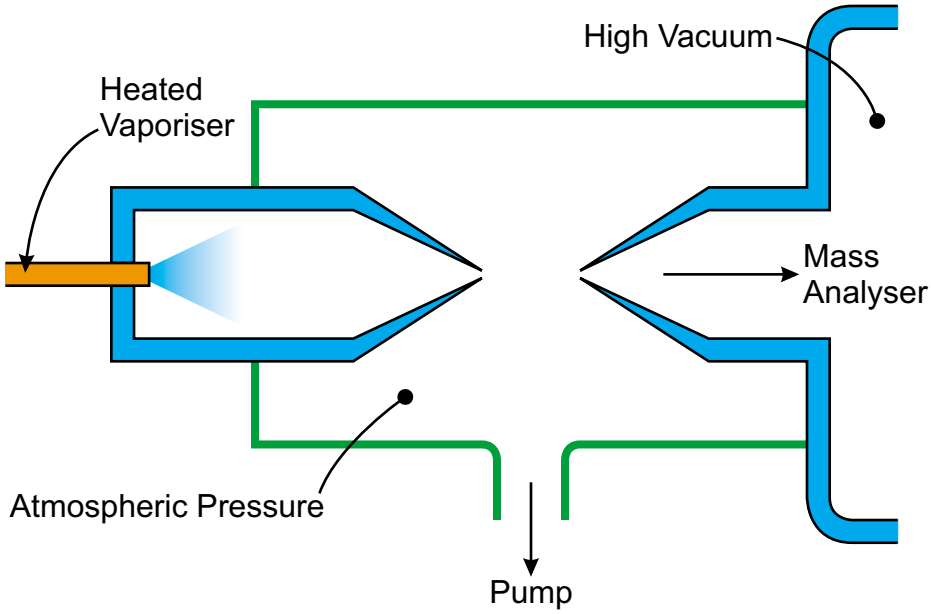

Figure 3.5. The jet separator as used for a liquid interface.

3.1.7. The Development of the Thermospray Interface

When a molecule is evaporated from a heated surface, energy from the surface is used to break bonds between the molecule and the surface. In the case of involatile molecules, energy is distributed among internal degrees of freedom and absorbed in decomposition reactions. The logical approach to evaporation would therefore be to minimise bonding to the surface while heating very rapidly, so that evaporation occurred before decomposition. Beuhler *et al.* investigated the competition between evaporation and decomposition for peptide molecules located on weakly interacting surfaces [26], finding rapid heating on Teflon surfaces to be effective. An approach based on rapid heating and the avoidance of surface interactions is the basis of thermospray.

The development of thermospray began with an instrument that used an IR laser to provide rapid heating [27]. Chromatographic eluate was sprayed as a liquid jet from a steel capillary into the path of the laser beam, which was powerful enough to vaporise all eluate at flow rates of up to 1 mL min^{-1}. This rapid heating, with no surface present, was shown to be efficient in producing a beam of vaporised eluate, which then intersected an electron beam for ionisation. As large amounts of solvent are present, this is a CI process. In later work, the investigators realised that if the

laser were simply used to heat the sprayer tip, the same results were obtained. The system was therefore simplified by replacing the laser with an oxy-hydrogen flame [28]. In an extension to this work it was noted that switching the electron source off did not remove the signal, indicating that another ionisation method was present [29]. This work concluded with the development of the thermospray interface described below [30].

Such a thermospray interface is illustrated in Figure 3.6. Chromatographic eluate flows through a flash vaporiser, resulting in a mist of droplets and vapour. Involatile molecules are preferentially retained within the droplets. The volatile electrolyte, ammonium acetate, is typically included in the mobile phase, giving the droplets a charge dependent on which ions were sampled in the process of forming the droplet. As solvent evaporates, involatile molecules can now evaporate as ions from the highly charged droplets. Ions are then electrostatically directed into the mass analyser, which is orthogonal to the jet, the solvent being pumped away. The systems are also often fitted with an electron gun to improve ionisation efficiency, with later models being fitted with a corona discharge electrode for the same purpose, resulting in a technique similar to APCI.

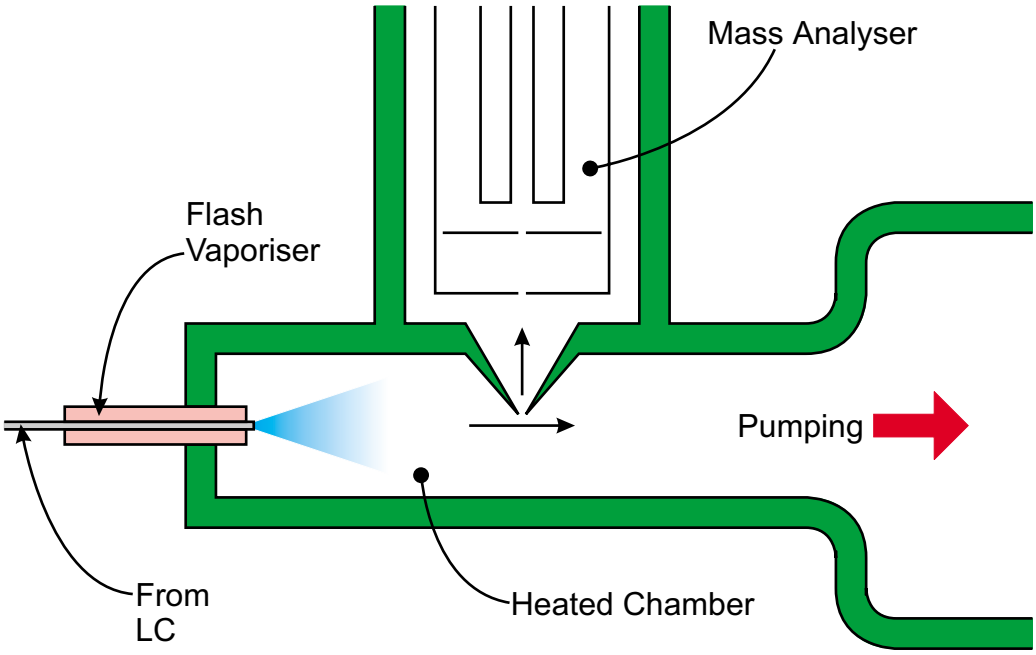

Figure 3.6. Schematic diagram of the thermospray interface.

Thermospray is essentially the culmination of vaporiser technology, with ever-faster heating favouring evaporation over decomposition. It represents an analytically useful solution to the problem of transferring involatile analytes from solution to the gas phase. Large, involatile analytes of major importance such as peptides and proteins cannot, however, be analysed by thermospray.

3.1.8. Electrospray

The development of electrospray ionisation (ESI) mass spectrometry has resulted in LC/MS becoming a routine technique in many analytical science laboratories. It appears that electrospray was first observed by Zeleny while conducting studies into electrical discharges from liquid points [31]. In this work a slight pressure was applied to a conductive liquid in a glass tube, which had at one end been pulled out to a fine needle, so that a droplet was produced at the needle tip. An electrical potential was then applied between the liquid and a large planar electrode. It was observed that under certain conditions a spray was produced that resulted in the production of very small (less than 1 μm in diameter) droplets [32]. This spray was described in greater detail and photographs presented in Zeleny's 1917 paper [33].

More detailed descriptions of the electrospray process can be found elsewhere [34,35], but an outline is provided here. Applying a potential of 2 – 3 kV to the tip of a narrow steel capillary that contains an electrolyte solution, which is 1 – 3 cm from a large planar electrode, results in electrospray. Considering the case where the capillary tip is held at a positive potential, the meniscus of the solution at the metal capillary tip will become enriched in positive electrolyte ions. This accumulated charge is pulled downfield towards the planar electrode, expanding the meniscus into a cone (the Taylor cone) as illustrated in Figure 3.7.

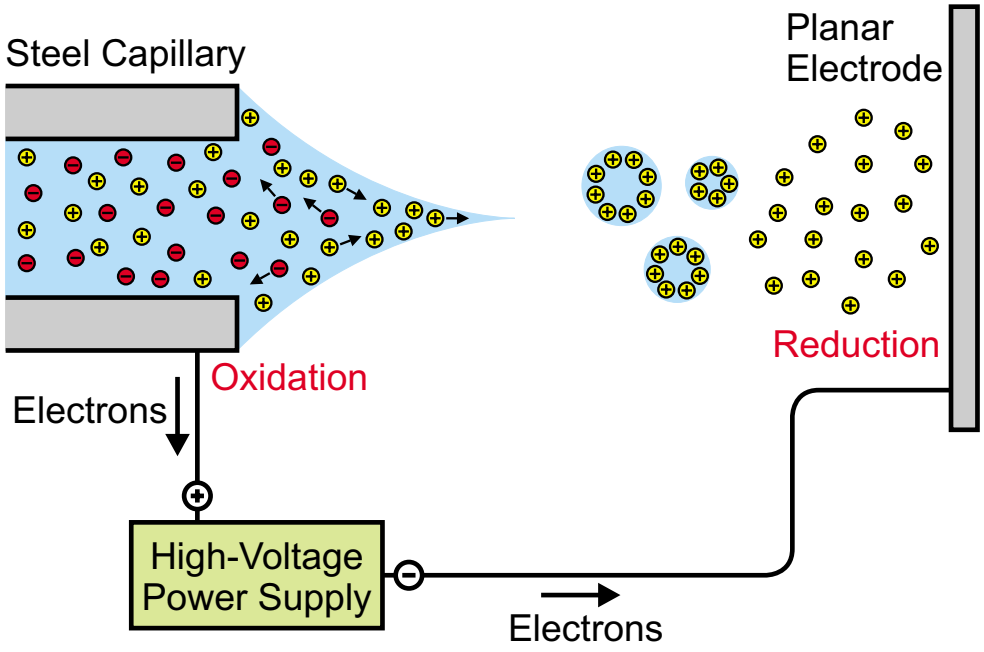

Figure 3.7. Diagram to explain the electrospray process. Applied potential causes charging that in turn causes the meniscus to move downfield, producing the Taylor cone, which destabilises to produce droplets that evaporate and divide to give free gas phase analyte ions.

At sufficiently high electrical potentials, a liquid jet emerges from the apex of the Taylor cone. In this jet the charge density is so high that the surface tension can no longer hold the emerging fluid. Charged droplets then emanate from the tip of the jet, stability being gained because the excess charges are spread over a larger surface area. In this way a fine spray of charged droplets of a single polarity is directed towards the counter electrode. As solvent evaporates, usually with the aid of heating, the droplets become smaller, but the charge that they carry remains constant. This results in droplet fission, spreading the charge over a larger surface area. Fission may happen a number of times, with the charge imbalance in the final droplets driving analyte charging and desorption.

The use of electrospray for the production of ions was first reported by Dole *et al.* in 1968 [36,37]. In their experiments, a dilute solution of polystyrene molecules was electrosprayed into a bath gas of nitrogen at atmospheric pressure. A small aperture, leading into a vacuum chamber, was used to sample the ions produced. The device used to investigate these ions was not, however, a mass spectrometer. A retarding

potential was applied to the ion beam and the effect of increasing this potential on the number of ions arriving at a detector was investigated. At the time, the only way to detect such slow moving, large ions was by means of a Faraday cup. This device detects charged particles independent of their mass or energy. The current detected is then amplified and measured, with sensitivity being limited by the noise of the amplifiers. Faraday cups are still used for isotope ratio measurements where absolute numbers of ions arriving are required. Iribarne and Thomson used mass spectrometry to study the evaporation of ions from the surface of highly charged water droplets that had been produced by electrospray [38,39], but it was Yamashita and Fenn [40,41] who first used electrospray ionisation for analytical work. They employed a quadrupole mass analyser instead of Dole's retarding potential, analysing low-mass analytes compatible with their mass analyser.

The greatest advantage of electrospray is that ions are produced with very little excess energy, meaning that very large and very involatile molecules can be analysed. Electrospray is currently the most universal interface between LC and mass spectrometry and is able to accept flow rates up to approximately 10 $\mu L\ min^{-1}$, requiring flow splitting when interfaced to many LC techniques. ESI/MS sensitivity, however, is largely concentration dependent, removing the disadvantage of flow splitting. Pneumatically assisted electrospray or ion spray was developed to increase the flow rate capable of being accepted into an electrospray source up to approximately 200 $\mu L\ min^{-1}$ [42], and is currently the most widely used form of ESI/MS. Essentially ion spray simply combines gas-assisted nebulisation with electrospray to accommodate higher flow rates.

A novel recent extension of ESI/MS is droplet electrospray. Here a piezoelectric buzzer is used to make a capillary vibrate such that the liquid held is emitted in the form of small droplets [43]. This work was originally performed to investigate the method of action of the electrospray process, but was later used for mass spectrometry [44]. Most LC/MS systems began their development as continuous flow liquid interfaces and were only later adapted for chromatography, so an interface based on a droplet dispenser may be developed in time. A key disadvantage of all electrospray systems, however, is that there is preferential ionisation of polar

analytes that migrate to the droplet surface, leaving non-polar analytes in the centre of the droplet.

3.1.9. Continuous Flow Fast Atom Bombardment

Continuous flow fast atom bombardment (CFFAB) was developed before ESI became the technique of choice and is still used in some laboratories. The advantage of conventional FAB, at that time, was that it was the only technique by which large biological molecules could be analysed. In a FAB source, a high-energy atom beam, typically composed of argon, is directed onto a sample dissolved in an involatile liquid matrix. When high-energy atoms strike the sample solution, pre-existing ions are ejected into the vacuum chamber and then directed into the mass analyser. FAB matrix is often chosen to contain components that promote ionisation of the sample, improving sensitivity. In the first LC/CFFAB/MS interface developed [45], FAB matrix was mixed with the chromatographic eluate, with the resulting mixture flowing into the high-vacuum chamber and being presented to the atom beam on a stainless steel frit. An improved interface was developed by Caprioli *et al.* [46] that did not use a frit, allowing flow rates of up to 10 μL min^{-1} to be accepted. Such flow rates, however, are obviously a major drawback of the technique, with most chromatographic eluate being discarded. When small-scale chromatography is used, however, this becomes less important. Caprioli has reviewed the development of such systems [47], with a key advantage over conventional FAB being the continuous renewal of the liquid surface. Conventional FAB suffers from a tendency for polar analytes to migrate to the inner part of a droplet while hydrophobic compounds concentrate on the droplet surface where ionisation is more effective. The continually renewed surface of CFFAB removes this selectivity to some degree.

3.1.10. Continuous Flow Matrix Assisted Laser Desorption Ionisation

A natural alternative to a high-energy atom beam as a way of adding energy to a sample is to use a laser. Use of a laser allows selective ionisation by adjustment of wavelength, but variable wavelength lasers are expensive and require skilled personnel. An alternative approach is provided by MALDI. In this technique analyte molecules are mixed with a matrix that is readily excited with a fixed wavelength

laser, and is able to transfer this energy to the analyte, resulting in the production of ions that are then directed towards the mass analyser [48]. The natural continuation of LC/CFFAB/MS is continuous flow MALDI, which was first demonstrated by Li *et al.* in 1993 [49]. In this work, a solution containing a mixture of both matrix and analyte was pumped into the mass spectrometer, being presented for laser irradiation on a stainless steel frit. Later work exchanged this inlet for a chromatographic system [50]. At roughly the same time, an aerosol MALDI interface was developed by Murray and Russell [51]. This device relied on passing a nebulised spray of fine droplets through the laser, producing ions that were then directed into a TOF mass analyser. Analyte was dissolved in matrix and pumped towards the source using a syringe pump. This work was extended to allow use as a chromatographic detector by adding the matrix post-column through a mixing tee [52].

3.1.11. Summary

The chronological development of LC/MS interfaces is summarised in Table 3.1. The pumping capacity problem was overcome easily with the adoption of differential pumping, with most techniques now requiring operation at atmospheric pressure to aid evaporation of solvent. The vaporisation problem has also been largely overcome, with few analytes being impossible to analyse by any technique. The one exception is waxes, important in the petrochemical industry, where field desorption still has a role to play. Their properties of being non-polar, involatile and thermally instable do not fit any interface, but they are rarely analysed chromatographically. Electrospray has become very important due to its ability to analyse non-volatile, polar molecules of biological interest, such a proteins and peptides, with some other techniques still being used for niche applications, especially where non-polar compounds are concerned. The main failure of electrospray, however, is its inability to accept non-volatile components in the chromatographic mobile phase, but no technique apart from the moving belt interface can solve this problem.

Date(s)	Refs.	Novel Features
1914-17	[31-33]	Electrospray process first observed
1968	[36,37]	Electrospray ionisation of macromolecules
1968-69	[7-10]	Direct liquid flow into a EI source
1973-80	[11-14]	Direct liquid flow into a CI source
1973-74	[15-19]	Atmospheric pressure ionisation
1974-80	[20-23]	Mechanical transfer interfaces
1975	[24]	Membrane Enrichment
1978	[25]	Jet Separator
1983	[27-30]	Development of thermospray ionisation
1984	[40,41]	Electrospray ionisation mass spectrometry
1985-86	[45-46]	Continuous flow FAB
1987	[42]	Ionspray
1993	[49-52]	Continuous flow MALDI
1994	[43,44]	Droplet electrospray

Table 3.1. Chronological development of LC/MS interfaces.

3.2. Coupling CE and CEC to Mass Spectrometry

Interfaces developed for CE/MS can, by and large, be applied to CEC/MS, but one distinct disadvantage of CE/MS does not apply to CEC/MS. In CE, vertical displacement of column inlet and outlet of even a few millimetres can lead to noticeable degradation of chromatographic performance. In CEC, the back pressures produced by the packed columns makes such alignment unnecessary. In terms of CE/MS, this means that direct connection to a high-vacuum chamber requires evacuation of the inlet region, making bubble formation a serious problem. For this reason, most CE/MS interfaces utilise atmospheric pressure ion sources. CEC systems on the other hand can be connected directly to vacuum chambers without significant loss in performance, offering a greater variety of interfacing strategies.

3.2.1. The Development of Interfaces for CE/MS

The first successful coupling of CE to mass spectrometry was reported by Smith's group at Pacific Northwest National Laboratory in 1987 [53]. In this work, the

column inlet was, in the usual manner, dipped into a vial containing mobile phase, while the outlet end of the column was surrounded by a stainless steel sheath as shown in Figure 3.8. Potentials of up to 60 kV could be applied to the inlet vial, while potentials of up to 5 kV could be applied to the sheath, allowing it to function both as CE cathode and electrospray needle. This interface, however, suffered from a relatively large dead volume at the outlet that reduced chromatographic efficiency.

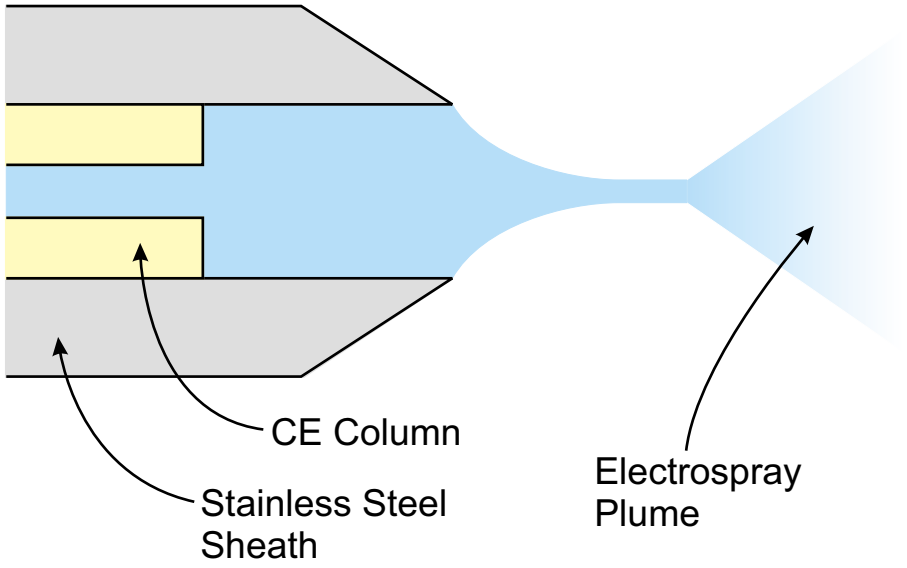

Figure 3.8. Schematic representation of the first successful CE/MS interface.

The same group, through the addition of a flowing liquid sheath, improved this early interface [54], as illustrated in Figure 3.9. Use of a liquid sheath improved electrospray efficiency, prevented analytes from contacting stainless steel surfaces, and reduced the dead volume of the system. Electrical connection is made through the sheath liquid, with a coaxial stream of gas being provided to suppress electrical discharges and to stabilise the spray. In both interfaces, quadrupole mass spectrometers were used as mass analysers. A key advantage of the liquid sheath interface is that solutes can be added through the sheath liquid; for example, adding acids to improve electrospray efficiency. A disadvantage of such interfaces is that dilution of eluate in sheath liquid reduces sensitivity.

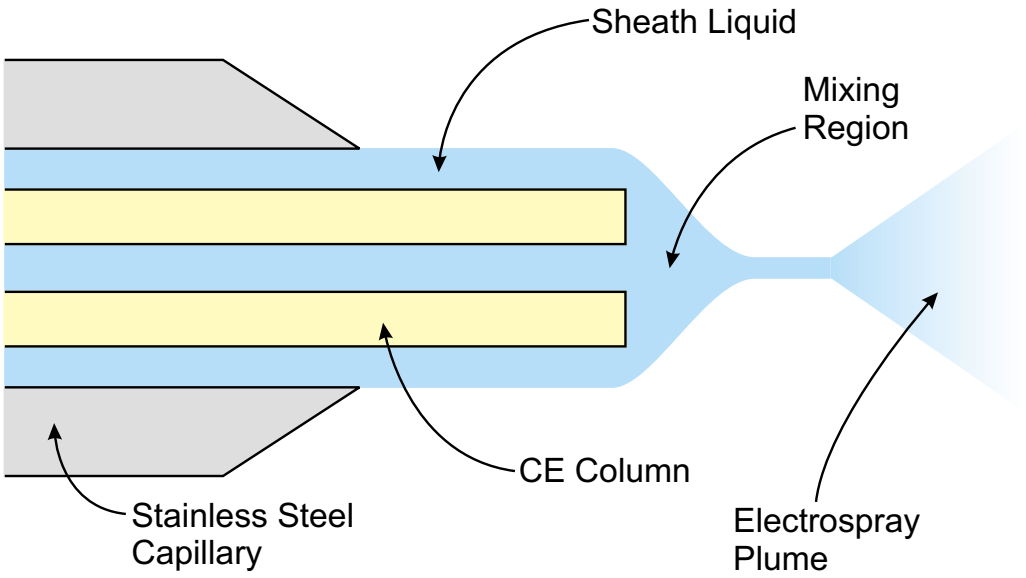

Figure 3.9. Schematic diagram of the sheath liquid interface for CE/MS.

Sheath liquid interfaces have become commonplace in CE/MS, with commercially produced devices now being available. A generalised sheath flow interface is illustrated in Figure 3.10. Smith's group further improved the performance of such interfaces by using very narrow ID capillaries and by etching the capillary tip to a taper using hydrofluoric acid [55]. Tapers were introduced in this case because it had been observed that electrospray often occurred from the outer edge of square cut capillaries. With very narrow ID capillaries, spraying from the outer edge was held to be likely to discriminate significantly in favour of the sheath liquid and against the column eluate.

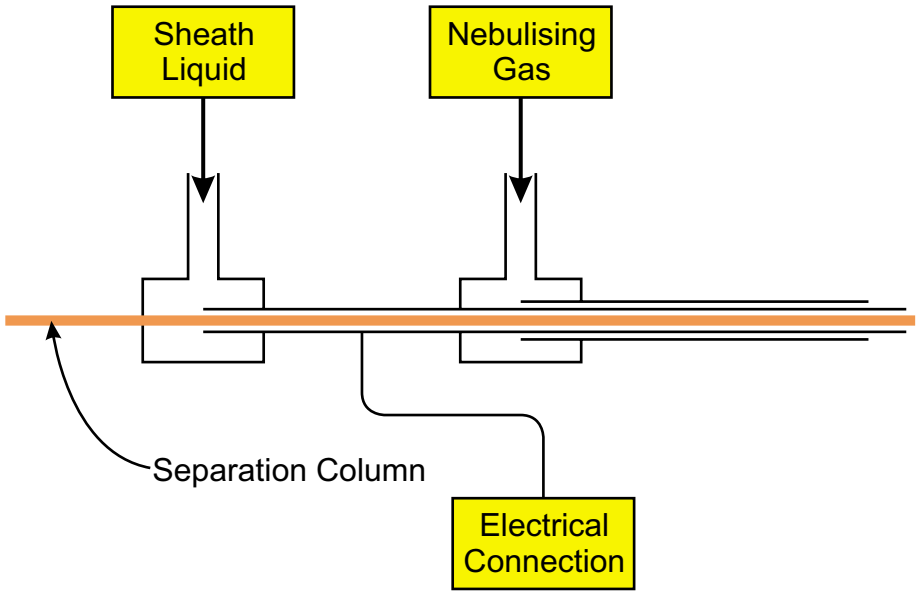

Figure 3.10. Generalised sheath liquid ESI interface for CE/MS. CE column runs through centre, with larger coaxial tubes carrying sheath liquid and nebulising gas. Electrical connection for ESI process and CE electrode through sheath liquid tube.

An alternative to the sheath flow interface that still makes use of added liquid is the liquid junction interface, first reported by Minard *et al.* [56]. In this interface, the CE capillary terminus is separated from a capillary running to a probe tip for CFFAB by a 20 µm gap. Both capillaries are carefully lined up so that their axes coincide, with the liquid junction being immersed in a vial that contains the FAB matrix. A schematic diagram of such an interface is shown in Figure 3.11. The CE mobile phase can be chosen to be optimal for the separation, with addition of matrix occurring post-column. Exact alignment of the capillaries is naturally critical. Further development of such interfaces, this time for ESI, was carried out by Lee *et al.* [57,58], with a hybrid liquid-junction coaxial interface for CFFAB being reported by Caprioli *et al.* [59].

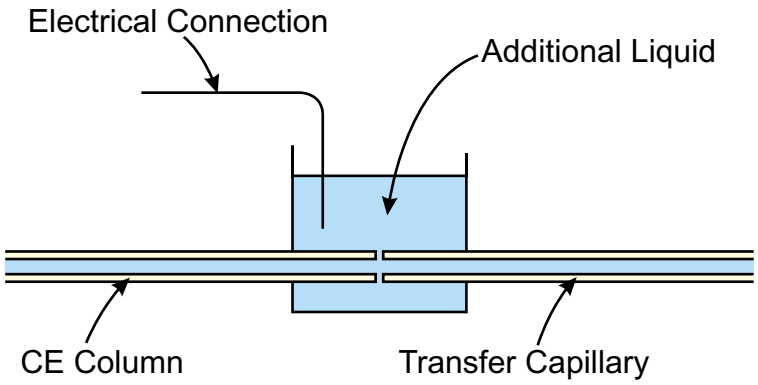

Figure 3.11. Schematic diagram of the liquid junction interface for CE/MS.

Since ESI/MS sensitivity is largely concentration dependent the addition of additional liquid is obviously a disadvantage. Chowdhury and Chait studied electrospray from finely polished, sharp needles, and determined that electrospray of largely aqueous solutions of high surface tension was possible without sheath liquid and nebulisation [60]. Smith's group used capillaries that had been etched to a fine point to demonstrate an improvement in sensitivity over sheath flow interfaces, using sulfur hexafluoride as sheath gas to suppress corona discharge [61]. This work was then extended by the same group to the development of a CE/ESI/MS interface, with electrical connection being made prior to the spray tip [62]. The early development of CE/MS interfaces has been reviewed comprehensively by Cai and Henion [63].

A further CE/MS interface, of direct relevance to the work reported in this thesis, was described by Chang and Yeung [64]. Their system is best classed as continuous flow MALDI, with the CE mobile phase containing $CuCl_2$ as matrix. The column inlet is placed in a vial while the outlet is inside the high-vacuum chamber of the mass spectrometer. A fine wire is used to make electrical contact inside the vacuum chamber for the CE cathode, with the tip of the capillary being subjected to laser irradiation at 248 nm. Whether the $CuCl_2$ acts as matrix or simply acts as an absorber for heating is unclear, but a single laser vaporisation and ionisation interface is obtained.

Finally, an interesting CE/MS interface was described by Preisler *et al.* [65]. This device is a hybrid of a liquid junction interface and a moving belt interface. At the end of the CE column a liquid junction facilitates the addition of MALDI matrix,

with this mixture being deposited onto a moving belt for solvent evaporation and presentation to the laser for the MALDI process. Such an interface could be used for CEC without modification. The ideal continuous flow MALDI interface, however, would be able to use a matrix that could be incorporated in the separation mobile phase, avoiding the use of junctions that inevitably degrade chromatographic efficiency.

3.2.2. The Development of Interfaces for CEC/MS

Early workers attempting to hyphenate CEC to mass spectrometry probably experienced reliability problems, which they tried to correct by pressurising the inlet vial. Pressurisation was first introduced into electrochromatographic systems by Tsuda in order to suppress bubble formation [66], resulting in a technique that is now known as pressurised electrochromatography (PEC). Pressurisation offers reduced analysis times and greater reliability, but efficiency is reduced due to the hybrid electroosmotic and pressurised nature of the flow. Verheij *et al.* were first to report the coupling of a PEC system to mass spectrometry, via a CFFAB interface, with FAB matrix being added to the chromatographic eluate using a liquid junction [67]. This work on PEC/MS was followed by the demonstration of an ESI interface by the same group [68] and by Schmeer *et al.* [69]. Gordon *et al.*, however, reported the first true CEC/MS interface, [70]. This interface was a CFFAB device, with FAB matrix being added in this case through a tee piece. The same group later reported the use of an ESI interface [71]. Despite this early interest in CFFAB, most reported interfaces have relied on ESI and have been of the CE/ESI/MS sheath liquid type, with good examples being provided by the work of Lane *et al.* [72,73].

A significant advance in ESI was provided by the introduction of the nanospray technique by Wilm and Mann [74]. These workers predicted proportionality between the two-thirds power of the flow rate and the size of droplets emitted from the tip of a stable Taylor cone. A larger proportion of analyte molecules are available for desorption from small droplets, making low flow rates desirable for the highest possible sensitivity. Such a system was realised experimentally by drawing capillaries to fine tips, coating then with gold for electrical connection, and filling them with ~ 1 μL of analyte solution. The tapered outlets of such capillaries were

measured to have diameters in the range 1 - 3 µm. This miniaturisation process was continued by Valaskovic *et al.* [75].

Such a strategy has been used for CEC/ESI/MS by Lord *et al.* [76]. Fused silica capillaries have been drawn to fine tapers, usually in the region of 10 µm, and then packed to produce chromatographic columns. A keystone effect prevents the packing material from leaving the column, while the exterior of the taper is coated in a conductive material to provide an electrical connection. Such systems represent the pinnacle of current CEC/ESI/MS interface development, with a packed taper being illustrated in Figure 3.12. One advantage of such a system is that there is no longer a sintered frit at the end of the packed bed, reducing the risk of bubble formation.

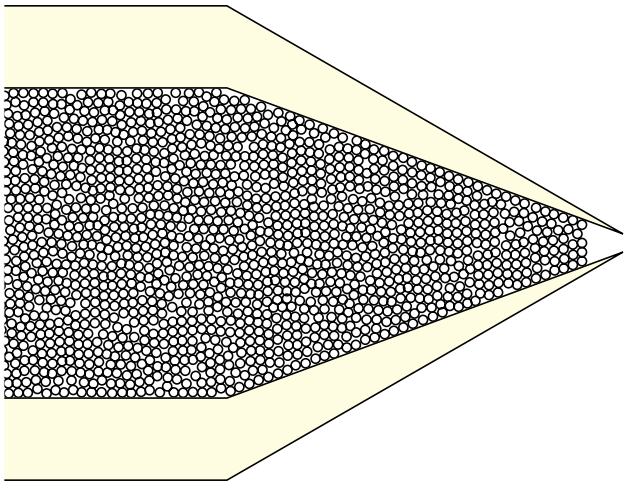

Figure 3.12. Column for CEC/ESI/MS produced by packing against a taper.

Such systems, however, are fragile and prone to blockages. An alternative method, designed to improve reliability, is to use a junction between the column and an unpacked needle. If the needle is blocked it can therefore be changed without discarding the column. The junction and unpacked section will, however, result in performance degradation.

3.3. Time-of-Flight Mass Spectrometry

Most LC/MS interfaces provide a continuous stream of ions to the mass spectrometer, but in this work, a pulsed source was used. TOF mass spectrometry is

characterised by being a pulsed rather than a continuous technique, and as such, is well suited to this application. TOF systems can record thousands of mass spectra per second, which is far in excess of most other mass analysers. A good introduction to TOF instrumentation and theory has been provided by Guilhaus [77], with an account focused more on applications being provided by Cotter [78]. Mamyrin has also recently reviewed the development of TOF instrumentation [79].

3.3.1. Time-of-Flight Fundamentals

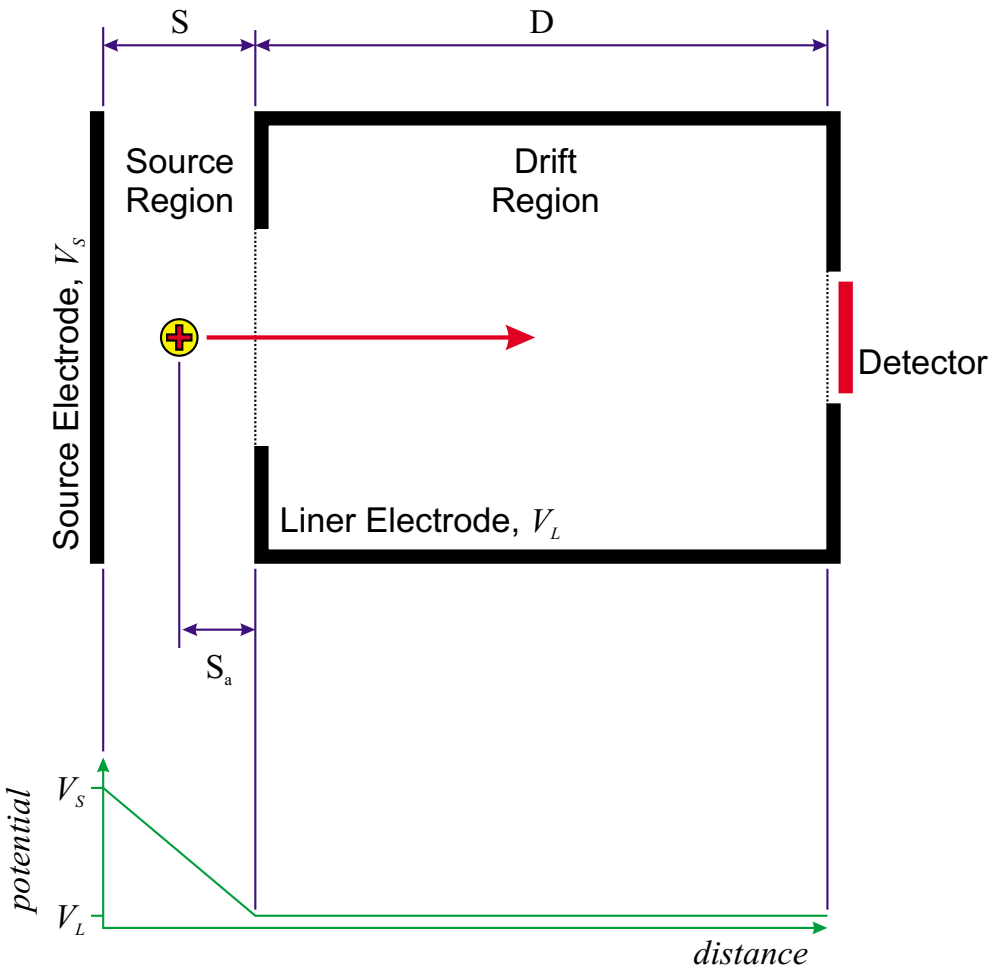

Figure 3.13. Schematic diagram showing the main parts of a single-field time-of-flight mass spectrometer.

The simplest possible TOF mass spectrometer consists of a drift region, which is held at a constant electrical potential, and a source region where a gradient in electrical potential exists. This gradient in electrical potential is used to accelerate

ions into the drift region. Ions would ideally be created instantaneously in the source region, all initially being located at the same point and having the same velocity. The electrical potential energy of an ion is equal to the product of its charge and the electrical potential at that point. The difference in electrical potential energy, ΔEPE, between an ion at the starting point indicated in Figure 3.13, and at any position in the drift region, is given by Equation 3.1,

$$\Delta EPE = q\left(\frac{S_a\left(V_S - V_L\right)}{S}\right) = qES_a \qquad \text{Equation 3.1}$$

where q is the charge on the ion, V_S is the potential of the source electrode, and V_L is the potential of the drift region. S is the distance between the source electrode and the beginning of the drift region, while S_a is the distance between the start point of the ion and the drift region. This expression is simplified by replacing $((V_S - V_L)/S)$ with E, the strength of the electric field established between the electrodes. ΔEPE is equal to the kinetic energy of the ion in the drift region, allowing the velocity of the ion to be calculated as indicated in Equation 3.2,

$$qES_a = \frac{1}{2}mu_D^2 \qquad \text{Equation 3.2}$$

where m is the mass of the ion and u_D is the velocity of the ion in the drift region. This expression can be rearranged as shown in Equation 3.3 to give u_D.

$$u_D = \sqrt{\frac{2qES_a}{m}} \qquad \text{Equation 3.3}$$

Knowledge of u_D then allows the time taken to pass through the drift region, t_D, to be calculated as shown in Equation 3.4.

$$t_D = \frac{D}{\sqrt{(2qES_a/m)}}$$ Equation 3.4

Here D is the distance travelled between the beginning of the drift region and the detector. To obtain the total flight time, however, the time spent in the source region must also be considered. The force, F, acting on an ion at the starting point is equal to the product of its charge and the electrical field strength. This force is also naturally equal to the product of the ionic mass, m, and the acceleration, a. These relationships are expressed in Equation 3.5.

$$F = qE = ma$$ Equation 3.5

The time taken to pass through the source region, t_S, can then easily be calculated if a standing start is assumed by dividing u_D by a, as indicated in Equation 3.6.

$$t_S = \left(\frac{u_D}{a}\right) = \sqrt{\frac{2mS_a}{qE}}$$ Equation 3.6

This gives a total flight time, t, as defined by Equation 3.7.

$$t = t_S + t_D = \sqrt{\frac{2mS_a}{qE}} + D\sqrt{\frac{m}{2qES_a}}$$ Equation 3.7

It can therefore by seen that t is proportional to the square root of (m/q), with q being replaced in the usual terminology with $z = (q/e)$, where e is the elementary charge. Additional time must also be added to take account of the response time of the detection system, meaning that an expression of the form shown in Equation 3.8 is required for calibration.

$$(m/z) = at^2 + b$$ Equation 3.8

Here, a and b are constants. Calibration, therefore, requires at minimum, two known masses, but naturally will be improved in accuracy with more information.

3.3.2. Maximising Resolution in TOF Mass Spectrometry

The m/z ratio resolution available for a TOF mass spectrometer is limited largely by variations in starting time, starting position and starting velocity of the ions to be analysed. Starting time variations can be minimised by reducing the duration of the ionisation process. In a mass spectrometer where a laser is used for ionisation, this would most simply be achieved by shortening the laser pulse so that it approached the digitisation rate of the signal from the detector. This would typically require laser pulses of nanosecond duration. An alternative solution is to increase the flight time by reducing the electric field used for acceleration or by lengthening the drift region. Lowering the accelerating field increases relative differences in velocity while lengthening the drift region quickly becomes impractical.

Loss of m/z ratio resolution resulting from ions created at different points in the source is also a problem. If all ions were created in the same plane perpendicular to the electric field, all ions with the same m/z ratio would gain the same amount of kinetic energy from the field and would arrive at the detector at the same time. However, ions are created in different planes, and although the laser must be focused to minimise this variance, some ions will start closer to the drift region and will be accelerated less than ions formed further away. The ions formed further away will therefore catch the slower ions, resulting in a space-time focus at a distance $2S_a$ from the source. This would theoretically be a good place for the detector, but insufficient temporal dispersion makes this impractical. Two-field ion extraction, as proposed by Wiley and McLaren in 1955 [80], can move this focus point to a more practical position.

Finally, the resolution loss arising from different starting velocities can be visualised by imagining two identical ions formed at exactly the same point in space and time, but with one ion moving away from the detector and one ion moving towards the detector. The ion moving away from the detector will have to be turned around by the field and sent back towards the detector, placing it considerably behind the ion

initially travelling towards the detector. Such effects can be minimised by using a very strong electric field, so that the difference in velocity is small compared to the resultant velocity. A further correction method, also suggested by Wiley and Mclaren [80], is to delay extraction for a short time after ion creation. Ions moving away from the detector will move to regions of higher potential, and hence will be accelerated for longer, while ions moving towards the detector will be accelerated for a shorter period of time. This time lag focusing however is only effective for a small m/z ratio range.

A far more effective method for reducing the effect of a spread in initial velocity, which translates into a spread in kinetic energy, is the reflectron invented by Mamyrin *et al.* [81]. This provides a way of focusing ions that have different initial kinetic energies, but which also have the same m/z ratio. Such a device is illustrated in Figure 3.14. The reflectron is located at the end of the flight tube and consists of a series of electrodes, running from the potential of the drift region up to a potential slightly higher than the source potential. Incoming ions penetrate the reflectron until they exchange all kinetic energy for potential energy, at which point they reverse and are accelerated back through the reflectron, emerging with the same kinetic energy as when they entered. Ions with greater kinetic energy penetrate the reflectron more deeply, and hence have longer flight paths, meaning that ions having different velocities will reach the detector at the same time.

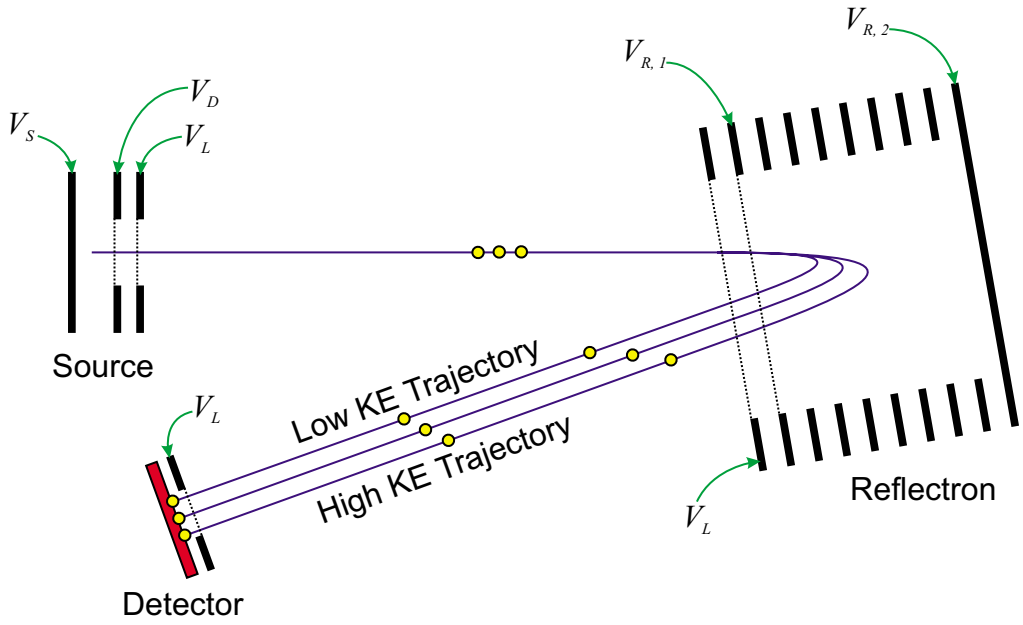

Figure 3.14. The reflectron and its role in correcting variance in initial kinetic energy.

In the Mamyrin design, the reflectron is set at a small angle to the initial ion path, resulting in exiting ions following a different flight path as they return. If the solid electrode labelled $V_{R,2}$ in Figure 3.14 is replaced by a grid, a detector can be located to allow monitoring of neutrals, which will not be deflected by the reflectron, or to allow the instrument to be used in linear mode. A secondary advantage of using a reflectron is that path length is increased, increasing flight time. Note that the instrument illustrated in Figure 3.14 has two-stage ion acceleration. In modern machines, a deflector is typically placed at the space-time focus, directing ions towards the reflectron. The space-time focus can be mirrored by the reflectron onto the detector, giving the highest possible level of performance. Such a configuration was used in the time-of-flight analyser employed in this work.

In typical use, the potential difference between $V_{R,1}$ and V_L is about two-thirds of the difference between V_S and V_L, with the potential difference between $V_{R,2}$ and V_L being a little greater than that between V_S and V_L. Hence, an ion entering the reflectron will first experience a region of strong electric field followed by a region of weaker electric field. This configuration is chosen to maximise penetration depth. The electrodes between $V_{R,1}$ and $V_{R,2}$ are present to make the electric field more

uniform throughout the reflectron. A representation of the electrical potentials within the instrument is given in Figure 3.15.

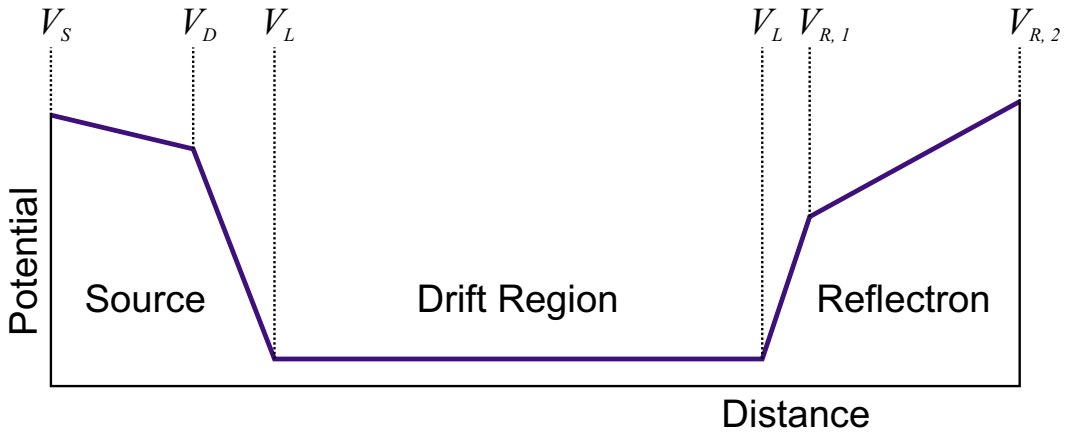

Figure 3.15. Plot of the electrical potentials within a TOF mass spectrometer equipped with a reflectron and two-stage ion extraction.

3.4. Use of an Ion Trap as a Storage Device

There are a number of methods for presenting ions to a TOF mass spectrometer. The approach taken in this work involved the use of a radio frequency (rf) only ion trap, used as a storage device, which was used to inject ions into the time-of-flight mass analyser. The ion trap provided a convenient means of decoupling the different timescales required for CEC separation and time-of-flight mass analysis.

An ion trap uses three electrodes to trap ions in a small volume. The structure of such a device is illustrated in Figure 3.16. The trap is cylindrically symmetrical and is composed of a ring electrode and two end cap electrodes. A large oscillating electrical potential is applied to the ring electrode, while the end cap electrodes are held at electrical ground. The mode of action of the trap is explained schematically in Figure 3.16. The diagram on the left-hand side (a) refers to the case where a cation is present and a large positive potential is being applied to the ring electrode. Considering first the radial direction, the cation will be forced towards the axis of the trap, while in the axial direction, it will move towards the end caps. The diagram on the right-hand side (b) refers to the case where a large negative potential is being applied. The cation is now attracted towards the ring electrode, moving away from

the axis, while in the axial direction it will move towards the centre of the trap. In this way, by means of rapidly oscillating potentials, the cation is focused towards the centre of the trap. The applied potentials and the frequency of oscillation of the ring electrode potential govern the *m*/*z* ratio range that can be trapped, with trapping frequencies typically being in the region of 1.1 MHz.

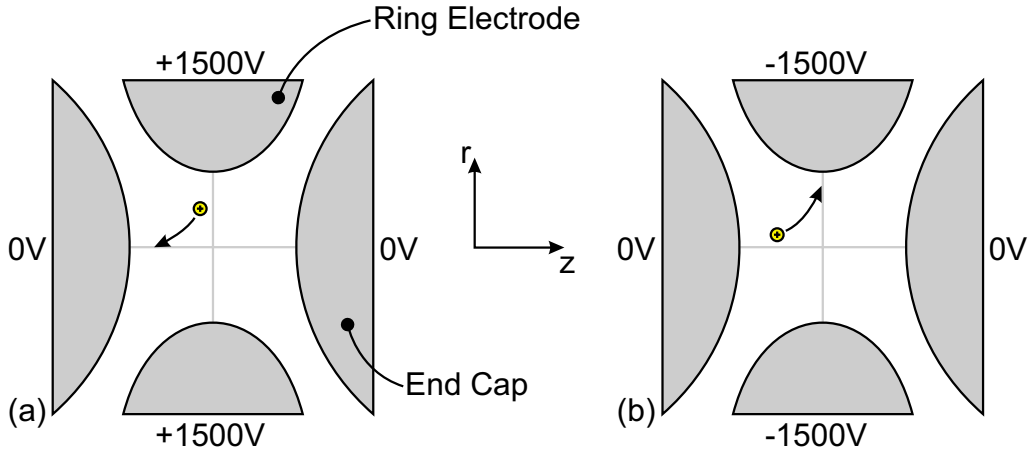

Figure 3.16. Diagram to explain the basic mode of action of a quadrupole ion trap. The trap is cylindrically symmetrical, with the r-axis and the z-axis as indicated. The diagram on the left-hand side (a) illustrates the situation when a large positive potential is applied to the ring electrode while the diagram on the right-hand side (b) illustrates the situation when a large negative potential is applied.

More detailed descriptions of the mode of action of the ion trap can be found elsewhere [82,83]. With the addition of helium to dampen trapped ion motions, an efficient ion storage device is obtained that can also be used as a mass spectrometer. In this work, however the ion trap was used purely in rf only mode to store and accumulate ions. The use of helium to dampen trapped ion motions results in a compressed cloud of ions with low kinetic energy that provides a suitable starting point for high-resolution TOF mass spectrometry. At the end of the trapping period, the trapping potential is switched off and an electrical potential pulse is applied to the end cap nearest the mass analyser to eject ions into the time-of-flight mass analyser. A hole is present in the centre of the electrode for this purpose.

3.5. Lasers in Mass Spectrometry

3.5.1. Laser Desorption

Lasers capable of outputting pulses of nanosecond duration are ideally suited to TOF mass spectrometry. Early examples of laser mass spectrometry were categorised as either multiphoton or desorption techniques [84]. Multiphoton techniques involve direct interaction of laser photons with individual molecules, atoms or ions in the gas phase, while desorption techniques involve the laser irradiation of solid phase samples. These solid phase samples typically consist of analyte adsorbed onto a substrate, with the principle advantage of laser desorption being the ability to vaporise involatile species without decomposition. Desorption techniques are used for larger, more complex molecules in the solid phase while multiphoton techniques are used for atoms or small molecules in the gas phase.

Posthumus *et al.* [85] demonstrated the use of pulsed infrared laser radiation ($\lambda = 10.6\ \mu m$) for the vaporisation and ionisation of involatile molecules such as oligosaccharides, nucleotides and peptides. Desorption is not a resonant process, so the wavelength employed is of little importance and there is little selectivity apart from a preference for polar molecules. An alternate strategy, first suggested by Cotter [84], is to reduce desorption power so that vaporisation is not followed by ionisation. Desorbed neutrals may then be ionised by multiphoton techniques, imparting a degree of selectivity to the experiment. Such two laser mass spectrometric experiments were first demonstrated by van Weyssenhoff *et al.* [86].

A number of explanations have been proposed for the laser desorption process, with the simplest of these being similar to those proposed for desorption of involatile molecules from weakly interacting conventionally heated surfaces that were mentioned previously [26]. Put simply, heating is so fast that weak bonds between adsorbate and substrate are broken, and vaporisation is achieved, before enough time has elapsed for stronger chemical bonds in the adsorbate to break and hence lead to decomposition. Laser heating also has the advantage over conventional heating in that energy can be directed and focused easily onto very localised regions of a sample.

An alternative explanation of the desorption process is provided by shock wave desorption. In this model, very fast laser heating is considered to result in rapid thermal expansion, causing desorption of molecules by momentum transfer. The heating rate must be very fast, and the laser must penetrate significantly into the sample. Lindner and Seydel performed an experiment, to test this hypothesis, where a thin layer of substrate was supported on a Formvar film, which was in turn was supported on a copper grid [87]. The laser beam was directed to the back of the sample, with ions released from the front of the sample directed into a TOF mass spectrometer, as illustrated in Figure 3.17. Very little fragmentation was observed, presumably because sufficient time was not available for the molecules to absorb internal energy.

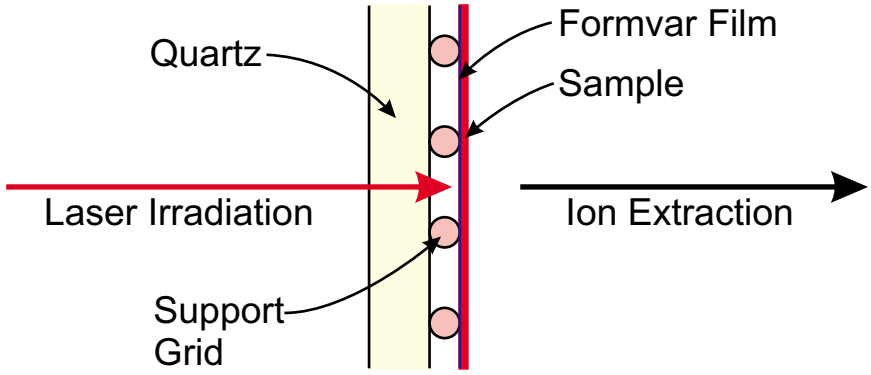

Figure 3.17. Apparatus used to investigate shock wave model of laser desorption.

In the CEC/MS interface described in this thesis, strictly, laser desorption was not performed. No substrate was present and the purpose of the IR laser was simply to assist vaporisation of chromatographic eluate by heating both the eluate and the capillary terminus in a similar manner to that described by Blackley *et al.* [27]. This fast heating would be expected to result in vaporisation of molecules that might otherwise have collected at the terminus. An improved strategy might have been to use resonant vaporisation, where laser wavelength is chosen to excite major mobile phase components such as water. An investigation based around an Er^{3+}:YAG laser that operates at 2.94 nm, and therefore would be expected to excite vibrational transitions in water, is reported in Section 6.6.

3.5.2. Laser Ionisation

Once gas phase molecules have been produced, multiphoton ionisation can be used to create ions for mass spectrometric analysis. Multiphoton ionisation is required because most molecules of interest have IPs that lie in the range 7 - 10 eV, requiring laser wavelengths that lie in the range 177 – 124 nm for single photon ionisation. Operating lasers in this range, however, is experimentally challenging due to radiation of this wavelength being strongly absorbed by atmospheric oxygen and water. Despite these difficulties, such laser sources have been successfully utilised [88], but it is more practical to use lasers outputting longer wavelengths. This, however, results in the requirement for more than one photon to be absorbed for ionisation.

Multiphoton ionisation is enhanced by choosing a laser wavelength that corresponds to excitation of the molecule into an intermediate electronic state, which must then be followed by a further photon for ionisation. Use of a real intermediate state increases the efficiency of the process, and also adds a degree of selectivity, resulting in a technique known as resonantly enhanced multiphoton ionisation (REMPI). In the present work, ions were produced from neutrals inside the ion trap, removing the possibility of transmission losses and reducing the complexity of the system. The selectivity arising from choice of laser wavelength can be used to ionise only one class of compounds out of a complex mixture of gas phase neutrals to simplify the analysis.

A final advantage of using ion trap storage over a purely TOF instrument is that ions produced at different times can be ejected into the mass spectrometer simultaneously. This obviously is of advantage for storing the results of many laser vaporisation laser ionisation cycles to increase selectivity, but it also avoids problems due to ions created during the vaporisation process. In a purely TOF mass analyser, these early ions will move towards the detector as soon as they are created, and will overlap the mass spectrum from the ionisation event, confusing the resulting data.

3.6. Ion Trap Storage Time-of-Flight Mass Spectrometry

The first ITS/TOF mass spectrometer was reported by Michael *et al.* in 1992 [89]. This device is illustrated in Figure 3.18. A syringe pump was used to deliver analyte solution through a 50 µm ID capillary, with a heater being used for vaporisation. With flow rates in the region of 50 µL min^{-1}, a differential pumping stage was required, with a skimmer being used to transfer vaporised analyte to the ion trap. The heater was set in the range 90 - 110ºC, but analyte temperature would be expected to be much lower due to expansion and solvent evaporation. UV laser radiation (λ = 266 nm) was used for ionisation, which passed through a hole in the ion trap ring electrode as illustrated in Figure 3.18. Ions created in this process are trapped by the oscillating potential applied to the ring electrode. Both end cap electrodes are maintained at 0 V for the duration of ion storage.

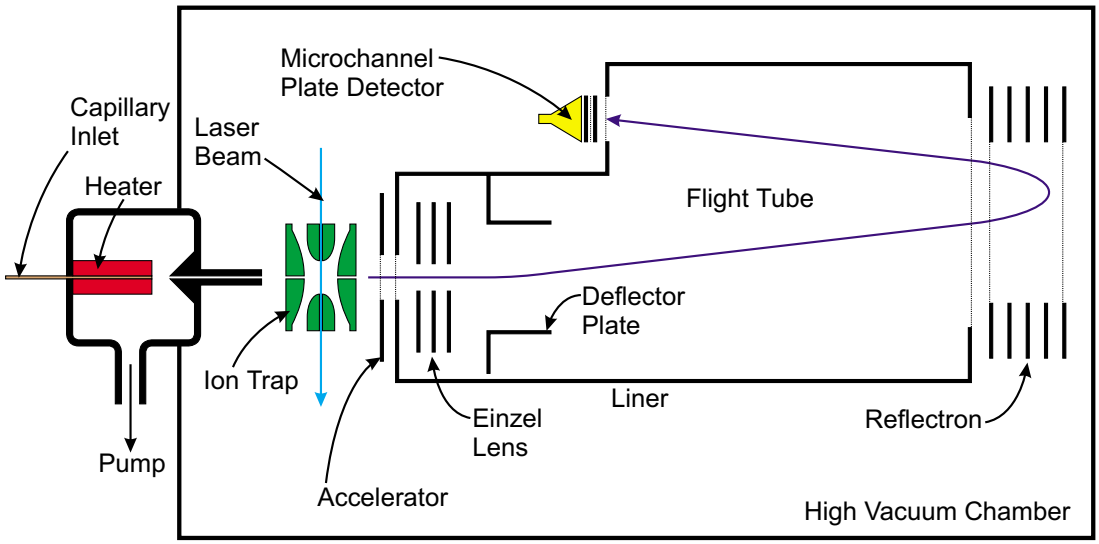

Figure 3.18. Schematic diagram of an ion trap storage reflectron time-of-flight mass spectrometer. Purple arrow indicates the flight path of the ions.

Extraction of ions into the mass analyser is accomplished by first switching off the oscillating potential applied to the ring electrode and then applying a dc pulse to the end cap closest to the flight tube. The flight tube uses a liner typically held in the region of -1300 V to allow the extraction process to function at relatively low voltages. Ions exiting the ion trap pass through an acceleration grid, followed by an Einzel lens, and are then deflected towards the reflectron and microchannel plate

(MCP) detector. Extraction was attempted without turning off the trapping potential, but was found to be unsatisfactory.

This work was extended with the addition of external ion sources to the system. First, a pneumatic nebuliser was used in conjunction with an electrical discharge to provide a stream of ions to the trap [90], followed by the addition of an ESI source [91]. A comparison of these atmospheric pressure ion sources is available [92]. The addition of these external sources naturally necessitated further ion optics and differential pumping prior to the ion trap. Also, in the case of ions formed outside the trap, a small positive voltage had to be applied to the ion trap end cap electrodes to retain high-energy ions. This work was followed by the addition of a MALDI source, where ionisation was performed inside the ion trap [93]. The sample solution was applied to a Macor probe tip, air dried and then the probe inserted directly into the ion trap through a hole in the ring electrode. The probe was inserted so that its tip was flush with the inner surface of the ring electrode. Laser irradiation at 266 nm was used in these studies.

Reports on the use of the system to gain fragmentation data with the ESI [94] and MALDI [95] sources followed. The ITS/TOF mass spectrometer has also been interfaced to CE [96,97]. The electrospray interface was used, with the terminus of the CE capillary etched to produce a fine needle and silver coated to establish an electrical contact. No sheath flow was required. Open-tubular CEC/MS has also been performed using an electrospray interface and the ITS/TOF [98]. A final reported use of the ITS/TOF by Lubman's group is worthy of note here [99]. In this work a continuous flow MALDI interface was reported, with an injection valve used to add samples to a continually running stream of liquid matrix. This stream was terminated in the ring electrode of the ion trap, with the use of a flow probe preventing electrical contact with the ring electrode. An IR heater was used to prevent freezing of the matrix, and a focused UV laser operating at 266 nm was used for sample photoionisation.

---

[1] J. G. Dorsey, *Microchem. J.*, **1999**, *61*, 6-11.

[2] W. H. McFadden, *J. Chromatogr. Sci.*, **1979**, *17*, 2-16.

[3] J. Abian, *J. Mass Spectrom.*, **1999**, *34*, 157-168.

[4] E. Gelpí, *J. Mass Spectrom.*, **2002**, *37*, 241-253.

[5] R. E. Lovins, S. R. Ellis, G. D. Tolbert and C. R. McKinney, *Anal. Chem.*, **1973**, *45*, 1553-1556.

[6] R. E. Lovins, J. Craig, F. Thomas and C. McKinney, *Anal. Biochem.*, **1972**, *47*, 539-549.

[7] V. L. Tal'roze, G. V. Karpov, I. G. Gorodetskii and V. E. Skurat, *Russ. J. Phys. Chem.*, **1968**, *42*, 1658-1664.

[8] V. L. Tal'roze, G. V. Karpov, I. G. Gorodetskii and V. E. Skurat, *Russ. J. Phys. Chem.*, **1968**, *42*, 1664-1667.

[9] V. L. Tal'roze, G. V. Karpov, I. G. Gorodetskii and V. E. Skurat, *Russ. J. Phys. Chem.*, **1969**, *43*, 198-201.

[10] V. L. Tal'roze, V. E. Skurat and G. V. Karpov, *Russ. J. Phys. Chem.*, **1969**, *43*, 241-242.

[11] M. A. Baldwin and F. W. McLafferty, *Org. Mass Spectrom.*, **1973**, *7*, 1111-1112.

[12] P. Arpino, M. A. Baldwin and F. W. McLafferty, *Biomed. Mass Spectrom.*, **1974**, *1*, 80-82.

[13] P. J. Arpino, B. G. Dawkins and F. W. McLafferty, *J. Chromatogr. Sci.*, **1974**, *12*, 574-578.

[14] A. Melera, *Adv. Mass Spectrom.*, **1980**, *8B*, 1597-1615.

[15] E. C. Horning, M. G. Horning, D. I. Carroll, I. Dzidic and R. N. Stillwell, *Anal. Chem.*, **1973**, *45*, 936-943.

[16] D. I. Carroll, I. Dzidic, R. N. Stillwell, M. G. Horning and E. C. Horning, *Anal. Chem.*, **1974**, *46*, 706-710.

[17] E. C. Horning, D. I. Carroll, I. Dzidic, K. D. Haegele, M. G. Horning and R. N. Stillwell, *J. Chromatogr.*, **1974**, *99*, 13-21.

[18] E. C. Horning, D. I. Carroll, I. Dzidic, K. D. Haegele, M. G. Horning and R. N. Stillwell, *J. Chromatogr. Sci.*, **1974**, *12*, 725-729.

[19] D. I. Carroll, I. Dzidic, R. N. Stillwell, K. D. Haegele and E. C. Horning, *Anal. Chem.*, **1975**, *47*, 2369-2373.

[20] R. P. W. Scott, C. G. Scott, M. Munroe and J. Hess, Jr., *J. Chromatogr.*, **1974**, *99*, 395-405.

[21] W. H. McFadden, H. L. Schwartz and L. Evans, *J. Chromatogr.*, **1976**, *122*, 389-396.

[22] R. D. Smith and A. L. Johnson, *Anal. Chem.*, **1981**, *53*, 738-739.

[23] M. J. Hayes, E. P. Lankmayer, P. Vouros, B. L. Karger and J. M. McGuire, *Anal. Chem.*, **1983**, *55*, 1745-1752.

[24] P. R. Jones and S. K. Yang, *Anal. Chem.*, **1975**, *47*, 1000-1003.

[25] T. Takeuchi, Y. Hirata and Y. Okumura, *Anal. Chem.*, **1978**, *50*, 659-660.

[26] R. J. Buehler, E. Flanigan, L. J. Greene and L. Friedman, *J. Am. Chem. Soc.*, **1974**, *96*, 3990-3999.

[27] C. R. Blakley, M. J. McAdams and M. L. Vestal, *J. Chromatogr.*, **1978**, *158*, 261-276.

[28] C. R. Blakley, J. J. Carmody and M. L. Vestal, *Anal. Chem.*, **1980**, *52*, 1636-1641.

[29] C. R. Blakley, J. J. Carmody and M. L. Vestal, *J. Am. Chem. Soc.*, **1980**, *102*, 5931-5933.

[30] C. R. Blakley and M. L. Vestel, *Anal. Chem.*, **1983**, *55*, 750-754.

[31] J. Zeleny, *Phys. Rev.*, **1914**, *3*, 69-91.

[32] J. Zeleny, *Proc. Camb. Philos. Soc.*, **1915**, *18*, 71-83.

[33] J. Zeleny, *Phys. Rev.*, **1917**, *10*, 1-6.

[34] R. B. Cole (Editor), *Electrospray Ionisation Mass Spectrometry: Fundamentals, Instrumentation and Applications*, John Wiley and Sons, New York, **1997**.

[35] R. B. Cole, *J. Mass Spectrom.*, **2000**, *35*, 763-772.

[36] M. Dole, R. L. Hines, L. L. Mack, R. C. Mobley, L. D. Ferguson and M. B. Alice, *Macromol.*, **1968**, *1*, 96-97.

[37] M. Dole, L. L. Mack, R. L. Hines, R. C. Mobley, L. D. Ferguson and M. B. Alice, *J. Chem. Phys.*, **1968**, *49*, 2240-2249.

[38] J. V. Iribarne and B. A. Thomson, *J. Chem. Phys.*, **1976**, *64*, 2287-2294.

[39] B. A. Thomson and J. V. Iribarne, *J. Chem. Phys.*, **1979**, *71*, 4451-4463.

[40] M. Yamashita and J. B. Fenn, *J. Phys. Chem.*, **1984**, *88*, 4451-4459.

[41] M. Yamashita and J. B. Fenn, *J. Phys. Chem.*, **1984**, *88*, 4671-4675.

[42] A. P. Bruins, T. R. Covey and J. D. Henion, *Anal. Chem.*, **1987**, *59*, 2642-2646.

[43] D. B. Hager and N. J. Dovichi, *Anal. Chem.*, **1994**, *66*, 1593-1594.

[44] D. B. Hager, N. J. Dovichi, J. Klassen and P. Kebarle, *Anal. Chem.*, **1994**, *66*, 3944-3949.

[45] Y. Ito, T. Takeuchi, D. Ishii and M. Goto, *J. Chromatogr.*, **1985**, *346*, 161-166.

[46] R. M. Caprioli, T. Fan and J. S. Cottrell, *Anal. Chem.*, **1986**, *58*, 2949-2954.

[47] R. M. Caprioli, *Anal. Chem.*, **1990**, *62*, 477A-485A.

[48] F. Hillenkamp, M. Karas, R. C. Beavis and B. T. Chait, *Anal. Chem.*, **1991**, *63*, 1193A-1203A.

[49] L. Li, A. P. L. Wang and L. D. Coulson, *Anal. Chem.*, **1993**, *65*, 493-495.

[50] D. S. Nagra and L. Li, *J. Chromatogr. A*, **1995**, *711*, 235-245.

[51] K. K. Murray and D. H. Russell, *Anal. Chem.*, **1993**, *65*, 2534-2537.

[52] K. K. Murray, T. M. Lewis, M. D. Besson and D. H. Russell, *Anal. Chem.*, **1994**, *66*, 1601-1609.

[53] J. A. Olivares, N. T. Nguyen, C. R. Yonker and R. D. Smith, *Anal. Chem.*, **1987**, *59*, 1230-1232.

[54] R. D. Smith, C. J. Barinaga and H. R. Udseth, *Anal. Chem.*, **1988**, *60*, 1948-1952.

[55] J. H. Wahl, D. R. Goodlet, H. R. Udseth and R. D. Smith, *Anal. Chem.*, **1992**, *64*, 3194-3196.

[56] R. D. Minard, D. Chin-Fatt, P. Curry, Jr. and A. G. Ewing in *Proceedings of the 36th Annual Conference on Mass Spectrometry and Allied Topics*, San Francisco, CA, **1988**, 950-951.

[57] E. D. Lee, W. Mück, J. D. Henion and T. R. Covey, *J. Chromatogr.*, **1988**, *458*, 313-321.

[58] E. D. Lee, W. M. Mück, J. D. Henion and T. R. Covey, *Biomed. Environ. Mass Spectrom.*, **1989**, *18*, 844-850.

[59] R. M. Caprioli, W. T. Moore, M. Martin, B. B. DaGue, K. Wilson and S. Moring, *J. Chromatogr.*, **1989**, *480*, 247-257.

[60] S. K. Chowdhury and B. T. Chait, *Anal. Chem.*, **1991**, *63*, 1660-1664.

[61] D. C. Gale and R. D. Smith, *Rapid Commun. Mass Spectrom.*, **1993**, *7*, 1017-1021.

[62] J. H. Wahl and R. D. Smith, *J. Cap. Elec.*, **1994**, *1*, 62-71.

[63] J. Cai and J. Henion, *J. Chromatogr. A*, **1995**, *703*, 667-692.

[64] S. Y. Chang and E. S. Yeung, *Anal. Chem.*, **1997**, *69*, 2251-2257.

[65] J. Preisler, P. Hu, T. Rejtar, and B. L. Karger, *Anal. Chem.*, **2000**, *72*, 4785-4795.

[66] T. Tsuda, *Anal. Chem.*, **1987**, *59*, 521-523.

[67] E. R. Verheij, U. R. Tjaden, W. M. A. Niessen and J. van der Greef, *J. Chromatogr.*, **1991**, *554*, 339-349.

[68] M. Hugener, A. P. Tinke, W. M. A. Niessen, U. R. Tjaden and J. van der Greef, *J. Chromatogr.*, **1993**, *647*, 375-385.

[69] K. Schmeer, B. Behnke and E. Bayer, *Anal. Chem.*, **1995**, *67*, 3656-3658.

[70] D. B. Gordon, G. A. Lord and D. S. Jones, *Rapid Commun. Mass Spectrom.*, **1994**, *8*, 544-548.

[71] D. B. Gordon, G. A. Lord, L. W. Tetler and C. M. Carr, *J. Chromatogr. A*, **1995**, *700*, 27-33.

[72] S. J. Lane, R. Boughtflower, C. Paterson and T. Underwood, *Rapid Commun. Mass Spectrom.*, **1995**, *9*, 1283-1287.

[73] S. J. Lane, R. Boughtflower, C. Paterson and M. Morris, *Rapid Commun. Mass Spectrom.*, **1996**, *10*, 733-736.

[74] M. S. Wilm and M. Mann, *Int. J. Mass Spectrom. Ion Processes*, **1994**, *136*, 167-180.

[75] G. A. Valaskovic, N. L. Kelleher, D. P. Little, D. J. Aaserud and F. W. McLafferty, *Anal. Chem.*, **1995**, *67*, 3802-3805.

[76] G. A. Lord, D. B. Gordon, P. Myers and B. W. King, *J. Chromatogr. A*, **1997**, *768*, 9-16.

[77] M. Guilhaus, *J. Mass Spectrom.*, **1995**, *30*, 1519-1532.

[78] R. J. Cotter, *Anal. Chem.*, **1992**, *64*, 1027A-1039A.

[79] B. A. Mamyrin, *Int. J. Mass Spectrom.*, **2001**, *206*, 251-266.

[80] W. C. Wiley and T. H. McLaren, *Rev. Sci. Instrum.*, **1955**, *20*, 1150-.

[81] B. A. Mamyrin, V. J. Karatajev, D. V. Schmikk and V. A. Zagulin, *Sov. Phys. JETP*, **1973**, *37*, 45-48.

[82] W. Paul, *Angew. Chem. Int. Ed. Engl.*, **1990**, *29*, 739-748.

[83] R. E. March, *J. Mass Spectrom.*, **1997**, *32*, 351-369.

[84] R. J. Cotter, *Anal. Chem.*, **1984**, *56*, 485A-504A.

[85] M. A. Posthumus, P. G. Kistemaker, H. L. C. Meuzelaar and M. C. Ten Noever de Brauw, *Anal. Chem.*, **1978**, *50*, 985-991.

[86] H. v. Weyssenhoff, H. L. Seltze, E. W. Schlag, *Z. Naturforsch.*, **1985**, *40a*, 674-676.

[87] B. Lindner and U. Seydel, *Anal. Chem.*, **1985**, *57*, 895-899.

[88] M. J. Dale, *Laser Desorption Laser Photoionisation Time-of-Flight Mass Spectrometry*, PhD Thesis, University of Edinburgh, **1994**.

[89] S. M. Michael, M. Chien and D. M. Lubman, *Rev. Sci. Instrum.*, **1992**, *63*, 4277-4284.

[90] B. M. Chien, S. M. Michael and D. M. Lubman, *Anal. Chem.*, **1993**, *65*, 1916-1924.

[91] S. M. Michael, B. M. Chien and D. M. Lubman, *Anal. Chem.*, **1993**, *65*, 2614-2620.

[92] B. M. Chien, S. M. Michael and D. M. Lubman, *Int. J. Mass Spectrom. Ion Processes*, **1994**, *131*, 149-179.

[93] B. M. Chien, S. M. Michael and D. M. Lubman, *Rapid Commun. Mass Spectrom.*, **1993**, *7*, 837-843.

[94] B. M. Chien and D. M. Lubman, *Anal. Chem.*, **1994**, *66*, 1630-1636.

[95] S. T. Fountain, H. Lee and D. M. Lubman, *Rapid Commun. Mass Spectrom.*, **1994**, *8*, 407-416.

[96] J. -T. Wu, M. G. Qian, M. X. Li, L. Liu and D. M. Lubman, *Anal. Chem.*, **1996**, *68*, 3388-3396.

[97] M. X. Li, J. -T. Wu, L. Liu and D. M. Lubman, *Rapid Commun. Mass Spectrom.*, **1997**, *11*, 99-108.

[98] J. –T. Wu, P. Huang, M. X. Li, M. G. Qian and D. M. Lubman, *Anal. Chem.*, **1997**, *69*, 320-326.

[99] L. He, L. Liang and D. M. Lubman, *Anal. Chem.*, **1995**, *67*, 4127-4132.

4. Chromatographic and Mass Spectrometric Instrumentation

In this chapter, a full description of the instrumentation used in this work is given. The method of preparation of columns for use in CE is described, along with the preparation of columns for use in CEC. This is followed by a description of how the shared electroseparation instrumentation was used for both techniques. HPLC data is compared with CEC data in Section 5.1, so the operation of the available HPLC instrument is also described. Certain tests, which were carried out to evaluate the performance of the separation instruments, are then described. This is followed by a description of the ITS/TOF mass spectrometer used in this work. The lasers used for vaporisation and ionisation are then introduced, prefaced with the instrumentation used to control their timing. Finally, the oscilloscope used to collect raw data and the computer system used to store and process this data are detailed.

4.1. The Separation Column

4.1.1. Properties of Fused Silica Capillaries

Glass tubes have been used to contain stationary phases since the inception of chromatography [1]. Most glasses are mixtures of SiO_2 and significant quantities of metal oxides [2]. For example, the major components of ordinary window or bottle glass (soda lime glass) are SiO_2, Na_2O and CaO, present at 74%, 16% and 5%, respectively, by mass. The major components of laboratory glass (borosilicate glass) in contrast are SiO_2, B_2O_3 and Na_2O, present at 80%, 13% and 4%, respectively, by mass. Soda lime glass is poorly resistant to high temperatures and sudden changes in temperature, while borosilicate glass has high resistance to temperature change and chemical corrosion. Fused silica is a type of glass that is almost 100% SiO_2.

The primary advantage of using glasses when making capillary columns is that they can be drawn out from blanks to the required dimensions. Drawn glass capillary tubing was introduced in the field of GC by Desty *et al.* in 1959 [3]. Fused silica capillaries were not introduced to GC until 1979 by Dandeneau and Zerenner [4],

presumably because drawing fused silica requires much higher temperatures than those required for metal oxide rich glasses. Fused silica was immediately recognised as having superior flexibility, and being inherently more inert than metal oxide rich glasses. Bare fused silica, however, rapidly becomes weak and brittle on exposure to moist air due to stress corrosion [5], requiring an external coating to maintain strength and flexibility. Coatings can also improve the mechanical properties of metal oxide rich glass capillaries [6], but such capillaries have not gained widespread acceptance. Using fused silica in place of other well-understood glasses, however, required new surface coating methods to be developed.

Fused silica is produced from the fusion of silica sand at very high temperatures (> 2000ºC) using either an electrically powered furnace or a flame fusion process. The properties of fused silica are summarised below [7].

- Transparent from 180 to 3500 nm
- Chemically resistant to acids, except phosphoric acid above 200ºC and hydrofluoric acid at all temperatures; slow reaction with alkalis and some metal oxides
- Good electrical insulator (2×10^{14} ohm cm at 20ºC)
- Low thermal conductivity and thermal expansion
- Can be polished to a fine finish

The fused silica capillaries used in this work were supplied by Composite Metal Services (Worcester, UK) [8] but were manufactured by Polymicro Technologies (Phoenix, AZ, USA) [9]. The capillaries used were all circular cylindrical tubes, although square cylindrical tubes are also available from Polymicro Technologies. Polymicro Technologies supply capillaries with IDs ranging from 2 to 700 µm and outer diameters (ODs) ranging from 150 to 850 µm. The most common capillary used here has an ID = 100 ± 6 µm and an OD = 363 ± 12 µm, with a coating thickness of approximately 20 µm giving a final average OD of 403 µm. Polymicro Technologies claim that their fused silica capillaries can withstand pressures of over 10^5 psi (0.69×10^9 Pa), but it must be borne in mind that a small scratch that allows moisture to reach the bare fused silica can make the capillary very brittle. Usually the coating material is a polyimide, but a less robust transparent coating is also available.

With standard polyimide coating the capillary is flexible, robust, and is useable up to 350°C.

4.1.2. Preparation of Fused Silica Capillaries for use in Separations

When cutting a section of capillary to a desired length it is essential that end faces are obtained that are clean, flat and perpendicular with respect to the capillary axis. Good quality cuts are vital for use in analytical separations. The capillary can be cut using a device such as Supelco's (Poole, UK) [10] Capillary Cleaving Tool. This tool has sapphire cutting edges that are used to cut through the polyimide capillary coating to score the underlying fused silica. The capillary is then pulled apart and the new end faces are carefully inspected. An alternative cleaving tool, which requires less dexterity, is Scientific Glass Technology's (Middelburg, The Netherlands) [11] Shortix Capillary Column Cutter. This device clamps the capillary in place and uses a rotating diamond blade to cut the capillary. Results using this tool were found to be good, although not significantly better than those found with the simpler cleaving tool.

In order to produce an absorbance detection window, the polyimide capillary coating must be removed. There are a variety of approaches to accomplish this. The easiest method is to simply burn off the coating using a flame, with cool flames (e.g. butane flame from a cigarette lighter) leaving the capillary brittle at the window and hot flames (oxy-hydrogen flame is recommended by Polymicro Technologies) causing less damage. Very hot flames, however, are difficult to use in a standard laboratory environment, and all flames tend to produce windows that are too wide. Ovens capable of temperatures in the region of 600°C can be used to remove the polyimide from large sections of capillary with minimal damage, but are not suitable for the production of windows. Similar but localised conditions are obtained with an electric heating coil [12], with good results being obtained provided that the capillary does not touch the coil. A further method is to use hot (100°C) sulfuric acid, which, as with the very hot flame, requires a specialised laboratory set up. Polymicro Technologies state that the best method to remove the polyimide coating is to burn it off using a continuous wave (i.e. not pulsed) CO_2 laser. However, absorbance

window strength was rarely critical, so the most common methods employed were electric heating coils and cool flames.

To perform CE all that is required is that the capillary is cut to an appropriate length, and a window for absorbance detection is made at an appropriate location. The capillary may then be mounted in an appropriate instrument and conditioned ready for use. For CEC, however, a stationary phase must be added and retained.

4.1.3. Stationary Phases

Stationary phases can be bonded to the inner surface of especially narrow capillaries to produce a chromatographic column [13], but it was usual in the present work to pack wider capillaries with silica particles to which the stationary phase had already been bonded. The simplest stationary phases are composed of porous silica spheres, with consistent pore size, and a narrow particle size distribution, to which hydrocarbon chains of a certain length have been bonded. This results in the presence of a hydrophobic environment in the vicinity of the surface. Hydrophilic analytes move quickly through the column, while hydrophobic analytes are retained in the stationary phase. This type of chromatography is classed as 'reversed phase'. Hydrophobic molecules can be made to move more quickly through the column by increasing the hydrophobicity of the mobile phase. Hydrophilic molecules on the other hand may be difficult to separate, and might best be analysed under 'normal phase' conditions.

HPLC stationary phases are often used in CEC without any modification. Stationary phases in CEC, however, are required to provide surface charges to support EOF. Stationary phases consisting of silica particles coated in hydrocarbon chains will contain a good number of residual non-derivatised silanol groups that will dissociate under appropriate conditions to produce the required charged surface. However, low surface charge concentration will, especially at low pH, result in low EOF rates. Moreover, modern stationary phases are designed to cap as many of these groups as possible, since they can result in interactions between analyte and surface that are detrimental to the separation.

To address these problems new CEC stationary phases have been developed, which incorporate charged groups to increase the EOF rate, and which also widen the pH range over which CEC can be performed effectively. A common solution is to use short hydrocarbon chains capped with sulfonic acid groups. This type of stationary phase is known as Strong Cation Exchange (SCX) due to its original purpose. A mixture of sulfonic acid terminated hydrocarbon chains and bare hydrocarbon chains can be used to produce what is known as Mixed Mode stationary phase. In this work two types of stationary phase have been used for CEC, specifically Hypersil Mixed Mode (3 µm diameter particles) and Hypersil ODS (octadecylsilyl) (3 µm diameter particles). The performance of such stationary phases in CEC has been investigated by Smith and Evans [14].

4.1.4. Mobile Phases

CE mobile phases are typically aqueous electrolytes, while for CEC they usually consist of a mixture of an aqueous electrolyte and acetonitrile or methanol. A considerable amount of organic solvent is required in the CEC mobile phases in order to perform reversed phase chromatography. CEC mobile phase mixtures are made up as aqueous solutions of electrolyte in water to which an appropriate volume of acetonitrile or methanol is added. It is essential for both techniques that mobile phases are carefully degassed immediately prior to use by stirring while under vacuum or while sparging with helium. Mobile phase degassing is most critical in CEC due to the fact that flushing the column with fresh mobile phase is much more difficult than in CE. A high-pressure pump must be used, and with all handling there is a risk of damaging the column.

Commonly used electrolytes included sodium phosphate, ammonium acetate, and tris(hydroxymethyl)aminomethane (TRIS). Ammonium acetate, being volatile, is especially suitable for mass spectrometry, while TRIS was useful because of its low conductivity. These electrolytes were often used as pH buffers, but were not exclusively used in their pH buffering ranges. While application of large electrical potentials to aqueous solutions will naturally result in the production of H^+ ions at the anode and OH^- ions at the cathode, production of only small amounts would be

expected due to the low currents found when performing CE and CEC. Changes in pH would therefore be expected to be small. However, use of this effect has interestingly been made in capillary isoelectric focusing [15].

4.1.5. Packing Capillaries for CEC

(1) Capillary Packing Apparatus

The apparatus used to pack fused silica capillaries with stationary phase coated silica particles is similar to that described previously by Boughtflower *et al.* [16,17] and is illustrated in Figure 4.1 below. To successfully produce a packed column, a well-suspended slurry of particles is forced as rapidly as possible into an empty capillary. The heart of the apparatus is the slurry ultrasonication chamber [17]. This chamber has a volume of ~ 4 mL, and is used to maintain a suspension of the slurry just before and during the packing process. Solvent is delivered into the chamber at high pressure with slurry being forced out of the chamber into the capillary.

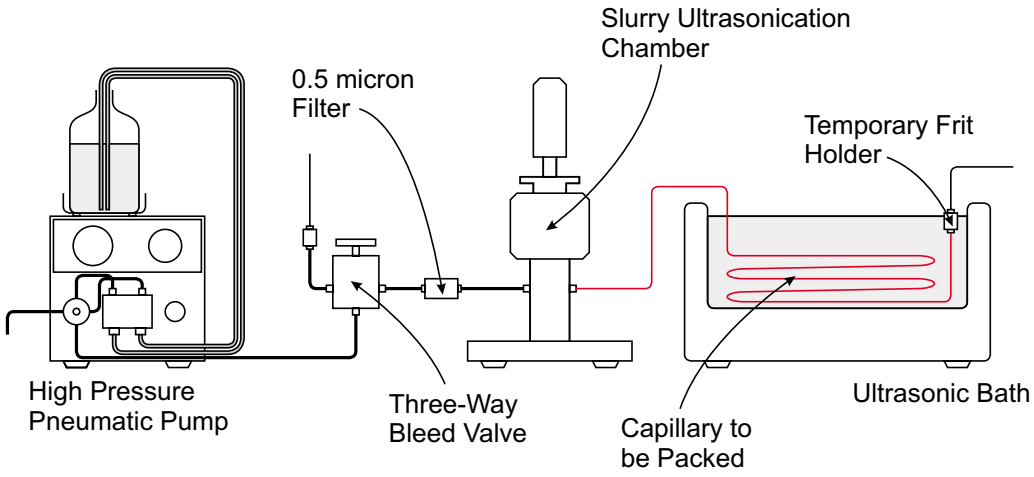

Figure 4.1. Apparatus used for the production of packed columns. The capillary to be packed is highlighted in red.

The high-pressure pneumatic pump that powers the system is a Knauer (Berlin, Germany) [18] WellChrom Pneumatic HPLC Pump K-1900, fitted with a 100 mL pump head, which is capable of a maximum output pressure of 1000 bar and a maximum flow rate of 300 mL min^{-1}. The pump itself is powered by compressed air and is connected via a three-way bleed valve followed by a 0.5 µm filter to the slurry

ultrasonication chamber. The purpose of the bleed valve is to allow system pressure to be reduced slowly at the end of the packing process in order to avoid disturbing the newly packed bed. The filter is included to prevent silica stationary phase particles from being washed back through the system and damaging the valve or the pump. A length of narrow capillary is fitted to the third port of the bleed valve to provide some resistance to flow, therefore assisting in the process of gently reducing system pressure.

The slurry ultrasonication chamber is illustrated in greater detail in Figure 4.2. The ultrasonic probe tip is directly attached to an ultrasonic probe. The probe and associated control electronics, designated the Miniprobe 55T, were obtained from Kerry Ultrasonics (Hitchin, UK) [19] and are capable of delivering ultrasound at 55 kHz with a maximum power output of 25 W. The point where the probe tip is clamped into the chamber is a vibrational node in order to avoid damping the output. Polyetheretherketone (PEEK) washers compress a Kalrez O-ring (supplied by James Walker (Old Woking, UK) [20]) into the available space to make the seal between the chamber and the probe tip. Kalrez and PEEK were chosen because of their excellent chemical resistance. The seal between the upper and lower parts of the chamber is achieved using another Kalrez O-ring, while other connections are sealed with standard chromatographic fittings and Teflon tape.

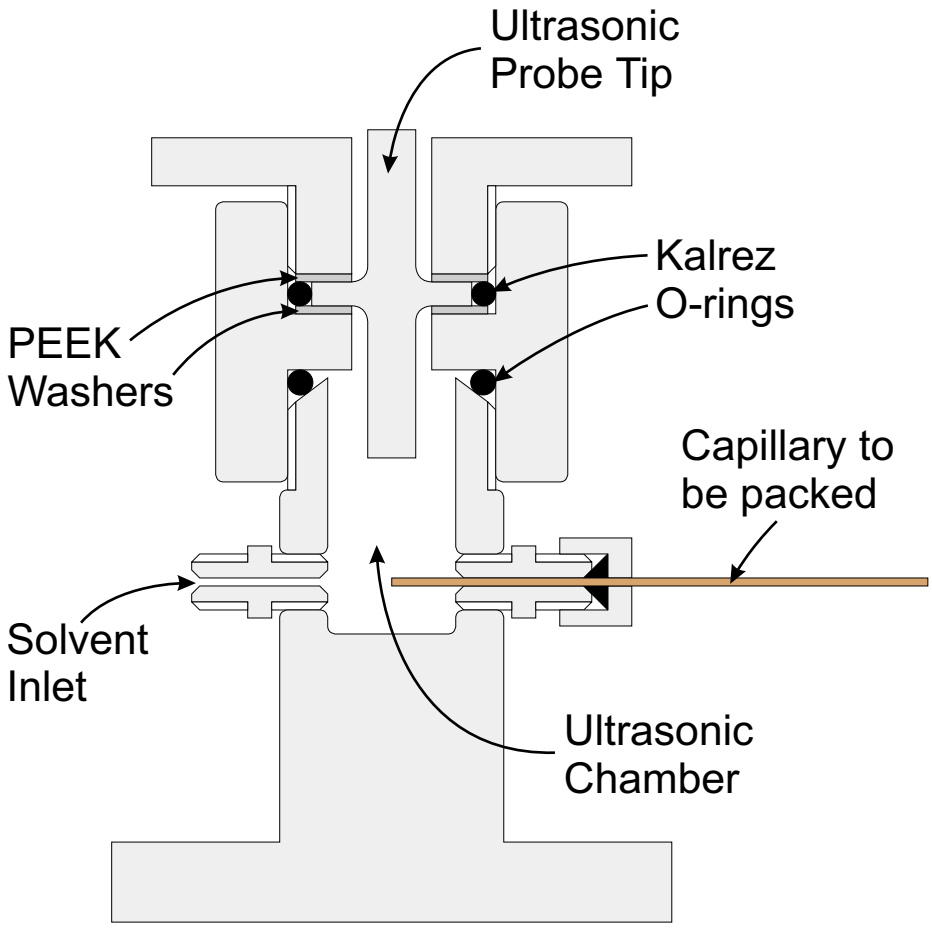

Figure 4.2. Detailed view of the slurry ultrasonication chamber.

The capillary to be packed is connected directly to the slurry chamber, with its inlet located close to the centre of the chamber. The outlet is terminated in a union, illustrated in Figure 4.3, that contains a fine steel mesh (temporary frit) that allows solvent but not packing material to pass [21]. The union is connected to a further section of narrow capillary to allow solvent flow out of the column to be easily observed. As much as possible of the capillary to be packed is immersed in an ultrasonic bath, reducing the probability of void formation during packing [22].

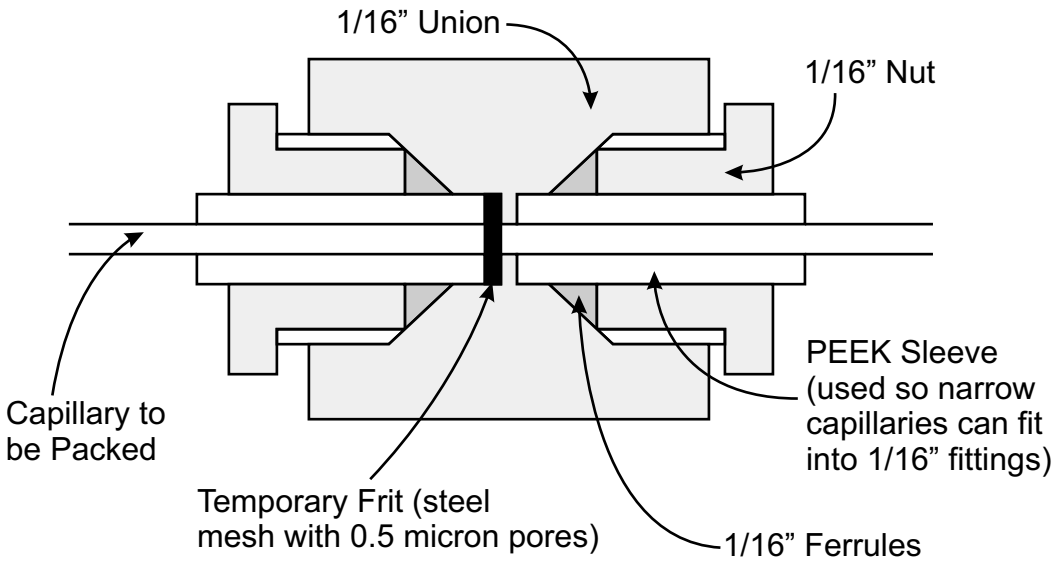

Figure 4.3. Union used to hold the temporary frit to the end of the capillary to be packed.

(2) Capillary Packing Procedure

Before use, the filter is checked to ensure adequate flow, and the tubing prior to the slurry chamber is flushed with the packing solvent, acetone (chosen for its low viscosity). The capillary is then connected to the slurry chamber, with its inlet positioned approximately at the centre of the chamber, as illustrated in Figure 4.2. For a 100 µm ID capillary, lengths of over 1 m can be packed successfully. The temporary frit is then attached to the capillary outlet. The capillary must initially be dry. Since as much of the capillary as possible should be immersed in the ultrasonic bath, it is typically wound around a support frame.

A slurry of the required stationary phase coated silica particles is prepared at a concentration of $\sim 100\ \mathrm{mg\ mL^{-1}}$ in acetone. This slurry is then subjected to ultrasonication for at least fifteen minutes to ensure a consistent suspension. Around 3 mL of this slurry is transferred quickly to the slurry chamber, and the ultrasonic probe switched on to maintain the suspension. The ultrasonic bath should also be switched on at this point. The pump is then switched on without delay, applying a pressure of around 800 bar to the system. The slurry is forced out of the chamber and down the column at high speed. Rapid column packing is essential to reduce the

probability of void formation in the packed bed. Pressure is applied for around fifteen minutes before being gently released using the three-way valve.

When the pressure is released, the remaining slurry can be recovered from the packing chamber and used again. The nascent column is detached and the packing chamber replaced with a chromatographic union (after the tubing has been purged with water). An electric heating coil (Innovatech, Stevenage, UK) [23] is then added to the system. The electric heating coil is used to produce retaining frits by sintering silica particles together, and was placed near the union that replaces the slurry chamber. The purging process is essential because the volume of the pump and tubing is very large in relation to the flow rates found when packing. Without purging new solvent would never reach the column. Purging also blows surplus packing material from the filter and nearby tubing, prolonging filter life. Water, because of its relatively high viscosity, is used in order to collapse voids that might have formed during the packing process. When the column is re-attached, the pump is used to apply a pressure of 800 bar, and the system is left to equilibrate for about twelve hours. No ultrasound is required during this time.

At the end of this period it should be evident that a small volume of water has flowed through the column. The change of solvent also allows the packed bed to be inspected (easiest when held against a matt black background) for any major faults. A frit is then burned at the high-pressure end of the column and the pressure released. The column must be carefully cut at the point where the frit has been made. The temporary frit holder is then removed, the column is reversed, and water is made to flow in the opposite direction (applied pressure 800 bar) in a further attempt to compress the packed bed. After a few more hours, a final frit is burned at the new high-pressure end to complete the column. The column is now ready to be filled with degassed mobile phase and used. Columns are stored so that they do not dry out, the ends being immersed in small solvent-filled vials, sealed with septa to minimise evaporation. Columns can be safely stored in this way for several weeks, with the limiting factor being evaporation of the solvent.

Although every effort is made to compress the packed bed, the column may settle in use due to attraction of the negatively charged silica particles to the anode. This

results in a much more uniformly packed bed, but with a void at the cathode end of the column. This void is removed by attaching the column to the high-pressure pump again, burning a new frit, and then cutting off the section containing the void. A finished column may also be divided up to make a number of smaller columns of a particular desired length. It is important to remember that frits can only be produced under high-pressures and while solvent is flowing.

When producing a capillary for use with absorbance detection, a window is burned before beginning the packing process. The window must be protected during the packing process to avoid fractures. When the column is packed, the initial high-pressure end should be the capillary outlet, and the first frit burned should be at the window. When the column is reversed, the packing material in the intended open part of the column is washed out, and a frit at the capillary inlet can be produced. The reason for making the window before packing is that the window should be as close to the terminal frit as possible. Burning the window on top of the frit location means that the frit gets heated twice, increasing both fragility and the possibility of a blockage forming.

4.1.6. Capillary Images

In this subsection, several images are presented to illustrate important capillary features. Figure 4.4 shows an open capillary while Figure 4.5 shows a packed capillary. Both capillaries are of equal size and are both polyimide coated. Figure 4.6 illustrates typical column damage that is found at the capillary inlet and suspected to be due to arcing that is possibly occurring within bubbles. Figure 4.7 shows a retaining frit at a capillary terminus while Figure 4.8 shows a retaining frit located at an absorbance detection window.

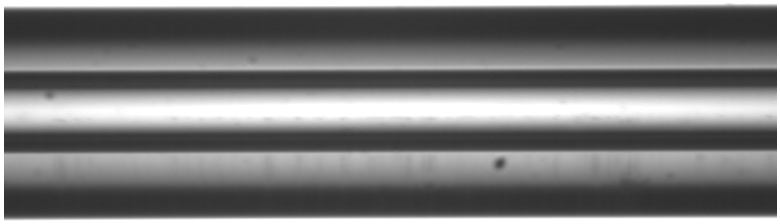

Figure 4.4. Microscope image of an open 100 µm ID, 363 µm OD capillary with polyimide coating intact (total OD = 403 µm). The total OD can be used to give a scale for this image, but the ID is misleading due to refraction in these circular cylindrical capillaries.

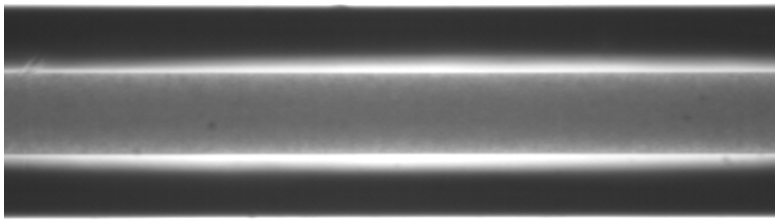

Figure 4.5. Packed column for comparison with previous figure. The polyimide coating is intact and the column dimensions are the same as for Figure 4.4.

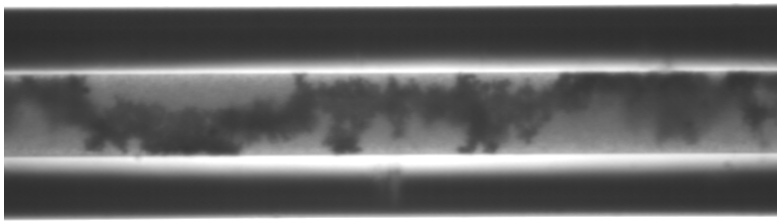

Figure 4.6. Permanent damage caused to packed bed by arcing that is occasionally found near the capillary inlet. The polyimide coating is intact and the column dimensions are the same as for Figure 4.4.

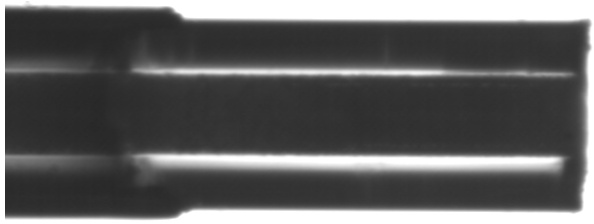

Figure 4.7. Column terminal frit showing the polyimide coating partially removed.

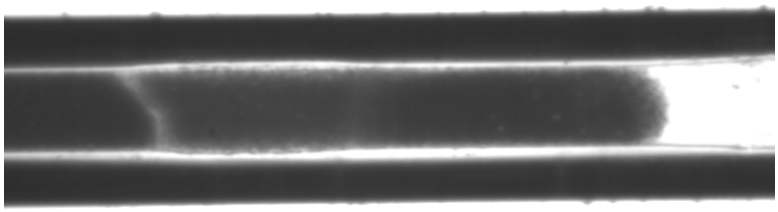

Figure 4.8. Column terminal frit at window. The polyimide coating has been removed and the extent of the frit can easily be seen. It is approximately 1 mm long.

Columns typically end their useful lives due to fractures. Baeuml and Welsch [24] recently suggested that fractures result from acetonitrile causing the capillary coating to swell, but it could be that this swelling simply exposes the capillary to attack by water. It is also possible that the high electrical potentials used are responsible in some way for fractures since columns can be reliably stored for long periods of time without significant degradation in performance. Further work is required in this area.

4.2. Separation Instrumentation

Two instruments were available that were designed for CE. In this section, these instruments are described, together with the procedural modifications required to enable them to be used for CEC. An instrument for the purpose of performing HPLC was also available, which is also described here. All three instruments are capable of outputting absorbance readings as voltages designed for chart recorders, with a device used to permit such analogue data to be recorded to a PC described to complete this section.

4.2.1. Isco 3850 Capillary Electropherograph

The essential components of a CE instrument are an absorbance detector, a high voltage power supply, some means of standardising sample injection, and some means of flushing the capillary. The Isco (Lincoln, NE, USA) [25] 3850 Capillary Electropherograph performs single channel absorbance detection in the range from 190 to 360 nm (deuterium lamp). Absorbance data is output as an analogue signal, with a full range of either 10 mV or 1 V (this at maximum corresponds to an absorbance of 0.002). Electronic smoothing of the output is performed, with a rise time of 0.8 seconds commonly used. The Isco instrument can apply electrical potentials of between –30 and +30 kV in 100 V steps, with current output limited to a maximum of 300 μA.

The capillary inlet is held in a positioning arm, which moves it between an inlet mobile phase reservoir, a sample introduction device and a syringe port for flushing the column. In the unmodified instrument, the high voltage power supply only serves the inlet mobile phase reservoir, with injection being achieved via a flow splitting device, using a small syringe to make the injection. The Electromigration Injection Control Accessory (used in all cases) exchanges the flow splitting device for a sample vial. This sample vial is connected to the high voltage power supply, with the positioning arm able to dip the capillary inlet into the sample vial. This configuration is illustrated in Figure 4.9. The capillary is held in the positioning arm by a soft ferrule, which also allows a tight seal to be made with the flushing block, allowing solvent to be pushed through the column with a syringe. For the ‘Inject’ and ‘Run’ positions the capillary is merely suspended in the solutions. Use of the positioning arm helps standardise the injection process, improving reproducibility. Injection timing is controlled by the Electromigration Injection Control Accessory and, by means of a sealed outlet mobile phase reservoir, vacuum injections can also be performed. The potential necessary for injection is fixed at 5 kV with a rise time of approximately three seconds.

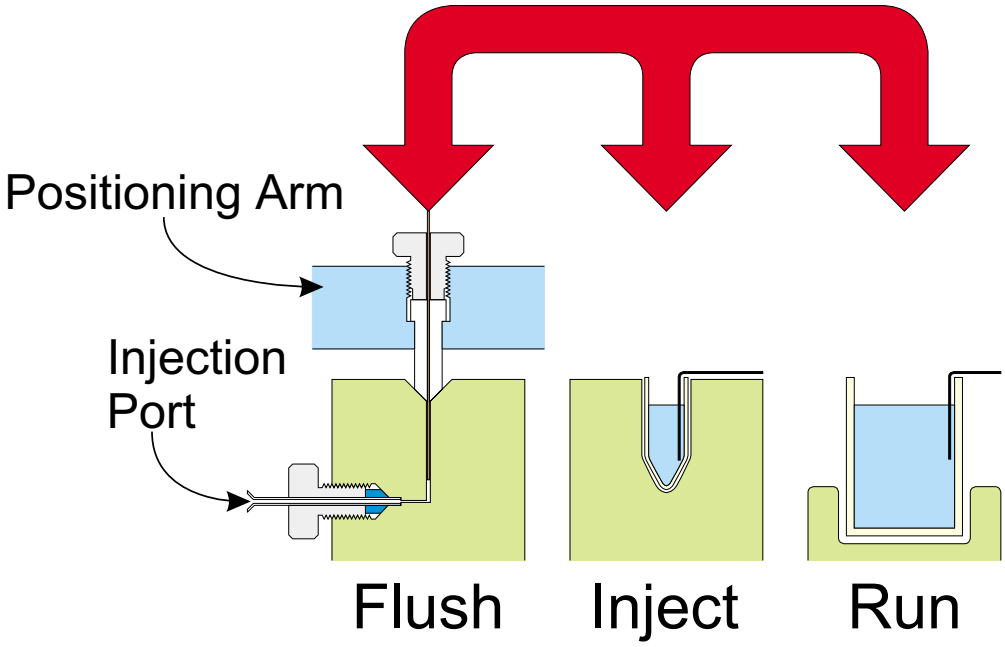

Figure 4.9. Diagrammatic representation of the role of the Isco instrument's positioning arm in capillary flushing and sample injection. The positioning arm lifts and rotates to move the capillary between positions.

The Isco instrument can accommodate capillaries with a minimum length of 30 cm to the window and 50 cm in total. The capillary outlet is placed in a sealed vial (illustrated in Figure 4.10) to which a vacuum can be applied for the purpose of making injections. Care must always be taken to ensure that liquid levels in all vials are equal, thus avoiding siphoning, which degrades the quality of the separation due to the development of laminar flow.

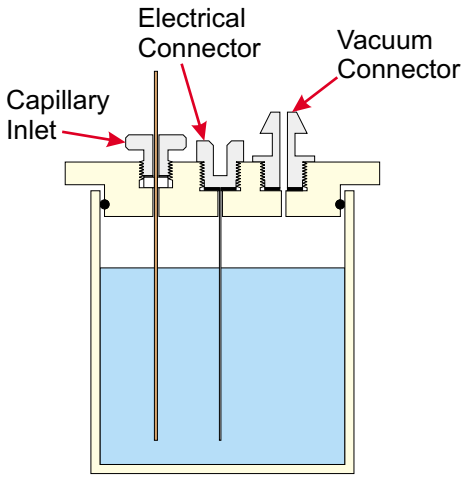

Figure 4.10. Outlet vial used to allow vacuum injections when performing CE.

A typical CE run starts by fitting the capillary into the system and then filling it through the flushing port with 0.1 M NaOH. This etches the inner surface of the capillary, exposing more silanol groups and hence increasing the EOF rate. The capillary is left for some time before being flushed again with 0.1 M NaOH followed by water and then finally with degassed mobile phase. The capillary is moved quickly from the flush position to the run position, and the running potential is applied. If a reasonable current is obtained, the column is allowed to equilibrate for some time. The expected current varies with the mobile phase utilised, while equilibration should ideally be allowed for 30 minutes. If a reasonable current is not obtained, the column is flushed again to remove air bubbles that are likely to have been formed. After equilibration, sample injection is performed by switching off the high voltage, moving the positioning arm to the sample position and applying the injection potential. At the end of the injection period the potential is switched off, and the positioning arm is moved back to the inlet mobile phase reservoir and the running potential applied. The positioning arm aids precision, but a good deal of operator skill is still required.

When using the Isco instrument for CEC the only operational differences are that the column cannot be flushed using a syringe and vacuum injections cannot be performed. Surface treatment with sodium hydroxide is not performed, as this would be expected to damage the stationary phase. A high-pressure pump is used to flush the column and injections can only be performed by application of an electrical

potential. Flushing is only required when installing a new column or when an old column fails due to bubble formation, but should be avoided as it can lead to damage to the column inlet. With a well packed column, flushing is avoided by refilling the inlet mobile phase reservoir with degassed mobile phase at least once a day, and then running the column to flush it with freshly degassed mobile phase.

4.2.2. Waters Capillary Ion Analyzer

The chief advantage of the Waters Capillary Ion Analyzer (CIA) over the Isco instrument is the fully automated injection capability. Like the Isco instrument, the CIA instrument is capable of providing running potentials of between –30 and +30 kV in 100 V steps, but injection is possible at any applied potential within this range (at the same polarity as the running potential). Absorbance detection, however, is achieved by means of a fixed wavelength (214 nm) detector based on a zinc lamp. Therefore, to change detection wavelength the entire detector unit must be exchanged.

The operation of the CIA instrument is based around a carousel that holds four inlet mobile phase reservoirs and twenty sample vials (0.5 mL Eppendorf tubes). These are arranged in four groups, each group of five sharing the same mobile phase reservoir. The high-voltage electrode and capillary inlet are held close together in an arm above the carousel. The carousel is lowered, rotated, and then brought back up again to change the vial or reservoir into which the electrode and capillary are dipped. The capillary outlet originally terminated in a similar carousel designed for fraction collection, but this device has been discarded. Instead the capillary is terminated in an outlet mobile phase reservoir identical to that on the Isco instrument, see Figure 4.10. It was not possible to perform vacuum injections, but the vacuum connector on the outlet mobile phase reservoir was used for flushing the column. The electrode and capillary arm are manually lifted and rotated to access wash vials, again using an applied vacuum to draw liquid through the capillary.

Once a column has been mounted into the system, the electrode and capillary arm are moved to a wash vial filled with 0.1 M NaOH, and a vacuum is applied to flush the column. The column is then flushed with water from a second wash vial. Mobile

phase reservoirs are then filled and finally the vacuum system flushes the column with freshly degassed mobile phase. As with the Isco instrument, before commencing a series of experiments, the levels of mobile phase reservoirs and sample vials should be checked to ensure they are equal. Once flushing is complete the running potential is applied and the resulting current checked to ensure the system is operating properly. The column is then allowed to equilibrate for approximately 30 minutes under the applied potential that will be used for the separation.

The CIA instrument is programmed to control the injection process. The electrical potential applied during an injection, and its duration, are entered into the system. Injection by raising the inlet to promote siphoning is also possible, but was not used. Absorbance data is output either as 10 mV full-scale or 1 V per absorbance unit (designed for use with different chart recorders). When in full-scale mode, the most sensitive setting is 0.001, meaning that a 10 mV signal change represents an absorbance change of 0.001. It is also possible to record the current, and to synchronise injection with an external data system. Such a system, however, was not available, so instead the exact injection time was obtained from chromatogram baseline disturbances. Such baseline disturbances arise from electrical interference within the instrument and are shown in Figure 4.11. The double negative peaks arise when the carousel moves to the sample vial and then after injection when it returns to the inlet mobile phase reservoir. The second peak in the second pair is associated with the running potential being applied. Similar baseline disturbance is evident when using the Isco instrument.

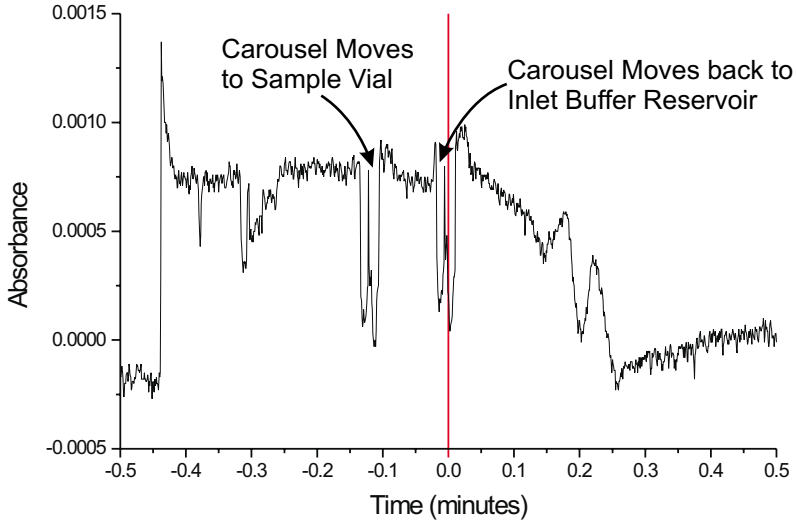

Figure 4.11. Baseline disturbance found during sample injection.

When using the CIA instrument for CEC, vacuum flushing of the columns is not possible, as with the Isco instrument, and therefore a high-pressure pump is utilised. Again it should be noted that flushing with sodium hydroxide is not performed to avoid damaging the stationary phase. With care, flushing is limited by regularly replacing the mobile phase in the inlet reservoir. In both CE and CEC modes, baseline disturbance in the chromatograms can be used to determine the exact start time of a chromatographic run.

4.2.3. Waters 2690 Separations Module and Waters 486 Tunable Absorbance Detector

An instrumental system for HPLC must provide a steady flow of well-mixed degassed mobile phase, some means of injecting sample into the mobile phase stream, and an absorbance detector. The instrument should be programmable so that the proportions of each component of the mobile phase can be varied with time. A sample carousel should be available to allow a large number of samples to be run automatically and the data stored for later analysis. The Waters 2690 Separations Module has a carousel system capable of holding 120 sample vials and is equipped with four solvent reservoirs. The solvent inputs are all equipped with helium sparging, and system control is achieved using an in-built computer. External computer control and data storage are possible but were not employed. Detection is

achieved using a single channel Waters 486 Tunable Absorbance Detector that is capable of operating between 190 and 380 nm. One volt per absorbance unit and 10 mV full-scale outputs are available for recording chromatograms. The instrument is also equipped with a column oven.

4.2.4. Pico Technology ADC-42

Chromatographic data was recorded to a PC using a Pico Technology (St Neots, UK) [26] ADC-42 analogue to digital converter (ADC). The key properties of this device are listed below.

- Fits directly to, and is powered by, the PC parallel port
- Records voltages in the range –5 to +5 V
- 12 bit voltage resolution over this range
- Time resolution of 50 ms
- Software provided so that it works like a chart recorder or an oscilloscope

Since the resolution of the ADC is limited to 2.44 mV, the 10 mV full-scale outputs on the Isco instrument and the CIA instrument could not be used. In the case of the Isco instrument, the ADC was connected directly to the 'One Volt Full Scale' output, while in the case of the CIA instrument the 'One Volt per Absorbance Unit' output was connected to the device via an amplifier. The amplifier was built in-house and provided $\times 100$ voltage amplification. The software supplied with the ADC was capable of displaying a chromatogram in real time, but chromatograms were recorded blind (drawing the graph on screen results in loss of data). Data was exported from the Pico Technology software as an ASCII file for further analysis.

4.3. Evaluation of the Separation Instrument

Some simple tests were performed to characterise and evaluate the performance of the CIA instrument and the HPLC instrument, which are detailed in this section.

4.3.1. Estimating Detector Efficiency for the Waters Capillary Ion Analyzer

The efficiency of the detector system in the CIA instrument was estimated by performing a simple experiment. A 100 µm ID column of total length 100 cm and length to absorbance detection window of 76 cm was filled with 50 mM ammonium acetate and was run at an electrical potential of 20 kV. Five consecutive injections were made of 100, 200, 300, 400 and finally 500 µM 1-naphthalene sulfonic acid in 50 mM ammonium acetate, with injections being performed by programming the instrument to apply 5 kV for 5 seconds while the capillary inlet was dipped into the sample vial. All five runs were recorded as one electropherogram that is shown in Figure 4.12. Baseline disturbances were used to indicate the start time of each individual run and to provide a measure of mobile phase flow rate. This showed that the time required for a neutral solute to reach the detector was 8.562 ± 0.009 minutes, the error being expressed as one standard deviation, corresponding to a flow rate of 690 ± 60 nL min^{-1}. The error increases in going from time to flow rate (0.1% to 8.5%) largely because the ID of the capillary is specified by the manufacturer as 100 ± 6 µm.

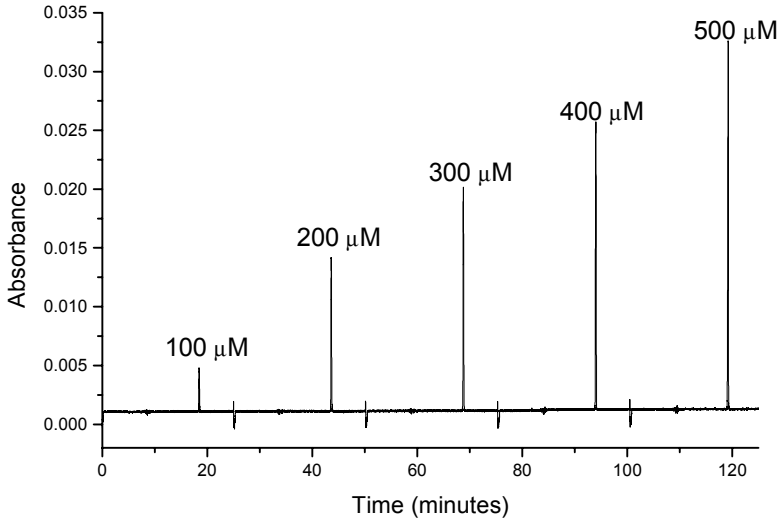

Figure 4.12. Consecutive injections of 1-naphthalene sulfonic acid solutions used to estimate CIA instrument detector efficiency. Zero time marks the beginning of the first run with each run lasting 25 minutes.

Using the flow rate calculated above the time axis was converted to a cumulative volume past detector axis and peak areas in volume units (absorbance has no units) were determined using Microcal Software's (Northampton, MA) [27] Origin 5.0. The amount of 1-naphthalene sulfonic acid injected onto the column was then calculated using the concentration of the solution injected and the injection volume. The injection volume was obtained from a consideration of the measured volumetric flow rate at 20 kV, the injection potential, and the injection time. It must be noted that an injection at 5 kV for 5 s really means ramping from 0 to 5 kV in around three seconds and then holding at 5 kV for the remaining two seconds. The injection was therefore regarded as being at 3.5 kV for 5 s. Because applied potential is proportional to flow rate it is easy to calculate the injection volume, which was just over 10 nL. The injection volume can then easily be converted to injection amount. The resulting data for injection amount and peak areas is given in Table 4.1.

Concentration of injected solution (µM).	Amount injected (picomoles)	Peak Area (nL)
100	1.0166	0.6124
200	2.0333	1.5230
300	3.0499	2.0178
400	4.0666	2.6236
500	5.0832	3.2991

Table 4.1. Peak areas resulting from the electrokinetic injection of various amounts of 1-naphthalene sulfonic acid.

The peak areas resulting from the injection of 1-naphthalene sulfonic acid were then plotted against the amount of sample injected, as shown in Figure 4.13. The line shown is a 'line of regression of *y* on *x*', that is, a line showing how *y* varies when *x* is set to chosen values, and was used to obtain averaged data. The product-moment correlation coefficient, *r*, was calculated to be 0.9974 while a 3.6% error was found in the calculated gradient.

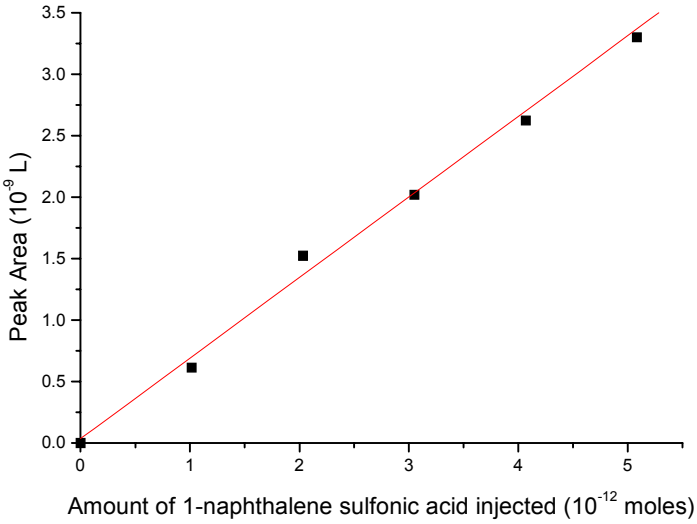

Figure 4.13. Graph of measured peak area versus amount of 1-naphthalene sulfonic acid injected for estimation of CIA instrument detector efficiency.

Using this data a standardised peak area for a 500 µM solution (5.0832 picomoles injected) was calculated as 3.324 nL. The detection cell is approximately 2 mm long,

giving a volume of 15.7 nL for a 100 µm ID capillary (this value is cancelled out making its exact magnitude unimportant). If the whole peak filled the absorbance cell as a square pulse the absorbance recorded would be 0.212 (real peaks are considerably longer than 2 mm). With knowledge of the injection amount, the size of the detection cell and the molar absorptivity constant of the analyte, an expected absorbance can also be calculated. First, if the whole injected amount filled the cell the concentration would be 324 µM. Second, the molar absorptivity constant for 1-naphthalene sulfonic acid in 50 mM ammonium acetate was found by experiment to be 4.204×10^6 M^{-1} m^{-1}. Using Beer's law and assuming a path length of 100 µm the expected absorbance can then be calculated to be 0.136. Therefore it can be seen that the instrument is in fact reading a higher value than would be expected, 0.212 recorded versus 0.136 expected. With careful consideration of the errors this difference could be used to correct recorded data. A likely source of systematic error is the refractive and reflective qualities of circular cylindrical tubes. This data does, however, show that the detector is producing a useable output.

4.3.2. Characterisation of Waters 2690 Separations Module and Waters 486 Tunable Absorbance Detector

In chromatography, great care and attention are paid to obtaining symmetrical peaks. Tailing is especially common with fronting being less often encountered. A typical HPLC injection valve is designed to switch a plug of analyte solution into the mobile phase stream, with this plug naturally tending with time towards a Gaussian distribution due to the action of diffusion. The input from an injection valve is of course made up of overlapping bands that are separated as they pass through the column. In a pure separation technique, such as chromatography, peaks cannot narrow and therefore the final peak shape is dependent on the input shape. A good way to test a system, apart from the chromatographic column, is to simply remove the column and observe what happens when an injection is made.

Figure 4.14 shows the result of a 10 µL injection of the instrument development test mixture (each component at 500 µM in acetonitrile) performed using the HPLC instrument described above. The solvent flow was simply acetonitrile at 1 mL min^{-1},

with the injection valve of the instrument being connected to the absorbance detector via approximately 50 cm of narrow PEEK tubing. Detection was performed at a wavelength of 214 nm. Significant tailing of the peak was observed. While it cannot be said whether this is mainly due to the injection valve, the detector, or associated interconnects, it is clear that degradation of chromatographic performance occurs that is not related to the chromatographic column. Figure 4.15 shows the results of a related experiment where the HPLC instrument was used to provide a flow of solvent, again acetonitrile at 1 mL min^{-1}, while a third party injection valve was connected to the usual absorbance detector using a short length of narrow PEEK tubing. The instrument development test mixture (again with each component at 500 µM in acetonitrile) was used and detection was performed at a wavelength of 214 nm. The valve used was a Valco C14W1 1 µL injection valve, and as can be seen, a similar level of performance was observed. Chromatographic efficiency is clearly reduced by valves, tubing and interconnects, which may be a significant part of total degradation when a column is connected. CE and CEC benefit from a simpler injection system that avoids such problems.

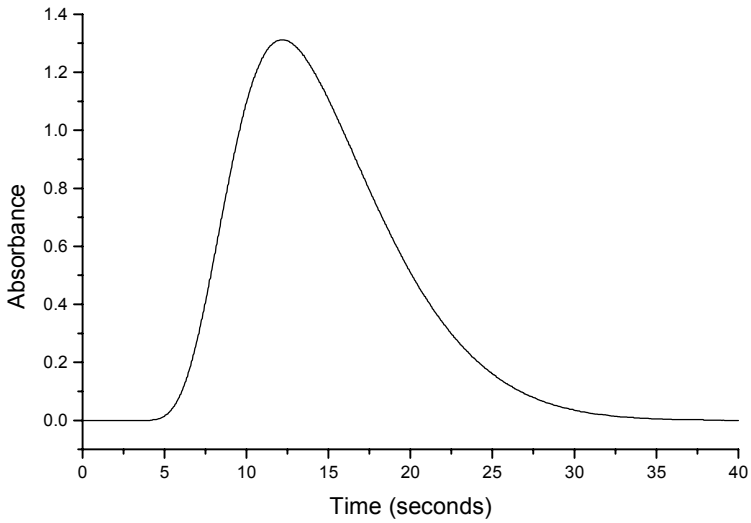

Figure 4.14. Result of direct connection of the Waters 2690 Separations Module to the Waters 486 Tunable Absorbance Detector via approximately 50 cm of 0.005" (127 µm) ID PEEK tubing between injection valve and detector. Sample injected was 10 µL of 500 µM instrument development test mixture.

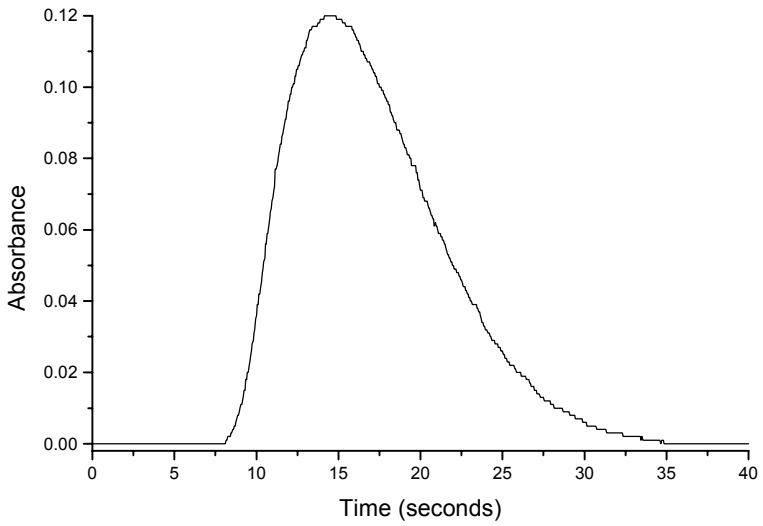

Figure 4.15. Result of direct connection of Valco C14W1 injection valve to Waters 486 Tunable Absorbance Detector via 27 cm of 0.0025" (63.5 µm) ID PEEK tubing. Sample injected was 1 µL of 500 µM instrument development test mixture.

To give a numerical value to peak asymmetry, the apex of the peak must first be located. The differences in time between the points on either side of the apex that are at 10% of full peak height and the apex itself are then presented as a ratio. This ratio is of the forward part of the peak width over the rearward part, and hence will give small numbers for tailing peaks. For the injection valve fitted to the Waters 2690 Separations Module, a value of 0.41 was obtained, while a slightly better result of 0.44 was obtained with the Valco C14W1 valve. Both systems, however, result in relatively poorly symmetrical peaks.

The contribution to the variance, σ^2, of a Gaussian curve from travelling through the tubes employed here can also be calculated for comparison. The required expression, given as Equation 4.1, was originally developed by Taylor [28], and can be compared with Equation 2.10. In this expression, u is the average mobile phase velocity, d_i is the inner diameter of the tube, L is the length of the tube, and D_m is the diffusion constant of a solute in the mobile phase. D_m is taken to be 10^{-9} m^2 s^{-1} here, which is a ballpark figure for a small molecule in a common solvent, while all other quantities have been given above. The contribution to the variance for the longer,

wider tube would therefore be 0.111 m^2, while that for the shorter, narrower tube would be 0.060 m^2. These contributions to total variance appear to be large, but given that liquid flows through the wider tube at 1.32 m s^{-1}, and through the narrower tube at 5.26 m s^{-1}, variance expressed in time units will be small. A contribution should strictly also be added for diffusion, but the high flow rates utilised mean that dispersion originating from diffusion will be negligible in comparison with that originating from laminar flow.

$$\sigma^2 = \frac{u d_i^2 L}{96 D_m} \qquad \text{Equation 4.1.}$$

4.4. Description of the Ion Trap Storage Time-of-Flight Mass Spectrometer

The mass spectrometer and associated power supplies were manufactured by the R. M. Jordan Company (Grass Valley, CA, USA) [29]. The design of this instrument originates from the work of Lubman *et al.* [30,31]. The mass spectrometer is illustrated in Figure 4.16. The source region of the instrument is housed in a large cubical vacuum chamber, of approximate dimensions $30 \times 30 \times 30$ cm, in order to provide easy access. This chamber is equipped with three fused silica windows for laser access (windows may be exchanged to allow lasers operating at $\lambda > \sim 3$ μm to enter the chamber). The source chamber is pumped with a Pfeiffer TPH2000 2,000 L s^{-1} turbomolecular pump, backed by an Edwards E2M40 two stage rotary pump combined with an Edwards EH250 mechanical booster. This pumping system was chosen to ensure vacuum performance even when pumping relatively large volumes of solvent vapour. The source chamber was separated from the TOF chamber using a gate valve, allowing isolation of the ion trap from the flight tube. The TOF chamber is pumped with an Edwards EXT250 250 L s^{-1} turbomolecular pump backed by an Edwards E2M18 two stage rotary pump. The ultimate vacuum (no solvent input) obtained in the source chamber was 5×10^{-8} mbar, while that obtained in the TOF chamber was 2×10^{-8} mbar. Typical working pressures (solvent

flow at typical CEC volumetric flow rates) were 2×10^{-6} and 4×10^{-7} mbar, respectively. These pressures were measured using Penning gauges.

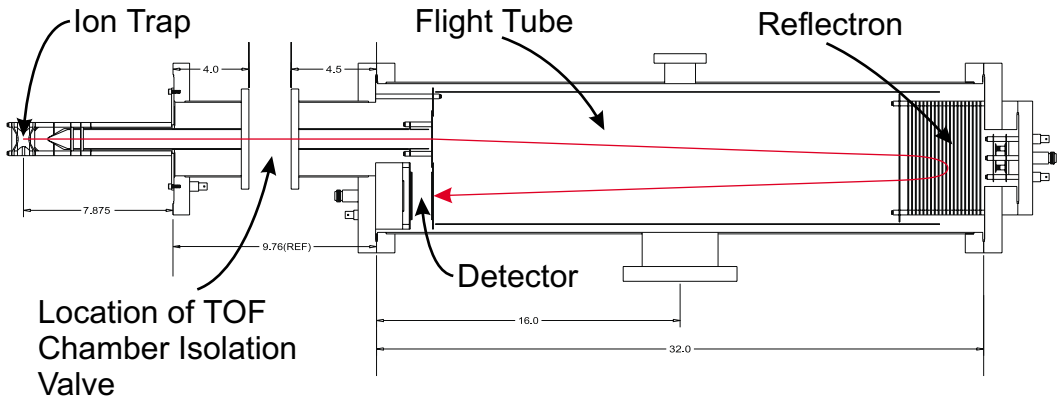

Figure 4.16. Side view of the ion trap storage time-of-flight mass spectrometer used in these experiments. Dimensions are in inches while the pathway followed by ions is highlighted in red. Expansions presented below.

Figure 4.17 is an enlargement of Figure 4.16 showing the source region of the ITS/TOF mass spectrometer. The ion trap comprises two end caps and a ring electrode. Ions can be either produced *in situ* or produced externally and then guided into the ion trap. An electrical potential pulse is applied to the end cap nearer to the flight tube to expel ions into the mass analyser. The ion trap is described in more detail in Section 4.5. The arrangement of electrodes that are used to focus the ion beam into the TOF mass analyser are also represented schematically in Figure 4.18.

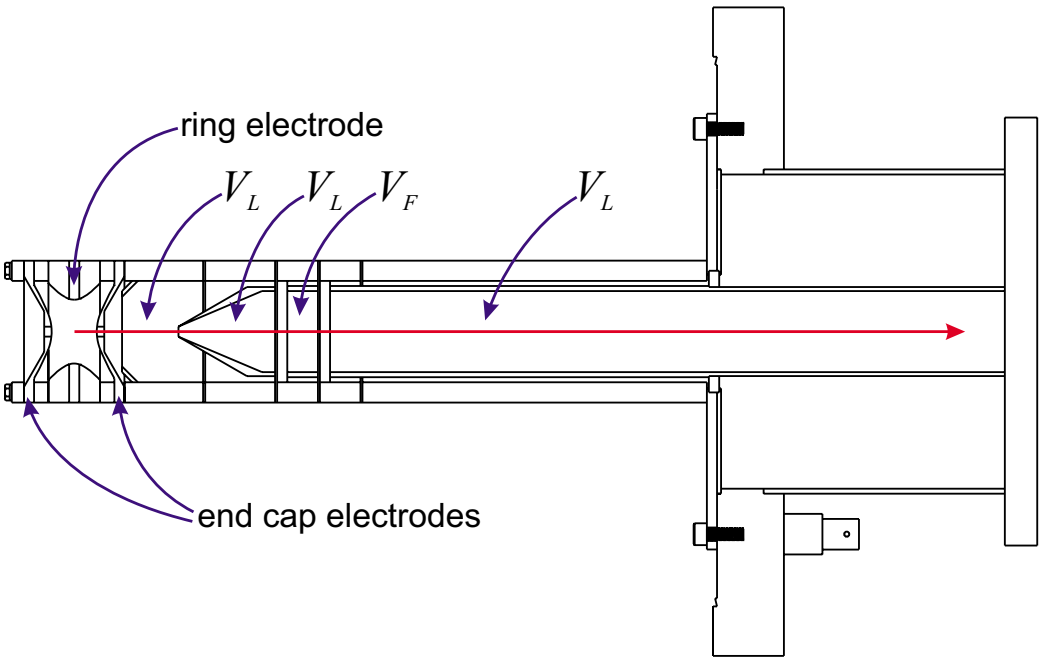

Figure 4.17. Enlargement of the source region of the mass spectrometer, with ion trajectory indicated in red.

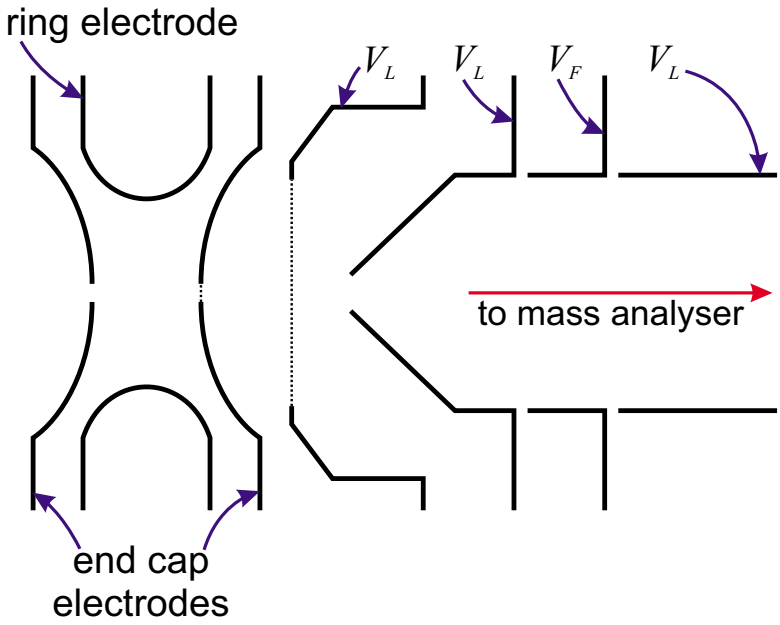

Figure 4.18. Schematic diagram of the electrodes that constitute the source region of the mass spectrometer, with dashed lines indicating grids.

Deflection plates, shown in Figure 4.19, are located just before the entrance to the flight tube to steer ions to either the linear or reflectron MCP detector. The flight

tube is equipped with a liner that allows it to be held at a specified electrical potential relative to ground. By holding the liner at a negative high potential, the positive high potentials that must be applied to the other electrodes are reduced. This reduces the risk of arcing. Certain electrodes are held at liner potential (V_L) as indicated in Figure 4.17, Figure 4.19 and Figure 4.20.

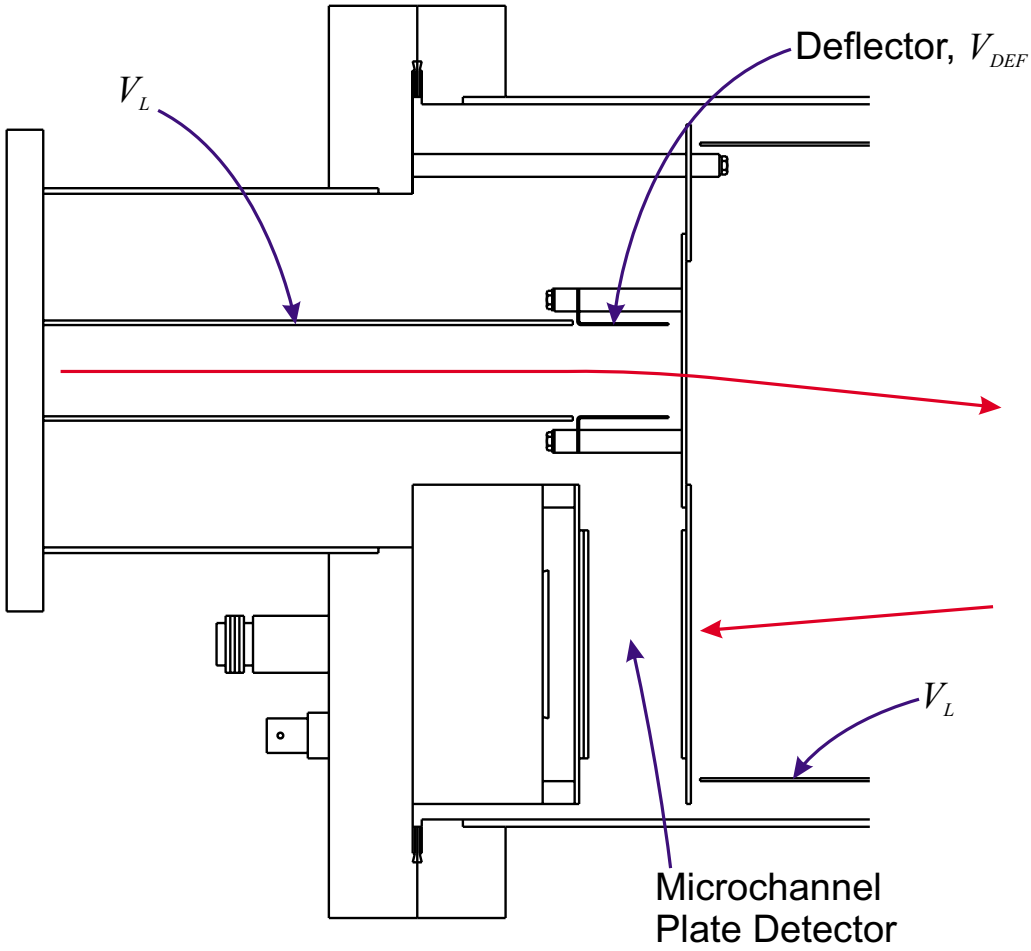

Figure 4.19. Central section of mass spectrometer showing the deflector and final MCP detector, with ion trajectory indicated in red.

At the end of the flight tube, ions pass through a grid held at the liner potential before entering the reflectron, which is a region of linear potential gradient used as an ion mirror and to improve resolution. An enlargement of this region of the instrument is given as Figure 4.20. The ions reverse direction in the reflectron and fly back towards the MCP detector illustrated in Figure 4.19.

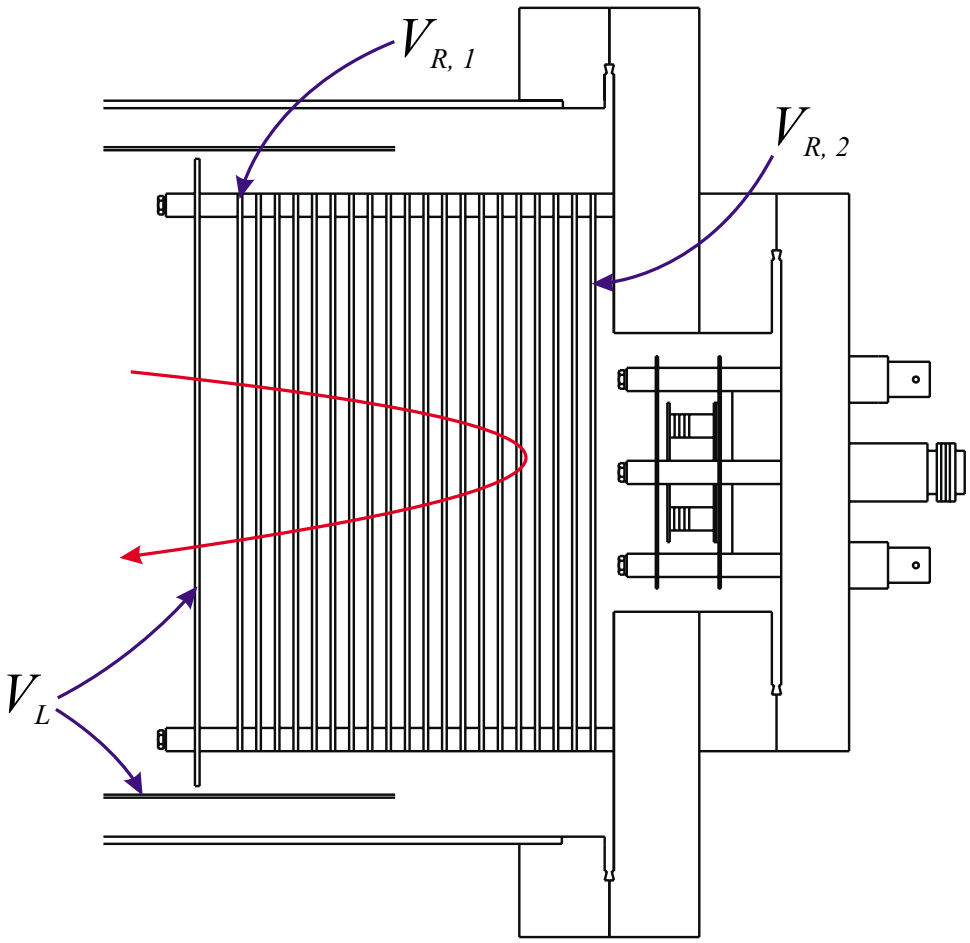

Figure 4.20. Detail of the reflectron end of the mass spectrometer. Ion trajectory indicated in red.

The potentials applied to the electrodes are supplied and controlled by two units. The Quadrupole Ion Trap Power Supply allows control of the amplitude of the rf potential applied to the ring electrode of the ion trap (0 - 5000 V) and adjustment of the extraction pulse amplitude (0 - 400 V). The extraction pulse is applied to the ring electrode nearest the flight tube. During extraction the rf potential may either be switched off or left on. Switching off the rf is synchronised with the rf voltage going through zero in the positive direction, and it may be chosen whether the extraction pulse is synchronised with the phase of the rf. In this work it was found that the best results were obtained by switching off the rf potential during extraction, but not synchronising the extraction pulse with the phase of the rf.

The electrodes, other than those that constitute the ion trap, are controlled by the Ion Trap Angular Reflectron (ITAR) Time Of Flight Power Supply. The liner (V_L), focus (V_F), deflector (V_{DEF}), reflectron voltages ($V_{R,1}$ and $V_{R,2}$), and the voltages applied across the MCP detector are all controlled via this unit. At maximum the first MCP is held at -2200 V, the second at -1200 V, while the final MCP is held at -200 V. In this work the first plate was typically held at –1600 V to prolong detector life. Electrons leaving the final plate hit an impedance matched 50 Ω conical anode, held at ground potential, which was connected directly to the oscilloscope.

4.5. The Ion Trap Interface

Arguably, the most important part of the whole system is the interface where analytes are converted into gas phase ions. This occurs within the ion trap, which is illustrated from the side in Figure 4.21 and from above in Figure 4.22.

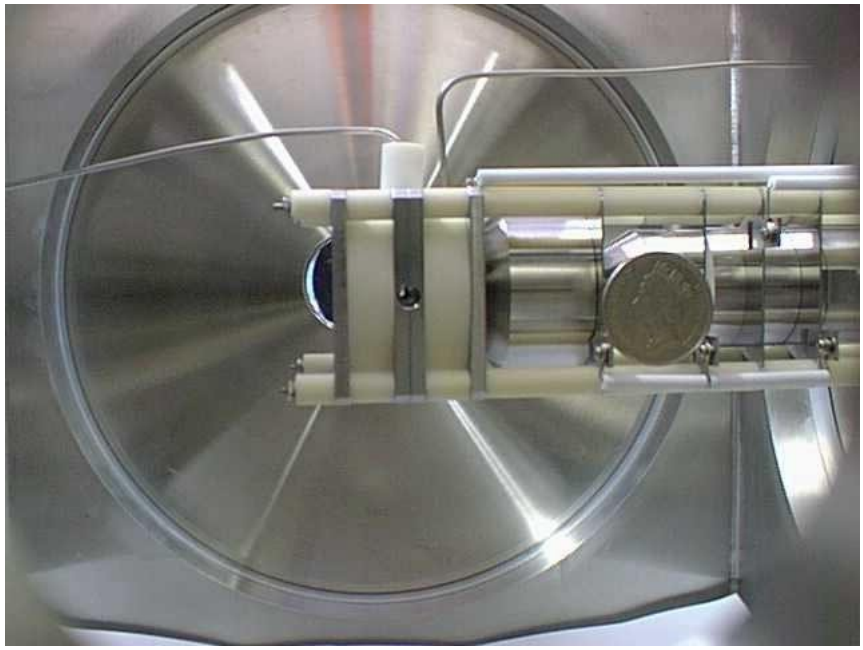

Figure 4.21. Photograph of ion trap assembly and nearby ion optics from the side. The small stainless steel tube on the right-hand side supplies helium to the trap, while the tube on the left-hand side can be used to supply analyte vapour. A ten pence coin (diameter ~ 24.5 mm) provides a scale. The internal dimensions of enclosing vacuum chamber are approximately 30 × 30 × 30 cm.

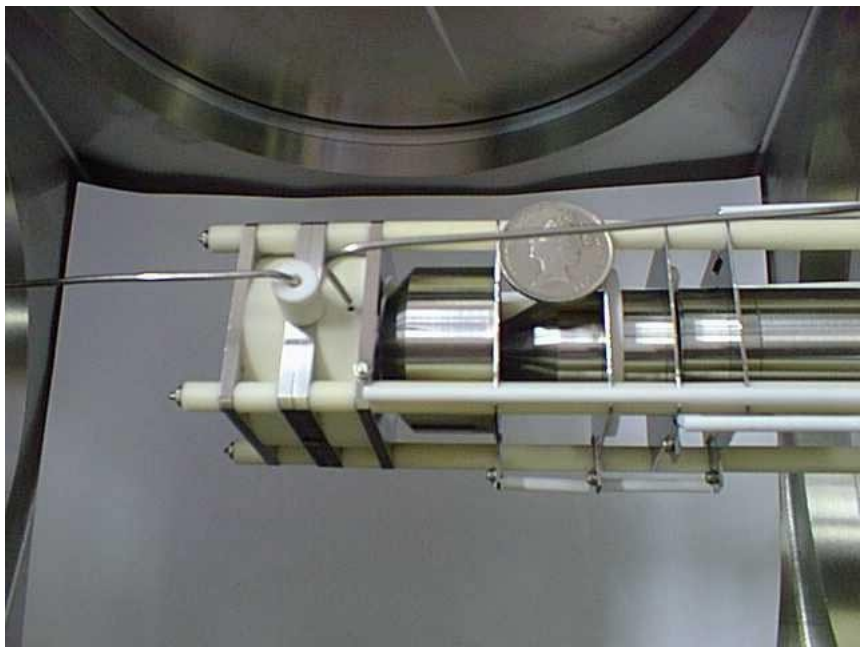

Figure 4.22. Photograph of ion trap assembly and nearby ion optics from the above. Note that stainless steel tube on the right-hand side (helium supply) should be inserted into the hole in the ceramic ring. The analyte supply (left-hand tube) can also be inserted through a similar hole in the other ceramic ring.

The exact shape and structure of the ion trap are represented diagrammatically in Figure 4.23 and Figure 4.24. The various electrodes that constitute the ion trap and nearby ion optics, as illustrated photographically in Figure 4.21 and Figure 4.22, are mounted on four ceramic tubes. Steel rods run through these tubes, insulated from the electrodes, to strengthen the assembly. Ceramic spacers separate individual electrodes, which are present both for insulation and to define the exact shape of the assembly. Additional ceramic rings are used to allow the trap to be held at a slightly higher pressure than the enclosing vacuum chamber. Higher pressures in the trap region are generated by continuous addition of helium or solvent vapour to the trap. These ceramic rings can be removed to allow the trap to operate at the pressure of the enclosing chamber.

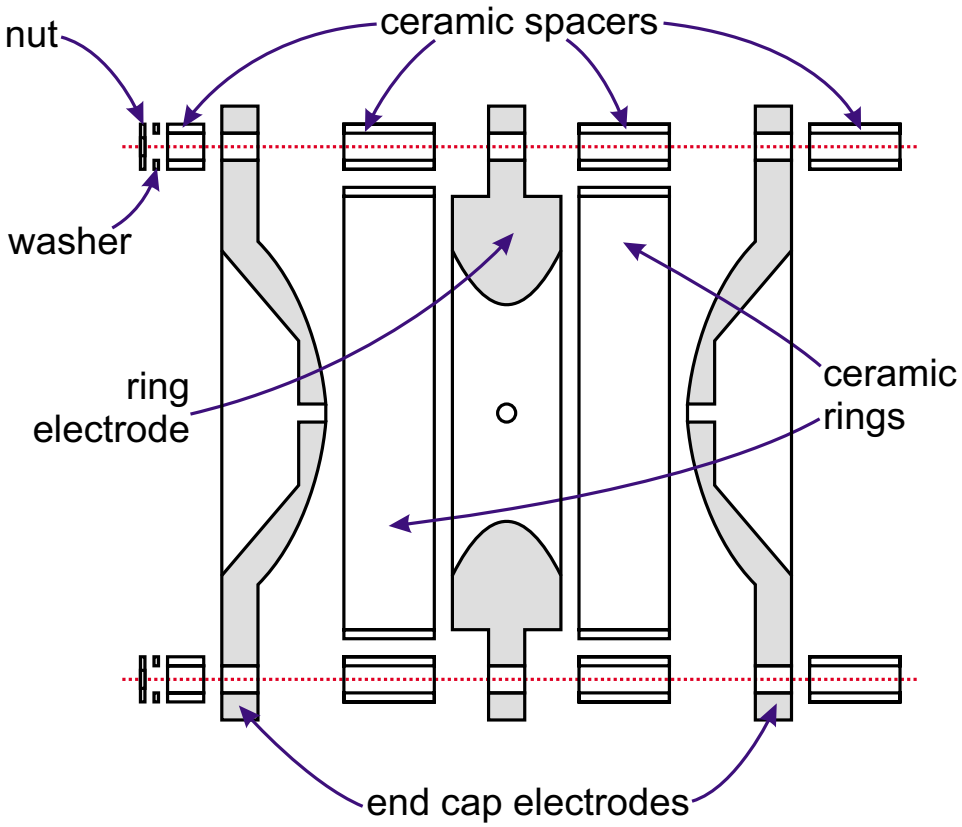

Figure 4.23. Exploded diagram of ion trap assembly, with the red dashed lines indicating the position of the supporting tubes.

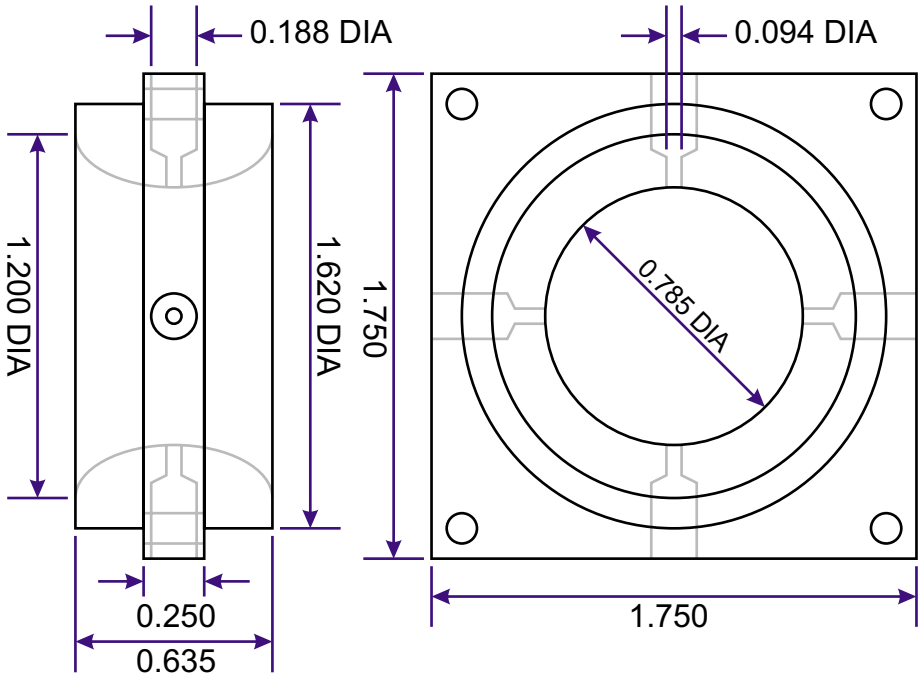

Figure 4.24. Ion trap ring electrode, with key dimensions given in inches.

When ions are produced within the trap, transmission losses associated with external ion production are avoided. The ring electrode of the ion trap contains four circular holes, of greater diameter at the end distant from the parabolic surface, as indicated in Figure 4.24, providing access to the trap for lasers and to provide a location for a sample holder. The lower hole typically contains the sample holder requiring the desorption laser to be trained on the sample through the top hole. The ionisation laser passes above the sample holder through the side holes. The sample holder may either consist of a paste of analyte on a ceramic probe or a fused silica capillary that is mounted flush to the parabolic inner surface of the ring electrode. The ionisation laser fires approximately 30 μs later than the desorption laser. This delay allows desorbed molecules to expand into the path of the ionisation laser. The orientation of the laser beams is illustrated in Figure 4.25.

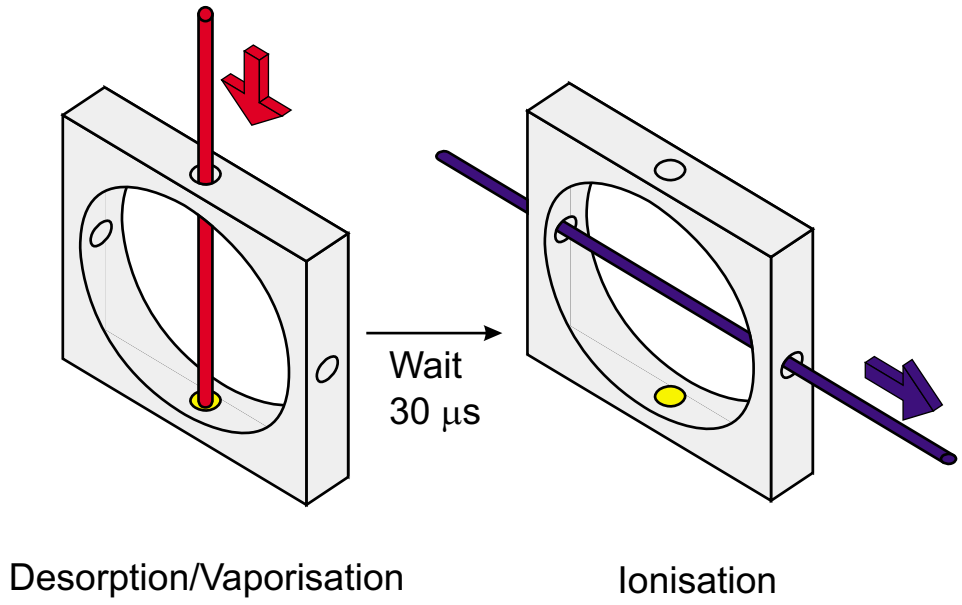

Figure 4.25. Schematic of how the lasers are used within the ion trap. The ring electrode shape has been simplified for clarity. Sample position shown in yellow.

4.6. Control of Experimental Timing

Fine control of experimental timing was essential in many aspects of this project, with laser control requiring 10^{-7} s resolution. When precise timing was required, a delay generator was utilised. This instrument is designed to output trigger pulses at specified delays from an input trigger pulse. Such pulses are used to trigger events;

for example, laser firing or starting to record data using an oscilloscope. An example timing schematic is shown in Figure 4.26. The input trigger, which can be internally generated, initiates the experiment when the voltage has risen past a set threshold value. There is then a short fixed delay before a zero time output pulse is delivered. This delay is 35 ns for the EG&G Instruments (Wokingham, UK) 9650A [32] four-channel digital delay generator, which was used for the bulk of the experiments in this work. The EG&G 9650A can provide four pulses, which are delivered at variable intervals from this zero time pulse, with a short delay after the end of the final pulse before another input trigger pulse can be accepted.

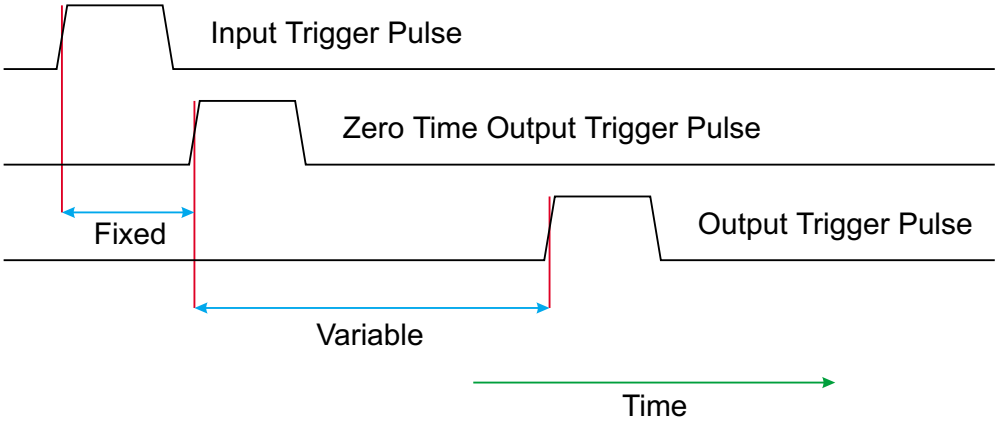

Figure 4.26. Schematic of a timing sequence.

The time delays between the four pulses can be controlled to a resolution of 10 ps and pulse widths are variable between 30 ns and 1 ms. If precisely defined output pulses are required two channels can be combined through a separate output. The instrument is able to accept various types of input trigger pulses, with output pulse amplitude being selectable from a number of common values. For most experiments, the EG&G 9650A was run from an internal trigger.

4.7. Lasers

When using pulsed lasers careful control of experimental timing is essential. Photodiodes were used to check the temporal uniformity of laser pulses and to monitor timing drift. Generally drift was negligible compared with the time scales of these experiments. Power was monitored, for Q-switched Nd^{3+}:YAG laser output at

1064 and 266 nm, using a Molectron (Portland, OR, USA) [33] PM500A laser power meter, in conjunction with a Molectron PM10V1 probe. Readings taken with these devices are compared with those obtained using a Scientech (Boulder, CO, USA) [34] Astral AA30 laser power meter in conjunction with a Scientech AC25UV probe to check calibration. A Molectron J3-09 pyroelectric laser energy detector, in conjunction with an oscilloscope, was used for long wavelength radiation, although this can also be used for visible and ultraviolet radiation. This device is used in a similar manner to the photodiodes.

4.7.1. Quantel Brilliant

The Quantel (Les Ulis, France) [35] Brilliant laser is a Q-switched Nd^{3+}:YAG laser capable of outputting 360 mJ pulses at a wavelength of 1064 nm and a repetition rate of 10 Hz. The gain medium of this laser consists of Nd^{3+} ions at a low concentration in yttrium aluminium garnet (YAG), which is $Y_3Al_5O_{12}$. The active medium is pumped by a flashlamp, while the laser is controlled by flashlamp and Q-switch timing pulses. When the laser is run in internal mode, these two pulses are produced internally and the delay between them is set using the laser's Remote Control Box (approximately 180 to 390 μs). This delay governs laser output power, with a shorter delay resulting in a higher output power. If timing is only required to microsecond resolution the 'Q-switch Out' pulse can be used to base experimental timing. The delay between this pulse and emission of laser radiation is approximately 80 ns. In this work the flashlamp pulse was controlled externally, while the delay before the Q-switch pulse was governed by the Remote Control Box. It is possible to provide both pulses for very close control of experimental timing.

In this work the laser was not used at its fundamental frequency (1064 nm), but was used in conjunction with harmonic generation modules to provide laser pulses of up to 40 mJ at 266 nm. In this mode, pulse widths are ~ 5 ns, with a beam diameter of ~ 4 mm. Typically the laser light was steered using two quartz prisms, sometimes followed by a quartz lens, before entering the source chamber of the mass spectrometer through a fused silica window.

4.7.2. Continuum Minilite

The Continuum (Santa Clara, CA, USA) [36] Minilite laser is a compact, simple to use, Q-switched Nd^{3+}:YAG laser. The laser offers operation in either high or low power mode, low power mode providing approximately 10% of the intensity of the high power mode. The laser accepts a 'Fire Laser' trigger, which results in laser radiation 238 ms later, with flashlamp and Q-Switch triggers for timing control. This laser was used at 1064 nm, giving pulses of up to 25 mJ (width ~ 5 ns). Laser light was typically steered using two quartz prisms followed by an iris and a lens before entering the source chamber of the mass spectrometer through a fused silica window.

4.7.3. Bioptic Lasersysteme Bioscope

The Bioptic Lasersysteme (Berlin, Germany) [37] Bioscope laser is a Q-switched Er^{3+}:YAG laser, which provides a source of 2.94 μm radiation with a maximum power output of 10 mJ and a maximum repetition rate of 10 Hz. Pulse width is ~ 50 ns, with a built in power meter monitoring output. The beam diameter is ~ 1 mm. In internal control mode the Bioscope provides a timing pulse synchronised to, but occurring a little later than, emission of laser radiation (delay negligible in experimental timing scales used here). It is possible to trigger the laser externally. Using the Molectron J3-09 pyroelectric laser energy detector, the delay between an external trigger and emission is determined as 140 μs. In use the laser is directed into the vacuum chamber through a calcium fluoride window by means of two mirrors, with a calcium fluoride lens of focal length 30 cm being used in some experiments. Due to strong absorbance by water vapour in the atmosphere, the path length of the laser outside the vacuum chamber is kept as short as possible.

4.7.4. Alltec AL861

The Alltec (Lübeck, Germany) [38] AL861 laser is a transverse excitation atmospheric (TEA) CO_2 laser capable of generating 100 ns pulses of 10.6 μm radiation at a maximum repetition rate of 50 Hz. To operate, the laser required a gas mixture of 4% CO and 12% CO_2 with the balance being made up with helium. The laser can be externally triggered. The laser beam is directed into the chamber using

two gold coated mirrors and collimated by an iris. The beam is focused into the chamber by a sodium chloride lens (f = 30 cm).

4.8. The LeCroy 9350M 500 MHz Digital Oscilloscope

An oscilloscope is used to observe transient signals, recording variations in voltage against time. If the transient signal is not a voltage, in the required range, some form of transducer is required. TOF experiments require the determination of the time it takes ions to reach the detector. The detector provides a voltage proportional to the number of ions arriving and the oscilloscope displays the TOF spectrum.

A LeCroy (Chestnut Ridge, NY, USA) [39] 9350M two-channel digital oscilloscope, which has a bandwidth of 500 MHz, was used in this work. Oscilloscope bandwidth is specified as the frequency at which a sinusoidal input signal is attenuated to 70.7% of the signal's true amplitude and hence measures how well the oscilloscope responds to rapidly changing signals. The oscilloscope was also capable of recording voltages at a rate of up to 500 MHz (2 ns resolution) for up to 100,000 points (200 µs at maximum resolution). It is possible to combine both channels to double the sampling rate (1 ns resolution) and increase the number of points that could be recorded to 250,000 (250 µs at maximum resolution). However, with typical TOF spectrum peaks spanning around 100 ns, combined channel operation was not required. Voltage resolution is 8 bit making it essential that the oscilloscope recorded the narrowest possible voltage range to span the entire signal. Maximum voltage resolution was 0.0625 mV, obtained on the 2 mV per division scale (eight divisions are present). Offset controls can be used to make most efficient use of the available resolution. Averaging of successive spectra enhances voltage resolution to give smoother peaks with less noise. The oscilloscope has a floppy disk drive for saving data but may also be remotely controlled.

The oscilloscope trigger is synchronised with the voltage pulse that accelerates ions into the TOF chamber. Usually Channel 1 is used to accept this external voltage pulse, being used to trigger the recording of data on Channel 2. A dedicated trigger channel is also available for use with single-channel operation. Vertical sensitivity

and offset must be set for each channel along with the time resolution. The oscilloscope was set to produce a summed average of a number of TOF spectra.

4.9. Experimental Timing Schematic

Since the maximum repetition rate of the experiment is 10 Hz, the EG&G 9650A delay generator is programmed to provide three pulses every 100 ms. The first pulse triggers the desorption laser, the second the ionisation laser, and the third ejects ions from the trap. Ejection of ions from the trap follows the trigger pulse, after a short delay to allow the rf field to be switched off. This timing sequence is illustrated in Figure 4.27, shown with common values for the time delays. Due to the requirement for the delay generator to deliver all delays before a new set of pulses can be delivered, a second pulse generator was required for trapping times of greater than one laser cycle. In this case a Stanford Research Systems (Sunnyvale, CA, USA) [40] *DG535* digital delay generator was used.

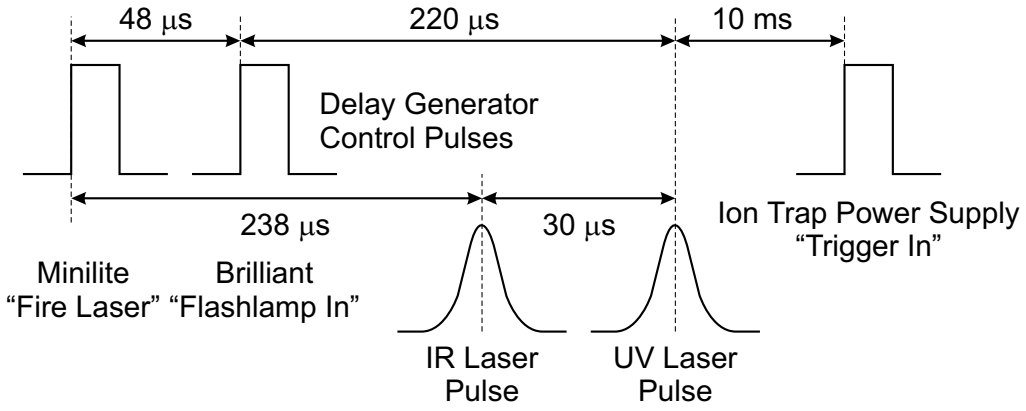

Figure 4.27. Example experimental timing sequence. Switching off is followed a short time later by the extraction pulse.

4.10. Acquisition of CEC/MS Data

The oscilloscope floppy disk drive can be used to transfer data to a PC for further analysis, but a method for recording large amounts of data in real time was required in order to obtain the consecutive TOF spectra that constitute CEC/MS data. Initial work made use of a Stanford Research Systems SR250 Gated Integrator and Boxcar Averager. This instrument allowed a selected ion chromatogram to be recorded for a

single analyte with known flight time. While useful for instrument testing, a method that allowed the whole TOF spectrum to be recorded was required.

The approach adopted was to connect the oscilloscope to a PC running National Instruments' LabVIEW software using an IEEE-488 cable. While there are many routes to instrument control and data acquisition, the advantage of LabVIEW was in the availability of instrument drivers and the graphical programming language that made the process simple and development rapid. A suite of programs was written (based upon earlier work by David P. A. Kilgour [41]) for real-time oscilloscope control and data acquisition, and for off-line data manipulation. To illustrate the capabilities of LabVIEW a program written to integrate peaks is described below. The graphical code is shown in Figure 4.28 and is explained in more detail in the following text. This code is part of the program used to produce selected ion chromatograms.

4.10.1. The Peak Integration Program

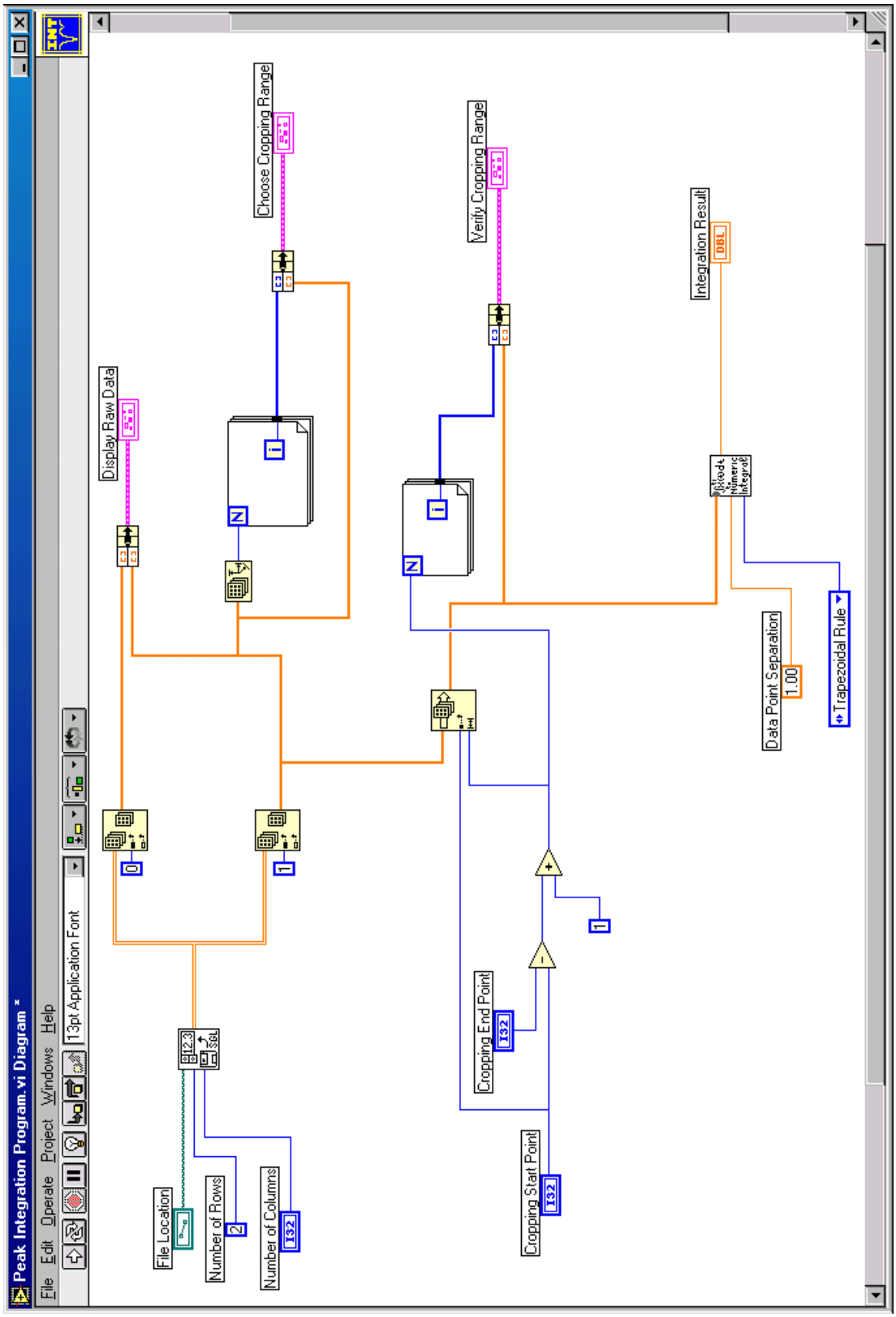

Figure 4.28. LabVIEW graphical code for the Peak Integration Program.

Data processing is not performed in real time to make data acquisition as rapid as possible. The first thing the Peak Integration Program must do is read the TOF spectrum from disk. Spectra are stored as binary files, to save space, and are composed of two long rows of data. The first row is an array of flight times and the second row is the corresponding voltages. LabVIEW is based on graphical representations of functions wired together to form a program. To illustrate this, the Peak Integration Program, shown in Figure 4.28, is broken up into its constituent parts and described below.

To the left in Figure 4.29 are three inputs, while to the right is a function that reads a binary file from disk. The inputs tell the program where to find the file, and how much of the file to read. This function outputs a two-dimensional array to the far right, represented as a double orange line. The number of rows in this work is always 2 (pre-set), while the number of columns and file location vary, being made available as inputs to the operator. Most spectra covered 100 µs at 2 ns resolution and hence would be expected to contain 50,000 points. Recording, however, begins at -1 ns and then every 2 ns until ended at 100,001 ns giving an array of 50,002 points.

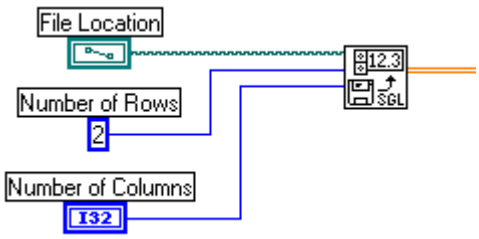

Figure 4.29. Loading a TOF spectrum into the Peak Integration Program.

The next step in the program separates time and amplitude arrays. Obtaining a one-dimensional time array is shown in Figure 4.30. The two-dimensional array enters the 'Index Array' function from the left, while a one-dimensional array exits to the right. The two boxes in the lower left corner of the function control how the one-dimensional array is produced. The upper box is active and refers to rows while the lower box refers to columns and is inactive. The zero attached to the upper of the two boxes outputs the first row of the two-dimensional array as a one-dimensional array. Substituting 0 for 1 outputs the second row (amplitude array).

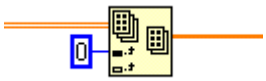

Figure 4.30. Outputting the first row of a two-dimensional array.

Now the TOF spectrum has been separated into a time array and an amplitude array. It is desirable to put these back together to check the original spectrum. The separated arrays are recombined as shown in Figure 4.31 using the 'Bundle' function to producing a line plot visible in the user interface.

Figure 4.31. Plotting raw data to guard against mistakes.

Integration limits are defined in terms of array index to simplify the program, although a less natural operator interaction is required. This section of the program plots the amplitude array against element number. The amplitude array enters from the left and the wire splits to make a copy. The 'Array Size' function gives the size of the array and by connection to the 'While Loop' controls the number of times the loop cycles. The loop outputs the index number. In the case of the 50,002 point arrays, the loop outputs an array of integers from 0 to 50,001. This is plotted against the amplitude array, allowing the user to determine between which array elements the peak should be integrated.

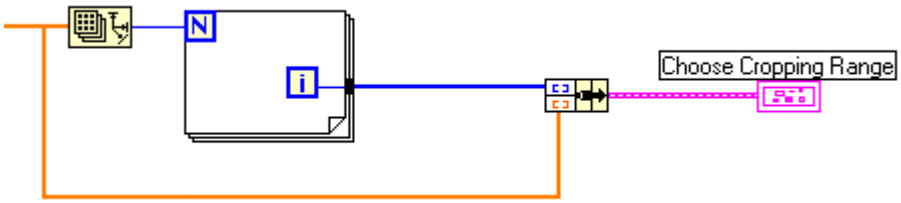

Figure 4.32. Plotting an array against array element number.

Once the peak has been identified and the array elements between which to integrate have been decided, the amplitude array is cropped. The 'Array Subset' function is used for this purpose. The one-dimensional amplitude array to be cropped enters

from above, while the cropped array is outputted below and to the right, see Figure 4.33. The two connectors in the lower left-hand corner of the function control the process. The upper connector governs at which point the cut is begun while the lower governs the number of elements before the second cut. The start and end points are input by the operator, guided by the chopping range graph, and from these the start point and the number of elements to output is determined. The cropped array is then plotted against a series of integers as previously to verify that the cropping has been successful.

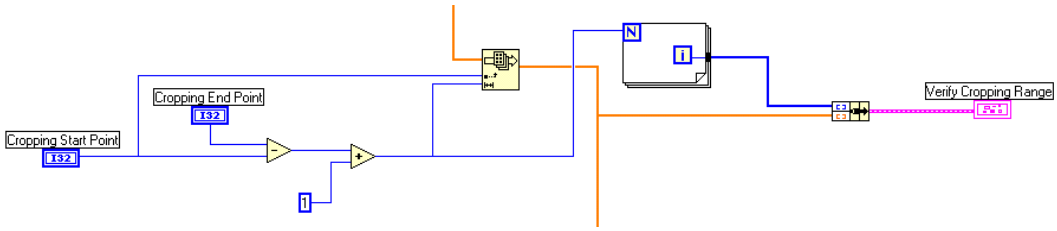

Figure 4.33. Cropping out a section of an array and plotting against new element numbers.

Finally, integration is performed. The cropped array enters the 'Numeric Integration' function from above while the integration result is outputted to the right, see Figure 4.34. Because the peaks are negative the output is negative. The action of this function is controlled by two inputs in the lower left-hand corner. The upper controls the gap between array points. As only relative data is required this is set to 1. The lower controls the integration method and is set to the trapezoidal rule (explained in Figure 4.35). The integration result is output in units of volts multiplied by the time difference between each point. Typically this would be 2 ns V, so simply multiplying by two gives data in units of 10^{-9} V s.

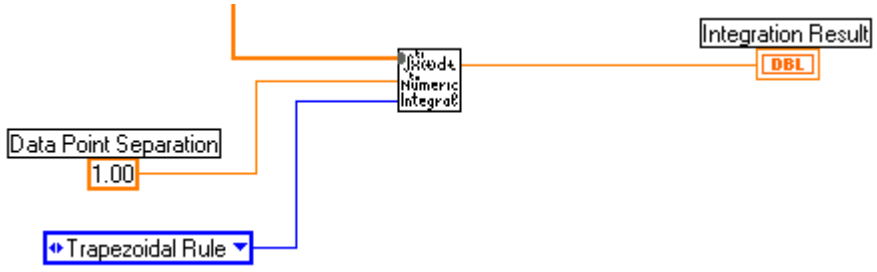

Figure 4.34. Program fragment used to determine peak area.

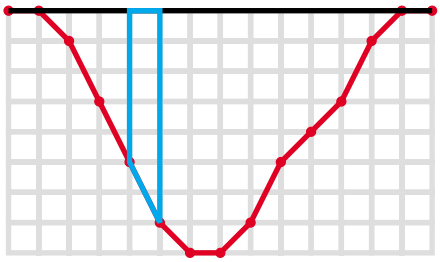

Figure 4.35. To obtain peak areas, trapezoids (blue) are drawn between consecutive data points (red) and the base line (black). Consecutive trapezoids are then added together to give the peak area.

The integration windows employed are narrow because the area calculated is relative to the time axis. If the baseline has an offset, different results will be obtained for the same peak as shown in Figure 4.36. The most serious case (third in Figure 4.36) is found when the baseline has a negative offset in relation to the peaks. In the TOF spectra recorded it was not uncommon for the baseline to exhibit a negative offset. Therefore, either a baseline must be defined or integration must be performed over relatively narrow time windows. LabVIEW can not easily be made to draw a baseline, so narrow integration windows were used.

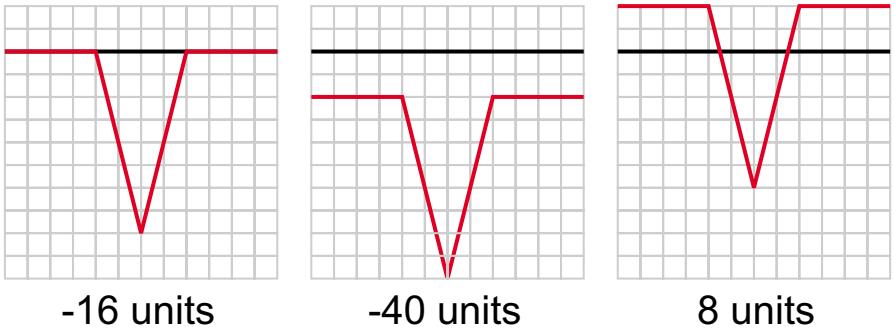

Figure 4.36. A demonstration of the LabVIEW integration process. The black line represents the time axis.

The user interface for this program is illustrated below in Figure 4.37. It is possible to zoom in on the peaks in each graph to set the cropping range. The user must enter the location of the file, the expected number of columns and the cropping range to obtain the integration result.

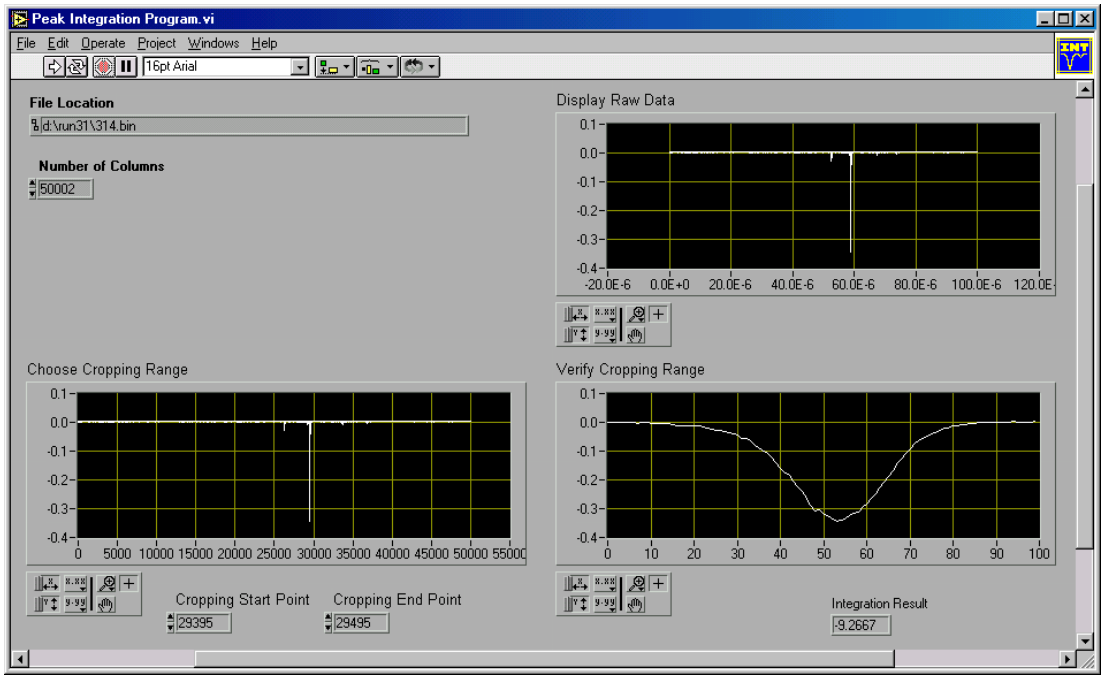

Figure 4.37. User interface for Peak Integration Program

The Peak Integration Program is used as part of the Selected Ion Chromatogram Program. The Peak Integration Program first determines the area to be cropped, then the selected ion chromatogram program takes over. This takes a set of consecutively recorded TOF spectra and collects the integration result for each spectrum. Using time data recorded with the spectra, a plot of peak area against time is produced that can be saved to disk as an ASCII file. Numerous selected ion chromatograms can be superimposed to give something that resembles a chromatogram obtained by measurements of absorbance. Because the Selected Ion Chromatogram Program uses the Peak Integration Program often in the region of 1,000 times in order to produce a chromatogram, the need to keep programs as simple as possible to optimise speed is immediately apparent. To produce a thousand point selected ion chromatogram from 1,000 TOF spectra (approximately 35 minutes run time) would take approximately five minutes.

4.10.2. Recording TOF Data in Real Time

The aim of the real time acquisition program was simply to set up the oscilloscope and then record mass spectra at known time intervals. Due to the time required for

transfer of TOF spectra from the oscilloscope to the PC, ten spectra were recorded into oscilloscope memory and a summed average then transferred to the PC. This data was displayed and saved to disk by the PC. The whole operation generally took 2.2 ± 0.1 seconds (error expressed as a standard deviation), allowing ~ 27 TOF spectra to be recorded per minute. Variation in cycle time can be attributed to background processes occurring in the PC. Hence, in any cycle, approximately one second was spent recording data while 1.2 seconds was spent on data transfer. Faster transfer would improve the resolution of recorded data.

The LabVIEW program designed to record chromatographic data is shown as a flow chart in Figure 4.38. The program first initialises communication with the oscilloscope before setting up the oscilloscope timing, referred to as its 'Timebase'. This sets up the amount of time, referenced to the trigger pulse, during which voltage data is recorded. This is followed by vertical set up for oscilloscope Channel 1 (trigger) and then separately for Channel 2 (TOF spectrum). These settings control the range of voltage recorded and must be set so that the signal fills the available space for maximum resolution but does not go off scale. The previous functions are performed only once during a run while the following are repeated many times until the end of the run.

The trigger is set up for every mass spectrum recorded, just as a trigger must be obtained for every spectrum displayed using an oscilloscope. Data recording begins either before or after the trigger. The next programmed task is setting up mathematical functions performed by the oscilloscope. In all runs the oscilloscope was programmed to record ten mass spectra into memory and then convert these into a summed average. The program is then forced to wait until ten spectra have been recorded. On completion the averaged data is passed from the oscilloscope to the PC. The data arrives in the format of t_0, Δt and an amplitude array. This data is converted to a time versus amplitude array and then saved to disk. Each TOF spectrum is saved individually, with consecutive filenames. The program then returns to setting up the oscilloscope trigger provided that the operator has not requested the program to stop. Each loop is accompanied by the time being added to a separate file. All files are

stored in the same folder. The end result is a folder that contains consecutively numbered mass spectra plus a file that details the time at which each was recorded.

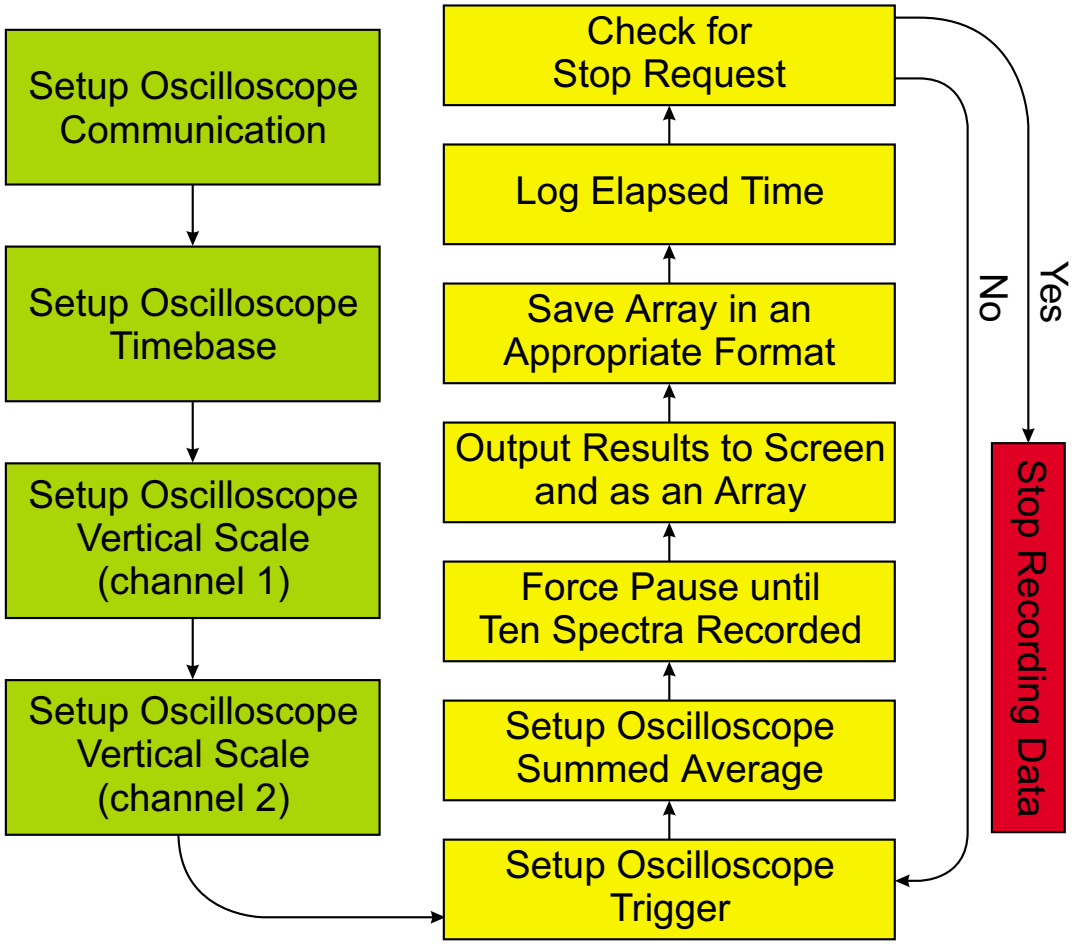

Figure 4.38. Flow chart representation of LC/MS LabVIEW program

---

[1] M. Tswett, *Ber. der deutschen bot. Gesellsch.*, **1906**, *24*, 384-393.

[2] *Chemistry of Glass*, published on the internet by the Corning Museum of Glass, Corning, NY, USA. Available at http://www.cmog.org/page.cfm?page=284 (December 2002).

[3] D. H. Desty, A. Goldup and B. H. F. Whyman, *J. Inst. Petrol.*, **1959**, *45*, 287-298.

[4] R. D. Dandeneau and E. H. Zerenner, *J. High Res. Chromatogr.*, **1979**, *2*, 351-356.

[5] T. A. Michalske and S. W. Freiman, *Nature*, **1982**, *295*, 511-512.

[6] K. L. Ogan, C. Reese and R. P. W. Scott, *J. Chromatogr. Sci.*, **1982**, *20*, 425-428.

[7] *Fused Quartz and Fused Silica Data Sheet*, published on the internet by Saint-Gobain Quartz, Wallsend, UK. Available at http://www.sgquartz.com/downloads/Fused%20Quartz%20&%20Fused%20Silica%20Data%20Sheet.pdf (December 2002).

[8] Further information available at http://www.compmetals.com

[9] Further information available at http://www.polymicro.com

[10] Further information available at http://www.sigmaaldrich.com

[11] Further information available at http://www.sgt-nl.com

[12] J. A. Lux, U. Häusig and G. Schomburg, *J. High Res. Chromatogr.*, **1990**, *13*, 373-374.

[13] T. Tsuda, K. Nomura and G. Nakagawa, *J. Chromatogr.*, **1982**, *248*, 241-247.

[14] N. Smith and M. B. Evans, *J. Chromatogr. A*, **1999**, *832*, 41-54.

[15] T. Huang, X. Z. Wu and J. Pawliszyn, *Anal. Chem.*, **2000**, *72*, 4758-4761.

[16] R. J. Boughtflower, T. Underwood and C. J. Paterson, *Chromatographia*, **1995**, *40*, 329-335.

[17] R. J. Boughtflower, T. Underwood and J. Maddin, *Chromatographia*, **1995**, *41*, 398-402.

[18] Further information available at http://www.knauer.net

[19] Further information available at http://www.kerry.co.uk

[20] Further information available at http://www.jameswalker.co.uk

[21] S. E. van den Bosch, S. Heemstra, J. C. Kraak and H. Poppe, *J. Chromatogr. A*, **1996**, *755*, 165-177.

[22] R. J. Boughtflower and C. J. Paterson, personal communication.

[23] Further information available at http://www.innovatech-uk.co.uk

[24] F. Baeuml and T. Welsch, *J. Chromatogr. A*, **2002**, *961*, 35-44.

[25] Further information available at http://www.isco.com

[26] Further information available at http://www.picotech.com

[27] Microcal Software has changed name to OriginLab. Information about their products can be found at http://www.originlab.com

[28] G. Taylor, *Proc. Roy. Soc. (Lond.)*, **1953**, *A219*, 186-203.

[29] Further information available at http://www.rmjordan.com

[30] S. M. Michael, M. Chien and D. M. Lubman, *Rev. Sci. Instrum.*, **1992**, *63*, 4277-4284.

[31] B. M. Chien, S. M. Michael and D. M. Lubman, *Int. J. Mass Spectrom. Ion Processes*, **1994**, *131*, 149-179.

[32] The *9650A* is now sold by Signal Recovery (http://www.signalrecovery.com)

[33] Further information available at http://www.molectron.com

[34] Further information available at http://www.scientech-inc.com

[35] Further information available at http://www.quantel.fr

[36] Further information available at http://www.continuumlasers.com

[37] Further information available at http://www.bioptic.de

[38] Further information available at http://www.alltec.com

[39] Further information available at http://www.lecroy.com

[40] Further information available at http://www.srsys.com

[41] D. P. A. Kilgour, *Development and Applications of Instrumental Chemical Analysis*, PhD Thesis, University of Edinburgh, **2002**.

5. Development of a Junction for Connection of CEC Columns to the ITS/TOF Mass Spectrometer

In this Chapter, work carried out to develop an electrically earthed junction, for connecting CEC columns to the ITS/TOF mass spectrometer, is described. The CEC column would ideally terminate at the point of sample vaporisation, but making an electrical connection to the column at this point would be difficult since the column terminus would be located inside the ion trap. One might conceive a system where the CEC column was mounted in a conducting sleeve, which in turn was mounted in an insulating ceramic sleeve. Such a system could be inserted in the 0.094" diameter hole drilled through the ion trap ring electrode, and with care, would be expected not to affect the function of the ion trap. The difficulty of constructing such an assembly, however, and the risk of laser damage to the column terminal frit, resulted in an alternative strategy being pursued. The CEC column is instead terminated in an electrically earthed junction, some distance from the point of sample vaporisation, with eluate being passed through an open capillary to the vaporisation point. Early versions of this junction between the separation column and the transfer capillary were found to degrade chromatographic performance significantly, and considerable effort was devoted towards developing an improved junction.

5.1. Characterisation of CEC Separation for a Suitable Test Mixture for Instrument Development

To aid in evaluation and development of the interface, a simple and reliable CEC separation was required. A test mixture was devised that consisted of acenaphthene, biphenyl, naphthalene, phenanthrene (Aldrich) and fluorene (BDH). These molecules were chosen both because they are amenable to laser ionisation at 266 nm and because they are important environmental pollutants. CEC analysis of polycyclic aromatic hydrocarbons has previously been reported [1,2]. Their structures, along with molecular masses and gas phase ionisation potentials [3], are given in Table 5.1. Test mixture solutions typically contained each component at a concentration of either 5 mM or 500 μM, with acetonitrile (Fisher) used as solvent.

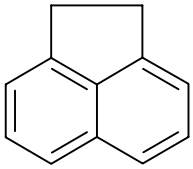	Acenaphthene (FW = 154.21) (IP = 7.68 eV)
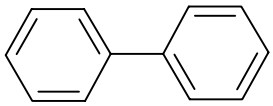	Biphenyl (FW = 154.21) (IP = 7.95 eV)
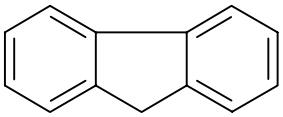	Fluorene (FW = 166.22) (IP = 7.89 eV)
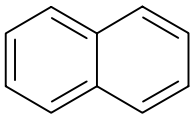	Naphthalene (FW = 128.17) (IP = 8.14 eV)
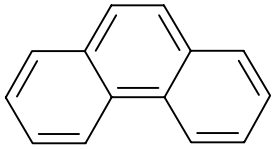	Phenanthrene (FW = 178.23) (IP = 7.86 eV)

Table 5.1. Structures of the components of the instrument development test mixture, along with molecular masses and gas phase ionisation potentials.

The test mixture was separated on a column packed in the usual manner with Hypersil Mixed Mode stationary phase (3 μm diameter particles); a mixture of ODS and SCX stationary phases designed to offer increased EOF over a wider pH range. The mobile phase consisted of 25% 50 mM aqueous (double distilled water) ammonium acetate (Prolabo) adjusted to pH 6.0 using acetic acid (Fisher), 75% acetonitrile. Ammonium acetate was chosen as electrolyte because its volatility makes it compatible with mass spectrometry.

The elution order was initially determined by running test mixtures that had either been spiked with or did not contain one particular component, using absorbance detection at 214 nm. Naphthalene was first to elute, followed by biphenyl, acenaphthene, fluorene and then finally phenanthrene. A sample CEC chromatogram obtained using the CIA instrument is shown in Figure 5.1. This method and test mixture were chosen in part so that the third and fourth peaks were closely spaced to

provide an easy indication of chromatographic efficiency. The slight baseline undulation is due to an ageing zinc lamp in the absorbance detection module of the CIA instrument.

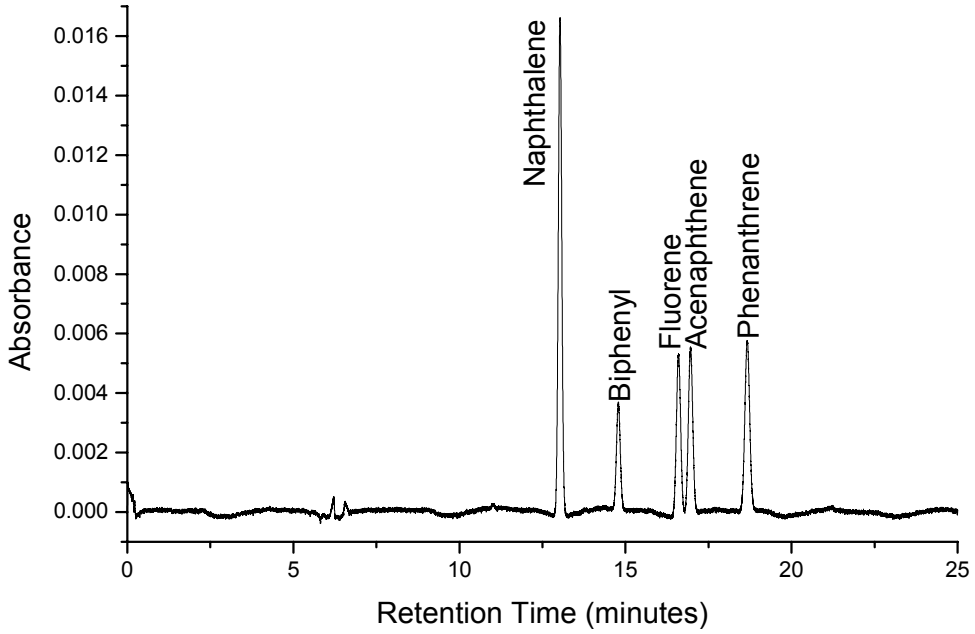

Figure 5.1. Example CEC chromatogram for the instrument development test mixture. Each component was present at 500 µM in acetonitrile. CEC separation recorded using absorbance detection at 214 nm.

The column used to produce the chromatogram shown in Figure 5.1 had a packed length from inlet to window of 432 mm and a total length of 624 mm. The column ID was 100 µm, with injection achieved by application of 5 kV for 5 seconds, with a running potential of 30 kV. Data was recorded using a PC fitted with the Pico Technology ADC-42 analogue to digital converter. Chromatographic efficiencies for each peak are listed in Table 5.2, being expressed as a plate number obtained from measurements of half height peak width. The baseline disturbance that can be seen in the chromatogram, at a retention time of ~ 6.5 minutes, marks the solvent front from the injection. This shows that the mobile phase velocity was ~ 1 mm s^{-1}.

Analyte	Efficiency (N)	Efficiency (N/m)
Naphthalene	70,000	162,000
Biphenyl	73,000	168,000
Fluorene	76,000	176,000
Acenaphthene	73,000	170,000
Phenanthrene	71,000	162,000

Table 5.2. Efficiencies for the CEC chromatogram of the instrument development test mixture displayed in Figure 5.1 expressed as a plate number (N), and as a number of plates per metre (N/m).

For comparison, separation of the instrument development test mixture was attempted by HPLC using the Waters 2690 Separations Module and the Waters 486 Tunable Absorbance Detector. The column used here was a Phenomenex (Torrance, CA, USA) [4] Prodigy (column length = 150 mm and ID = 2 mm), which is based on porous silica particles of 5 µm diameter coated with 'ODS (3)' (a C18, end-capped stationary phase). The column was chosen to be as similar as possible to the CEC columns prepared in this work. Data was recorded at 214 nm, while the mobile phase utilised was 50% 50 mM ammonium acetate adjusted to pH 6.0 with acetic acid, 50% acetonitrile. Using an identical mobile phase to that employed for CEC, no separation was achieved. The flow rate of the mixed mobile phase was set to 0.5 mL min^{-1}, and the resulting chromatogram is shown in Figure 5.2. This shows a separation to have been achieved at relatively low chromatographic efficiency. Selection of a more appropriate column and more extensive method development could perhaps improve chromatographic efficiency. This result does, however, illustrate that although HPLC is not capable of such high separation efficiencies as CEC, selectivity can be enough to answer the analytical question.

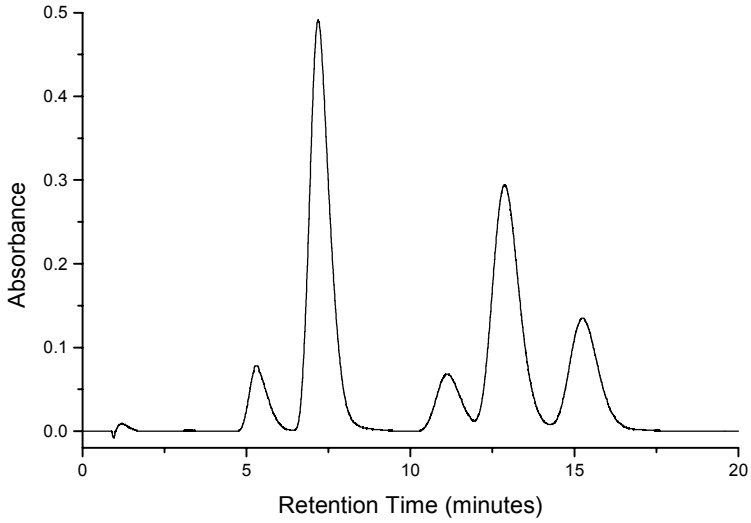

Figure 5.2. HPLC separation of instrument development test mixture using a Phenomenex Prodigy C18 column and a mobile phase consisting of equal amounts of acetonitrile and 50 mM ammonium acetate adjusted to pH 6.0 with acetic acid.

5.2. An Operational Simplification: The Transfer Capillary

A typical chromatographic column for use in CEC consists of a narrow fused-silica capillary, packed from the inlet to an absorbance detection window, with an unpacked region beyond the window (as illustrated in Figure 2.15). The capillary is usually packed with porous silica particles to which the stationary phase has been chemically bonded. Silica particles at each end of the packed bed are sintered to produce the frits that retain the packing material, while the absorbance detection window is produced by removing the protective capillary coating at the end of the packed bed. When coupling to mass spectrometry, this window is often retained to provide additional information, but the requirement for an absorbance detection window is removed. The capillary can therefore be packed throughout its entire length, from inlet to the outlet, simplifying the system.

As mentioned above, terminating the column at the vaporisation point was deemed to be too difficult. The column was therefore terminated in an electrically grounded junction, using a narrow capillary to transfer column eluate to the vaporisation point. Such a system is illustrated in Figure 5.3, and would be expected to allow

independent optimisation of chromatographic system and interface. Placing the junction outside the vacuum chamber would also allow column swapping without the interruption caused by opening the chamber.

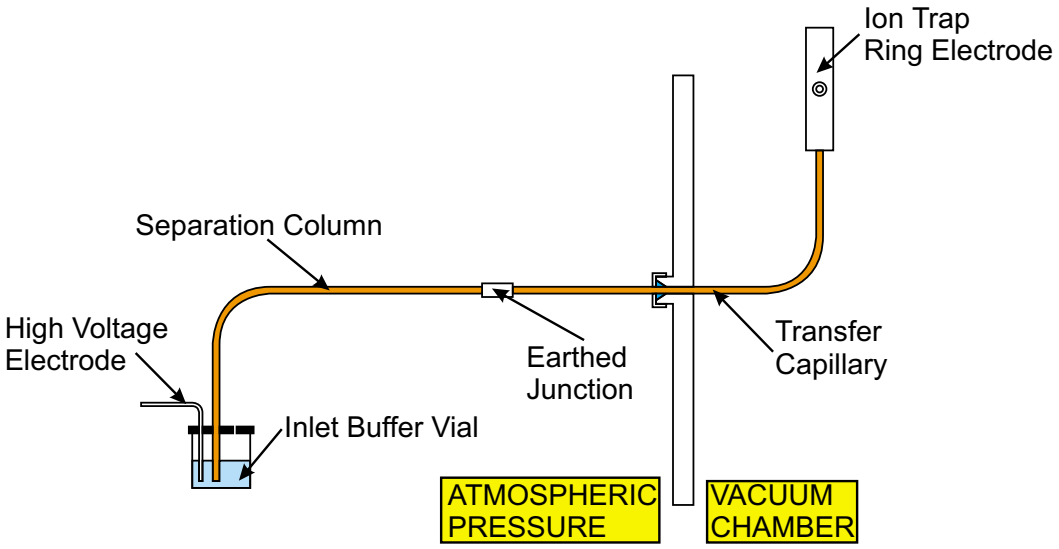

Figure 5.3. Use of a transfer capillary between the separation column and ion trap as an operational simplification.

Because liquid flow through the transfer capillary must originate from a pressure gradient, the flow will be laminar and will result in a loss of chromatographic efficiency. Degradation is minimised by using a transfer capillary of reduced ID in comparison with the separation column [5]. For a transfer capillary half the length of the separation capillary, when connecting a 100 µm ID separation column to a 25 µm ID transfer capillary, the decrease in efficiency, expressed as a plate number, is predicted to be 17% [5]. This theoretical data does of course assume a perfect joint between the separation column and transfer capillary. A further advantage of this system might arise from the pressure generated by the column that is used to push mobile phase through the transfer capillary. It has been suggested that pressurisation is useful to suppress gas bubble formation [6,7], which is often thought to occur at the exit frit [8]. If the mobile phase is assumed to be flowing at 1 mm s^{-1} through a separation column of 100 µm ID with a bed porosity of 0.4 [9], the volumetric flow rate can be calculated to be 3.14 nL s^{-1}. To maintain this flow rate through a transfer capillary of 25 µm ID and length 0.5 m filled with a mobile phase having a viscosity

of 0.369×10^{-3} N m^{-2} s (acetonitrile), the pressure differential required is only 0.6 atmospheres (see Equation 2.3). Bubble suppression is therefore an unlikely beneficial side effect of the transfer capillary, as the terminus of the separation column is at a lower pressure in the interface than in stand-alone CEC.

5.3. Simulation of Fluid Flows through Capillary Junctions

Typical CEC flow rates are measured using the time required for an unretained analyte to pass through the column, and tend to fall in the range from 1.0 to 2.0 mm s^{-1}. Assuming a packed bed porosity of 0.4 [9], and that the ID of the separation column is 100 µm, typical volumetric flow rates through the column fall in the range from 190 to 380 nL min^{-1}. On passing through a junction between capillaries of differing ID this volumetric flow rate must be maintained. Therefore, connecting a 100 µm ID packed column to a 33⅓ µm ID unpacked transfer capillary (3:1 contraction ratio) would result in a typical mobile phase flow rate in the transfer capillary in the range from 3.6 to 7.2 mm s^{-1}. This ballpark figure, however, provides limited information about the effect that a junction will have on a chromatographic band. Computational fluid dynamics (CFD) modelling was therefore used to provide further information about the physical processes that occur at a junction. Dr George Alder (School of Engineering and Electronics, University of Edinburgh) kindly assisted by performing these simulations. Computer simulations of electrokinetic transport in microfabricated channel structures have previously been reported [10].

Fluent's (Lebanon, NH, USA) [11] Fluent 4.4.4 CFD software was used to investigate the optimum geometry for the junction between the separation column and the transfer capillary. Band dispersion was modelled for situations that are difficult to test directly by experiment. The modelling process is quite distinct from any practical experiment that can be performed because the width, profile and concentration of the incoming band can be arbitrarily selected. Volumes of fluid are labelled and then observed as they pass through a system. For any CFD calculation, boundary conditions must first be established, with the geometrical conditions used here illustrated in Figure 5.4.

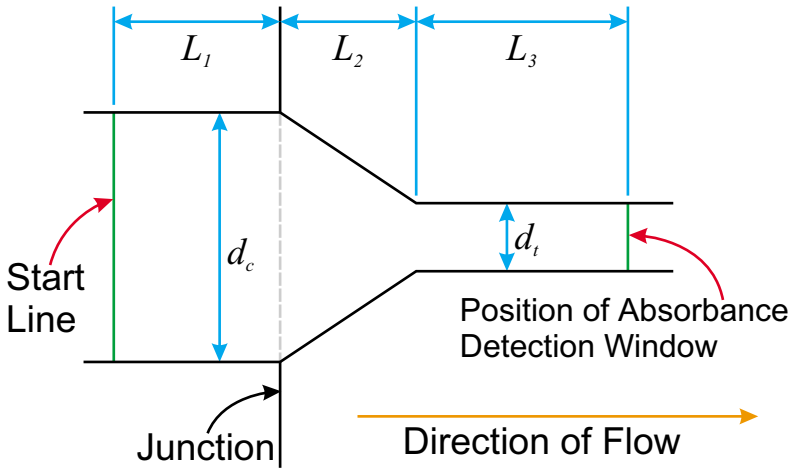

Figure 5.4. Geometrical boundary conditions used for CFD calculations.

Boundary conditions describing fluid motion are also required. Fluid enters from the left with a uniform velocity parallel to the axis of the capillary, which is constant across the capillary diameter, in order to represent the flat flow profile found with EOF. On crossing the start line, laminar flow conditions are imposed: the magnitude of the flow velocity varies in a parabolic fashion across the diameter of the capillary, from zero at the walls to a maximum in the centre. This represents the pressure drive (originating from EOF in the chromatographic column) that pushes fluid through the transfer capillary.

L_1 is a short length between the start line and the junction that is necessary due to the impossibility of starting the calculation at the junction when $L_2 = 0$. When $L_2 > 0$, therefore, $L_1 = 0$. L_2 is a transitional section between the separation column (ID = d_c) and the transfer capillary (ID = d_t). This transitional section is conical to maintain radial symmetry. Simulated chromatographic bands are observed at a distance ($L_2 + L_3$) from the junction. The system modelled here has a diffusion coefficient of 10^{-9} m^2 s^{-1}, a viscosity of 10^{-3} N m^{-2} s and a density of 10^3 kg m^{-3}. These conditions are similar to the behaviour of a small molecule in water, but essentially the program is monitoring the movement of labelled water. The incoming band profile is triangular to provide a representation of the Gaussian bands found in real systems. In the next two sections, two contrasting geometries are investigated

5.3.1. The Butt Joint Configuration

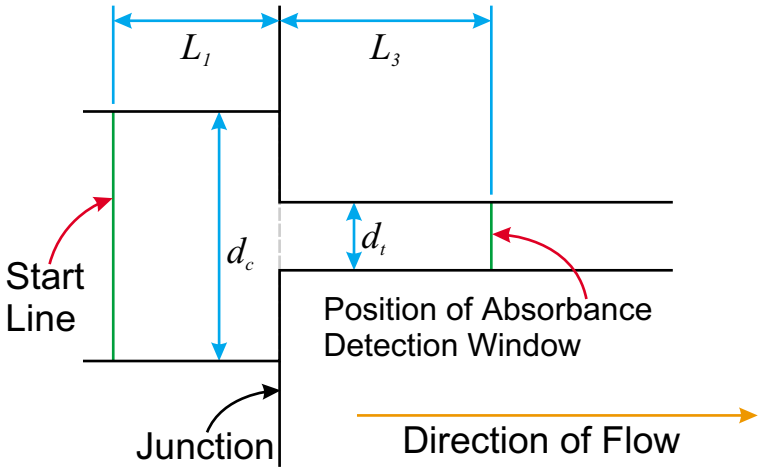

Figure 5.5. Geometrical boundary conditions for the butt joint configuration.

The simplest joint is the butt joint, where the two capillaries of differing ID are simply butted together. The simplified geometrical boundary conditions for this case are shown in Figure 5.5. As there is no transitional zone, $L_2 = 0$. Due to the nature of the computation, edges were rounded to reduce calculation time. Some calculations were, however, performed for square edges. The results are compared with those for simulations using rounded edges in Figure 5.6. This shows a simulated chromatographic band recorded using a virtual absorbance detector at $(L_2 + L_3) = 2.5$ mm for a 3:1 contraction ratio (100 µm ID capillary connected to a 33⅓ µm ID capillary). The test band has a base width of 2 s and a maximum concentration of 0.5 (arbitrary units), originating from a start line 0.1 mm before the junction ($L_1 = 0.1$ mm) with incoming velocity being 0.1 mm s^{-1}. Rounding the edges has only a slight effect on the results, while significantly reducing calculation time. The maximum concentration can be seen to be significantly reduced from 0.50 to ~ 0.11 (arbitrary units) when moving from a wider to a narrower capillary. It should also be noted that concentration is plotted against time, not absorbance as is typically found in a chromatogram.

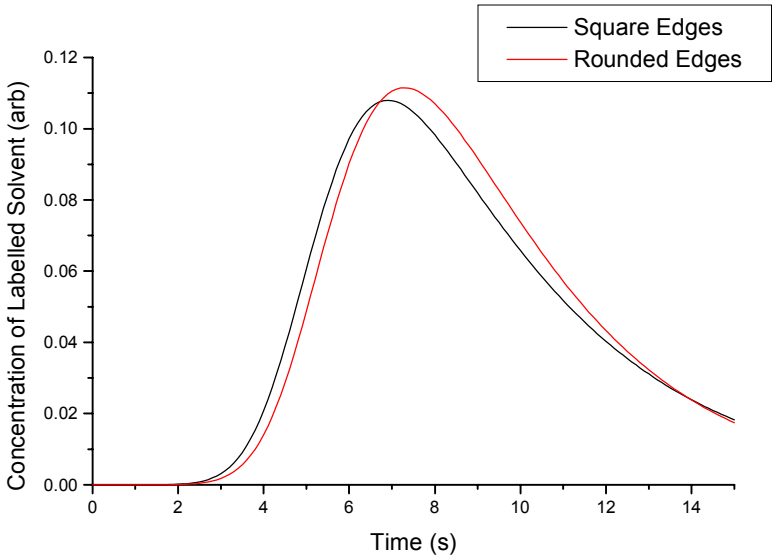

Figure 5.6. Effect of simplifying CFD calculation by rounding edges for the butt joint configuration.

The computational grid used in the rounded butt joint configuration is shown in Figure 5.7. The dependence of results on the chosen grid was tested by doubling the number of grid points and also by halving the time interval between each calculation. In all cases reported here, no significant dependence was found on grid density or time interval between each calculation. Due to the symmetry of the capillaries studied, radial sections were considered in all calculations and results are presented as radial sections.

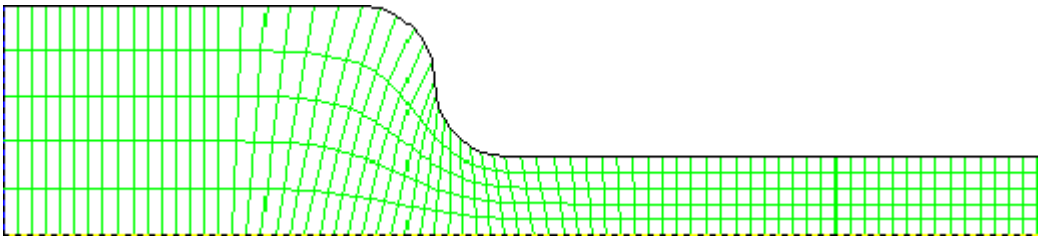

Figure 5.7. Computational grid used for the rounded butt joint configuration.

Figure 5.8 shows the variations in fluid flow velocity magnitude throughout a rounded butt interconnect, with hotter colours representing higher magnitudes for the conditions outlined above (red represents the highest velocity magnitudes, falling

through orange, yellow, green and blue to indigo and violet). Of note is the large stagnant area in the larger capillary.

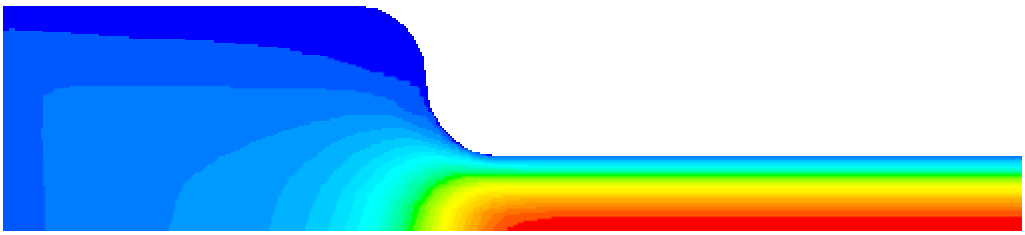

Figure 5.8. Variation in the magnitude of the fluid velocity through a rounded butt interconnect.

Because the start point in this simulation is some distance from the joint, a laminar flow velocity profile will develop before the joint. In a real system, laminar flow should only be found beyond the electrical ground point, although modelling what happens at this point would be difficult. The electrical field characteristics at the end of the column would be expected to be complicated as shown in Figure 5.9.

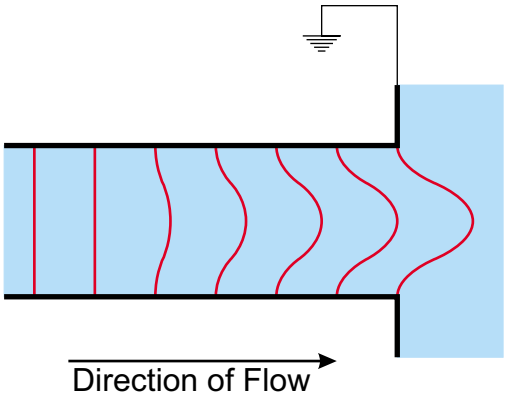

Figure 5.9. Schematic distorted electrical field contours found at the earthed terminus of a capillary (exiting into a large reservoir).

In Figure 5.8, the most noticeable feature is the high central velocity in the smaller capillary due to conservation of volumetric flow rate. The expected acceleration of the fluid as it enters the smaller capillary can easily be seen. The CFD calculation, being able to provide flow velocity information for any point, goes far beyond the predictive power of any bulk flow calculation. Figure 5.10 depicts the progression of an originally triangular labelled solvent band through the butt joint interconnect as a

sequence of images where a hotter colour represents a higher labelled solvent concentration. Conditions are as described above. The ten frames are consecutive and equally spaced in time.

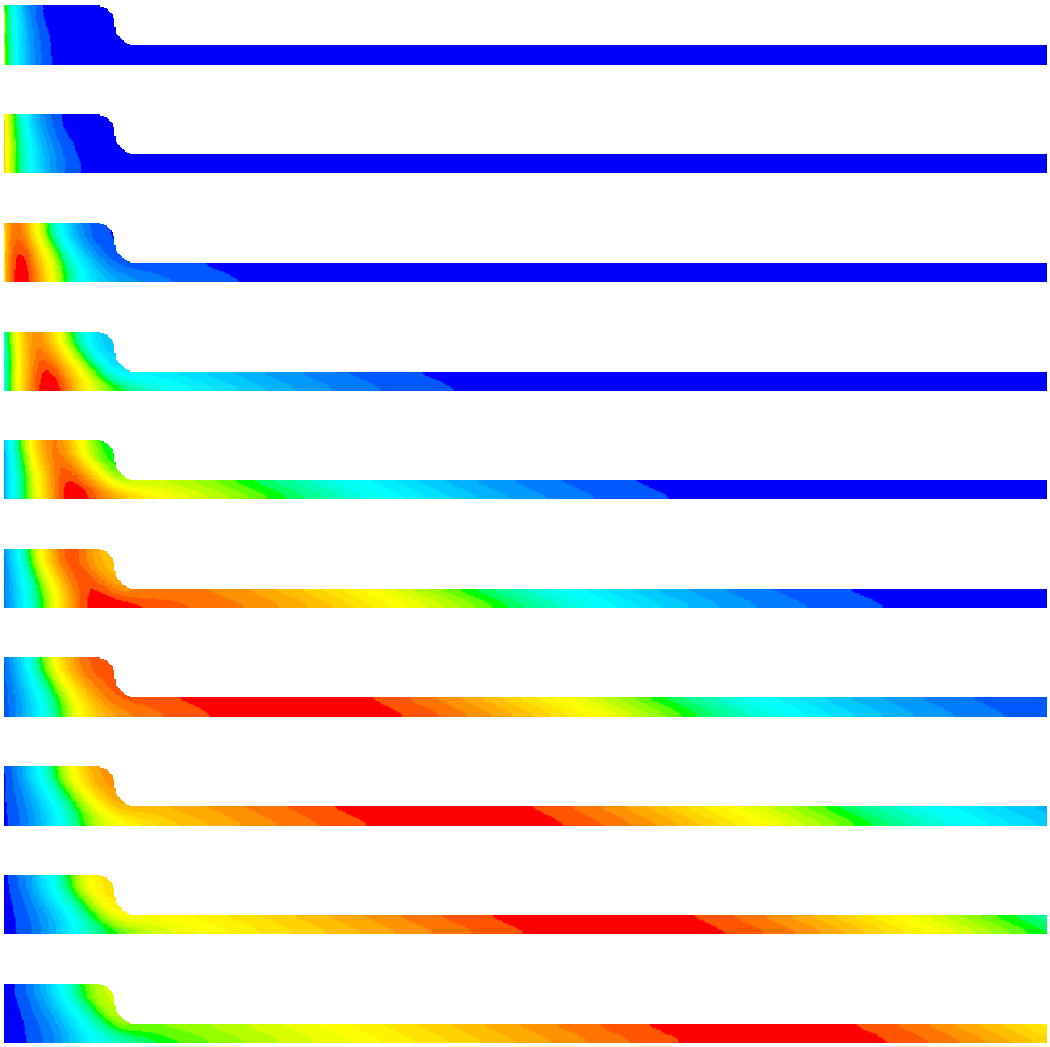

Figure 5.10. Progression of a band of labelled solvent through a rounded butt interconnect

These flow profile sequences show that when a butt connection is used, employing a contraction ratio of 3:1, there is clearly a stagnation volume in the corner of the larger capillary where a small amount of the original labelled solvent is trapped. Given that the original incoming band has a symmetric triangular distribution, the band exiting the junction develops significant tailing. This would be detrimental to any chromatographic separation.

5.3.2. The Conical Inlet Configuration

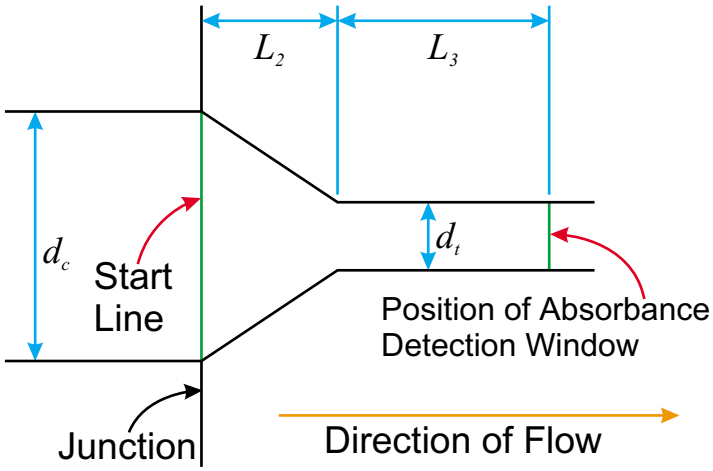

Figure 5.11. Geometrical boundary conditions for the conical inlet configuration.

An improved way of coupling the two capillaries would be to construct a conical inlet into the narrower capillary. The simplified geometrical boundary conditions for such a configuration are shown in Figure 5.11. In this model the simulation is started at the junction ($L_1 = 0$), with L_2 being equal to 0.1 mm. Simulated chromatographic data is again recorded a small distance along the transfer capillary. Locating the start line at the beginning of the inlet allows closer modelling of the real system. The variation in the magnitude of the flow velocity through the conical inlet is illustrated in Figure 5.12.

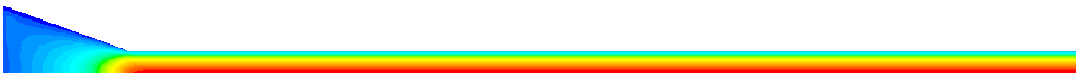

Figure 5.12. Variation in the magnitude of the fluid velocity through the conical inlet interconnect.

As with the simple butt joint, the flow velocity in the smaller capillary is naturally much greater than that in the larger capillary. The stagnant volume seen in Figure 5.8 is not seen in this case. The progress of a solute band through the tapered inlet is shown below in Figure 5.13. As with the butt joint, a triangular band with a base width of 2 s and a maximum concentration of 0.5 enters from the left at a velocity of 0.1 mm s^{-1}.

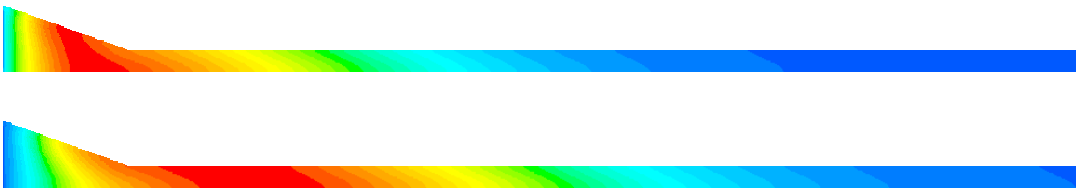

Figure 5.13. Progression of a band of labelled solvent through a conical inlet interconnect.

A comparison of the results obtained for the butt joint and the tapered inlet is shown in Figure 5.14. The data shown in both cases was obtained using a virtual absorbance detection window at $(L_2 + L_3) = 2.5$ mm. Dispersion introduced by the butt joint can be seen to be greater than that introduced using the conical inlet. The half height width of the peak associated with the conical inlet is 3.4 s, while that associated with the butt joint is 5.9 s. As the chromatographic efficiency expressed as a plate number is proportional to the inverse square of peak width, efficiency in plate number terms would differ by a factor of approximately three. Along with a significant increase in chromatographic resolution when the conical inlet is used, the maximum concentration is also higher, resulting in improved sensitivity. The integrated area for each peak must naturally be the same in both cases, but in a real system an intense peak helps bring a weak signal above the noise.

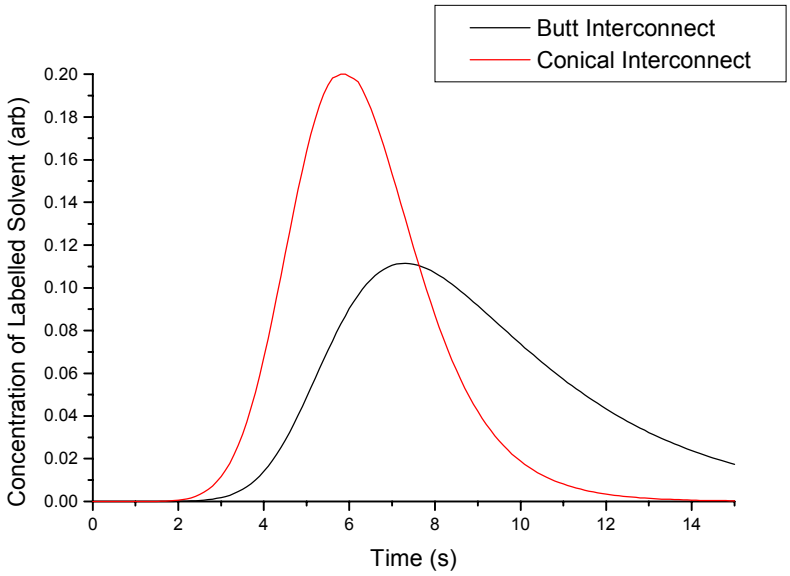

Figure 5.14. Comparison of dispersion between butt and conical inlet interconnects

Conical capillary inlets can be manufactured by etching the narrower capillary using hydrofluoric acid to increase the ID to that of the wider capillary [12]. Capillary action draws the acid into the capillary causing a natural taper to develop, while the polymeric coating protects the outside of the capillary. The capillary must then be ground down to the required ID. This process is explained schematically in Figure 5.15.

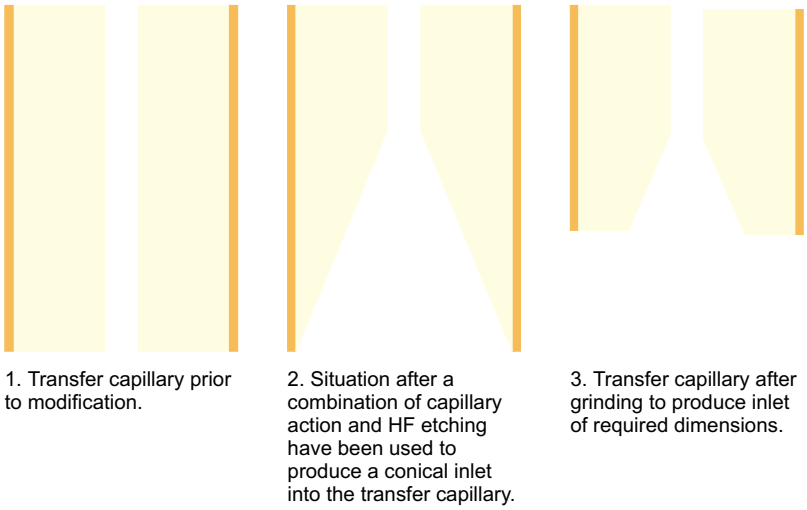

Figure 5.15. Production of conical inlet transfer capillaries.

Conical inlets have clearly been shown to offer superior theoretical performance to simple butt joints, but fabrication of such inlets proved to be difficult. The central problem was in grinding capillaries down to flat ends after etching. Therefore, all work here uses simple butt joint connections. Furthermore, in real junctions, it is not obvious what the effect of the terminal electrode will be. Circulation and mixing may occur, and non-symmetrical gaps between the capillaries, which are bound to be present in real systems, complicate the situation still further. Alignment problems that might be present are illustrated in Figure 5.16. The likely effect of packing materials is also not clear. Efforts were therefore focused on producing junctions with properly aligned capillary axes and narrow gaps.

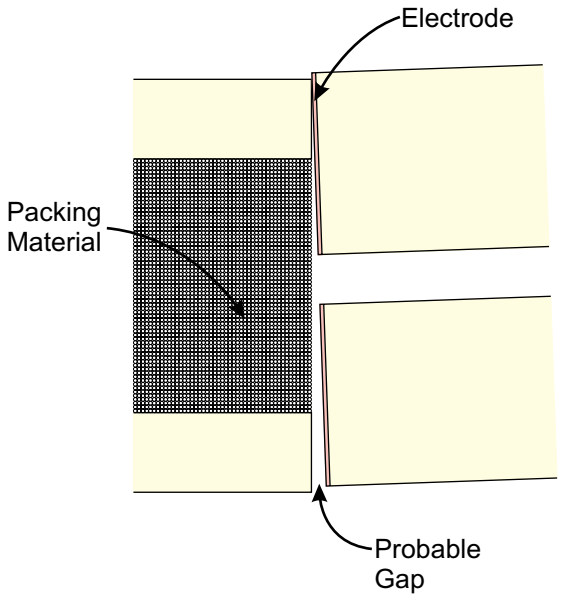

Figure 5.16. Exaggerated significant features of a real capillary junction that may be more important than idealised geometries.

5.4. Preliminary Laser Induced Fluorescence Imaging of a Solute Band being driven through an Open Capillary by a Combination of Electrophoresis and EOF

Ideally, CFD simulations would be supported by the imaging of real bands passing through real junctions. Observation of a solute band both before and after a structure such as a retaining frit or a capillary junction, using a standard absorbance detector,

is useful in order to discover how best to improve such structures. However, being able to watch what happens across the capillary diameter as the band passes through such a structure offers an understanding of how to improve the structure rather than just a measure of how well it functions. As a feasibility study, laser induced fluorescence (LIF) imaging has been used to observe a band of fluorescent dye being driven through an open capillary by a combination of electrophoresis and EOF.

Imaging of solute movements in CE was first reported as a means to improve the effectiveness of liquid junctions [13]. This work attempted to optimise junction dimensions, along with the composition of the buffer bathing the junction, by imaging the progress of a solute band passing through the junction. The solute band was a coloured dye, and a microscope equipped with a video camera was used to record images. Liquid junctions are used in coupling CE to mass spectrometry, as detailed in Section 3.2.1, and also in making grounded capillary unions [14]. Taylor and Yeung made a comparison of EOF and hydrostatic flow, using LIF imaging techniques to allow less concentrated dye solutions to be used [15]. Such work is limited, however, by using injected bands, which will naturally spread through the action of diffusion as they pass through the capillary. These workers addressed this problem by collecting long exposure images of fluorescing particles as they are washed through the capillary by EOF. The resulting streaks provided a measure of fluid velocity at a particular radial position.

At roughly the same time, Tsuda *et al.* imaged the progress of a dye through rectangular capillaries, chosen for better detection limits and more efficient heat dissipation [16]. The next significant progress, however, resulted from the work of Lempert et al. [17]. In this work caged dyes were introduced, which in their initial state are non-fluorescent, but which become fluorescent when activated by a laser. The activation laser is used to activate all dye molecules in a plane, allowing conventional LIF imaging of the movement of such planes. Paul *et al.* used this technique to demonstrate the difference between pressurised flow and EOF in CE, with impressive results being obtained [18]. Caged dyes, however, are expensive.

LIF imaging has also been used by Nilsson *et al.* to image entire CE columns, allowing the progress of separating fluorescent bands to be monitored [19-21]. This

method, although providing limited information about the variation in fluid velocity across a capillary diameter, has been applied to packed columns. The detrimental effects of frits on separation efficiency have been clearly demonstrated [22,23]. Further to this, the use of confocal microscopy to investigate solute distribution in packed beds under CEC conditions has recently been reported [24]. Certain solutes were shown to be found preferentially inside porous packing particles while others were shown to be outside. This technique is powerful enough to obtain information about radial variations in concentration in packed columns, allowing systematic development of retaining frits and junctions between packed and unpacked columns.

To investigate whether a basic imaging system could be produced in our lab, a 100 µm ID capillary, coated in a transparent protective polymeric coating, was mounted in the apparatus shown in Figure 5.17. The capillary was prepared for use by flushing with 0.1 M NaOH, followed by water, followed by mobile phase that had been degassed by sparging with helium while stirring. The mobile phase utilised was 50 mM aqueous (double distilled water) Na_2HPO_4 (BDH) that had been adjusted to pH 3.5 using phosphoric acid (Fisher). In a CE experiment performed using the Isco instrument, a sample of 282 µM rhodamine 6G (Lambda Physik, Göttingen, Germany [25]) in methanol (Fisher) was injected by application of 5 kV to the sample vial for 5 seconds. The structure of rhodamine 6G is given in Figure 5.18. The applied running potential was 20 kV. The total length of the capillary was 100 cm, with observations being made at a point 37 cm from the capillary inlet.

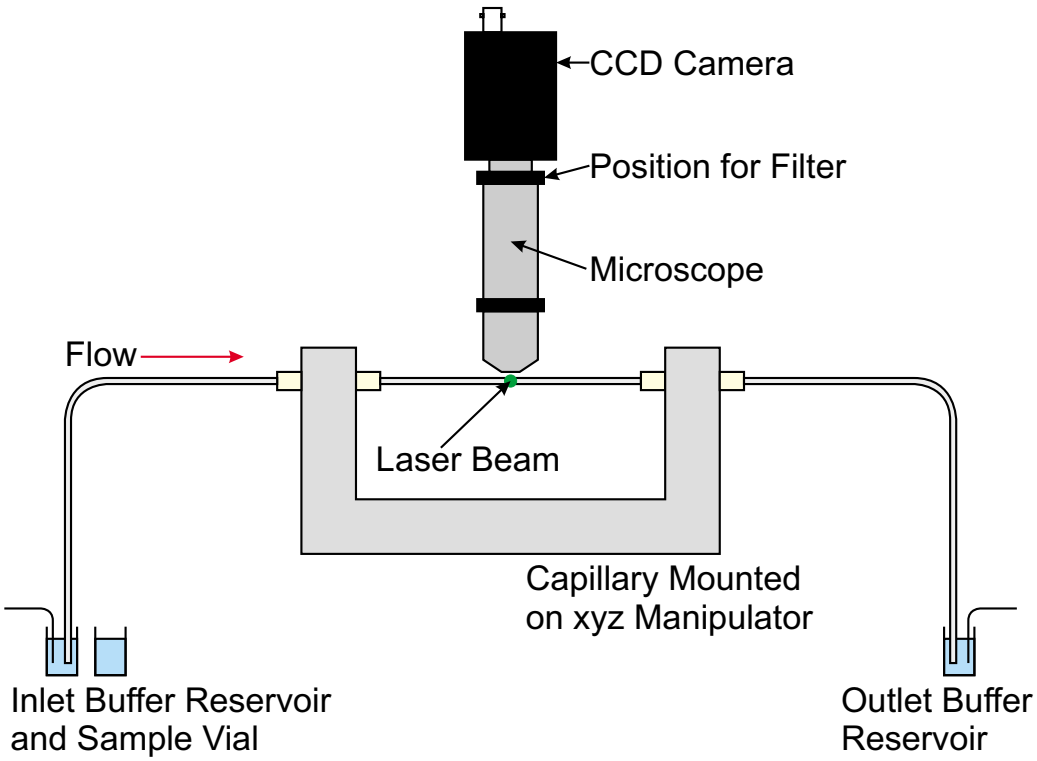

Figure 5.17. Experimental set up for observing analyte bands by laser induced fluorescence imaging. Laser beam is perpendicular to the plane of the paper.

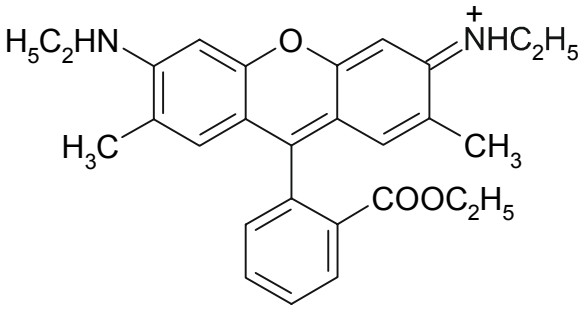

Figure 5.18. The structure of rhodamine 6G as used in these experiments.

Rhodamine 6G has an absorption maximum at 528 nm in ethanol and a fluorescence maximum at 556 nm in ethanol, and under the conditions used in this experiment was positively charged [26]. Excitation was achieved using the focused output from an argon-ion laser operating at 514 nm. The resulting fluorescence was observed orthogonally though a Prior Scientific (Cambridge, UK) [27] microscope using a sensitive Pulnix (Sunnyvale, CA, USA) [28] PU2015 CCD video camera. A glass filter (OG550, 3 mm thick, supplied by Comar Instruments, Cambridge, UK) was

utilised to reject the excitation wavelength. The signal was captured using a Data Translation (Marlboro, MA, USA) [29] DT355 frame grabber and analysed with Impuls's (Gilching, Germany) [30] Vision S image processing software. Figure 5.19 shows a series of frames recorded as the dye passed the detection point. Seven frames (taken at 25 frames per second) separate each image. The characteristic flat flow profile can clearly be seen in each frame.

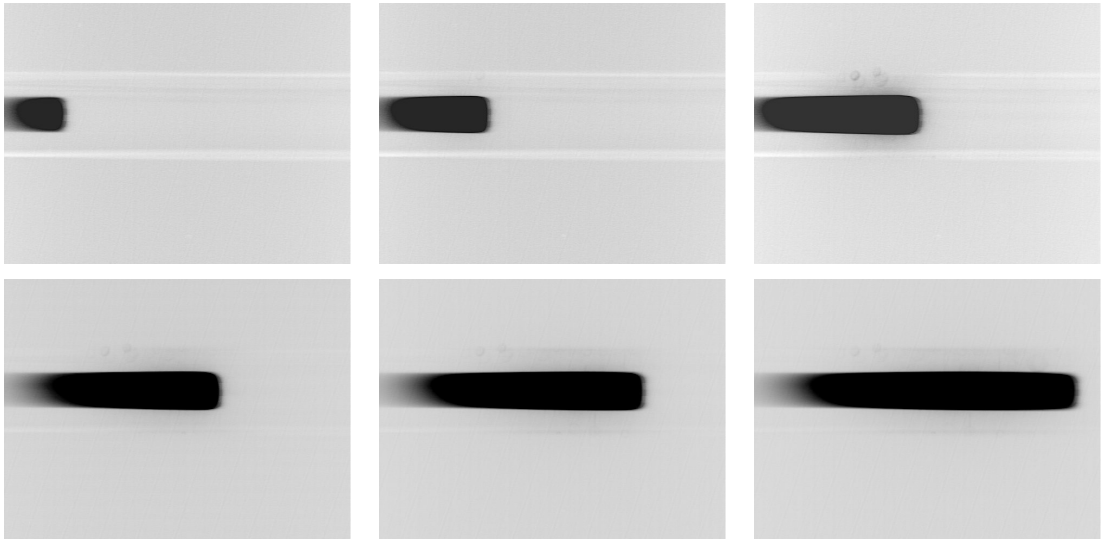

Figure 5.19. Consecutive LIF images for a solution of rhodamine 6G being driven through a 100 µm ID fused silica capillary by a combination of electrophoresis and EOF.

The ideal result would be a band of Gaussian profile, but a sharp front followed by a long tail is obtained. A Gaussian peak in this context would appear as a gradual darkening followed by a gradual lightening. What also might be expected, given the high analyte concentration, would be fronting, that is, there would be a gradual darkening followed by a more rapid lightening. This was not observed, however, indicating that sample capacity has probably not been exceeded. It must be noted that the camera was saturated immediately so possible detail of a gradually darkening image as the peak arrives is hidden and only a sharp front is observed. Severe tailing is likely to be due to interaction between the positively charged dye and the negatively charged capillary walls. It is fortuitous that the over concentration results in a sharp band that might be utilised for testing the quality of junctions. Any turbulence in a junction should disrupt the flat flow front. Unfortunately, however, it

would be difficult to produce a transparent junction that could be used to observe any effects. Stephen Hay continued this work as a BSc final year project in our group [31]. The effect of tight turns in the capillary was investigated with some success.

5.5. Preliminary Study into Imaging Analyte Bands in Packed Columns

Being able to directly view the progression of analyte bands through packed columns would be even more desirable than monitoring progression through open tubes, especially for watching bands crossing retaining frits. However, the packing material will be expected to efficiently scatter light making the collection of useful data difficult. A possible solution is provided by the use of columns packed with non-porous bare silica particles. These non-porous particles are less efficient at scattering light and hence may allow useful information to be obtained. Although mass transfer through pores inside particles is important, the bulk of the flow passes between particles. In order to explore the feasibility of making such measurements a column was packed as usual except that rather than placing the exit frit just before the window it was placed at the end of the column. The section of capillary exposed at the window was therefore packed and detection was attempted through this medium using the usual absorbance detector fitted in the CIA instrument. A column was also made that was packed in the same manner with porous silica based Hypersil Mixed Mode stationary phase to act as a control.

A 100 µm ID capillary packed with Hypersil Mixed Mode stationary phase was filled with a mobile phase that consisted of 25% 50 mM aqueous ammonium acetate that had been adjusted to pH 6.0 using acetic acid, 75% acetonitrile. The total length of the column was 695 mm while the window was located 503 mm from the inlet. Detection was achieved at a wavelength of 214 nm, while the running potential was 20 kV. Injection of a sample of 50 mM naphthalene in acetonitrile was achieved by application of 5 kV for 5 seconds. The resulting chromatogram is shown in Figure 5.20.

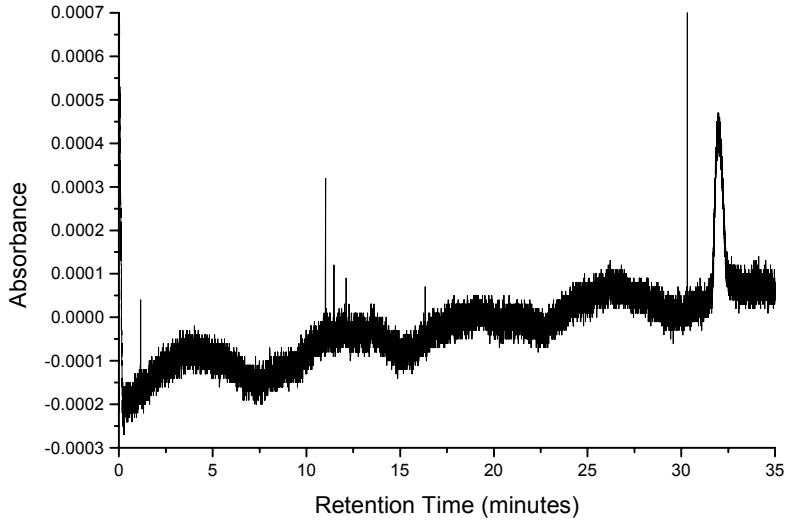

Figure 5.20. Absorbance detection on packed bed using a column packed with Hypersil Mixed Mode stationary phase. Sample was 50 mM naphthalene.

Naphthalene was chosen as a simple molecule with strong absorbance at 214 nm. The relatively high concentration of naphthalene used (50 mM) and the resulting small peak shows that detection on the packed bed in columns packed with porous silica particles is likely to be difficult. Such high concentrations will run the risk of exceeding the sample capacity of the column, preventing good quality chromatographic bands from being eluted, although the peak shape obtained in Figure 5.20 is good. The column was then modified by burning a new frit just before the detection window, removing the old exit frit at the column outlet and then flushing the column using the high-pressure pump to remove excess stationary phase. The column was therefore returned to the standard configuration in order to determine whether the column was fully functional and whether the packed bed detection data was reliable. The column was replaced in the Waters CIA instrument and filled with the same mobile phase. Running potential was increased to 25 kV, while the column was naturally slightly shorter. The chromatogram obtained for a test mixture of acenaphthene, biphenyl, fluorine, naphthalene and phenanthrene, each present at 500 µM in acetonitrile, is presented for comparison in Figure 5.21.

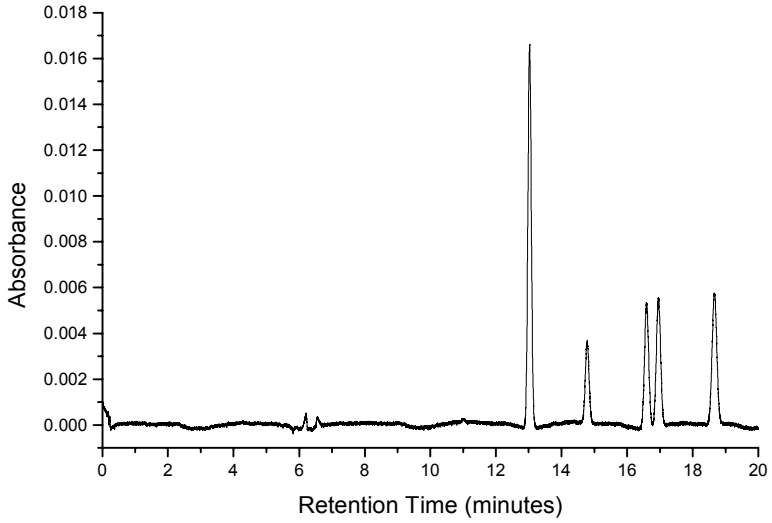

Figure 5.21. Test chromatogram used to ensure that column was performing adequately after on packed bed detection experiments.

Having shown that detection on the packed bed is possible, but of little use with porous stationary phases, a column was packed with non-porous bare silica particles. The same mobile phase as above was used at a running potential of 20 kV, with sample injection again being performed by application of 5 kV for 5 seconds. The total length of the column used was 457 mm, with the window being placed 285 mm from the inlet. A sample of 5 mM naphthalene in acetonitrile was investigated. The resulting chromatogram is shown in Figure 5.22. A good peak is obtained for naphthalene, which will have been washed through the column by the EOF. The small peak before the main peak is likely to be baseline disturbance originating from the injection. An enlarged view of this eluting peak is presented in Figure 5.23 showing that it is reasonably symmetrical, and could be used to monitor dispersion of bands passing through particular systems.

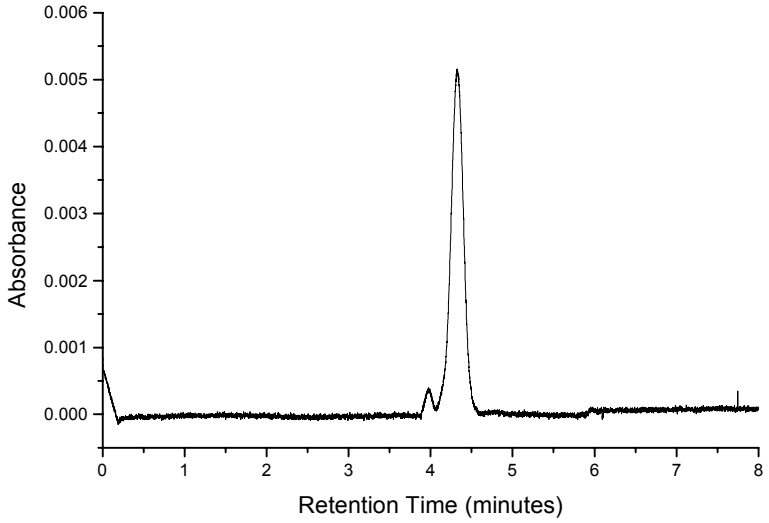

Figure 5.22. Absorbance detection of an unretained peak through the packed bed of a column packed with non-porous bare silica particles.

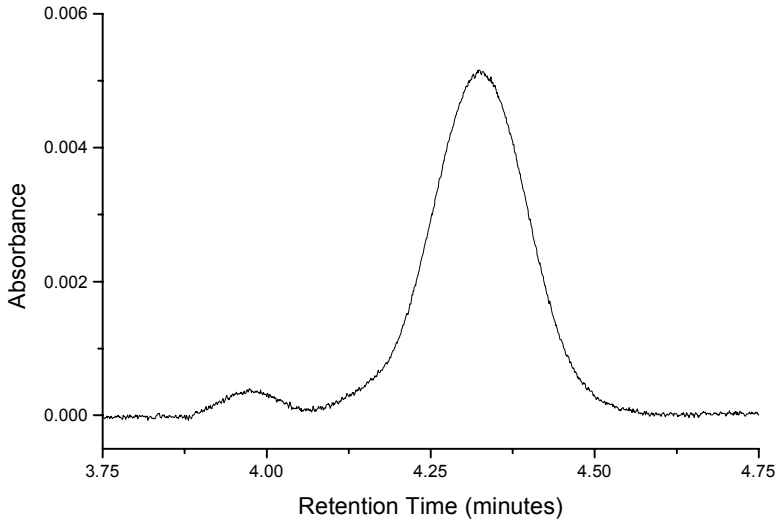

Figure 5.23. Enlarged view of peak profile from Figure 5.22 for the purpose of displaying the peak shape.

Ultimately, frits made using non-porous silica particles will be different from those made using porous silica particles to which a stationary phase is bonded. The packed bed structure of pores and channels, however, will be the same and it may be

possible to extract some useful information. The chief advantage would be that detection could be performed after one frit, rather than the usual system where detection is performed downstream from two frits. A more elegant experiment might be to utilise a dual detector system where a packed window was followed by a conventional window, with a frit or other structure between the windows. With both windows being placed close together a good before and after picture could be obtained. Such a system, however, was not readily available.

5.6. Development of an Efficient Earthed Junction

The junction between the separation column and the transfer capillary is predictably a critical point in the system. Early experiments utilised Upchurch Zero Dead Volume (ZDV) unions that are adequate for joining stainless steel tubing of relatively large ID, but degrade the efficiency of the separation with the narrow capillaries used in CEC. Figure 5.24 illustrates ZDV unions designed for use with 1/16" (1.5875 mm) stainless steel tubing being used with that tubing and being used with narrow capillaries. A narrowing in bore is found at the centre of the union to aid correct positioning of the tubing. The narrowed bore should be matched to the ID of the tubing used and is typically 0.010" (0.254 mm) or 0.020" (0.508 mm). The swept volumes for 0.010" and 0.020" 'thru-holes' are given as 25 nL and 134 nL, respectively, by the manufacturer. This gives the length of the narrowed section as 0.49 mm for the 0.010" case and 0.66 mm for the 0.020" case. With care, very good junctions can be produced.

However, attempts to join fused silica capillaries with an OD of approximately 0.4 mm (including polyimide coating) using sleeves made of polymeric tubing resulted in the ZDV degrading the efficiency of the separation. The volume contained in a packed column of length 500 mm, with an ID of 100 µm and a bed porosity of 0.4 is approximately 1.57 µL. This is large in comparison with the swept volume. The design of the union, however, makes it very hard to obtain the ideal swept volume because the capillary is mounted in polymeric tubing, which leads to alignment and positioning problems. ZDV unions can also be obtained without the

region of narrowed bore, but while such joints would seem to be useful for reducing dead volume, the production of an ideal joint becomes even harder.

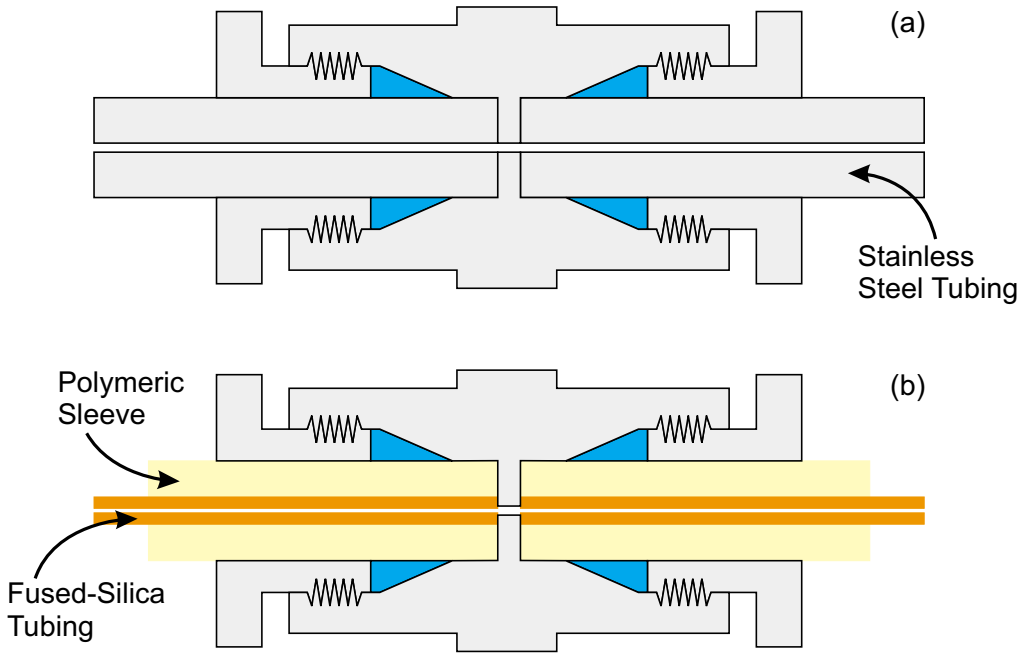

Figure 5.24. Cross-sectional views of an Upchurch Zero Dead Volume union used to join (a) stainless steel tubing versus (b) fused silica capillaries.

Although use of a ZDV union was not ideal, it did provide a reliable way of electrically earthing the separation column as the metal body of the union is in direct contact with the mobile phase. Due to the poor chromatographic performance of the ZDV union, however, an improved junction was desirable. Liquid junctions, although typically used for the addition of make-up flow, provide the first examples of efficient capillary junctions [14]. In the example given, the junction was required as a means of grounding a CE column, with electrolyte after the junction flowing to an electrochemical detector. The junction was chosen to be very narrow to allow electrical connection, but to minimise mass transfer with the liquid in which the junction is immersed. Another reported method, this time designed for CEC, is to use sleeves of tightly fitting tubing to make the junction, coating either capillary terminus with graphite paste to provide a connection to electrical ground [5]. With some similar type of electrical coating, the heat shrink tubing reported by Rapp and Bayer

could also be used [32]. All three types of junction can only withstand low pressures, but as mentioned previously (Section 5.2), high pressures would not be expected.

Heat-shrink tubing was investigated, but achieving correctly aligned junctions was very difficult. Utilisation of a Supelco Capillary Column Butt Connector (CCBC) union provided a good way to join capillaries, but did not provide a method for electrically earthing the terminus of the separation column. The CCBC union is based upon a double-tapered ferrule. The capillaries are butted together in the ferrule, followed by the assembly being tightened, compressing the ferrule and producing a joint capable of withstanding moderate pressures. The double-tapered ferrule is, unfortunately, made from a non-conductive polymeric material. Numerous solutions involving conductive paint and fine wires were attempted, but were all found to be both unreliable and technically difficult to implement. A relatively simple solution involved coating the transfer capillary with copper using an Edwards E12E4 Vacuum Coating Unit [33]. The coating is relatively thin and reasonably robust, and is ideal for making electrically earthed junctions. The CCBC union as used is illustrated in Figure 5.25.

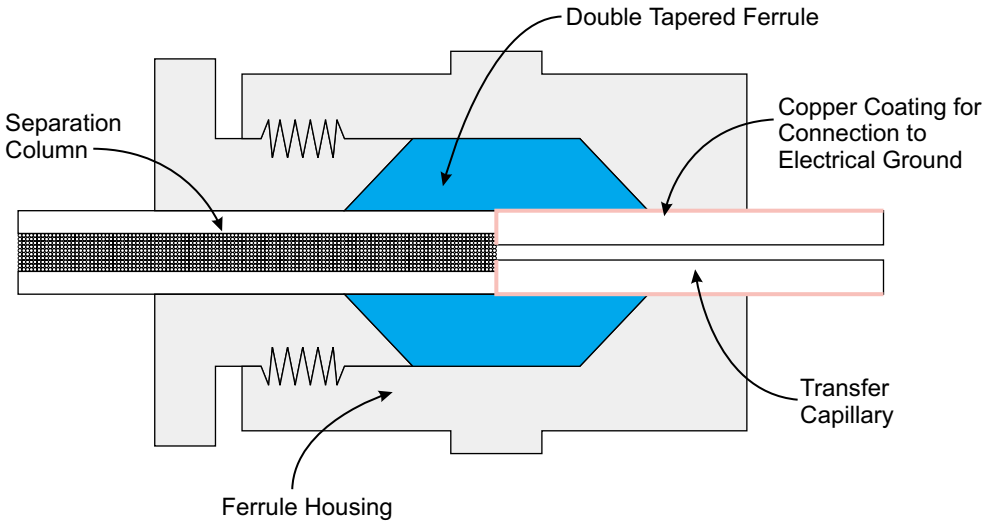

Figure 5.25. Simplified cross-section of Supelco Capillary Column Butt Connector showing the separation column entering from the left and the narrower transfer capillary exiting to the right. The double-tapered ferrule is highlighted in blue, and the copper coating of the transfer capillary in pink.

The CCBC union was first tested without the conductive coating. A capillary of 100 µm ID was prepared in the usual manner with a total length of 848 mm, and a length from inlet to absorbance detection window of 601 mm. The capillary was mounted in the Isco instrument and detection performed at 210 nm with a time constant of 0.4 seconds. The column was filled with 50 mM ammonium acetate (pH allowed to remain at unadjusted value of 7.0) that had been degassed by sparging with helium. Injection was performed by applying 5 kV to the sample vial for 5 seconds, while a running potential of 15 kV was used giving a recorded current of circa 75 µA. 1 mM 1-naphthalene sulfonic acid in water was injected, with the recorded electropherogram reproduced as Figure 5.26.

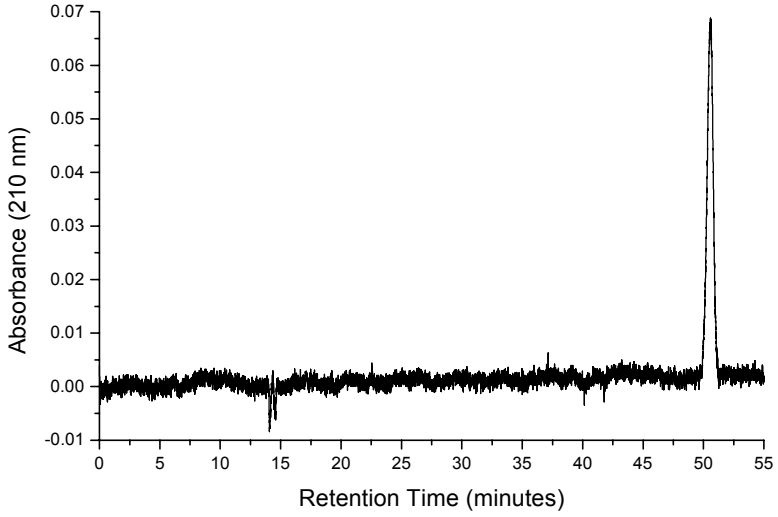

Figure 5.26. CE electropherogram for the injection of 1 mM 1-naphthalene sulfonic acid onto a fused silica capillary of 100 µm ID recorded at a running potential of 15 kV.

The capillary was then broken 424 mm from the inlet and repaired using the CCBC union. The experiment was repeated and the resulting electropherogram is shown in Figure 5.27. The peak is largely similar, although a shift to shorter retention times after the break is obvious. Retention times in CE shorten with column use as NaOH washes increase the surface concentration of silanol groups, but for unretained peaks to appear approximately 1.5 minutes sooner in retention time is unusual. Separation

efficiency for the unbroken capillary was 45,000 (74,000 per metre) theoretical plates while that for the broken capillary was 35,000 (59,000 per metre) theoretical plates, showing a 21% decrease in chromatographic efficiency. The CCBC union proved to be effective in largely retaining separation efficiency through a junction.

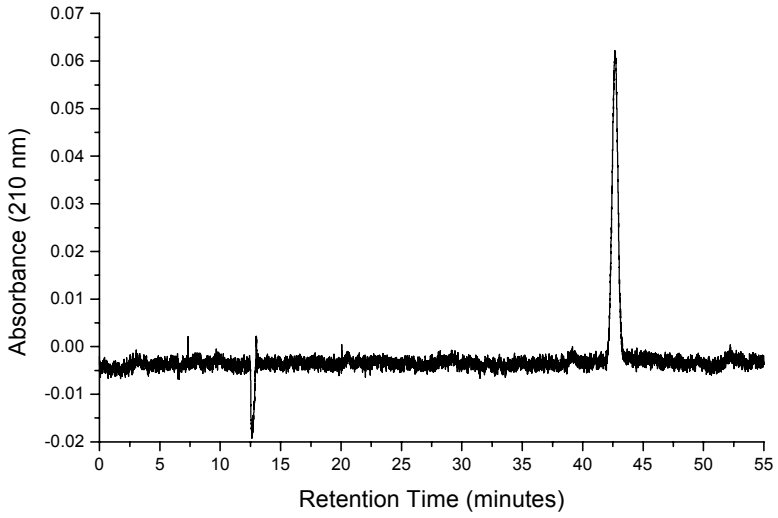

Figure 5.27. CE electropherogram for the injection of 1 mM 1-naphthalene sulfonic acid onto a fused silica capillary that had been broken and then repaired using a Supelco Capillary Column Butt Connector.

A more representative test of this new capillary jointing strategy for CEC columns was carried out using a 304 mm column with an ID of 100 µm packed with 3 µm diameter Hypersil ODS stationary phase. This was connected to a transfer capillary of length 440 mm and ID equal to 25 µm. The end of the transfer capillary that was used in the junction was coated with copper to provide a connection to electrical ground. The system was filled with a mobile phase composed of 25% 5 mM TRIS (Sigma), 75% acetonitrile. The system was run at an applied potential of 25 kV on the Isco instrument, which resulted in a current of 2 µA. The test sample consisted of thiourea, benzamide, anisole, benzophenone and biphenyl, each present at 1 mg mL^{-1} in acetonitrile. Injection was achieved by application of 5 kV to the sample vial for 5 s, with an absorbance detection window being placed 97 mm along the transfer capillary from the junction. Detection was performed at 210 nm, with an absorbance

range of 0.01 (absolute absorbance values plotted) and a time constant of 0.4 s. The resulting CEC chromatogram is shown in Figure 5.28.

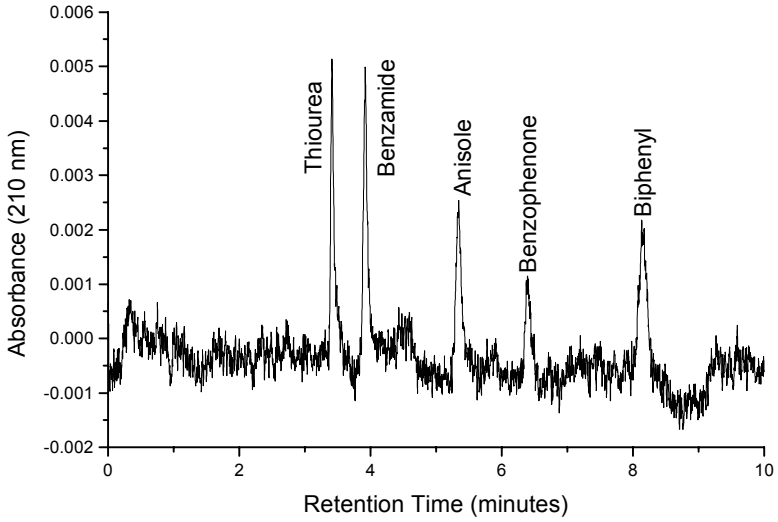

Figure 5.28. CEC separation of a mixture of thiourea, benzamide, anisole, benzophenone and biphenyl recorded using an absorbance window in the transfer capillary.

Chromatographic efficiencies expressed as a number of theoretical plates for the chromatogram displayed in Figure 5.28 are given in Table 5.3. Although the data quality appears relatively poor, it must be remembered that detection is occurring in a very small absorbance cell, forced by the use of a 25 µm ID transfer capillary.

Analyte	**Efficiency (N)**	**Efficiency (N/m)**
Thiourea	25,000	62,000
Benzamide	22,000	54,000
Anisole	19,000	48,000
Benzophenone	27,000	68,000
Biphenyl	20,000	51,000

Table 5.3. CEC chromatographic efficiencies, expressed as plate numbers, for the separation of a mixture of thiourea, benzamide, anisole, benzophenone and biphenyl found when testing the Supelco Capillary Column Butt Connector.

5.7. Investigating Reproducibility in CEC

In any analytical technique, reproducibility is essential. CEC is typically regarded as being less reproducible than HPLC, and hence a brief study was undertaken. A CEC column was produced that was packed with Hypersil Mixed Mode stationary phase (3 µm diameter particles) which was of total length 699 mm, with a packed length from the inlet to an absorbance detection window of 434 mm. The column was filled with a mobile phase that consisted of 25% 50 mM ammonium acetate that had been adjusted to pH 6.0 with acetic acid, 75% acetonitrile. The column was mounted in the CIA instrument, forcing absorbance detection to be carried out at a wavelength of 214 nm. A running potential of 30 kV was applied, while injection was achieved by application of 5 kV for 5 seconds to the sample vial. First, a sample of 1.3 mM thiourea in acetonitrile was investigated, with three consecutive runs being recorded. The resulting chromatogram in the region of the eluting band is shown in Figure 5.29. The retention times for thiourea, which is regarded as an unretained marker, were 6.257, 6.247 and 6.224 minutes for the first, second and third peak, respectively. Although the standard deviation is only 0.017 minutes (approximately 1 second), there is a possible trend towards shorter retention times.

A possible explanation for this reduction in retention time is heating. As the column warms under applied potential, mobile phase viscosity will fall, leading to an increased EOF rate (see Equation 2.7). In a CE separation this heating would result in a severe loss of performance, but in CEC, due to the packing material preventing the development of convection currents, only a moderate loss of performance would be expected. Allowing the column to equilibrate for sufficient time before use should preclude this problem, with further improvements being offered by the use of systems designed to accurately regulate column temperature.

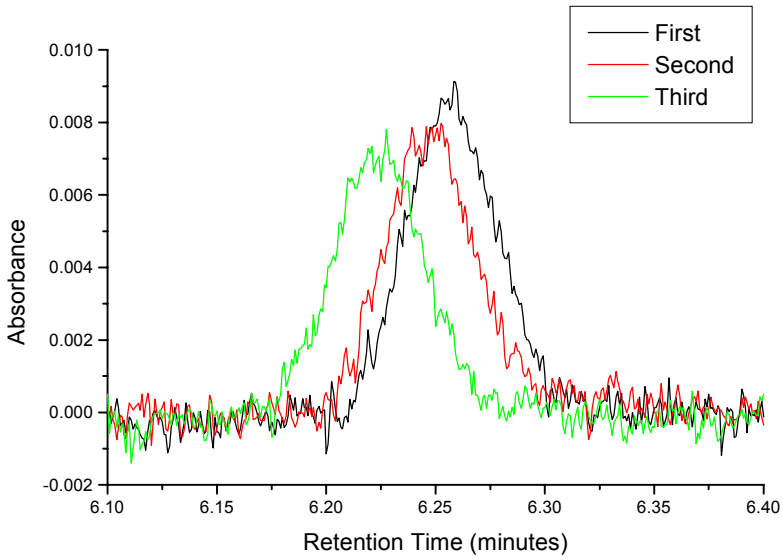

Figure 5.29. Three consecutive injections of 1.3 mM thiourea onto a CEC column packed with Hypersil Mixed Mode stationary phase to illustrate the level of reproducibility available in CEC.

To further investigate reproducibility, the instrument development test mixture with each component present at 2 mM in acetonitrile, was analysed in three consecutive injections using the method described above. The resulting chromatograms are shown in Figure 5.30. An enlarged view of the last four eluting bands in these chromatograms is shown in Figure 5.31. For naphthalene, the retention times, efficiency and peak asymmetry from these three consecutive runs are given in Table 5.4.

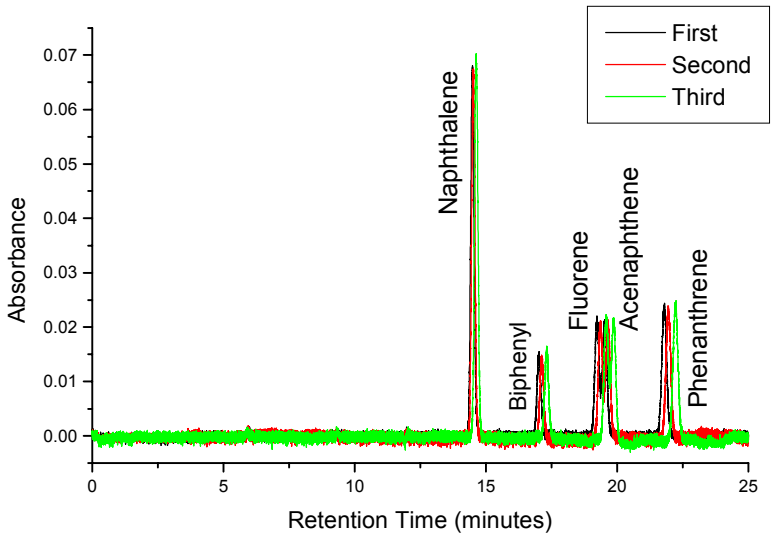

Figure 5.30. The result of three consecutive injections of the instrument development text mixture, with each component at 2 mM in acetonitrile, onto a CEC column packed with Hypersil Mixed Mode stationary phase.

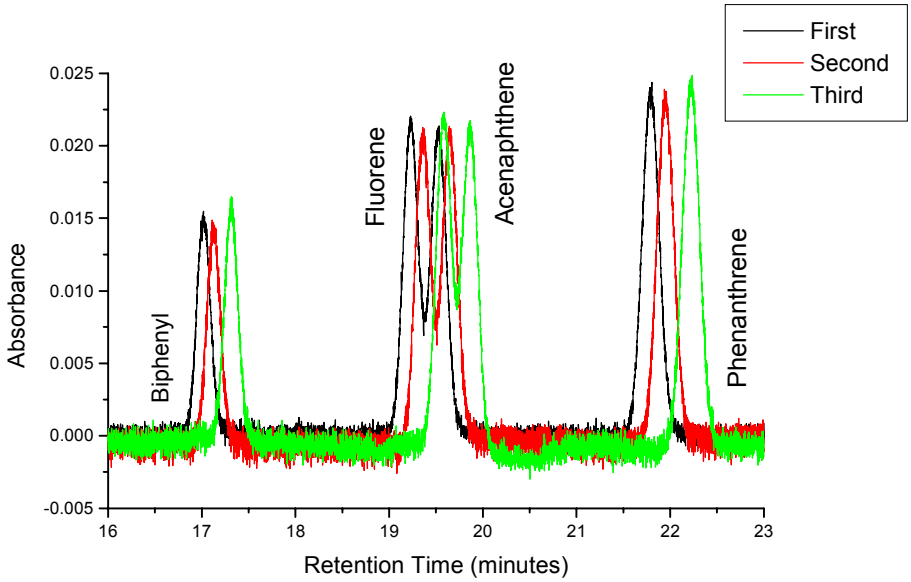

Figure 5.31. Enlarged view of the chromatogram presented in Figure 5.30 showing the final four peaks in greater detail. Note that baseline resolution has not been achieved for fluorene and acenaphthene.

Run	Retention Time (minutes)	Efficiency (N)	Efficiency (N/m)	Asymmetry
First	14.48	53,000	76,000	0.88
Second	14.52	55,000	79,000	0.96
Third	14.63	52,000	75,000	0.97

Table 5.4. Key indicators of chromatographic performance for the naphthalene peak in three consecutive separations of the instrument development test mixture.

In the case of the unretained marker, thiourea, a possible trend towards shorter retention times was observed, while with the instrument development test mixture, there is a possible trend towards longer retention times. No clear trend is seen in efficiency or peak asymmetry, with the peaks moderately tailing. When performing CEC on a regular basis, it is noticeable that retention times often increase through the course of a day. This lengthening in retention time is reversed when the column is flushed with freshly degassed mobile phase, with the apparent trend as the column ages being towards shorter retention times.

The trend towards longer retention times over longer periods of time is probably due to stationary phase damage. Hydrocarbon chains that constitute the stationary phase will break off from support particles as the column ages, exposing silanol groups and leading to an increase in EOF and a reduction in retention times. The daily trend towards longer retention times is more difficult to explain. Since flushing the column with freshly degassed mobile phase typically brought retention times back to normal, some degradation of the mobile phase in use other than heating may be the cause. This is most likely to be solvent evaporation from buffer reservoirs resulting in a more concentrated mobile phase. Gas concentration in the mobile phase will also rise. Replacing old mobile phase with freshly degassed mobile phase improves the situation, but using pressurised flow to purge the column offers better results. Ultimately the best solution would be sealed buffer reservoirs, mounted in a system capable of accurate temperature control.

5.8. Concluding Remarks

The additional challenges associated with terminating the CEC column in some structure mounted in the ring electrode of the ion trap were avoided by using a transfer capillary. These challenges are making an effective electrical connection and avoiding laser damage to the terminal frit. The transfer capillary is connected to the terminus of the CEC column through a junction, which must also allow electrical connection to be made. CFD calculations were used to investigate the ideal configuration for such a junction, but the practical difficulties of producing such junctions meant that simpler strategies were followed. Initial attempts to fabricate real junctions suffered from poor alignment, while use of junctions based on double tapered ferrules resulted in problems with electrical connection. Vacuum coating with copper was eventually identified as the best route towards reliable electrical connection, resulting in a junction that was proved to be effective. Preliminary attempts to image solute flows under EOF conditions were partially successful.

---

[1] C. Yan, R. Dadoo, H. Zhao, R. N. Zare and D. J. Rakestraw, *Anal. Chem.*, **1995**, *67*, 2026-2029.

[2] R. Dadoo, R. N. Zare, C. Yan and D. S. Anex, *Anal. Chem.*, 1998, 70, 4787-4792.

[3] D. R. Lide (Editor), *CRC Handbook of Chemistry and Physics (Seventy Fourth Edition)*, CRC Press, Boca Raton, FL, **1993**.

[4] Further information available at http://www.phenomenex.com

[5] R. J. Boughtflower, C. J. Paterson and J. H. Knox, *J. Chromatogr. A*, **2000**, *887*, 409-420.

[6] T. Tsuda, *Anal. Chem.*, **1987**, *59*, 521-523.

[7] N. W. Smith and M. B. Evans, *Chromatographia*, **1994**, *38*, 649-657.

[8] H. Rebscher and U. Pyell, *Chromatographia*, **1994**, *38*, 737-743.

[9] J. C. Giddings, *Dynamics of Chromatography, Part I, Principles and Theory*, Marcel Dekker, New York, **1965**.

[10] S. V. Ermakov, S. C. Jacobson and J. M. Ramsey, *Anal. Chem.*, **1998**, *70*, 4494-4504.

[11] Further information available at http://www.fluent.com

[12] M. E. P. Hows and D. Perrett, *Chromatographia*, **1996**, *43*, 200-204.

[13] W. G. Kuhr, L. Licklider and L. Amankwa, *Anal. Chem.*, **1993**, *65*, 277-282.

[14] R. A. Wallingford and A. G. Ewing, *Anal. Chem.*, **1987**, *59*, 1762-1766.

[15] J. A. Taylor and E. S. Yeung, *Anal. Chem.*, **1993**, *65*, 2928-2932.

[16] T. Tsuda, M. Ikedo, G. Jones, R. Dadoo and R. N. Zare, *J. Chromatogr.*, **1993**, *632*, 201-207.

[17] W. R. Lempert, K. Magee, P. Ronney, K. R. Gee and R. P. Haughland, *Exp. Fluids*, **1995**, *18*, 249-257.

[18] P. H. Paul, M. G. Garguilo and D. J. Rakestraw, *Anal. Chem.*, **1998**, *70*, 2459-2467.

[19] S. Nilsson, J. Johansson, M. Mecklenburg, S. Birnbaum, S. Svanberg, K. -G. Wahlund, K. Mosbach, A. Miyabayashi and P. -O. Larsson, *J. Cap. Elec.*, **1995**, *2*, 46-52.

[20] J. Johansson, D. T. Witte, M. Larsson and S. Nilsson, *Anal. Chem.*, **1996**, *68*, 2766-2770.

[21] T. Johansson, M. Petersson, J. Johansson and S. Nilsson, *Anal. Chem.*, **1999**, *71*, 4190-4197.

[22] B. Behnke, J. Johansson, S. Zhang, E. Bayer and S. Nilsson, *J. Chromatogr. A.*, **1998**, *818*, 257-259.

[23] B. Behnke, J. Johansson, E. Bayer and S. Nilsson, *Electrophoresis*, **2000**, *21*, 3102-3108.

[24] M. Lowry, Y. He and L. Geng, *Anal. Chem.*, **2002**, *74*, 1811-1818.

[25] Further information available at http://www.lambdaphysik.com

[26] U. Brackmann, *Lambdachrome® Laser Dyes (Third Edition)*, published on the internet by Lambda Physik, Goettingen, Germany. Available at http://216.218.202.68/pdf/pdf_54.pdf (December 2002).

[27] Further information available at http://www.prior.com

[28] Further information available at http://www.pulnix.com

[29] Further information available at http://www.datx.com

[30] Further information available at http://www.impuls-imaging.com

[31] S. J. Hay, *The Development of Micro Total Analysis Systems*, BSc Final Year Project, University of Edinburgh, **2001**.

[32] E. Rapp and E. Bayer, *J. Chromatogr. A*, **2000**, *887*, 367-378.

[33] This instrument is essentially a high vacuum bell jar equipped with electrical feed-throughs. A tungsten wire crucible containing the metal with which to coat is suspended between the electrodes in the vacuum chamber, while the capillary to be coated is suspended above the crucible in an appropriate orientation. Passing current between the electrodes heats the crucible and melts the coating metal. Due to the high vacuum, evaporated metal atoms can travel some distance and hence are able to coat the capillary.

6. Combining Capillary Electrochromatography with Ion Trap Storage Time-of-Flight Mass Spectrometry

The small volumetric flow rates encountered in CEC, unlike those found in HPLC, allow termination of the separation column inside a high-vacuum chamber. This removes the need for the differential pumping stages that are typically encountered in atmospheric pressure ion sources. In the interface employed in this work, molecules are vaporised using a pulsed IR laser that is focused onto liquid flowing out of the capillary and then ionised after a short delay using a pulsed UV laser. Vaporisation and ionisation are separated both spatially and temporally, allowing separate optimisation. Ionisation laser wavelength is chosen to provide a degree of selectivity, while vaporisation efficiency should be largely insensitive to the wavelength chosen. It is important to note that sample vaporisation and ionisation both occur inside the ion trap, which is used as a storage device rather than as a stand-alone mass spectrometer, to avoid transmission loses. Vaporised chromatographic mobile phase molecules act in place of helium as buffer gas to damp trapped ion motions in order to improve mass spectrometric resolution. Ions may be accumulated in the trap for a number of laser vaporisation laser ionisation cycles before finally being ejected into a TOF mass analyser.

6.1. Initial Tuning of the ITS/TOF Mass Spectrometer

6.1.1. Instrument Tuning with a Gaseous Analyte: Aniline

The chromatographic system described in Chapter 5 is designed to provide a continuous flow of eluate, which most of the time will consist solely of the mobile phase. Occasionally, for short periods of time, dissolved analyte will also be present. Even then, however, analyte concentration will be changing rapidly with time. Such a system is obviously not suitable for tuning the mass spectrometer. An alternative system capable of providing a continuous flow of analyte was required, with the simplest solution being to allow the analyte to enter as a gas. Naturally, no vaporisation laser is required, but all other operating parameters can be thoroughly investigated. The gaseous analyte chosen was aniline vapour, which was produced by

placing liquid aniline in an evacuated chamber that was connected via a length of stainless steel tubing to the ion trap. Evaporated aniline passes through this tube, entering the trap through a hole cut in the ceramic ring furthest from the mass analyser. Helium is allowed to enter through a hole cut in the ceramic ring closest to the mass analyser. The ion trap structure is described fully in Section 4.5.

With a continuous analyte source available, voltages applied to the ion optics, experimental timing, and the amount of helium used were tuned to obtain the optimum signal. The fourth harmonic output of the Quantel Brilliant laser (λ = 266 nm) was employed for sample ionisation, operating at 10 Hz and providing 4 mJ pulses. Once optimum settings had been identified for other parts of the instrument, the effect of ion trap storage time on molecular ion peak area was investigated. Molecular ion peak area is used as a measure since this is what will be used to produce selected ion chromatograms from CEC/MS data. For aniline, having a molecular mass of 93, the molecular ion will also have a m/z ratio equal to 93 since laser ionisation acts by removing a single electron. A relatively narrow integration window of 200 ns was used to provide a balance between good signal to noise and obtaining a strong signal. Initially, storage times of less than 100 ms were investigated, with the results plotted as Figure 6.1. The trap was also used for accumulation, the difference between accumulation and storage being that ions were collected from more than one laser shot. In this case, ejection of ions into the mass analyser occurred 10 ms after the final laser shot. The results of these experiments are plotted in Figure 6.2.

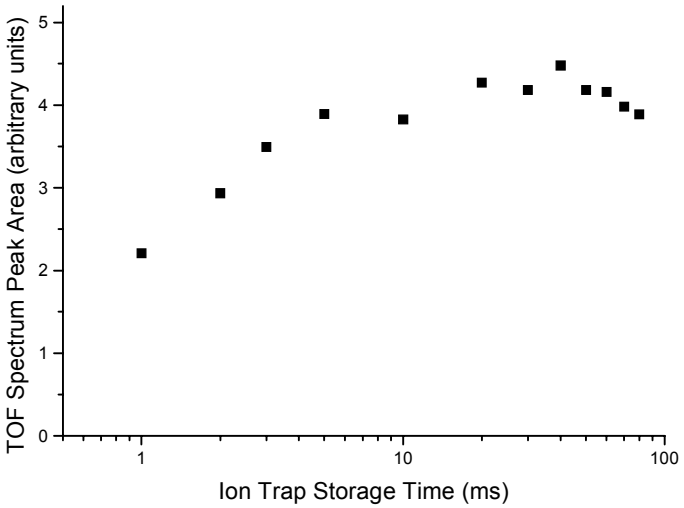

Figure 6.1. Comparison of molecular ion peak area with storage time for aniline vapour.

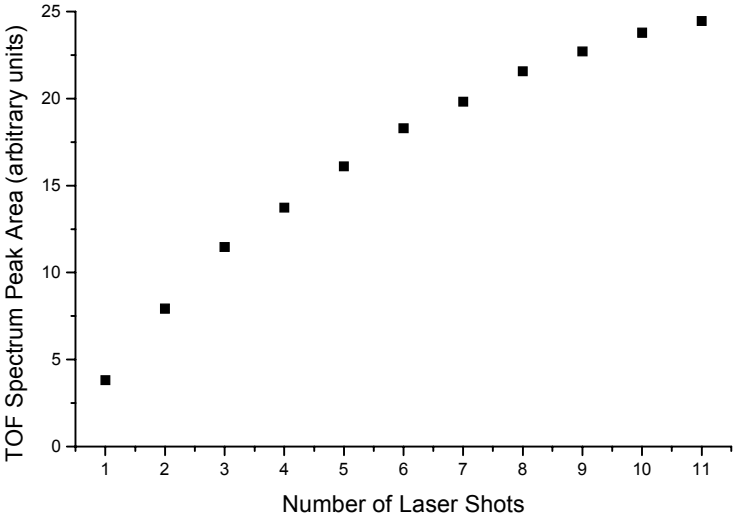

Figure 6.2. Effect of accumulating ions over a number of laser shots on aniline molecular ion peak area.

Ions stored in an ion trap are focused towards the centre of the trap as they lose energy due to collisions with the buffer gas. There is a reduction in variation in ion velocity and ion location for the trapped ions, resulting in TOF spectrum peaks on ejection that are both narrow and intense. This naturally makes the amount of added

buffer gas critical. Ions ejected too early from the trap into the TOF mass analyser give rise to wide peaks, because they have relatively widely varying initial velocities and locations. Total peak area will fall too, as ions at the edge of the cloud can no longer reach the detector. If ions remain in the trap for too long, although the peak will continue to sharpen, peak area will be lowered as ions undergo reactions or escape from the trap. If reactions result in charged species, other peaks will be seen. When peak area is used to evaluate the effect of ion trap storage time, peaks that are wider than the integration window will result in especially low values, while narrow peaks will result in high values. The 200 ns window employed in this work is a little wider than most TOF spectrum peaks.

It can be seen from Figure 6.1 that, for storage times in the region of 1 ms, peak area is small. Peak areas for the storage times investigated that were over 10 ms, however, are considerably larger and relatively constant. This is as would be expected, giving 10 ms as the minimum time required for adequate damping. A slight tail off is observed at the longest storage times, indicating losses from the trap and possibly reactions. Figure 6.2 shows that when more than one ionisation laser pulse is used before ejection into the TOF mass analyser to create ions, the molecular ion peak area is seen to increase. As the number of ionisation laser pulses increases, the rate of increase is seen to diminish. The signal intensity would be expected to level off, as the trap becomes full.

6.1.2. Instrument Tuning with a Solid Analyte: Tryptophan

Although the tuning data collected with aniline was useful, the removal of the requirement for a vaporisation laser meant that a critical part of the experiment was ignored. An involatile solid sample was therefore investigated. Tryptophan (Aldrich) was suspended in a minimum amount of methanol and applied as a paste to a sample probe that fitted into the ring electrode of the ion trap. The sample probe was made of a non-conductive material and presents samples for desorption in the position indicated in Figure 4.25. The Alltec AL861 CO_2 laser ($\lambda = 10.6$ µm) was used for sample desorption and was focused onto the sample probe. The fourth harmonic output of the Quantel Brilliant laser ($\lambda = 266$ nm) was used for sample ionisation,

operating at 10 Hz and providing 4 mJ pulses. The voltages applied to the ion optics and the amount of helium allowed to enter the trap were tuned to optimise the signal. A representative TOF spectrum obtained is shown in Figure 6.3. Use of a solid sample on an immovable target meant that extensive investigation of trapping time was not possible, as the sample was exhausted in less than five minutes.

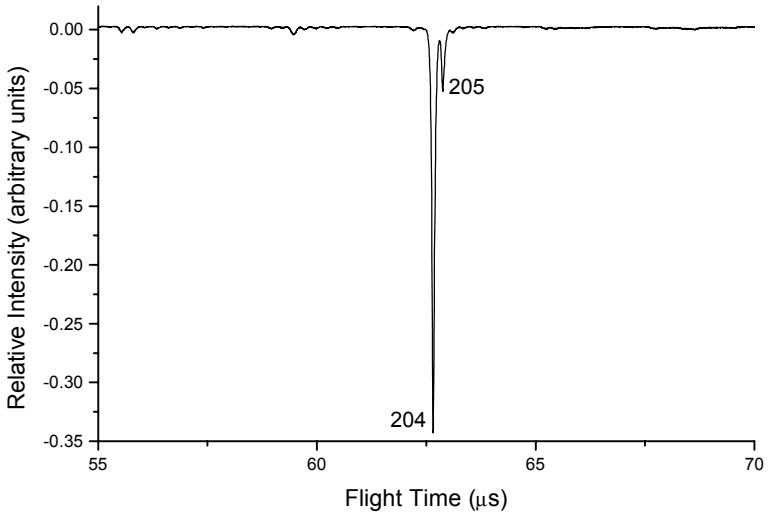

Figure 6.3. TOF spectrum of tryptophan. Desorption achieved using a CO_2 laser operating at 10.6 μm, with ionisation achieved using the fourth harmonic output of a Nd^{3+}:YAG laser (266 nm). Arbitrary units are in fact the signal obtained from the MCP detector in volts. Peak labels are *m*/*z* ratios.

The trapping time utilised in this experiment was 95 ms, with the aim being to produce an intense, narrow peak. The peak resolution expressed as peak time divided by half height peak width is 920. As mentioned above, solid samples are quickly exhausted, and furthermore, may be a poor guide to the behaviour of liquid flowing out of a capillary. Although desorption of solids and vaporisation of liquids both rely on fast heating, they are distinct techniques. Use of a solid sample was therefore not an ideal way to tune the instrument. A system was required that would mimic the combination of chromatographic column and transfer capillary while providing a constant supply of analyte.

6.2. Constant Analyte Introduction System for Instrument Tuning

In order to characterise and further develop the interface, a simple analyte delivery system that was similar to the combination of separation column and transfer capillary was required. A solution was devised that consisted of a long piece of fused silica capillary of ID = 25 µm, which terminated in the ring electrode of the ion trap in the same way as the transfer capillary. The other end of the capillary was placed in a sample reservoir outside the vacuum chamber, as illustrated in Figure 6.4. The pressure differential across the capillary causes liquid to flow towards the ion trap, while the narrow capillary provides a flow rate of the same order as that found in CEC. This is similar to Tal'roze's leak inlet [1-4]. The system can be used to mimic a continually eluting analyte band and is ideal for system tuning, with volumetric flow rate being estimated using Equation 2.3. Initial experiments utilised the Alltec AL861 CO_2 laser for vaporisation, but radiation of this wavelength was found to damage the transfer capillary terminus. Vaporisation was therefore attempted with the Continuum Minilite laser, operating at its fundamental frequency of 1064 nm.

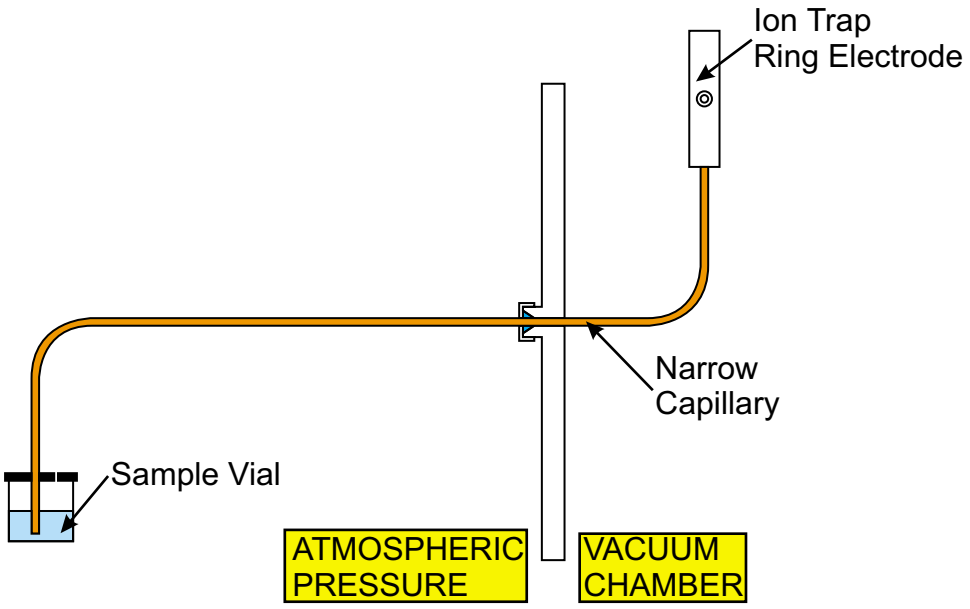

Figure 6.4. Simple analyte introduction system used for instrumental tuning and characterisation.

6.2.1. Behaviour of Liquid Entering the Ion Trap

A major concern with the introduction of liquids through a capillary into a high-vacuum chamber is that rapid evaporation of liquid inside the capillary may lead to flow stoppage through freezing of the solvent. Such problems have been reported by many workers, and were even mentioned in the very first LC/MS experiments performed [1-4]. Interestingly, when He *et al.* used a similar mass spectrometer to the one used in this work, for continuous flow MALDI, an IR heater was used to prevent freezing of the liquid matrix [5].

In order to gain a better idea of the physical processes that occur when liquids enter a vacuum chamber, through a narrow capillary at low volumetric flow rates, solvent outflow from the capillary terminus was observed using a video camera. The capillary was mounted inside the vacuum chamber, close to a window to allow observation, and various liquids and solutions were introduced through the capillary. The vacuum chamber was held at 10^{-3} mbar to mimic conditions inside the trap. When a good clean cut was made, and the capillary coating had been burnt off, the behaviour was reproducible. A solvent bubble would form, which eventually reaches a limiting size, with excess solvent running down the outside of the capillary. This behaviour was seen in the case of acetonitrile, water and methanol, as well as a solution of naphthalene at 5 mM in acetonitrile.

When the 1064 nm output of the Continuum Minilite laser (the laser used for vaporisation in most CEC/MS experiments) was focused onto the end of the capillary, at typical experimental power output settings, no solvent bubble was observed to form. Figure 6.5 shows the case where a solvent bubble was allowed to form, with a shutter used to block the laser, followed by the shutter being opened to permit the laser to strike the tip of the capillary. With the video camera recording at a rate of 25 frames per second, and the laser firing ten times a second, some frames were over exposed because they coincided with laser irradiation. Therefore, the frames shown here were recorded between laser pulses. Image 1 was recorded before the shutter was opened, with the following images showing the reduction in size of the solvent bubble due to the laser. The solvent used here was acetonitrile, with the laser power being higher than would typically be used in a CEC/MS experiment to

speed up the process (the available recording system could only operate for a short period of time).

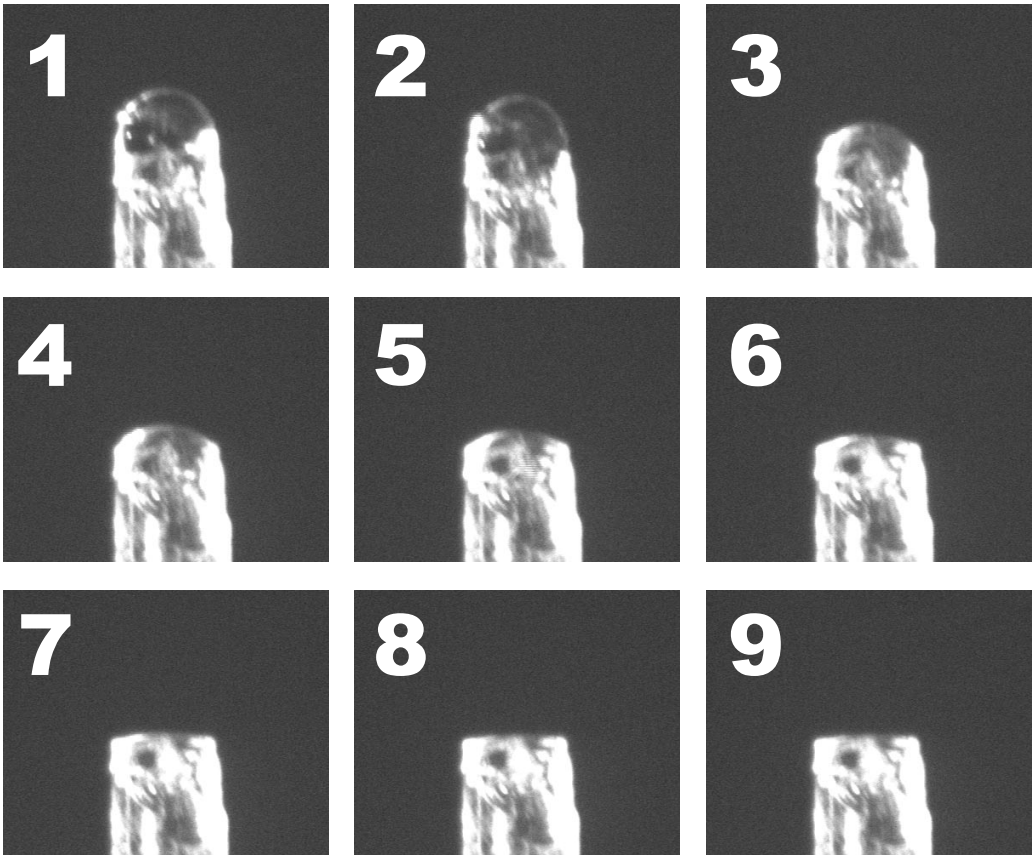

Figure 6.5. Series of nine frames showing the effect of laser irradiation (1064 nm) on an acetonitrile droplet. Frames separated by 0.2 seconds. For scale, the width of the capillary is ~ 400 μm.

A wide variety of behaviour, however, was observed unless great care was taken with preparation of the capillary tip. A typical pattern was that upon admission of solvent, a droplet would form at the end of the capillary. This droplet would increase in size until it would suddenly flash freeze. The frozen droplet would then fall off the capillary tip and be replaced by extruded slugs of solvent ice for some time. A droplet would then begin to form as before and the process would repeat. A sequence of images illustrating this behaviour is shown in Figure 6.6. Here the solvent is again acetonitrile. Similar behaviour was observed with water and methanol. Eventually, however, this behaviour tended to settle down to a small bubble with excess solvent

running down the outside of the capillary as before. Use of long equilibration times is therefore recommended to ensure stable operation of the system.

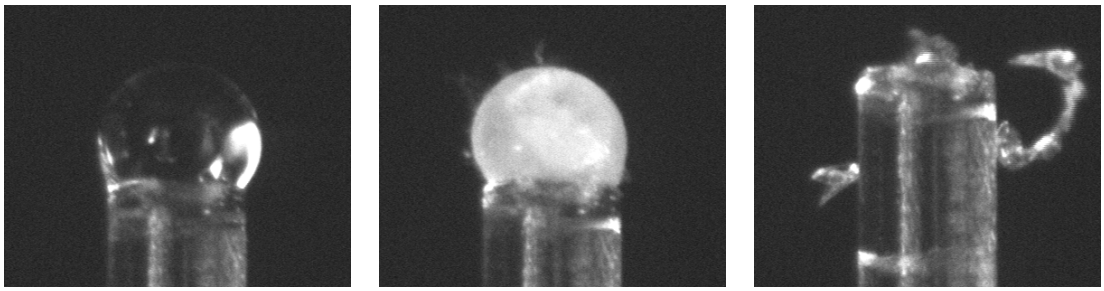

Figure 6.6. Images showing non-ideal behaviour at the capillary tip inside the vacuum chamber. Sometimes a solvent droplet forms, which then freezes and falls off the tip, followed by extrusion of slugs of solvent ice before a return to droplet formation. For scale, the width of the capillary is ~ 400 µm.

In one extreme case a particle may have become trapped at the capillary orifice, causing long strands of solvent ice to be extruded. A representative image is shown in Figure 6.7. The liquid in this case was acetonitrile.

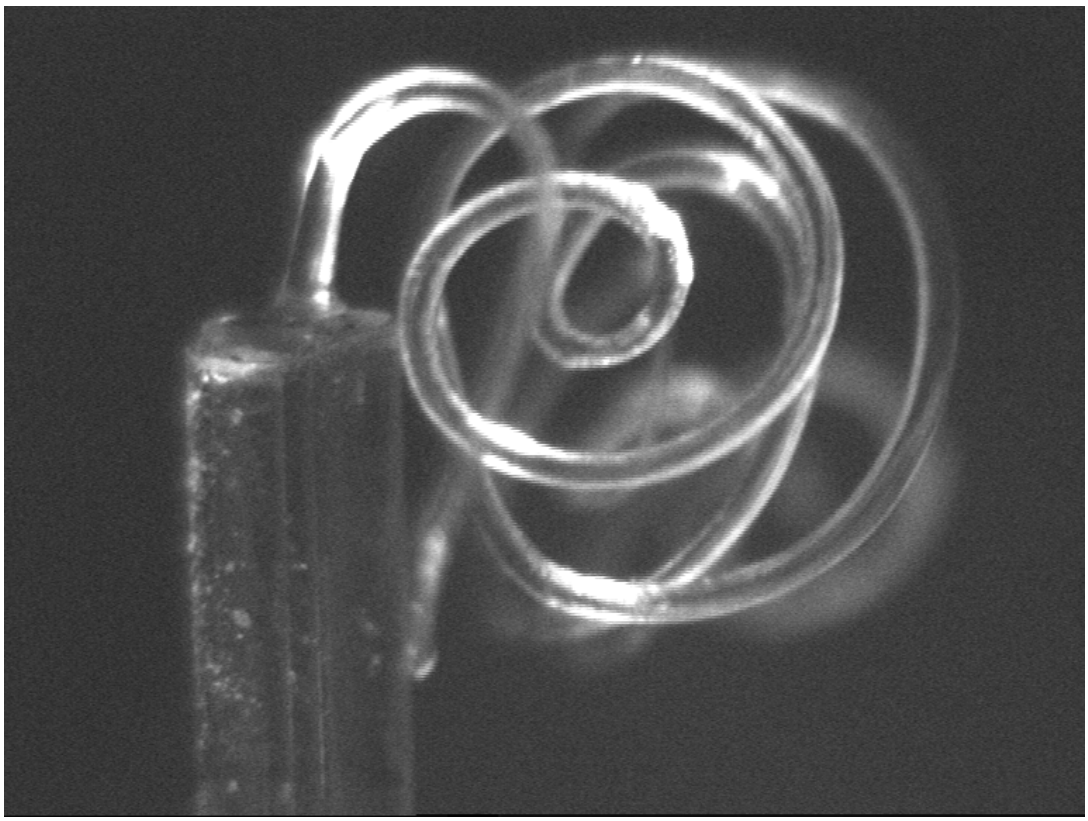

Figure 6.7. Extrusion of acetonitrile solvent ice fibre from capillary tip into high vacuum chamber. For scale, the width of the capillary is ~ 400 µm.

6.2.2. Determining the Optimum Settings for the ITS/TOF Mass Spectrometer

Although the simple, constant flow, analyte introduction system was prone to occasional problems, these were the same problems that would be expected when using a chromatographic column and a transfer capillary. This analyte introduction system was therefore used to tune the ITS/TOF mass spectrometer. The analytes used in the instrument development test mixture were each dissolved in acetonitrile and allowed to flow into the instrument. Sample vaporisation was carried out using the Continuum Minilite laser, operating at 1064 nm, while the fourth harmonic of the Quantel Brilliant laser ($\lambda = 266$ nm) was used for sample ionisation. The desorption laser was triggered to fire 30 µs before the ionisation laser, with the ion trap storage time set to various values.

It was found that most available variables had largely the same optimum values for different analytes and for different trapping times. An exception is the amplitude of the rf trapping potential, where the optimum value is mass dependent. Once chosen, timing settings were held constant throughout these experiments in order to allow comparisons to be made. Addition of helium degraded the quality of the spectra, probably because solvent vapour provided sufficient buffer gas, making no additional gas necessary. The typical operating settings are listed in Table 6.1. A good average value for the amplitude of the rf trapping potential is provided in the table. The voltage applied to the first MCP was chosen as a compromise between maximising sensitivity and prolonging detector life.

Amplitude of rf Trapping Potential	1525 V
Extraction Pulse Potential	-193 V
Liner Potential, V_L	-1127 V
Focus Potential, V_F	-87 V
Deflector Potential, V_{DEF}	-1093 V
Reflectron Voltage 1, $V_{R,1}$	-288 V
Reflectron Voltage 2, $V_{R,2}$	123 V
Voltage applied to first MCP	-1598 V

Table 6.1. Typical operating parameters for the ITS/TOF mass spectrometer.

6.3. Characterisation of the Ion Trap

Ion trap storage time and buffer gas pressure are the two parameters observed to have greatest effect of the resulting TOF spectra. These parameters were investigated in order to determine the optimum settings. Since it was observed that additional helium degraded the quality of the spectra obtained when liquids were flowing into the trap, the effect of lowering the pressure inside the ion trap was investigated. The ceramic rings that make up the ion trap housing (see Section 4.5) fit snugly, allowing the ion trap to be held at a slightly higher pressure than the enclosing chamber. Ion trap pressure is estimated to be in the region of 10^{-3} mbar. This pressure is a balance between liquid entering the trap and the rate at which the surrounding vacuum chamber 'pumps' the trap. Removing one of the ceramic rings can therefore lower

trap pressure. Imposing limitations on chromatographic parameters was avoided, but altering the flow rate into the trap would also allow control of trap pressure.

As the purpose of these experiments was to determine the optimum parameters for the collection of chromatographic data, molecular ion peak area using a narrow integration window was used for evaluation. The effect of the range over which integration was performed was also considered. Integration occurs after a run has been recorded, but operating parameters must be optimised with the typical integration window in mind.

6.3.1. Choosing the Optimum Ion Trap Storage Time

To ascertain the optimum ion storage time for liquid flowing into the trap, a 5 mM solution of naphthalene in acetonitrile was allowed to enter the trap through a 25 μm ID capillary of length 564 mm. Given that the viscosity of acetonitrile at room temperature (298 K) is 0.369×10^{-3} N m^{-2} s (0.369 centipoise), the volumetric flow rate into the ion trap can easily be estimated using Equation 2.3. The flow rate was estimated to be 280 nL min^{-1}, assuming that dissolved naphthalene makes only a negligible contribution to the viscosity of acetonitrile. Ion trap storage time was examined with the experiment configured as described above. All spectra are the summed average of 100 raw data traces unless stated otherwise. Figure 6.8 shows a comparison of the TOF spectrum for a relatively short storage time (10 μs) with that for a relatively long storage time (90 ms), with an enlarged view of the molecular ion peak shown in Figure 6.9. A maximum storage time of 90 ms was chosen because with both lasers firing at 10 Hz, it was a convenient place to stop before the next laser pulse. The lasers can be fired at frequencies of less than 10 Hz, but output tends be reduced in quality away from this optimum value. Naphthalene has a molecular mass of 128, meaning that the molecular ion would be expected to have a $m/z = 128$. The smaller peak, labelled as $m/z = 169$, is likely to be an acetonitrile adduct.

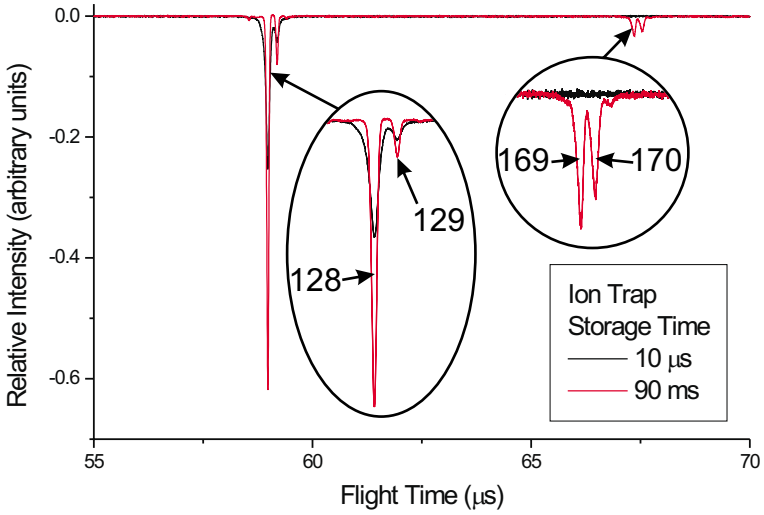

Figure 6.8. Comparison of the effect of short and long trapping times on the TOF spectrum of naphthalene. Sample is 5 mM naphthalene in acetonitrile, entering at a flow rate 280 nL min^{-1}. Laser vaporisation at 1064 nm, laser ionisation at 266 nm, ceramic rings in place. Peak labels are *m*/*z* ratios.

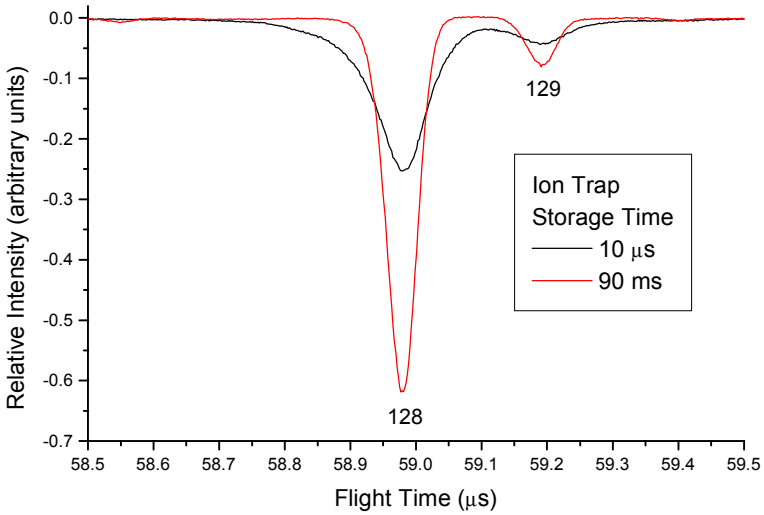

Figure 6.9. Enlargement of the TOF spectrum for naphthalene from Figure 6.8 in the region of the naphthalene molecular ion. Peak labels are *m*/*z* ratios.

It can clearly be seen that the longer storage time gives a sharper naphthalene molecular ion peak that can be entirely contained within the 200 ns integration window. The 10 μs naphthalene molecular ion peak can be seen to be wider than the

200 ns integration window, further reducing abundance in terms of measured peak area for selected ion chromatograms. This is as would be expected given that solvent vapour inside the trap should act as a buffer gas, in a similar manner to helium, to damp trapped ion motions and in time improve mass resolution. The resolution (expressed as peak apex time divided by half-height width) of the molecular ion peak recorded using a storage time of 10 µs is 630, while that recorded using a storage time of 90 ms in 1090. Another effect of longer trapping times is to increase the number of interactions between the trapped ions and between trapped ions and neutral buffer gas. This is illustrated in Figure 6.8 by the adduct peak present at the longer storage time. This is likely to be a naphthalene-acetonitrile adduct arising from the collision of a naphthalene ion with an acetonitrile molecule. Data was recorded for 36 different ion trap storage times, ranging from 10 µs to 90 ms, and analysed using the peak integration program. Figure 6.10 summarises this information on molecular ion peak area for various trapping times. It can be seen that peak area is largely constant between 0.1 and 10 ms. Longer storage times, however, give the highest mass spectrometric resolution, suggesting that 10 ms is the best choice when collecting data.

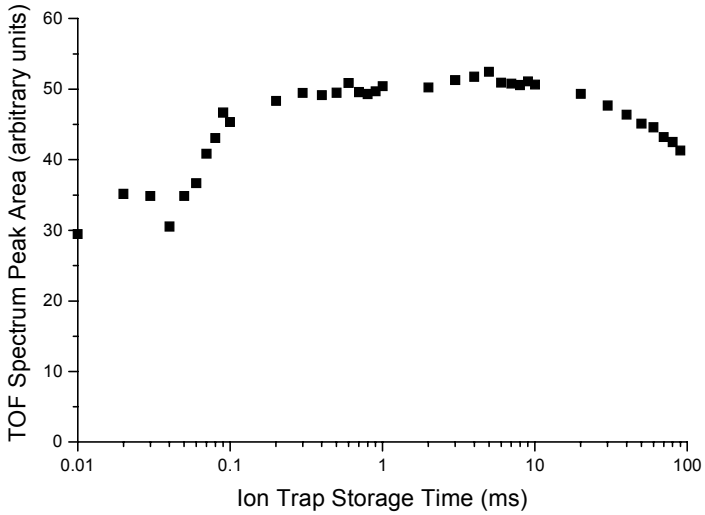

Figure 6.10. Variation of molecular ion peak area in the TOF spectrum of naphthalene with storage time. Sample was 5 mM naphthalene in acetonitrile, entering at a flow rate 280 nL min^{-1}. Laser vaporisation at 1064 nm, laser ionisation at 266 nm, ceramic rings in place.

Figure 6.11 shows a plot of similar data recorded under identical experimental conditions except that the concentration of naphthalene used in this case was 500 µM in acetonitrile. It is interesting to note that the molecular ion peak area is greater than one tenth of that found for the more concentrated 5 mM solution, indicating perhaps that the trap is close to being full in the former case. Another interesting feature is that at longer trapping times the molecular ion peak area does not decrease. This must be because ion-molecule reactions are less likely due to the lower concentration of ions in the trap. This data as a whole suggests that, as when using a gaseous analyte, a trapping time of 10 ms is optimal for production of selected ion chromatograms.

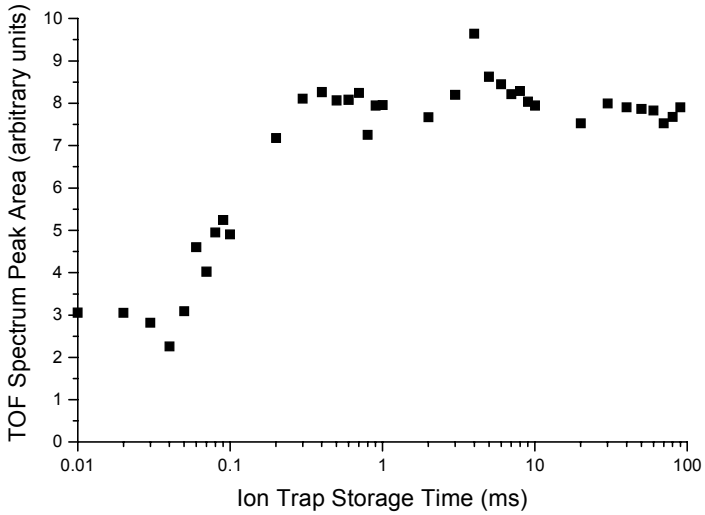

Figure 6.11. Variation of molecular ion peak area in the TOF spectrum of naphthalene with storage time. Sample was 500 µM naphthalene in acetonitrile, entering at a flow rate 280 nL min^{-1}. Laser vaporisation at 1064 nm, laser ionisation at 266 nm, ceramic rings in place.

Thus far, only trapping times up to 100 ms have been considered. Although likely to have no analytical use, it was interesting to investigate how long ions could be stored in the trap. Figure 6.12 shows data for the case of very long trapping times. As might have been expected, molecular ion peak area reduces gradually. It should, however, be noted that the ionisation laser is optimised for operation at 10 Hz, and moving to slower repetition rates reduces pulse energy somewhat. The first data point is for a storage time of 10 ms, with spectra thereafter recorded at 100 ms intervals up to 1010 ms.

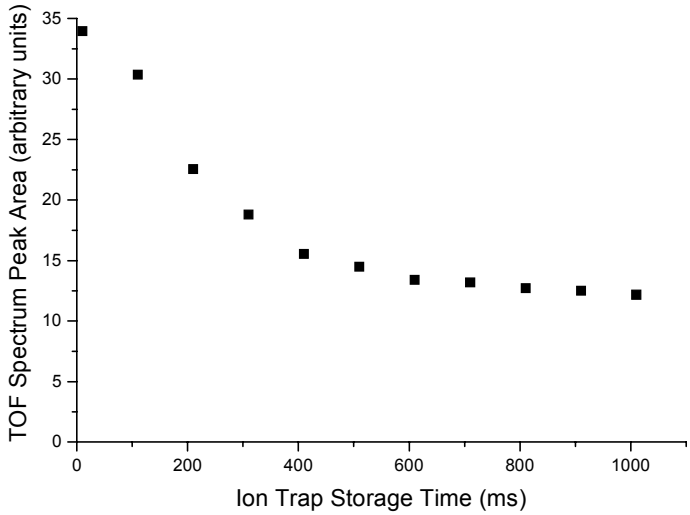

Figure 6.12. Variation of molecular ion peak area in the TOF spectrum of naphthalene with storage time. Storage times of over 100 ms are considered. Sample was 5 mM naphthalene in acetonitrile, entering at a flow rate 280 nL min^{-1}. Laser vaporisation at 1064 nm, laser ionisation at 266 nm, ceramic rings in place.

6.3.2. Evaluating the Effect of Internal Ion Trap Pressure

Using evaporating mobile phase as buffer gas is less convenient than helium because control over the internal pressure in the ion trap can only exerted by varying flow rate or by altering the trap housing. To investigate whether the internal ion trap pressure was too high, one of the ion trap ceramic rings was removed. This should lower the trap pressure to close to the pressure of the larger enclosing vacuum chamber. The spectra obtained for trapping times of 10 µs and 90 ms trapping are shown in Figure 6.13, with an enlargement of the molecular ion peak being shown in Figure 6.14. Variance in molecular ion peak area for a 200 ns integration window is shown in Figure 6.15. The data shown in Figure 6.13 and Figure 6.15 was generated in an identical manner to the data shown in Figure 6.8 and Figure 6.10, except for removal of a ceramic ring.

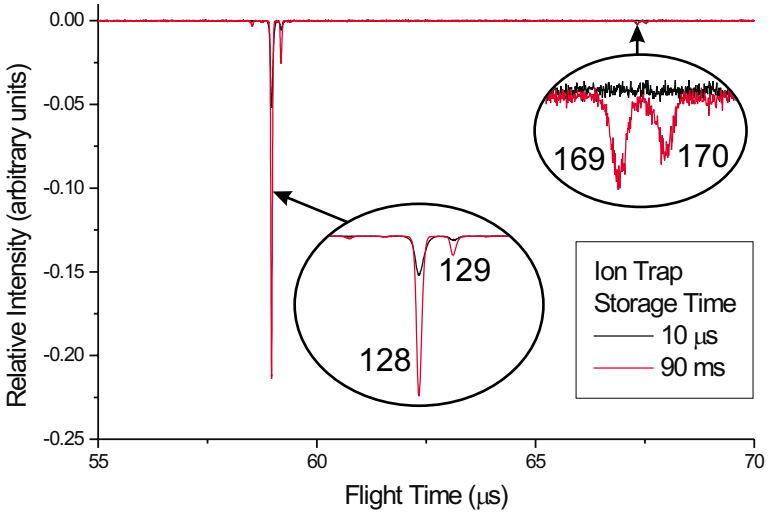

Figure 6.13. Comparison of the effect of short and long trapping times on the TOF spectrum of naphthalene. Sample is 5 mM naphthalene in acetonitrile, entering at a flow rate 280 nL min^{-1}. Laser vaporisation at 1064 nm, laser ionisation at 266 nm, one ceramic ring removed. Compare with Figure 6.8. Peak labels are *m*/*z* ratios.

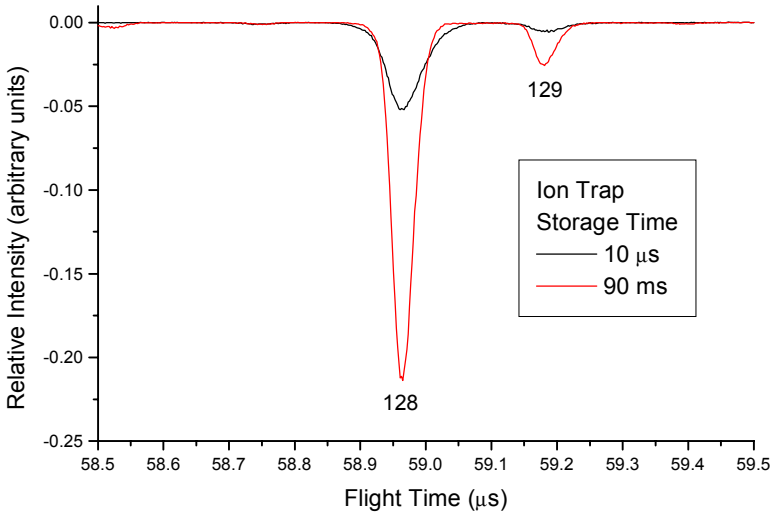

Figure 6.14. Enlargement of the TOF spectrum for naphthalene from Figure 6.13 in the region of the naphthalene molecular ion. Compare with Figure 6.9. Peak labels are *m*/*z* ratios.

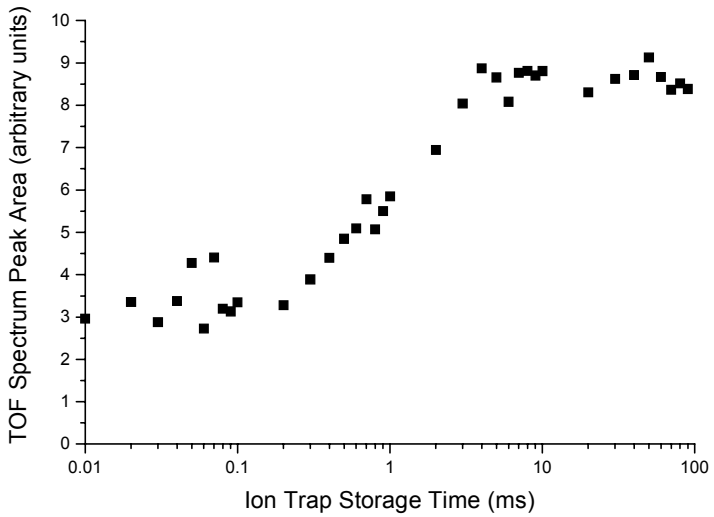

Figure 6.15. Variation of molecular ion peak area in the TOF spectrum of naphthalene with storage time. Sample was 5 mM naphthalene in acetonitrile, entering at a flow rate 280 nL min^{-1}. Laser vaporisation at 1064 nm, laser ionisation at 266 nm, one ceramic ring removed. Compare with Figure 6.10.

The shapes of the peaks in Figure 6.13 can be seen to be similar to those in Figure 6.8, but peak areas are clearly much reduced. This reduction in abundance is clear in the molecular ion peak and in the acetonitrile adduct peak ($m/z = 169$) that was recorded at a storage time of 90 ms. A 500 µM naphthalene in acetonitrile solution was also investigated, but in this case no signal could be obtained. This data implies that the low internal trap pressure resulting from the removal of one of the ceramic spacer rings allows analyte to be pumped away, possible before ionisation has occurred. The fact that the peaks are sharp seems to indicate that the limited focusing due to limited solvent vapour present was sufficient.

6.3.3. Accumulation for more than One Laser Cycle

One way to improve detection limits is to accumulate ions for more than one laser cycle. With the lasers firing every 100 ms, and storage possible for over a second, significant gains in sensitivity should be possible. Figure 6.16 shows how molecular ion peak area for a 500 µM solution of naphthalene in acetonitrile, entering the trap at the usual flow rate of 280 nL min^{-1}, increases with number of laser cycles. In each

case the summed average spectrum used to calculate the peak area was obtained 10 ms after the final laser pulse; that is, the storage times were 10 ms (1 cycle), 110 ms (2 cycles), 210 ms (3 cycles)…1010 ms (11 cycles). As expected a significant increase in sensitivity is obtained.

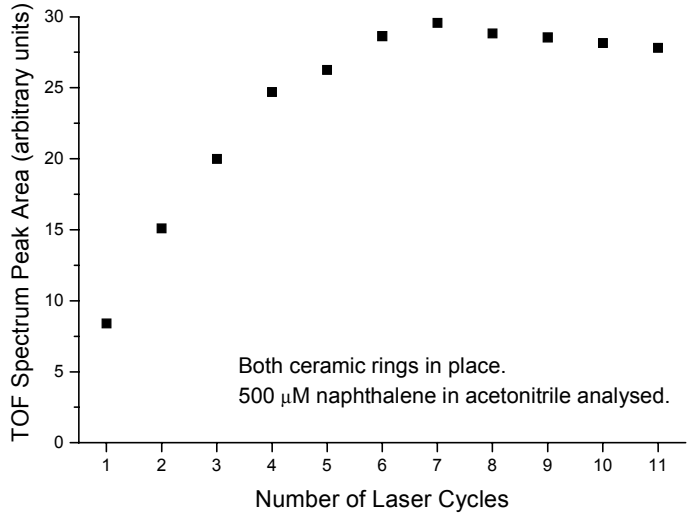

Figure 6.16. Variation of molecular ion peak area in the TOF spectrum of naphthalene with number of laser cycles over which accumulation was performed. Sample was 500 μM naphthalene in acetonitrile, entering at a flow rate 280 nL min^{-1}. Laser vaporisation at 1064 nm, laser ionisation at 266 nm, both ceramic rings in place.

Figure 6.17 shows the case when one ceramic ring is removed to improve pumping, in this case, with a solution of 5 mM naphthalene in acetonitrile. As expected, there is also a gradual increase in signal with number of laser cycles until a limiting value is reached. The signal for this much more concentrated sample, however, is similar to that for the 500 μM solution obtained with a higher internal trap pressure.

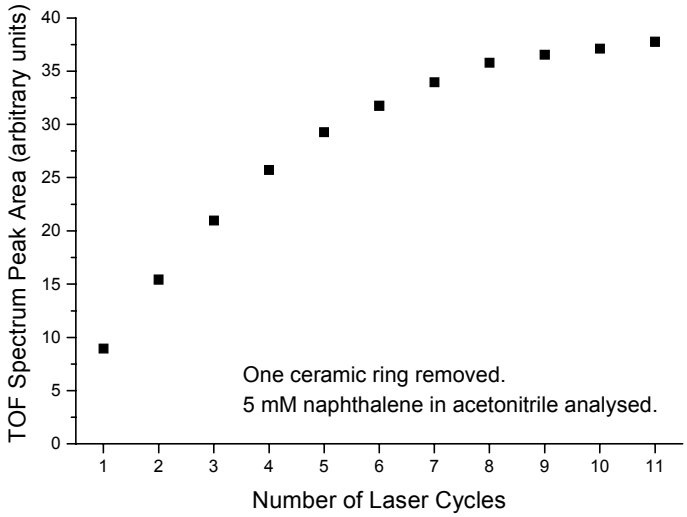

Figure 6.17. Variation of molecular ion peak area in the TOF spectrum of naphthalene with number of laser cycles over which accumulation was performed. Sample was 5 mM naphthalene in acetonitrile, entering at a flow rate 280 nL min^{-1}. Laser vaporisation at 1064 nm, laser ionisation at 266 nm, one ceramic ring removed.

When both spacer rings are in place and the concentration is increased from 500 µM to 5 mM, the use of multiple laser cycles confers no significant advantage as shown in Figure 6.18. It should be noted that the maximum signal is obtained with the spacer ring in place, and only two laser cycles have to occur before this maximum value is obtained. The most interesting feature of Figure 6.18 is the fact that molecular ion peak area decreases with increasing numbers of laser cycles. The reason for this behaviour is that this data is solely representative of molecular ion peak area. The TOF spectra corresponding to the first and last point in Figure 6.18 are shown in Figure 6.19.

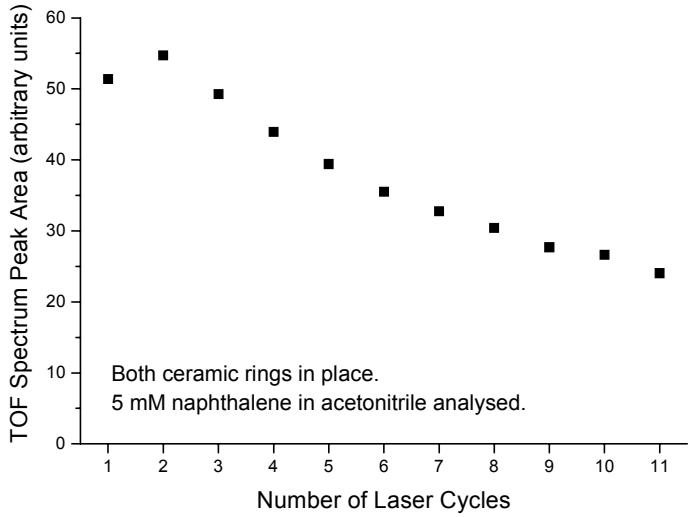

Figure 6.18. Variation of molecular ion peak area in the TOF spectrum of naphthalene with number of laser cycles over which accumulation was performed. Sample was 5 mM naphthalene in acetonitrile, entering at a flow rate 280 nL min^{-1}. Laser vaporisation at 1064 nm, laser ionisation at 266 nm, both ceramic rings in place.

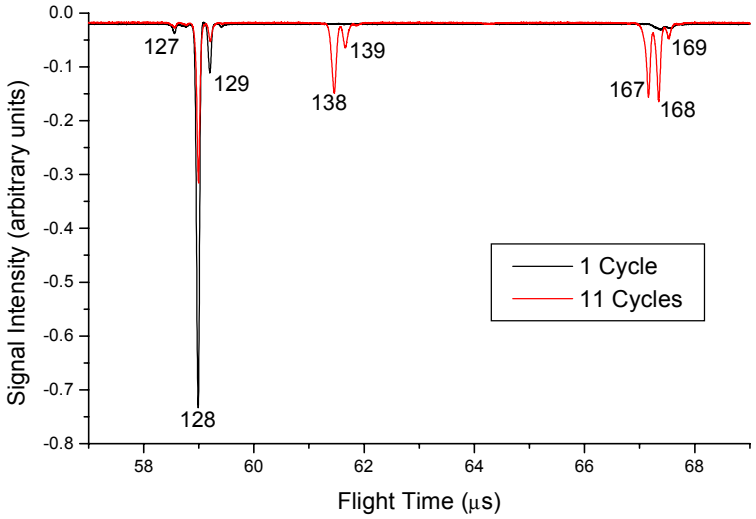

Figure 6.19. Comparison of TOF spectra for naphthalene after one laser cycle (storage time = 10 ms) versus eleven laser cycles (storage time = 1010 ms). Sample was 5 mM naphthalene in acetonitrile, entering at a flow rate 280 nL min^{-1}. Laser vaporisation at 1064 nm, laser ionisation at 266 nm, both ceramic rings in place. Peak labels are *m*/*z* ratios.

It can be seen that after eleven cycles the amount of signal originating from adducts is significant. The trap was probably full after two cycles and there is a large amount of time for ion-molecule reactions. The overall charge capacity of the trap can be monitored by integrating the peak area for all features in the TOF spectra. Figure 6.20 shows the peak areas for the first (*m*/*z* = 128, naphthalene molecular ion), second (*m*/*z* = 138, unknown adduct or breakdown product of adduct) and third (*m*/*z* = 168, suspected acetonitrile adduct) peak clusters, for the ITS/TOF data that is partially presented in Figure 6.19, along with their sum. It is suggested that the *m*/*z* = 138 peak is an adduct breakdown product since its growth lags behind the *m*/*z* = 168 peak. It is also interesting to note that the acetonitrile adduct, usually recorded at *m*/*z* = 169, seems to have lost a hydrogen atom to give a most abundant *m*/*z* = 168 at long storage times. The integration window used was widened to encompass the entire width of all the peaks in the cluster when constructing Figure 6.20. The overall signal is in fact fairly constant with increasing number of

laser cycles for this system, in which the trap is probably full immediately after the first laser shot.

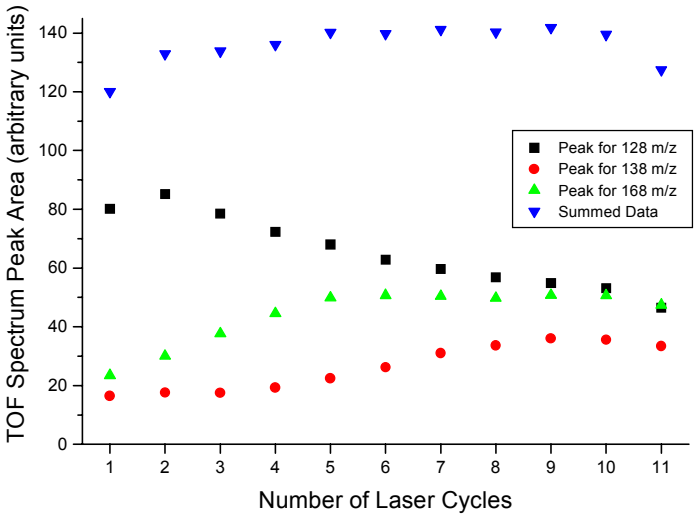

Figure 6.20. Observations on the decrease in molecular ion peak area being compensated by the increase in adduct ion peak area for same data as that used in Figure 6.18 and Figure 6.19.

The above experiments have shown that there is considerable advantage to be found in trapping ions for multiple laser cycles when analytes are present at low concentration. For the analysis of concentrated solutions there is less advantage unless some form of ion-molecule chemistry is desired. When using the system as a chromatographic detection method a balance must be struck between sensitivity and temporal resolution. Trapping for multiple cycles will increase sensitivity while reducing the number of spectra that are recorded. As TOF spectra with this system vary significantly from laser shot to laser shot this will require either collection of averaged data to be abandoned or will lead to large gaps between chromatographic data points. For example, waiting for ten laser shots for maximum sensitivity would require a little over one second, while data transfer would take a further 1.2 seconds, giving an acceptable total of 2.2 seconds. This data, however, would be very variable leading to chromatograms of varying intensity. If on the other hand, ten TOF spectra were averaged, an unacceptable 12.2 seconds would be found between each

chromatographic data point. The optimal situation would perhaps be to collect a small number of laser shots for samples at low concentration.

Variation in obtained signal with storage time was also investigated for phenanthrene, with similar results obtained. Unfortunately, however, when these experiments were extended to other compounds with strong absorbance at 266 nm, such as the amino acid tryptophan and the heavier PAH coronene (Acros), no signal could be obtained. Since both compounds have been successfully analysed as solids, it would appear that the vaporisation process is to blame. The IR laser has been shown in Section 6.2.1 to be capable of vaporising liquids at low flow rates, but the process does not seem to be able to force these relatively involatile molecules into the gas phase so that they become available for ionisation. Experiments were repeated with the IR laser switched off and similar results were obtained to when the laser was switched on, although an enhanced signal was observed for phenanthrene. This enhancement is probably due to laser heating promoting phenanthrene vaporisation, while the more volatile naphthalene does not require this heating. At any rate, for the low-mass PAHs studied, vaporisation seems to have been mainly by evaporation.

6.4. Determination of Detection Limits

The constant analyte introduction system described above was used to estimate the detection limits for the system. Solutions of naphthalene in acetonitrile were allowed to enter the system at a flow rate of 280 nL min^{-1}. Sample data is shown in Figure 6.21. This data was generated using a trapping time of 10 ms; that is, collection over only one laser shot was considered. Collection over more than one laser shot would improve overall detection limits. For a single laser shot the detection limit was found to be in the region of 100 nM. The displayed TOF spectra are the result of 100 summed TOF spectra, meaning that sample consumption for the 100 nM solution was approximately 5 femtomoles.

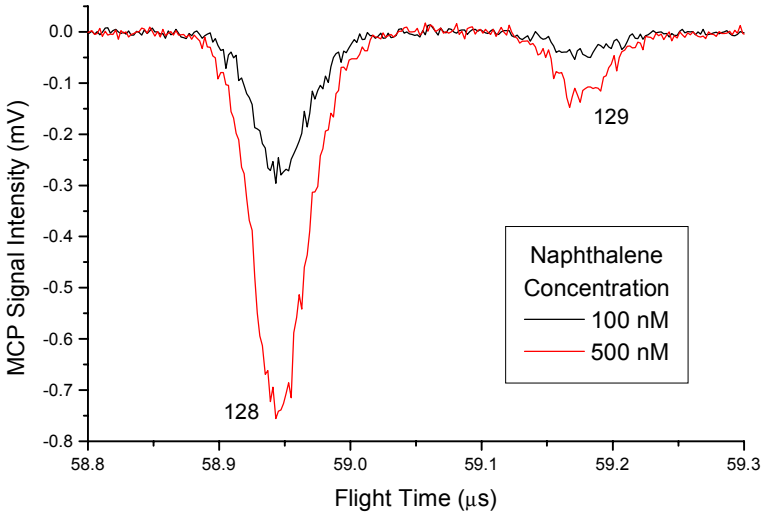

Figure 6.21. Estimation of the limit of detection for the two-laser mass spectrometry interface. Limit found using solutions of naphthalene in acetonitrile. Peak labels are *m*/*z* ratios.

6.5. CEC/MS Data Obtained Using the ITS/TOF Mass Spectrometer

Presented first is CEC/MS data obtained using the ZDV union illustrated in Figure 5.24. In this example, the standard separation described in Section 5.1 was not used, but the same instrumental development test mixture was used. Instead the mobile phase was 25% aqueous 5 mM TRIS adjusted to pH 8.0 with HCl, 75% acetonitrile, with a running potential of 30 kV and injection being performed by application of 5 kV for 5 seconds to the sample vial. The column was 220 mm long and was packed in the usual manner with Hypersil ODS stationary phase (3 μm diameter particles), with a transfer capillary of length 563 mm. The trap was used with ceramic rings in place and with an ion trap storage time of 10 ms. Resulting CEC/MS data is shown in Figure 6.22. The chromatographic efficiency for the naphthalene peak in terms of a plate number was calculated to be in the region of 3,000 (14,000 per metre). Calculation of efficiencies in term of plates per metre took no account of the length of the transfer capillary.

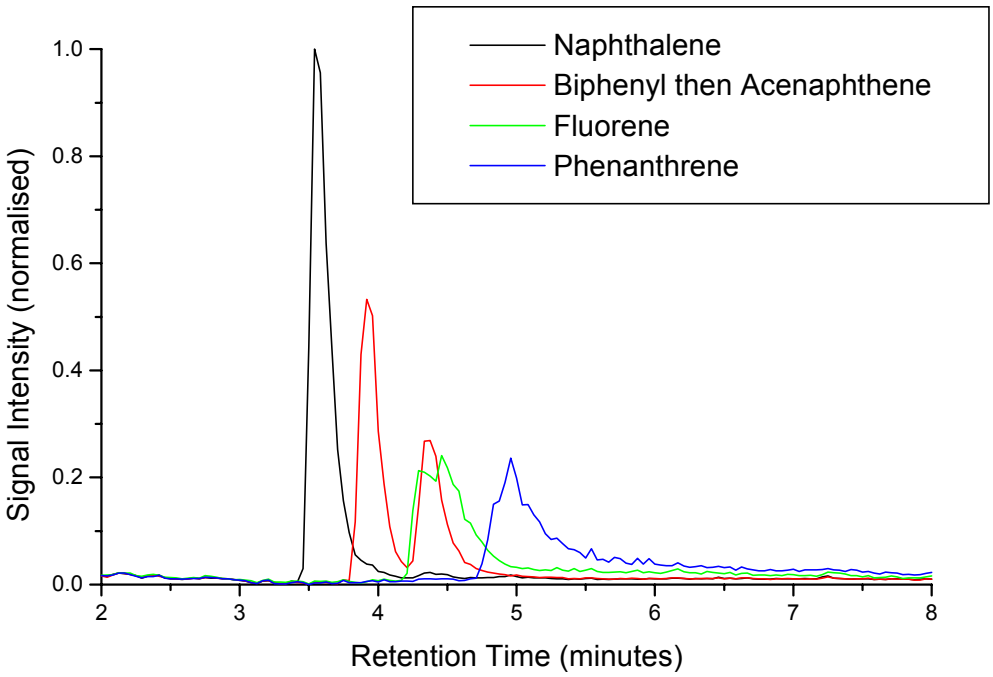

Figure 6.22. Early CEC/MS separation of naphthalene, biphenyl, fluorene, acenaphthene and phenanthrene using a ZDV union between the CEC column and the transfer capillary. Chromatogram comprises four overlaid selected ion chromatograms (biphenyl and acenaphthene have the same mass).

Following the successful production of an efficient earthed capillary junction based on the CCBC (see Figure 5.25) and the successful tuning and characterisation of the mass spectrometer, it was necessary to perform new CEC/MS experiments to investigate the performance of the entire system. For this purpose the instrument development test mixture was analysed with each component present at a concentration of 5 mM in acetonitrile. Injection was performed by applying a potential of 5 kV to the sample vial for 5 s, whilst the running potential was 30 kV. The CEC column employed had an ID = 100 µm and a length of 546 mm. It was connected to a transfer capillary of length 540 mm. The CEC column was packed with Hypersil Mixed Mode stationary phase (3 µm diameter particles) from inlet to outlet with no absorbance detection window. The column was mounted in the CIA instrument, which was used for automated injection and as the source of the applied potential for CEC. The trap was used with ceramic rings in place and with an ion trap

storage time of 10 ms. Accumulation of ions for more than one laser cycle was not investigated. Peak integration of the TOF spectra was performed, as usual, over 200 ns windows. The selected ion chromatograms that were obtained are shown in Figure 6.23.

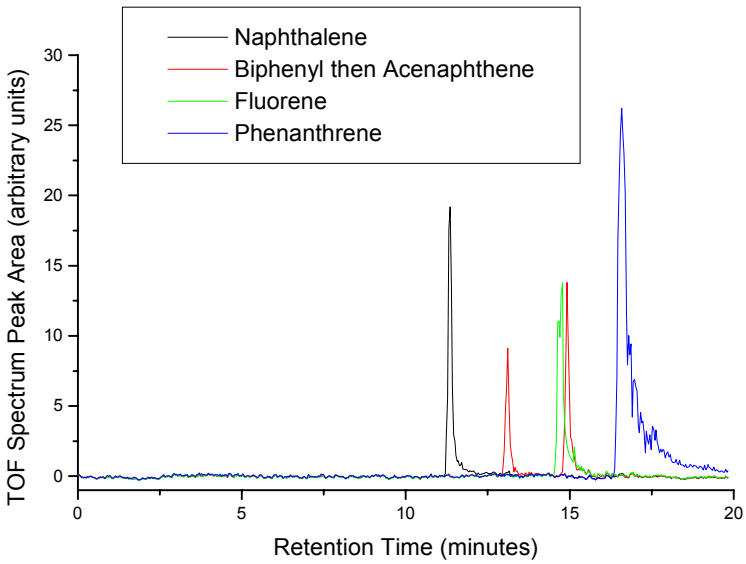

Figure 6.23. CEC/MS separation of naphthalene, biphenyl, fluorene, acenaphthene and phenanthrene. Chromatogram comprises four overlaid selected ion chromatograms (biphenyl and acenaphthene have the same mass).

The quality of the data is clearly much improved over that displayed in Figure 6.22. Fluorene and acenaphthene can be seen to be resolved, although not to the baseline. Considerable tailing is evident, as predicted by the CFD studies, with the tailing especially pronounced in the case of phenanthrene. This tailing, however, may be the result of sample remaining on the capillary tip for much longer than the analyte band is eluting due to inefficient vaporisation. The other PAHs would be expected to evaporate more readily than phenanthrene. As mentioned above, all five molecules will produce good signals with no vaporisation laser present, but less volatile phenanthrene noticeably benefits from the presence of the vaporisation laser. High vaporisation laser powers, however, can cause undesirable fragmentation. A solution to the tailing problem might be to use a high power vaporisation pulse while data was

transferring from the oscilloscope to the computer in order to clean the terminus of the transfer capillary prior to the next data acquisition cycle.

Table 6.2 gives a comparison between data recorded using on-column absorbance detection (see Figure 5.1) with that obtained using the ITS/TOF mass spectrometer (see Figure 6.23). All data was obtained from measurements of peak width at half height. It can be seen that the chromatographic efficiencies are fairly constant for on-column detection, while those for the TOF mass analyser vary considerably, and are about 55% of those for absorbance detection on average. The low sampling rate for the MS data effectively hides a decrease in chromatographic efficiency with retention time. The effect of a low sampling rate is illustrated in Figure 6.24. This decrease is due to the increase in tailing with retention time and is probably due to vaporisation efficiency as described above.

	CEC		**CEC/MS**	
Analyte	**N**	**N/m**	**N**	**N/m**
Naphthalene	70,000	162,000	55,000	100,000
Biphenyl	73,000	168,000	66,000	121,000
Fluorene	76,000	176,000	32,000	58,000
Acenaphthene	73,000	170,000	80,000	147,000
Phenanthrene	71,000	162,000	24,000	44,000

Table 6.2. Comparison of results obtained using on-column absorbance detection with those obtained using the TOF mass analyser.

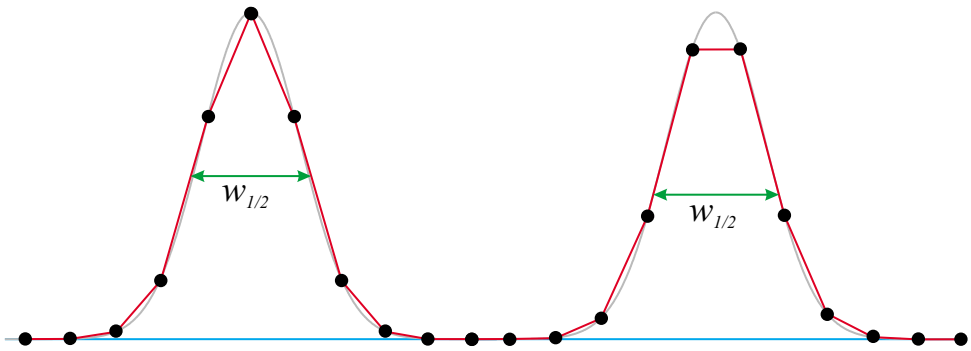

Figure 6.24. Effect of low sampling rate on recorded data. Different peak shapes are obtained when peak apex coincides with a sample point than when they do not coincide.

The selected ion chromatograms shown in Figure 6.23 were produced from a large number of TOF spectra. Individual TOF spectra for each compound in the test mixture, recorded at the retention time corresponding to maximum molecular ion signal intensity, are displayed in Figure 6.25. Signal intensity is generally lower than that found in the examples given previously, as with all parameters fixed for a chromatographic run, drift was often found to reduce intensities.

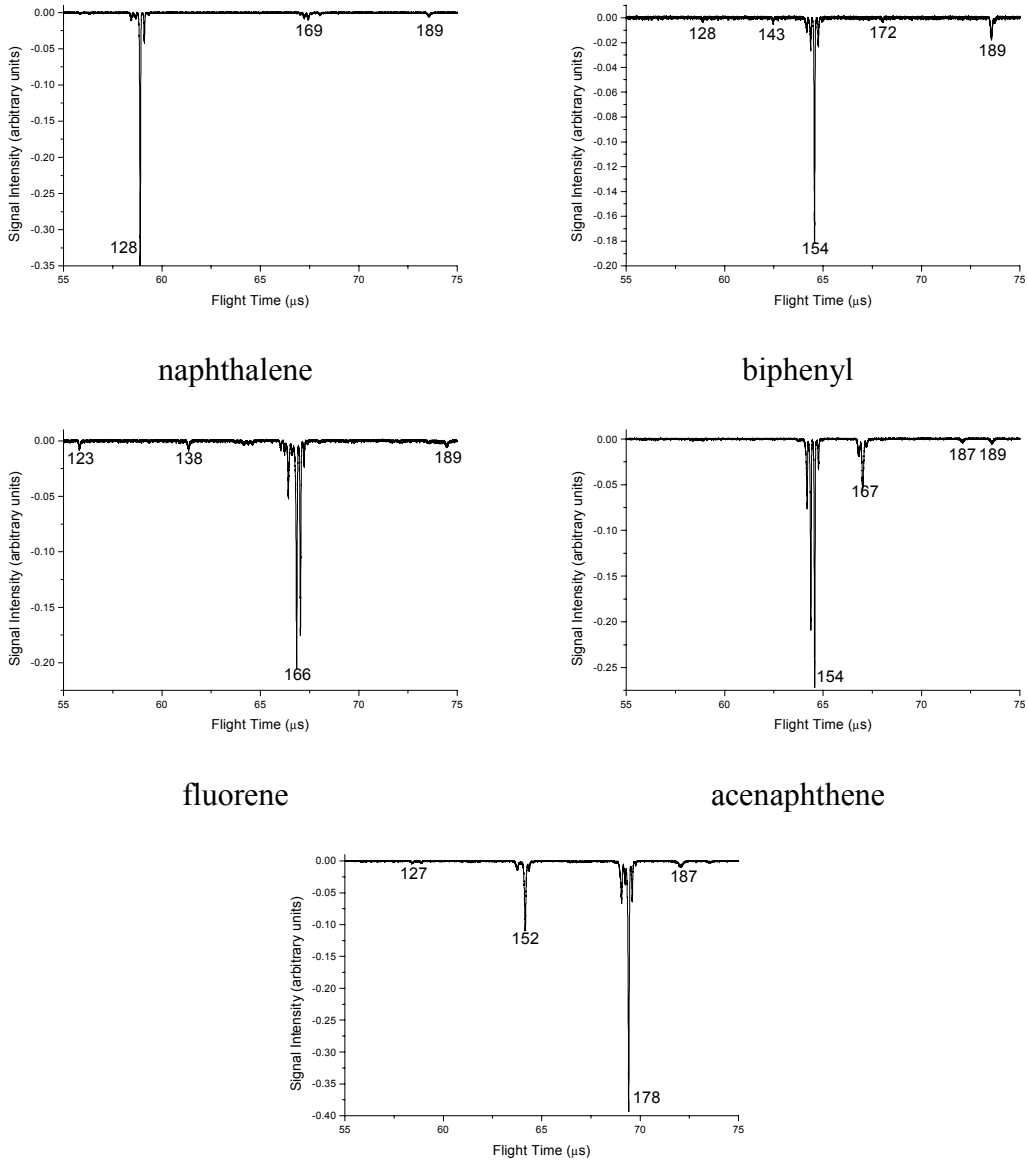

Figure 6.25. TOF spectra recorded at each chromatographic peak apex in Figure 6.23. Note that in the case of acenaphthene, the tail of the fluorene peak can still be seen. Peak labels are *m*/*z* ratios.

Figure 6.26 shows CEC/MS data recorded for the instrument development test mixture with each component now present at 500 μM. All other parameters were unchanged. As was found earlier, with data collected using the constant analyte introduction system, peak intensity falls by much less than the drop in concentration. This indicates that the ion trap was probably saturated at the higher concentration of 5mM. The normal rf trapping potential amplitude used was 1525 V, and since variation in amplitude had been observed to affect the performance of the ion trap with respect to *m*/*z* ratio, the effect on the TOF spectra was investigated. Figure 6.27 shows CEC/MS data recorded for the instrument development test mixture at 5 mM using an rf trapping potential amplitude of 1300 V, while Figure 6.28 shows similar data except that the rf trapping potential amplitude was set to the slightly higher value of 1400 V. Along with the data shown in Figure 6.23, which was recorded using an rf trapping potential of 1525 V, no clear trend can be seen. It appears that changing the rf trapping potential amplitude results in less variance than that which is found between identical potentials. These spectra, therefore, give a rough guide to the reproducibility available with this system.

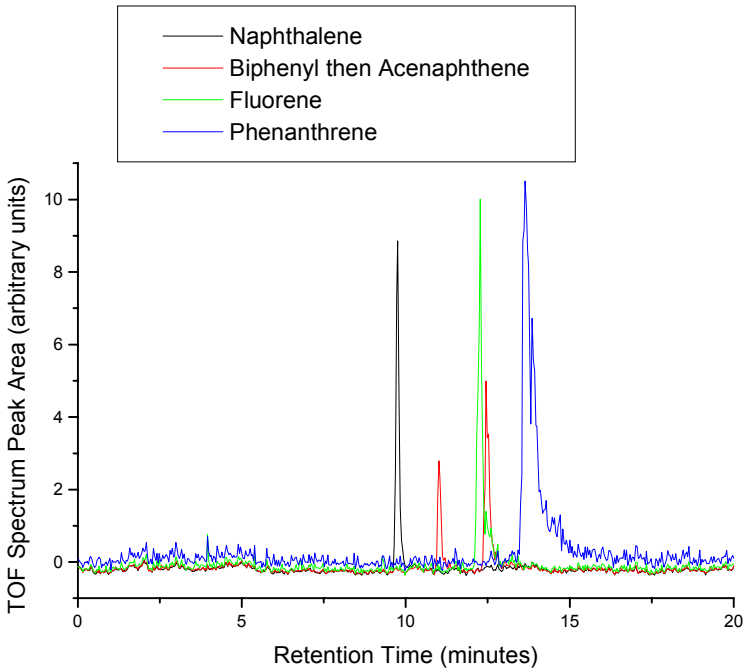

Figure 6.26. CEC/MS data for the analysis of the instrumental development test mixture with each component present at 500 µM in acetonitrile (rf peaks at 1525 V).

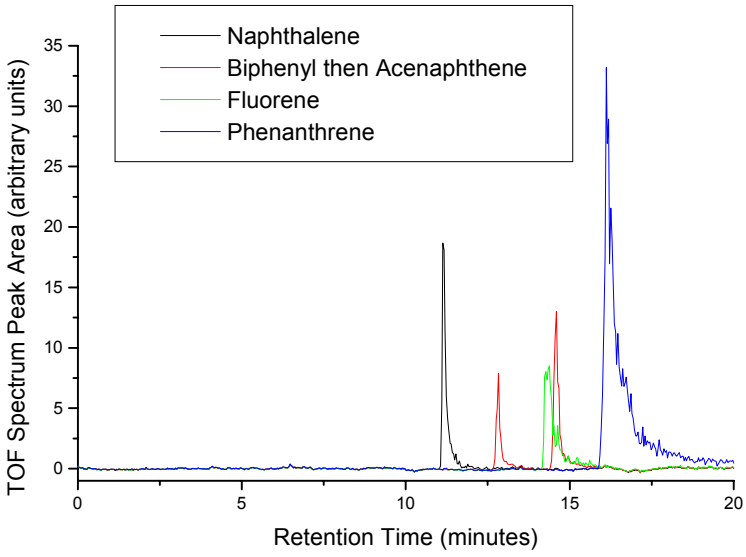

Figure 6.27. CEC/MS data for the analysis of the instrumental development test mixture with each component present at 5 mM in acetonitrile, with the rf trapping potential amplitude set to 1300 V.

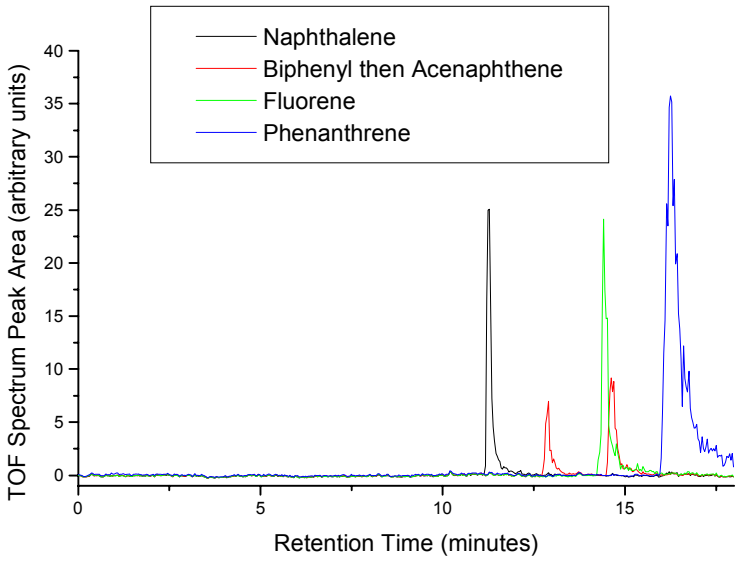

Figure 6.28. CEC/MS data for the analysis of the instrumental development test mixture with each component present at 5 mM in acetonitrile, with the rf trapping potential amplitude set to 1400 V.

6.6. Continuous Flow Liquid MALDI for Separation Interfaces

MALDI is a well-established desorption/ionisation technique that in its usual form is unsuitable for coupling to separation techniques. Continuous flow MALDI, as described in Section 3.1.10, is of greater interest to separation scientists. To be of substantial usefulness, however, the liquid matrix must be compatible with the separation technique of choice. It is of course possible to add the matrix post-column using a device such as a liquid junction, but this will inevitably lead to a loss of separation efficiency. Furthermore, large volume flows into high vacuum chambers will demand expensive pumping systems. The obvious solution is to find a laser that can excite common separation solvents, avoiding the need for unusual additives. Methanol, ethanol and most importantly water, all have strong absorption in the region of 3 µm, while an Er^{3+}:YAG laser is capable of output at 2.94 µm. This provides a means of inputting energy into these common solvents that may be transferred to a dissolved analyte resulting in desorption and ionisation. This would produce a widely applicable experimental technique.

MALDI using an Er^{3+}:YAG laser (2.94 μm) was first reported in 1990 by Overberg *et al.* [6]. Shortly thereafter, the same group reported the use of a CO_2 laser (10.6 μm) in MALDI [7]. Use of IR lasers has been shown to be superior to use of UV lasers in a number of cases, largely because less fragmentation is observed [8-12]. Furthermore, there are many more potential matrices available for MALDI using IR lasers because of strong absorption of many molecules in the IR spectral region. A promising matrix is therefore water, which has been used in MALDI in the ice form for vacuum system compatibility [13], and with the development of atmospheric pressure MALDI, has also been used as water droplets [14]. The correlation between absorption and ion formation in MALDI using IR lasers has been investigated [15]. Continuous flow IR MALDI has been implemented by Lawson and Murray, using an ethanol glycerol mixture as matrix [16].

To mimic a separation system, a system such as that illustrated in Figure 6.4 was used to provide a low flow rate of analyte solution. The Bioptic Lasersysteme Bioscope Er^{3+}:YAG laser was directed using two mirrors and focused using a calcium fluoride lens onto the sample position. A calcium fluoride window was fitted to the high vacuum chamber to permit entry of the laser beam. Radiation at 2.94 μM is significantly absorbed in the air, due to the presence of water vapour, and therefore the laser path length was kept as short as possible. Figure 6.29 shows the TOF spectrum obtained when a solution containing naphthalene at 23 mM and glycerol at 11 mM in ethanol was allowed to enter the trap through a capillary of 25 μm ID and of length, 519 mm. PAHs have already been analysed by IR MALDI, using a CO_2 laser (10.6 μm) and sulfolane as matrix [17]. This matrix was investigated in this work as part of a continuously flowing system, with the Er^{3+}:YAG laser, but no data could be obtained. An ion storage time of 210 ms was used, which means that three laser shots contributed to every TOF spectrum recorded. The pulse length of the Er^{3+}:YAG laser is relatively long at ~ 50 ns, making ion trap storage very useful for improving TOF spectrum resolution. For the data displayed, 1000 TOF spectra were summed. The mass spectrometer was used as described previously while the glycerol was present to guard against freezing of solvent as it enters the high vacuum chamber. This is intended to provide a smoother flow of analyte. The pulse energy

found with the laser varied shot to shot between 6 and 10 mJ. This low pulse energy suggested that laser heating might not be adequate and intermittent flow due to freezing might be obtained, necessitating the glycerol.

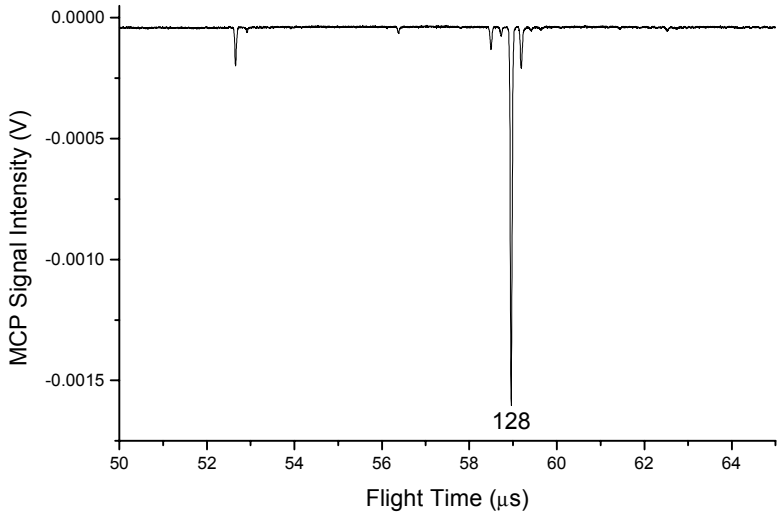

Figure 6.29. Signal obtained in a continuous flow MALDI experiment using an Er^{3+}:YAG laser operating at 2.94 μm to analyse a solution of naphthalene (23 mM) and glycerol (11 mM) in ethanol. Peak labels are *m*/*z* ratios.

As can be seen, a signal for the molecular ion of naphthalene is observed, but the intensity is low given the relatively high analyte concentration used. Phenanthrene was also investigated, using an 18 mM solution containing glycerol at 11 mM in ethanol, with all other conditions as described above. Again a signal of very low intensity was obtained as shown in Figure 6.30. After each experiment the capillary terminus was inspected for damage and laser alignment was verified. No problems were discovered in either case.

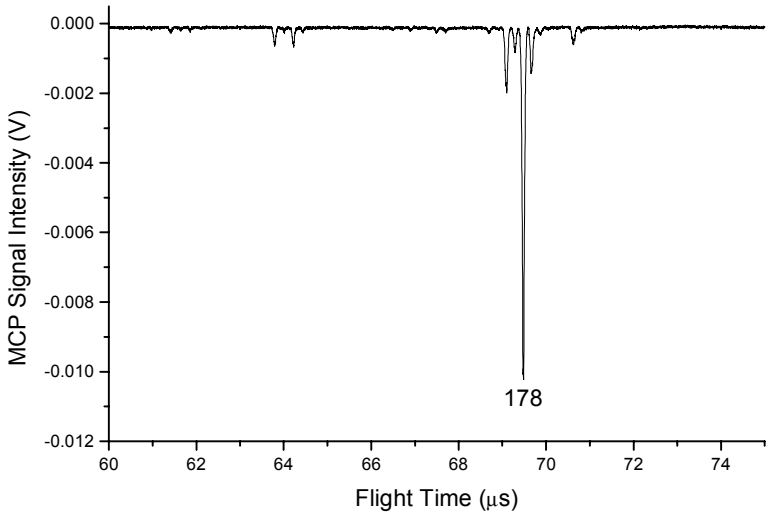

Figure 6.30. Signal obtained in a continuous flow MALDI experiment using an Er^{3+}:YAG laser operating at 2.94 mm to analyse a solution of phenanthrene (18 mM) and glycerol (11 mM) in ethanol. Peak labels are *m*/*z* ratios.

For means of comparison, a two-laser experiment was attempted. The Quantel Brilliant laser was used for ionisation, providing radiation at 266 nm as described previously. The configuration of the Bioptic Lasersysteme Bioscope laser was unchanged, but in this experiment it was used as a vaporisation laser. Using the same naphthalene solution as that described above, the UV laser was added into the system, firing ~ 30 μs after the IR laser. In this instance the trapping time was reduced to 10 ms so that only one delay generator was required. Figure 6.31 shows that a very large signal was obtained, although Figure 6.32 records that a similar result was obtained from use of the UV laser alone.

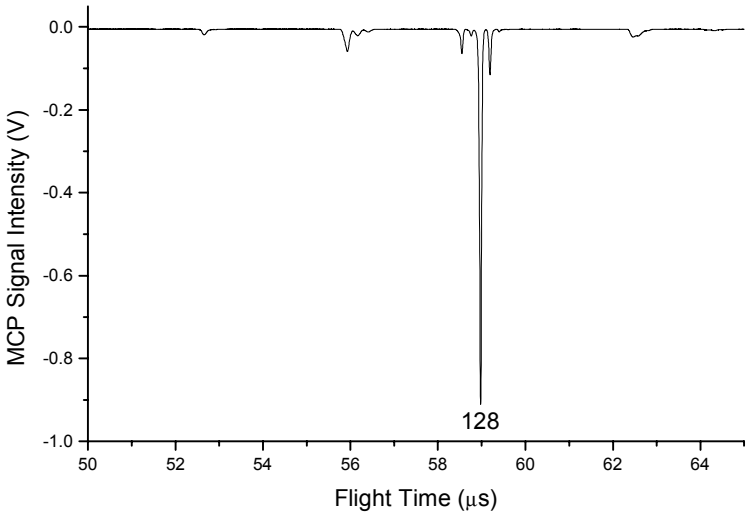

Figure 6.31. Two-laser MS experiment using an Er^{3+}:YAG laser operating at 2.94 μm for vaporisation along with a quadrupled Nd^{3+}:YAG laser operating at 266 nm for ionisation. Sample was naphthalene (23 mM) and glycerol (11 mM) in ethanol. Peak labels are *m*/*z* ratios.

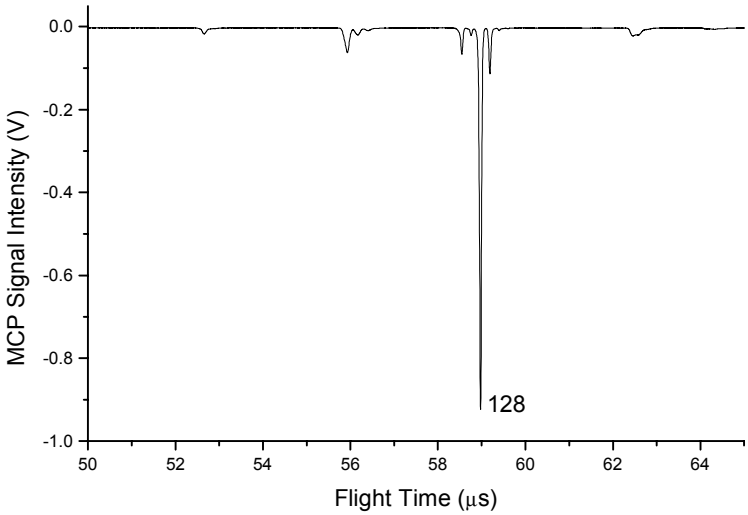

Figure 6.32. Signal recorded for naphthalene (23 mM) and glycerol (11 mM) in ethanol using the ionisation laser alone. Peak labels are *m*/*z* ratios.

Tryptophan solutions were also investigated, as examples of an involatile analyte systems, but no signal was obtained. Given that both analyte molecules for which a

signal was obtained (naphthalene and phenanthrene) are relatively volatile, this would seem to indicate that the Bioptic Lasersysteme Bioscope IR laser is not capable of inputting enough energy into the flowing liquid to result in vaporisation. What must have happened is that naphthalene and phenanthrene evaporated into the ion trap chamber and, in the case of the Bioptic Lasersysteme Bioscope IR laser alone, were ionised at very low efficiency. On addition of the Quantel Brilliant UV laser, ionisation became much more efficient and a large signal was obtained. The difference in intensity is due to the difference in photon energy between the two lasers. The gas phase ionisation potential of naphthalene is 8.14 eV [18], meaning that 20 photons would need to be absorbed from the Bioptic Lasersysteme Bioscope IR laser in order to achieve ionisation (2.94 μm corresponds to 0.42 eV while for comparison 266 nm corresponds to 4.66 eV). The gas phase ionisation potential of phenanthrene is slightly lower at 7.86 eV [18], requiring 19×0.42 eV photons. Use of the Bioptic Lasersysteme Bioscope IR laser desorption from a solid sample did, however, provide acceptable results, indicating that not enough power was available to vaporise the eluate at experimental flow rates.

An idea of the energy required can be obtained by consideration of the amount of energy needed to vaporise all solvent flowing into the vacuum chamber. The inner diameter of the capillary utilised was 25 μm, the viscosity of ethanol is 1.074×10^{-3} N m^{-2} s, the pressure difference along the capillary was 1.01×10^{5} N m^{-2} and the capillary length was 0.519 m. Using Equation 2.3, a value for the flow rate of approximately 100 nL min^{-1} is obtained, with the real flow rate likely to be lower due to the presence of dissolved analyte and glycerol (increased viscosity). This means that somewhere in the region of 0.17 nL of liquid will emerge ready for every laser shot. Given that the molar enthalpy of vaporisation for ethanol at atmospheric pressure when starting at 25°C is 42.32 kJ mol^{-1}, there would be a requirement for 1.3×10^{-4} J to be transferred from every laser shot to vaporise all solvent. As this process is occurring in a high vacuum chamber, the true value would be expected to be different, with evaporation into the chamber cooling the droplet. The number is likely to be of the correct order of magnitude, however. Laser pulse energy is much larger than 0.13 mJ, but transfer of energy to the solvent will be inefficient, and laser

energy will be attenuated through the air and the laser optics. It is certainly possible that the Bioptic Lasersysteme Bioscope IR laser does not provide enough power for these experiments. The long laser pulse length may be a contributory factor. Other experiments were attempted where a much longer capillary was utilised to lower the flow rate, but no signal was obtained in these cases either.

6.7. Concluding Remarks

A system for performing CEC/MS using laser vaporisation, laser ionisation and ion trap storage in conjunction with TOF mass spectrometry has been demonstrated in every aspect apart from laser vaporisation. Performance is good for volatile analytes, with chromatographic efficiencies having been largely retained when comparing absorbance detection with detection with mass spectrometry. The reasons for the lack of success with involatile analytes are not clear, but suspicion has naturally fallen on the vaporisation stage. The vaporisation laser was seen to have virtually no effect with naphthalene, but was seen to enhance phenanthrene signals somewhat. The molecules being similar, but phenanthrene being heavier, phenanthrene would be expected to require more energy for vaporisation. This seems to indicate that the laser is able to heat the capillary tip, promoting phenanthrene vaporisation. The experiments where the laser was observed to remove solvent droplets from the end of the capillary also indicate that vaporisation of some form is possible. The nature of what is occurring as liquids run into the vacuum chamber is therefore not well understood. After vaporisation, the greatest challenge in further system development is the data system.

---

[1] V. L. Tal'roze, G. V. Karpov, I. G. Gorodetskii and V. E. Skurat, *Russ. J. Phys. Chem.*, **1968**, *42*, 1658-1664.

[2] V. L. Tal'roze, G. V. Karpov, I. G. Gorodetskii and V. E. Skurat, *Russ. J. Phys. Chem.*, **1968**, *42*, 1664-1667.

[3] V. L. Tal'roze, G. V. Karpov, I. G. Gorodetskii and V. E. Skurat, *Russ. J. Phys. Chem.*, **1969**, *43*, 198-201.

[4] V. L. Tal'roze, V. E. Skurat and G. V. Karpov, *Russ. J. Phys. Chem.*, **1969**, *43*, 241-242.

[5] L. He, L. Liang and D. M. Lubman, *Anal. Chem.*, **1995**, *67*, 4127-4132.

[6] A. Overberg, M. Karas, U. Bahr, R. Kaufmann and F. Hillenkamp, *Rapid Commun. Mass Spectrom.*, **1990**, *4*, 293-296.

[7] A. Overberg, M. Karas and F. Hillenkamp, *Rapid Commun. Mass Spectrom*., **1991**, *5*, 128-131.

[8] E. Nordhoff, A. Ingendoh, R. Cramer, A. Overberg, B. Stahl, M. Karas, F. Hillenkamp and P. F. Crain, *Rapid Commun. Mass Spectrom.*, **1992**, *6*, 771-776.

[9] F. Hillenkamp, M. Karas and S. Berkenkamp in *Proceedings of the 43rd ASMS Conference on Mass Spectrometry and Allied Topics*, Atlanta, GA, **1995**, 357.

[10] S. Berkenkamp, C. Menzel, M. Karas and F. Hillenkamp, *Rapid Commun. Mass Spectrom.*, **1997**, *11*, 1399-1406.

[11] S. Niu, W. Zhang, B. T. Chait, *J. Am. Soc. Mass Spectrom.*, **1998**, *9*, 1-7.

[12] S. Berkenkamp, F. Kirpekar and F. Hillenkamp, *Science*, **1998**, *281*, 260-262.

[13] S. Berkenkamp, M. Karas and F. Hillenkamp, *Proc. Natl Acad. Sci. U.S.A.*, **1996**, *93*, 7003-7007.

[14] V. V. Laiko, N. I. Taranenko, V. D. Berkout, M. A. Yakshin, C. R. Prasad, H. S. Lee and V. M. Doroshenko, *J. Am. Soc. Mass Spectrom.*, **2002**, *13*, 354-361.

[15] V. L. Talrose, M. D. Person, R. M. Whittal, F. C. Walls, A. L. Burlingame and M. A. Baldwin, *Rapid Commun. Mass Spectrom.*, **1999**, *13*, 2191-2198.

[16] S. J. Lawson and K. K. Murray, *Rapid Commun. Mass Spectrom.*, **2000**, *14*, 129-134.

[17] S. N. Jackson and K. K. Murray, *Rapid Commun. Mass Spectrom.*, **2001**, *15*, 1448-1452.

[18] D. R. Lide (Editor), *CRC Handbook of Chemistry and Physics (Seventy Fourth Edition)*, CRC Press, Boca Raton, FL, **1993**.

7. Conclusion

A new instrument has been developed for on-line CEC/MS, based on a hybrid ITS/TOF mass spectrometer. The ion trap is used in rf-only mode, with dc-pulse ejection, to provide decoupling of the different timescales required for CEC separation and TOF mass analysis. The ion trap is capable of storing and accumulating ions prior to TOF mass analysis, enabling efficient ion detection. The instrument incorporates a laser vaporisation laser ionisation interface in which analytes are vaporised, directly from the end of the capillary coupling the working CEC column to the instrument, using 1064 nm radiation. Ions are obtained through UV photoionisation of the vaporised neutrals, using a wavelength chosen to be selective for the targeted analyte. This two-step approach can provide ultratrace analysis with high selectivity. Laser vaporisation and laser ionisation can be performed directly in the ion trap, avoiding the need for any ion transfer optics external to the trap. Software for data acquisition was developed using National Instruments' LabVIEW.

A key advantage of both CE and CEC over HPLC was demonstrated in the experiments described in Section 4.3.2. There, the combination of a typical HPLC injection and detection system was shown, simply by removing the column, to significantly degrade performance. In CE and CEC, the use of electrokinetic injection removes the need for injection valves, along with the associated tubing and connectors, while on-column absorbance detection removes the need for tubing and connections between the end of the column and the detector cell. This simplification contributes to the superior separation efficiencies reported in both CE and CEC. All attempts to join capillaries to enlarged detection cells, to increase sensitivity, have resulted in reduced separation efficiency.

Capillary junctions, however, were required to avoid the difficult task of terminating the CEC column in the ion trap ring electrode. It was decided to use a transfer capillary to carry eluate from the column to the vaporisation point, necessitating the fabrication of a junction that caused minimal degradation of chromatographic efficiency but which allowed electrical connection to be made. In Chapter 5, the development of a suitable junction was described. Theoretical work by Boughtflower *et al.* [1] showed that the transfer capillary should be significantly narrower than the separation column to

preserve chromatographic efficiency, so CFD simulations were performed to determine the ideal geometry for this junction. A conical inlet into the narrower capillary was shown to be significantly superior to simply butting the two columns together. In practice, however, production of these conical inlets proved too challenging and simple butt joints were used in the CEC/MS experiments described here.

To support this computational work, imaging of bands as they moved through capillary systems was attempted. This was achieved, for fluorescent molecules, by intersecting the column with a laser beam and using a microscope to observe the resulting fluorescence. The fluorescent dye was injected just like any other sample, and then travelled through the column under the influence of both the bulk EOF and electrophoresis. Sharp fronts were observed, and it was proposed that these could be used to probe the effect of capillary junctions and structures such as retaining frits. The inability to produce transparent junctions, however, brought this work to an end. It would, however, have been interesting to image the passage of a band across a retaining frit.

As a final extension to the imaging work, absorbance detection windows were constructed in packed regions of the capillary. Different packing materials were investigated, with porous silica particles found to scatter light and hence reduce detection sensitivity much more effectively than non-porous silica particles. It was proposed that non-porous particles might profitably be used in imaging studies. However, recent reports of confocal microscopy being used to image solute distribution in packed beds [2] offer superior data. These reported techniques probably provide the best way to investigate the processes occurring within retaining frits.

In practical terms, the greatest challenge in producing efficient junctions was in alignment. In junctions where polymeric sleeving was employed, alignment of the capillary axes and positioning the end faces close to each other were found to be virtually impossible. The best jointing strategy was found to be the use of double tapered ferrules. The capillaries to be joined are placed so that their junction is in the middle of the ferrule, with the ferrule housing allowing compression of the ferrule to hold the capillaries tightly in place. Such housings, however, caused the failure of graphite paint, forcing an alternative strategy of vacuum coating with copper. Such

junctions were shown to retain that majority of the chromatographic efficiency, while at the same time, providing a reliable connection to electrical ground.

The reproducibility of CEC separations was an issue that was briefly investigated. Retention times of retained solutes were seen to vary systematically through the course of a day, something that had been noticed throughout these experiments. Typically, during the course of a day, retention times of retained solutes will lengthen. On flushing the column with freshly degassed mobile phase, normal retention times are typically regained. This lengthening is probably due to mobile phase degradation. Solvent evaporation will result in a more concentrated mobile phase, which would naturally be expected to influence the separation. During the lifetime of a column, however, retention times tend to fall. This is probably due to exposure of additional surface silanol groups, through some degradation process, raising the EOF rate. It should also be noted that warming of mobile phase, due to resistive heating, would be expected to raise the EOF rate. Allowing time for thermal equilibrium to be obtained is therefore important.

The initial tuning of the ITS/TOF instrument and the CEC/MS experiments that were eventually performed are fully discussed in Chapter 6. The instrument proved to be very stable, with most settings kept constant throughout this work. The optimal ion trap storage time was found to be in the region of 10 ms, when only one laser cycle is being considered. Shorter times did not allow focusing of ions into the centre of the trap for efficient extraction into the TOF mass spectrometer, while longer times resulted in significant losses of molecular ion peak area, due both to ions leaving the trap and ion-molecule reactions. Storage over multiple laser cycles was shown to significantly increase the molecular ion peak area provided that the trap does not become full. The maximum m/z ratio resolution of the ITS/TOF instrument is ~ 1500.

The performance of the instrument was evaluated using PAHs, both because they are important environmental pollutants and because they are amenable to laser ionisation at 266 nm. Expressed as a number of plates per metre, an average chromatographic efficiency of 95,000 was obtained with a test mixture that consisted of acenaphthene, biphenyl, fluorene, naphthalene and phenanthrene. Furthermore, using the leak inlet, naphthalene was detected as a 100 nM solution in acetonitrile (one laser cycle only).

The CEC/MS data obtained showed that most chromatographic efficiency had been successfully retained. CEC/MS separation of a test mixture of PAHs was demonstrated. The combination of CEC with ITS/TOF mass spectrometry using a two-laser interface located inside an ion trap has been shown to be feasible. Most of the practical difficulties encountered were technical and could be overcome with improved instrumentation. A more serious problem is the lack of success with involatile analytes. All compounds analysed in solution were volatile, indicating that the laser vaporisation interface is not capable of the fast heating required to move compounds from solution to the gas phase. Further work is needed to fully investigate this problem. The vaporisation imaging studies that were carried out indicated that laser power was sufficient for vaporisation of large amounts of solvent, but no signal for an involatile analyte was ever obtained, at any laser intensity.

Improvements to the sensitivity and chromatographic efficiency of the system could be obtained by replacing the ion trap vacuum chamber with one that allowed much shorter transfer capillaries to be utilised. Eventual phasing out of transfer capillary use would be desirable, but it might be envisaged that exposing retaining frits to laser irradiation could prove problematic. Being able to swap columns without opening the chamber is useful, however, arguing in favour of retaining the transfer capillary. Considering the interface, use of lasers with higher repetition rates, but with the same output, could increase sensitivity. With the ideal trapping time being 10 ms, 100 Hz lasers would seem to be appropriate. Another innovation that could reduce peak tailing would be to introduce an occasional very high power laser pulse for the purpose of cleaning the desorption end of the transfer capillary. This would be likely to produce a large amount of fragment ions, which would need to be discarded before the next analytical laser pulse. The greatest practical problem, however, is loss of data when waiting for data transfer between the oscilloscope and the computer. Ideally, every TOF spectrum would be recorded for later investigation, but any reduction in the time taken to transfer data would be an improvement.

The possibility of performing continuous flow MALDI experiments in the ITS/TOF system was also investigated. An Er^{3+}:YAG laser (2.94 μm) was used, capable of exciting common solvents such as methanol, ethanol and water. Being able to use standard chromatographic solvents as matrix is a great improvement on other forms of

continuous flow MALDI where matrix is added to column eluate, resulting is reduced sensitivity and chromatographic efficiency. The system was shown to be functional, although no MALDI data could be obtained. It is postulated that low laser power was the problem.

Finally, in the appendix that follows this Chapter, a number of stand-alone CE experiments that were performed in addition to the main body of work are described. An effective CE method for the separation of the nucleotides AMP, CMP, GMP and TMP was developed, which was designed for use in studies of nucleotide binding to platinum aminophosphine complexes. The separation suffered a little from fronting, probably due to the sample capacity of the system having been exceeded, but baseline resolution was retained. The separation of histones was also investigated. Histones are very basic analytes, being prone to adsorption to silica surfaces, resulting in poor chromatography due to tailing. Several approaches proposed for histone separation were investigated, with the conclusion being that the CE/MS analysis of histones would require a radically different strategy to those reported in the literature. As future work, the use of capillaries made out of materials such as PEEK is suggested.

The final stand-alone CE experiments performed were concerned with increasing sample capacity, a problem encountered with the nucleotide binding studies. This was achieved by packing columns with non-porous silica particles to provide what might essentially be regarded as an array of interconnected narrow capillaries. Sample capacity is proportional to surface area, making these columns able to accept larger amounts of injected sample without compromising separation efficiency. Results showed that the sample capacity had indeed increased, evidenced by achieving symmetrical peaks on the packed column at concentrations where open columns delivered noticeably asymmetrical peaks. Separation efficiency, however, was lower than that typically found in open-column CE. Further work on this subject should probably be focused on packing the columns with smaller particles.

---

[1] R. J. Boughtflower, C. J. Paterson and J. H. Knox, *J. Chromatogr. A*, **2000**, *887*, 409-420.

[2] M. Lowry, Y. He and L. Geng, *Anal. Chem.*, **2002**, *74*, 1811-1818.

A. Capillary Electrophoresis Separations

This appendix describes the results of other experimental work that arose during the course of the principal project. A CE method was developed for the separation of nucleotides at physiological pH, which could be used to assess nucleotide binding, and separation strategies for histones were also investigated. The feasibility of increasing sample capacity in CE by using columns packed with bare non-porous silica was also examined.

A.1. Separation of Nucleotides by Capillary Electrophoresis

Tsuda was first to report nucleotide analysis by CE, using 0.02 M phosphate containing 0.5% ethylene glycol as electrophoretic medium [1,2]. Since nucleotides are negatively charged under most conditions, an improvement in analysis speed is offered by reversing column surface charge. Bare fused silica capillaries offer negatively charged surfaces, resulting in the direction of bulk flow being from anode to cathode. Negatively charged nucleotides will be attracted towards the anode, moving against the bulk flow. Faster analyses are therefore obtained if the surface charge is reversed and the bulk flow is made to run from cathode to anode. Huang *et al.* used cetyltrimethylammonium bromide as a dynamic coating agent to provide a positively charged surface and hence obtain faster analyses [3]. Separation efficiency was reduced, however, probably due to surface adsorption. Analysis of nucleotides by CE has been reviewed comprehensively by Geldert and Brown [4]. CE/ESI/MS analysis of nucleotides has also been reported [5].

The aim of the work described in this section was to develop a separation technique that could be used to analyse the binding of platinum aminophosphine complexes to nucleotides at physiological pH. A study of the interactions between nucleotides and cisplatin, *cis*-$[Pt(NH_3)_2Cl_2]$, using CE as an analytical tool, has recently been published [6]. The nucleotide, once bound to the complex, would be expected to migrate at a different velocity, due to having obtained a different hydrodynamic radius and also possibly a different charge. Reduced peak area would therefore be expected for each nucleotide at the anticipated retention time, along with new peaks

at different retention times. Analysis of these peaks could be used to calculate binding coefficients. Given the focus on binding it was essential that the CE separation protocol did not include any molecules that might be suspected to influence binding. Most published methods [4], however, contain various additives, such as ethylenediaminetetraacetic acid, that would cast doubt on any results obtained. A method free from modifiers, but still capable of delivering an adequate separation, was required.

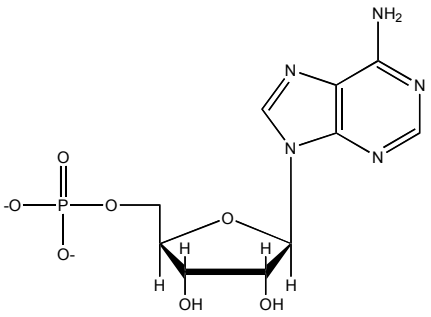

adenosine 5'-monophosphate

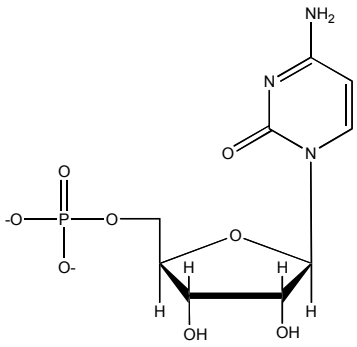

cytidine 5'-monophosphate

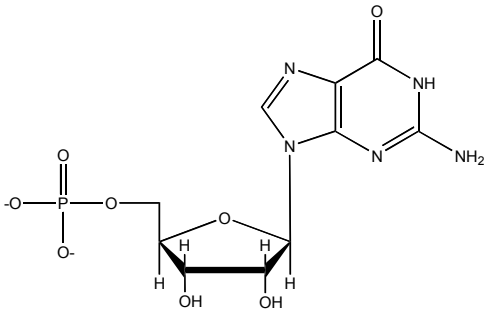

guanosine 5'-monophosphate

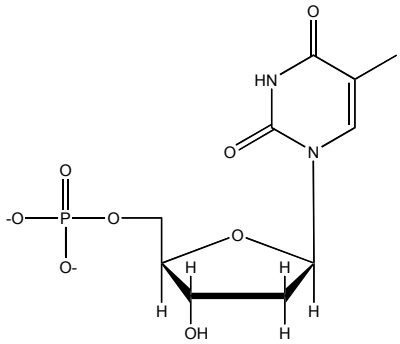

thymidine 5'-monophosphate

Figure A.1. Structures of the nucleotides investigated as would be found in a slightly alkaline (pH ~ 8) solution.

The structures of the nucleotides investigated are given in Figure A.1. Three are ribonucleotides (adenosine 5'-monophosphate (AMP), cytidine 5'-monophosphate (CMP) and guanosine 5'-monophosphate (GMP)) while one is a deoxyribonucelotide (thymidine 5'-monophosphate (TMP)). At close to neutral pH, all four are doubly negatively charged [7]. A 100 μm ID capillary was prepared that had a total length of

880 mm and a length between inlet and window of 630 mm. The column was filled with 20 mM Na_2HPO_4 that had been adjusted to pH 7.75, which had been degassed by sparging with helium while stirring. The efficiency of the separation was very sensitive to changes in pH. The column was mounted in the Isco instrument and used at an applied potential of 25 kV, which resulted in a current of 110 µA. Absorbance was recorded at a wavelength of 254 nm, with a time constant of 0.8 seconds, while injection was achieved by applying a vacuum to the outlet for 5 seconds. Vacuum injection was employed because injection by electromigration will discriminate against negatively charged ions. Each nucleotide was present at a concentration of 40 µm in water in the injected sample. Separation was achieved with baseline resolution as shown in Figure A.2. The region of the electropherogram where the nucleotides elute is shown expanded in Figure A.3.

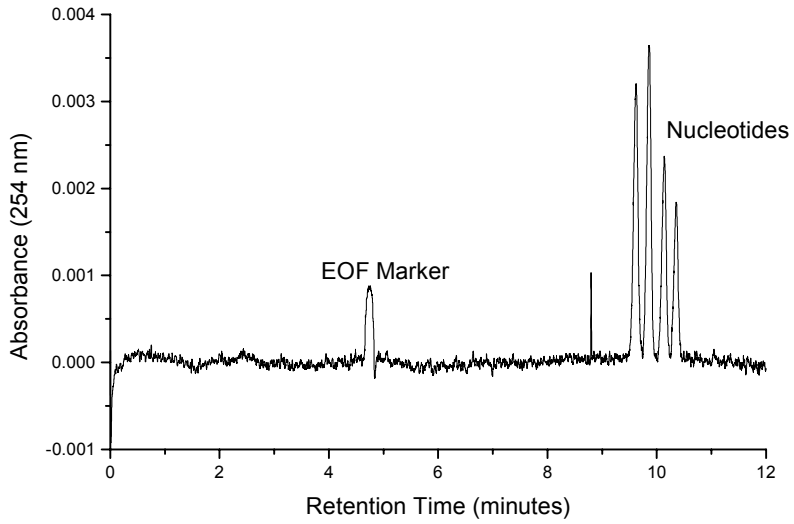

Figure A.2. Separation of nucleotides AMP, CMP, GMP and TMP by capillary electrophoresis at physiological pH without additives that might interfere with nucleotide binding.

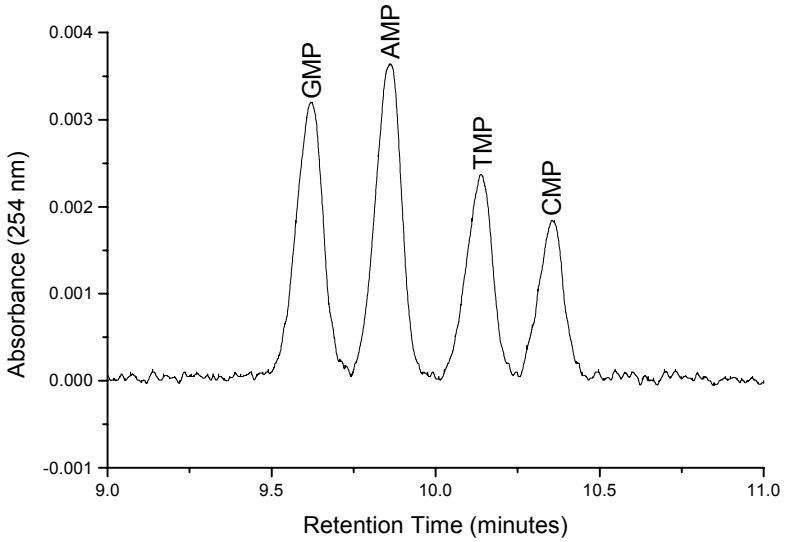

Figure A.3. Labelled expansion of the region in the electropherogram where the nucleotides elute.

It can be seen that there is slight fronting, especially evident on the earlier peaks, which is further evidenced by the separation efficiencies displayed in Table A.1. These efficiencies were calculated by taking measurements of half height peak width, using Equation 2.14 to give separation efficiency in terms of a plate number. Although plate numbers do not strictly apply to electrophoresis, use of this method of quantifying peak width in relation to retention time has become widespread. The fronting recorded was possibly due to exceeding the sample capacity of the column. Maximum peak area, however, was required for accurate determination of binding constants, so this fronting was tolerated provided that baseline resolution was obtained. The elution order was determined by spiking and removing particular components of the mixture. This work was begun in collaboration with E. Beth Watchman. She continued this work, and initial binding studies are reported in her PhD thesis [8].

Analyte	Efficiency (N)	Efficiency (N/m)
GMP	60,000	95,000
AMP	67,000	106,000
TMP	70,000	112,000
CMP	86,000	136,000

Table A.1. Chromatographic efficiencies expressed as plate numbers for the separation of the nucleotides AMP, CMP, GMP and TMP.

A.2. Separation of Histones by Capillary Electrophoresis

Histones are of great interest because they are the major structural proteins of chromatin and because they have a role in gene expression [9,10]. In simple terms, histones form a positively charged spindle about which negatively charged DNA is wound. Five classes of histones are found in nearly all eukaryotic cell types (H1, H2A, H2B, H3 and H4), with most classes displaying a complex pattern of variants. Histones are subject to post-translational modifications that include methylations, acetylations and phosphorylations of specific arginine, histidine, lysine, serine and threonine residues. These modifications are used to regulate the action of the protein, with many being reversible, but all decrease the amount of positive charge on the histones thereby significantly altering the interaction between the histone and DNA. The degree of modification varies enormously with species, tissue, and the stage of the cell cycle. An efficient CE method that could be interfaced to mass spectrometry would provide a useful analytical tool.

The basic amino acids, arginine, histidine and lysine, are present in high proportions in the histones, providing their positive charges for DNA binding, and making the proteins extremely basic (isoelectric point pH 10-12). The chief obstacle to effective analysis by CE is therefore adsorption onto silica tubing due to interactions with acidic silanol groups. Green and Jorgenson suggested the use of high ionic strength buffers to suppress adsorption of basic proteins [11]. In this work, however, use of a high pH buffer was recommended in order to reduce the charge on the analysed proteins. In the earliest reported CE separation of histones, on the other hand, a high ionic strength acidic buffer was used to limit adsorption onto the capillary [12]. Use

of acidic buffers reduces the proportion of silanol groups that are dissociated, and hence presenting binding sites, while use of high concentration buffers aims to out compete the histones for the remaining binding sites. A side effect is that EOF is reduced almost to zero and hence the separations are almost wholly electrophoretic. Subsequent studies have employed dynamic coating agents such as hydroxypropylmethyl cellulose (HPMC) to improve separation efficiency [13-16]. The addition of a long polymeric chain molecule such as HPMC is for the purpose of coating the inner wall of the capillary to further guard against undesirable interactions. However, choosing to operate under such acidic conditions ensures that the histones are very highly positively charged. Using the same logic, but moving to a more moderate pH, a more recently reported method uses 1,5-dimethyl-1,5-diazaundecamethylene polymethobromide (hexadimethrine bromide) as a dynamic surface modification reagent [17]. This work was largely successful, although severe fronting is evident in the electropherograms presented. The presence of large polymeric molecules and involatile salts in the mobile phase, however, would also almost certainly prevent histones from being detected by mass spectrometry. As the polymeric molecules and high salt concentrations are used primarily to prevent histone adsorption to the silica surface, there seems to be room for improvement either by permanently modifying the surface, or by using a material other than fused silica.

In initial trial experiments, a low pH was used along with a polymeric modifier to coat the inner capillary walls. A 75 μm ID column was prepared for CE that was of total length 767 mm, with a length from outlet to absorbance detection window of 534 mm. The column was then fitted into the CIA, but was not flushed in the usual manner with dilute NaOH, but only with water. The NaOH step was omitted, since etching the capillary to reveal more silanol groups was undesirable. The mobile phase used was prepared by adjusting an approximately 100 mM solution of phosphoric acid (88.36% phosphoric acid supplied by Fisher) in water to pH 2.0 with triethylamine (Fisons). Use of triethylamine as cation was recommended by Lindner *et al.* [16]. To this solution was then added 0.03% by mass HPMC (supplied by Aldrich with viscosity at 2% by mass in aqueous solution being equal to 4.0 N m^{-2} s). The mobile phase was degassed by stirring under vacuum (degassing by sparging

with helium resulted in the formation of soapy bubbles). All runs in this section were performed with an applied potential of 15 kV and detection was by achieved by measuring absorbance at a wavelength of 214 nm. Injection was performed electrokinetically by application of 10 kV for 5 seconds, although with the instrument taking ~ 5 seconds to ramp up to 10 kV this might better be described as a true 5 kV for 5 seconds injection.

The first sample investigated, however, was not a histone, but was 1 mg mL^{-1} arginine in water. The resulting electropherogram is shown in Figure A.4. Arginine was chosen because, as a small positively charged ion, it would be expected to interact strongly with the capillary wall. As can be seen there is strong tailing, indicating that this was indeed the case. The separation efficiency of the peak, originating from a measurement of half height width and expressed as a plate number, was acceptable at 69,000 (130,000 per metre), but the measured asymmetry ratio of 0.33 clearly indicates the severe tailing that is visible in Figure A.4.

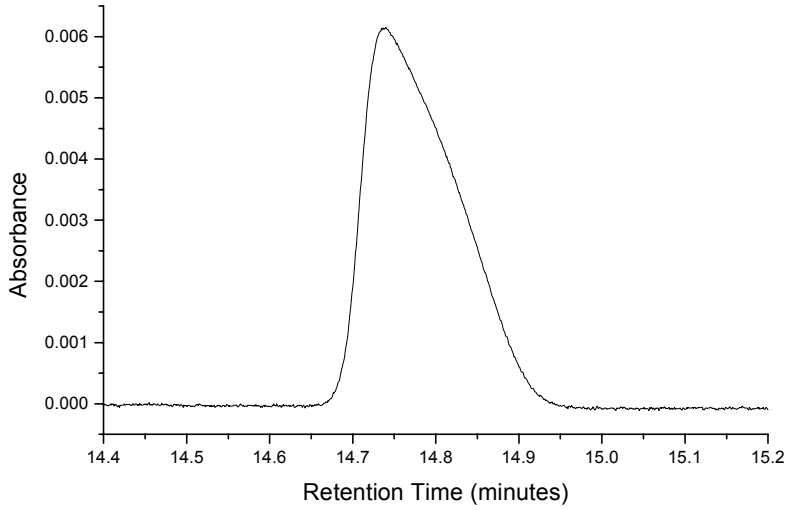

Figure A.4. Use of arginine as a probe to determine the success of surface deactivation strategies. Arginine injected onto a bare column containing a low pH mobile phase with the dynamic coating agent, HPMC, at 0.03%.

The results with arginine show that surface deactivation is not entirely effective, but the separation efficiency recorded was promising. A sample of H1 histones from

chicken erythrocytes was obtained from Dr James Allan (Institute of Cell and Molecular Biology, University of Edinburgh), diluted in a small amount of water and analysed as described above. The sample probably contained a good deal of salt and hence the analyte was likely to be very dilute. The resulting electropherogram is shown in Figure A.5.

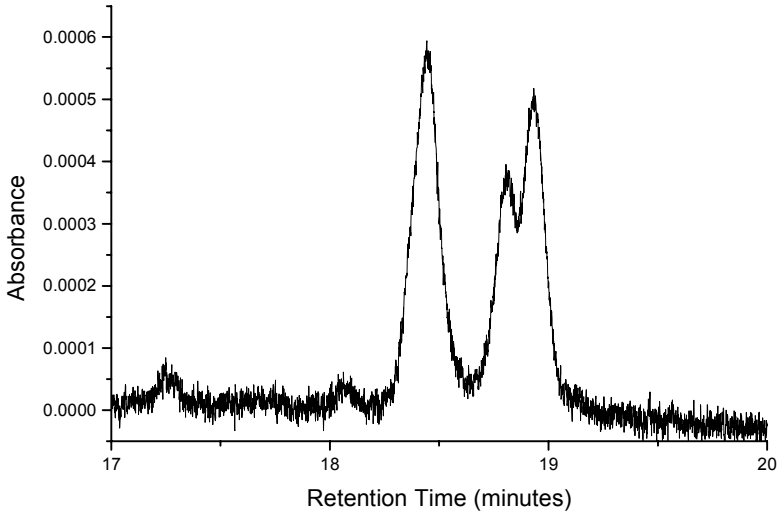

Figure A.5. Results from a CE separation of a sample of H1 histones originating from chicken erythrocytes.

The number of peaks that should have been obtained is greater than the three that are clearly visible, with others possibly hiding in the noise. The close to Gaussian peak shape of the large peak to earlier retention time, however, shows that surface deactivation has been more effective in this case than in the case of arginine. This is likely due to a reduced charge to mass ratio for the histones. The separation efficiency of the first strong peak, expressed as a plate number and obtained from a measurement of half height peak width, is excellent at 107,000 (201,000 per metre). Progress towards a mass spectrometry compatible separation would best be achieved, however, with permanently deactivated fused silica tubing or with tubing made of a different material. If mass spectrometric detection is utilised, there is no longer any requirement for a transparent capillary, and hence an opaque material such as PEEK could be used. PEEK capillaries of appropriate dimensions are readily available, are

likely to have significantly less polar surfaces, and could easily be added to an interface such as that shown in Figure 3.9. With the mass spectrometric system providing a further stage of separation, total electrophoretic resolution of all components is not necessarily required. It is, however, useful to have only to deal with two or three components at any one time rather than with the whole set.

A.3. Performing Capillary Electrophoresis on Packed Columns to Increase Sample Capacity

One of the most important limiting factors found in CE is relatively low sample capacity, as evidenced by the fronting mentioned in the previous sections of this appendix. Fronting has been linked to overloading since the inception of CE [18], and while careful choice of buffer can increase sample capacity [19], limitations on the amount of sample that can be injected is a real problem. Sample capacity is a measure of how much analyte can be loaded onto a column without adversely effecting the separation. When sample capacity is exceeded, peaks tend to front, becoming wider and reducing separation efficiency. Sample capacity is proportional to column surface area, so an effective method to increase relative sample capacity would be to use narrower capillaries. However, this will naturally result in a reduction in detection efficiency, as with open tubular CEC (see Section 2.7.3.). Bundles of narrow capillaries could be effective, but with the relatively large tolerances on capillary ID this would probably lead to smeared out peaks. Packed columns, however, are often regarded as bundled capillaries, so a possible solution would be to pack a capillary with non-porous bare silica particles to represent the inner surface of a CE capillary. This would essentially result in a bundle of very narrow capillaries, with the challenge being to avoid any chromatographic interaction. For systems such as the histones, this would be very difficult, but for other systems adsorption is less of a problem.

In order to investigate the feasibility of this approach, a 100 µm ID capillary was packed with non-porous bare silica particles of diameter equal to 2.8 µm, with the length to the detector being 308 mm and the total length of the column being 502 mm. The column was packed in the usual manner, although sedimentation in the

packing chamber with non-porous particles is more rapid than with porous particles, making the process less efficient. Before use the column was flushed with 0.1 M aqueous NaOH, for the same purpose as that with the open columns, using the high pressure pump. The mobile phase employed was 50 mM aqueous ammonium acetate, with a running potential of 25 kV being utilised. Injection was performed by application of 5 kV for 5 seconds. The CIA was used for these experiments, forcing absorbance detection to be fixed at a wavelength of 214 nm. Consecutive injections were made of 1-naphthalene sulfonic acid solutions at concentrations of 100, 200, 300, 400 and 500 µM in water. The run length was ten minutes. The resulting electropherogram for all the runs is shown in Figure A.6. An enlarged view of the eluting band for the 500 µM solution is shown in Figure A.7 so that the peak shape can be seen more clearly. For comparison, the peak obtained by running the same sample through an open column filled with the same mobile phase is presented in Figure A.8. The length of the separation capillary in this case was 1000 mm in total and 760 mm to the window. A running potential of 20 kV was applied and the sample injection was performed in the same manner as for the packed column. This data is presented in Section 4.3.1, where it is used for estimating detector efficiency. Figure A.8 is an enlargement of the electropherogram shown in Figure 4.12.

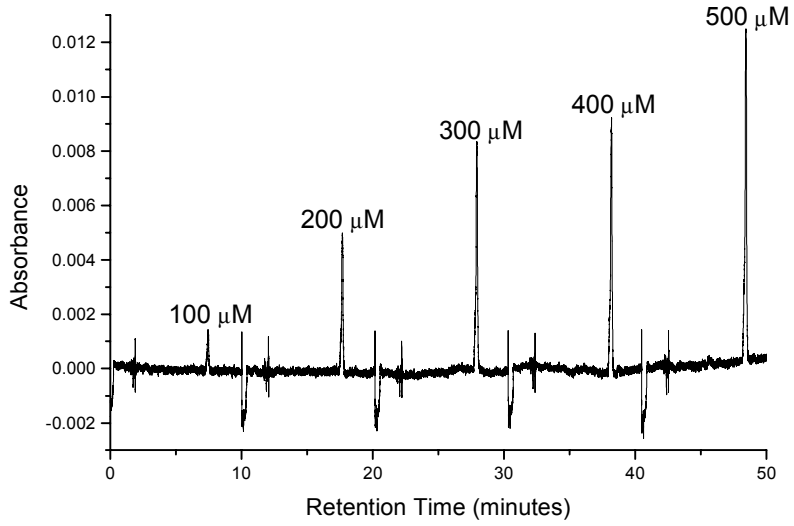

Figure A.6. Electropherogram showing consecutive injections of 1-naphthalene sulfonic acid solutions used to evaluate performance of packed CE columns. Zero time marks the beginning of the first run with each run lasting 10 minutes.

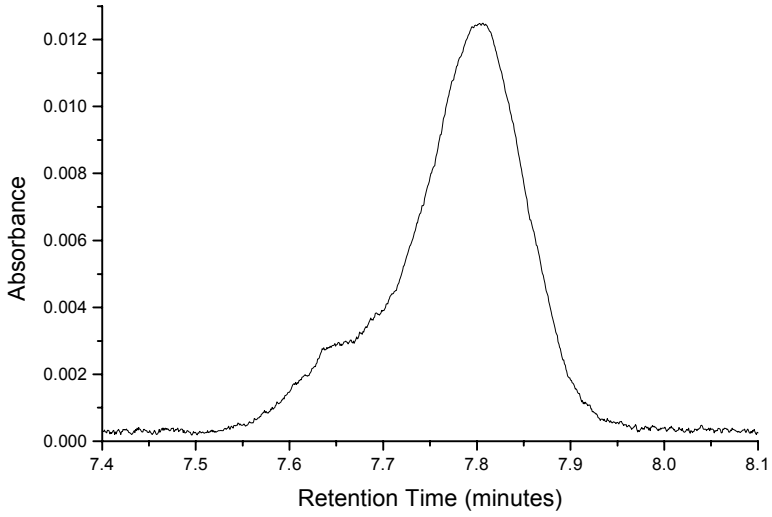

Figure A.7. Enlarged view of the eluting band for the 500 μM solution of 1-napthalene sulfonic acid shown in Figure A.6.

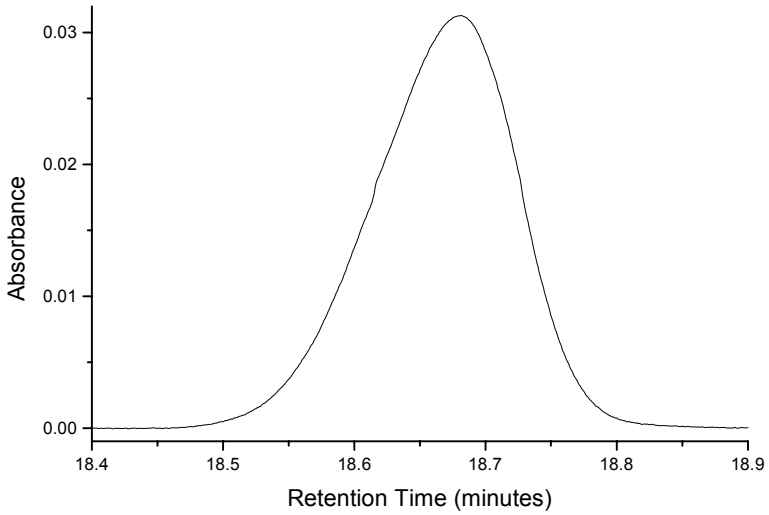

Figure A.8. Peak shape for a 500 µM solution of 1-napthalene sulfonic acid run on an open column run for comparison. Data is the same as that shown in Figure 4.12.

Comparing the electropherogram shown in Figure A.6 with that presented in Figure 4.12, which corresponds to an almost identical experiment using an unpacked open column, it can first be seen that the peaks are less intense. A noticeable feature in the enlarged view of the electropherogram for the 500µM solution of 1-nathalene sulfonic acid using the packed CE column is the small, partially resolved peak at slightly shorter retention time to the main peak. The identity of this impurity is unknown, but it is seen at all concentrations at a proportionate intensity. This minor peak results in an asymmetry ratio of 1.9 for the main peak, but this is misleading due to the impurity. The half height width, however, is in the region beyond the influence of the smaller peak. The value of 7.5 seconds at a retention time of 468.2 seconds allows calculation of the separation efficiency as 22,000 theoretical plates (71,000 per metre). For comparison the efficiency of the same peak for the open column experiments is 122,000 theoretical plates (161,000 per metre). It can clearly be seen, however, in Figure A.8 that the peak is fronting, indicating that the sample capacity of the column has been exceeded. The peak asymmetry ratio in this case is equal to 1.46. Data for each peak in Figure 4.12 is given in Table A.2. It can be seen that asymmetry rapidly increases with injected concentration, indicating that sample capacity has been exceeded. No such fronting is seen for the packed column.

This data does show, however, that although fronting is clearly evident in the open column data, the effect on separation efficiency as typically measured, is minor.

Concentration of 1-naphthalene sulfonic acid injected (μM)	Efficiency (N)	Efficiency (N/m)	Peak Asymmetry Ratio
100	127,000	168,000	1.00
200	129,000	170,000	1.21
300	129,000	170,000	1.26
400	122,000	160,000	1.37
500	122,000	161,000	1.46

Table A.2. Variation of efficiency and peak symmetry with concentration of 1-naphthalene sulfonic acid injected onto an open CE column. Original data is shown as Figure 4.12.

Figure A.9 provides a comparison of peak area with concentration of 1-naphthalene sulfonic acid injected. The product-moment correlation coefficient, *r*, was calculated to be 0.9845, considerably lower than that found for open column CE, but still indicating a largely straight line.

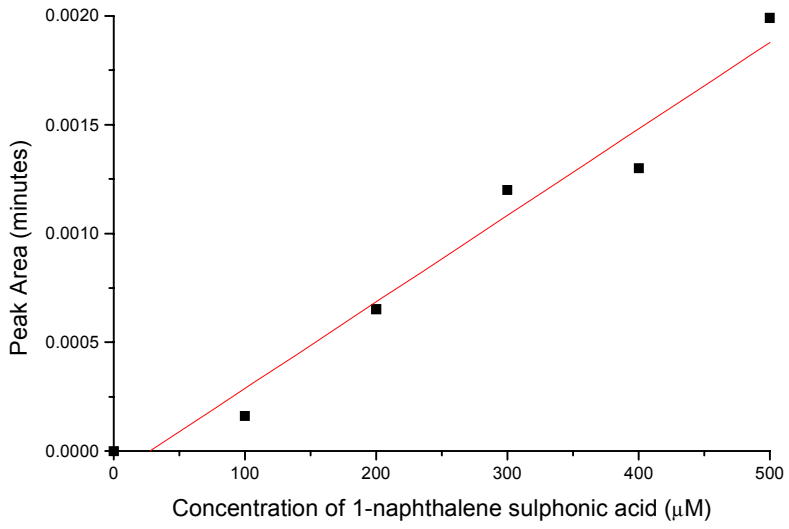

Figure A.9. Comparison of peak area with concentration of 1-naphthalene sulfonic acid injected for packed CE column (compare with Figure 4.13).

These initial results show that non-porous bare silica particles have potential for use in increasing CE sample capacity. Increased sample capacity was clearly demonstrated. The separation efficiencies obtained so far are poor compared with the open column technique, and increasing the surface area would increase the probability of undesirable interactions, but there is certainly scope for further investigation.

---

[1] T. Tsuda, G. Nakagawa, M. Sato and K. Yagi, *J. Appl. Biochem.*, **1983**, *5*, 330-336.

[2] T. Tsuda, K. Takagi, T. Watanabe and T. Satake, *J. High Resolut. Chromatogr. Chromatogr. Commun.*, **1988**, *11*, 721-723.

[3] X. Huang, J. B. Shear and R. N. Zare, *Anal. Chem.*, **1990**, *62*, 2051-2053.

[4] S. E. Geldart and P. R. Brown, *J. Chromatogr. A*, **1998**, *828*, 317-336.

[5] Z. Zhao, J. H. Wahl, H. R. Udseth, S. A. Hofstadler, A. F. Fuciarelli and R. D. Smith, *Electrophoresis*, **1995**, *16*, 389-395.

[6] A. Zenker, M. Galanski, T. L. Bereuter, B. K. Keppler and W. Lindner, *J. Chromatogr. A*, **1999**, *852*, 337-346.

[7] T. Hirakawa, S. Kobayashi and Y. Kiso, *J. Chromatogr.*, **1985**, *318*, 195-210.

[8] E. B. Watchman, *Platinum (II) Aminophosphine Anticancer Complexes and their Interactions with Nucleotides*, PhD Thesis, University of Edinburgh, **2001**.

[9] A. Wolffe, *Chromatin Structure and Function, Third Edition*, Academic Press, San Diego, **1998**.

[10] H. Gould (Editor), *Chromatin - A Practical Approach*, Oxford University Press, Oxford, **1998**.

[11] J. S. Green and J. W. Jorgenson, *J. Chromatogr.*, **1989**, *478*, 63-70.

[12] L. R. Gurley, J. E. London and J. G. Valdez, *J. Chromatogr.*, **1991**, *559*, 431-443.

[13] H. Lindner, W. Helliger, A. Dirschlmayer, H. Talasz, H. Wurm, B. Sarg and M. Jaquemar and B. Puschendorf, *J. Chromatogr.*, **1992**, *608*, 211-216.

[14] H. Lindner, W. Helliger, A. Dirschlmayer, M. Jaquemar and B. Puschendorf, *Biochem. J.*, **1992**, *283*, 467-471.

[15] H. Lindner, H. Wurm, A. Dirschlmayer, B. Sarg and W. Helliger, *Electrophoresis*, **1993**, *14*, 480-485.

[16] H. Lindner, W. Helliger, B. Sarg and C. Meraner, *Electrophoresis*, **1995**, *16*, 604-610.

[17] C. A. Mizzen and D. R. McLachlan, *Electrophoresis*, **2000**, *21*, 2359-2367.

[18] J. W. Jorgenson and K. D. Lukacs, *Science*, **1983**, *222*, 266-272.

[19] E. K. M. Andersson and I. Hägglund, *J. Chromatogr. A*, **2002**, *953*, 227-237.

B. Courses, Conferences and Other Activities

B.1. External Conferences and Meetings Attended

Second International Meeting on Capillary Electrochromatography (part of the Fifth International Symposium on Capillary Electrophoresis), University of York, Friday 28th August 1998.

Theory and Practice of Mass Spectrometry: A Technique for the New ICI, Rushpool Hall, Saltburn, Monday 9th to Wednesday 11th November 1998.

24th Annual Meeting of the British Mass Spectrometry Society, University of Reading, Sunday 12th to Wednesday 15th September 1999.

Desty Memorial Lecture for Innovation in Separation Science, The Royal Institution of Great Britain, London, Monday 18th October 1999.

Royal Society of Chemistry Annual Conference, University of Manchester Institute of Science and Technology, Sunday 16th to Thursday 20th April 2000.

15th International Mass Spectrometry Conference, Palacio de Congresos, Fira de Barcelona, Spain, Sunday 27th August to Friday 1st September 2000.

Pharmaceutical Analysis – Lab on a Chip (part of the 2000 British Pharmaceutical Conference and held in conjunction with the Joint Pharmaceutical Analysis Group), International Convention Centre, Birmingham, Monday 11th September 2000.

The Miniaturisation Revolution – Second British Mass Spectrometry Society Meeting on Miniaturisation – Current and Future Trends in Miniaturised Sample Handling, Separation and Detection Strategies, SmithKline Beecham Pharmaceuticals, Harlow, Wednesday 13th September 2000.

49th ASMS Conference on Mass Spectrometry and Allied Topics, Hyatt Regency Hotel, Chicago, USA, Sunday 27th to Thursday 31st May 2001.

B.2. Courses Attended

Induction Course for Laboratory Demonstrators, Wednesday 21st October 1998, one full day duration.

BP Team Development Course, Tuesday 14th and Wednesday 15th March 2000, two full days duration.

Mass Spectrometry (Lecture Course), Professor J. J. Monaghan, Autumn Term 2000, 5 hours in total duration as 5 one hour lectures.

Scientific Computing Tools: Introduction to Unix, Tuesday 6th and Wednesday 7th November 2001, 6 hours in total duration as two three hour sessions.

Scientific Computing Skills: LaTeX, Tuesday 13th and Wednesday 14th November 2001, 6 hours in total duration as two three hour sessions.

Scientific Computing Tools: Unix II, Tuesday 4th and Wednesday 5th December 2001, 6 hours in total duration as two three hour sessions.

Furthermore, I have attended and participated in Physical Section colloquia and informal meetings, both in Edinburgh and at Firbush Point Field Centre, Loch Tay. I have also, in addition, attended and arranged regular group meetings.

B.3. Other PhD Related Activities

Participated in the Pupil Researcher Initiative, primarily as a Researcher in Residence, being placed with George Heriot's School, Edinburgh. This involved attending approximately twenty lessons, each of seventy minutes duration, acting as a classroom assistant, helping students working on their Sixth Year Studies chemistry projects (Autumn Term 1999 and Spring Term 2000). Also participated in two 'Express Yourself' science conferences, chairing meetings and judging presentations (Glasgow Science Centre, Monday 11th June 2001 and The Royal Institution of Great Britain, London, Thursday September 27th 2001). Presented with a Science Communicator's Award by Professor Richard Brook, Chief Executive of the EPSRC, for these and other contributions to the Pupil Researcher Initiative.